DEVELOPMENT OF AN OPTIMUM ACETABULAR CUP PROSTHESIS

MARTIN J. MATHIAS

A thesis submitted in partial fulfilment of the requirement of Bournemouth University for the degree of Doctor of Philosophy

March 2004

Bournemouth University

In collaboration with

Orthodynamics Ltd.

Abstract

The aim of this research is to use advanced materials and state of the art Finite Element Analysis to produce a novel acetabular cup prosthesis. An investigation into current static and fatigue testing procedures for acetabular cup prostheses has identified current strengths and weakness and proposes a cheap, fast method that is closer to anatomical loading conditions.

The current trend of performing Total Hip Replacements (THR) on younger patients incurs an increasing number of revisions. Therefore, prolonging the life of a THR is of paramount importance and is the principal goal of this study. With this trend comes a new set of design goals driven by higher patient expectations of their THR. Younger patients not only require increased longevity from their prosthesis but also increased performance so as to be able to undertake more strenuous everyday activities, such as sports. Historically, the main objective of THR was to relieve pain and increase quality of life in the elderly and was not intended for young active patients. Previous research proposes that the acetabular cup design has far more impact on long-term survival of the THR than the femoral component. Optimising the acetabular cup prosthesis produces a highly complex problem where many of the individual design factors have massive impact on the system. A main aim is to develop a material or combination of materials to optimise the stress distribution in the system without sacrificing the service life of the THR. Of the 800,000 hip replacements carried out annually, many of the current acetabular cups have some form of polyethylene bearing surface. However, polyethylene wear debris is seen as a major contributing factor to bone resorption and hence prosthesis loosening. Changes in stress values, even caused by initial primary fixation during the operation, can result in stresses being transferred in an unrealistic manner. The effect is that the bone grows to differing thickness and strengths. This is known as remodelling. For optimisation of the acetabular cup, the properties of the natural hip must be retained by minimising both remodelling and bone resorption.

The present research, with collaboration from Orthodynamics Ltd., has produced novel composite acetabular cup prostheses with a ceramic on ceramic bearing surface that should last longer and perform better, thus reducing the necessity for costly and debilitating revisions later on in life. In addition, the use of the proposed novel anatomically orientated mechanical testing methods gave fast, cheap results and could also allow further research into fatigue failure of alumina bearing couples in THR.

Contents.

List of Figures

List of Tables

Publications Resulting From Thesis

1. Mathias, M., 2004, Development of an optimum acetabular cup prosthesis. In: Cobb, J. (editor), *3rd Academic Biomedical Engineering Research Group Workshop Proceedings,* Bournemouth, September 2002, ISBN 1-85899-178-1

Acknowledgements

The author wishes to acknowledge the help, support and encouragement received whilst undertaking the PhD research.

My supervisor, Dr Kamran Tabeshfar.

Orthodynamics Ltd of Christchurch in Dorset (UK), for their financial support and the manufacture of the specimens required for mechanical testing.

Dr John Bradley and Dr Darren Forrest of Orthodynamics Ltd. for their biomechanical expertise and support.

The Engineering and Physical Science Research Council and Bournemouth University for their financial support.

The staff of Design Engineering and Computing at Bournemouth University for their patience and support, especially the technicians at Tolpuddle House and Studland House.

Carolyn Mair for her continued encouragement and advice

Last but not least, my family and friends for their continued support, patience and encouragement.

Author's Declaration

This thesis is submitted for the degree of Doctor of Philosophy in the School of Design, Engineering & Computing, Bournemouth University. I am responsible for the work submitted in this thesis. The submitted work is original, except where references have been made to others. The research was carried out by myself in the period from October 1999 to March 2004 under the supervision of Dr. Kamran Tabeshfar in the School of Design, Engineering & Computing, Bournemouth University.

No part of this thesis, or any other work similar to it, has been, or is currently being submitted for any degree or any other qualification. This thesis is less than 40,000 words.

Martin Mathias

School of Design, Engineering & Computing,

Bournemouth University

UK

Nomenclature

a	crack length (m)
a_c	critical crack length (m)
A_0	initial crack length (m)
A	constant in the relationship between stress intensity factor and subcritical crack growth rate
B	minimum specimen thickness (m)
C	geometry correction factor
E	elastic modulus (Pa)
I	second moment of area (m^4)
K	stress intensity factor (MPa-$m^{1/2}$)
K_c	fracture toughness (MPa-$m^{1/2}$)
K_i	stress intensity factor corresponding to toughening mechanism i (MPa-$m^{1/2}$)
K_{ic}	fracture toughness or critical stress intensity (MPa-$m^{1/2}$)
K_s	shielding stress intensity factor (MPa-$m^{1/2}$)
K_{th}	subcritical crack growth intensity factor (MPa-$m^{1/2}$)
K_{tip}	stress intensity factor experienced at the crack tip (MPa-$m^{1/2}$)
n	exponent in the relationship between stress intensity factor and subcritical crack growth rate
W	minimum remaining uncracked specimen length (m)
Y	geometric flaw shape parameter

Greek letters

Δ	prefix indicating a range
σ	applied stress (MPa)
σ_{vm}	Von Mises-Hencky stress (MPa)
σ_{ys}	material yield stress (MPa)
σ_1	maximum principal stress (MPa)
σ_2	middle principal stress (MPa)
σ_3	minimum principal stress (MPa)

1 INTRODUCTION

1.1 Introduction to Total Hip Replacement

The hip joint can be simply described as spherical or ball and socket joint and is the connection between the pelvis and the longest bone in the body, the femur. The hip joint is one of the largest most heavily loaded joints in the body, with the ability to withstand forces many times greater than body weight.

The head of the femur represents approximately two thirds of a sphere and fits into the deep socket in the pelvis called the acetabulum. Both the acetabulum and the femoral head are largely covered in articular cartilage that acts as a bearing material, with synovial fluid as the lubricant. The hip joint allows backwards and forwards movement, inward and outward swing and some degree of rotation.

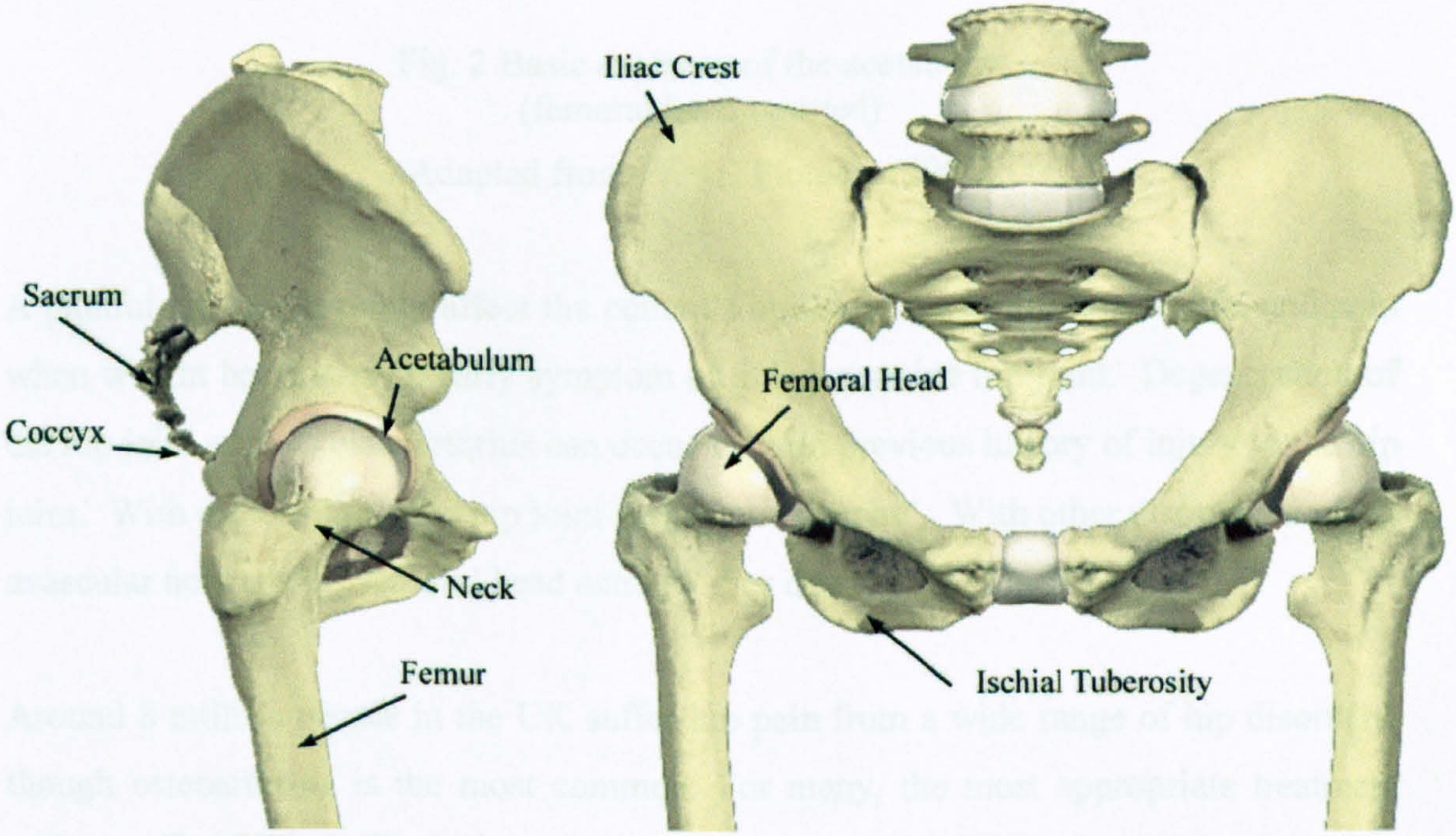

Fig. 1 Basic anatomy of the hip joint

Adapted from Primal Pictures (2003)

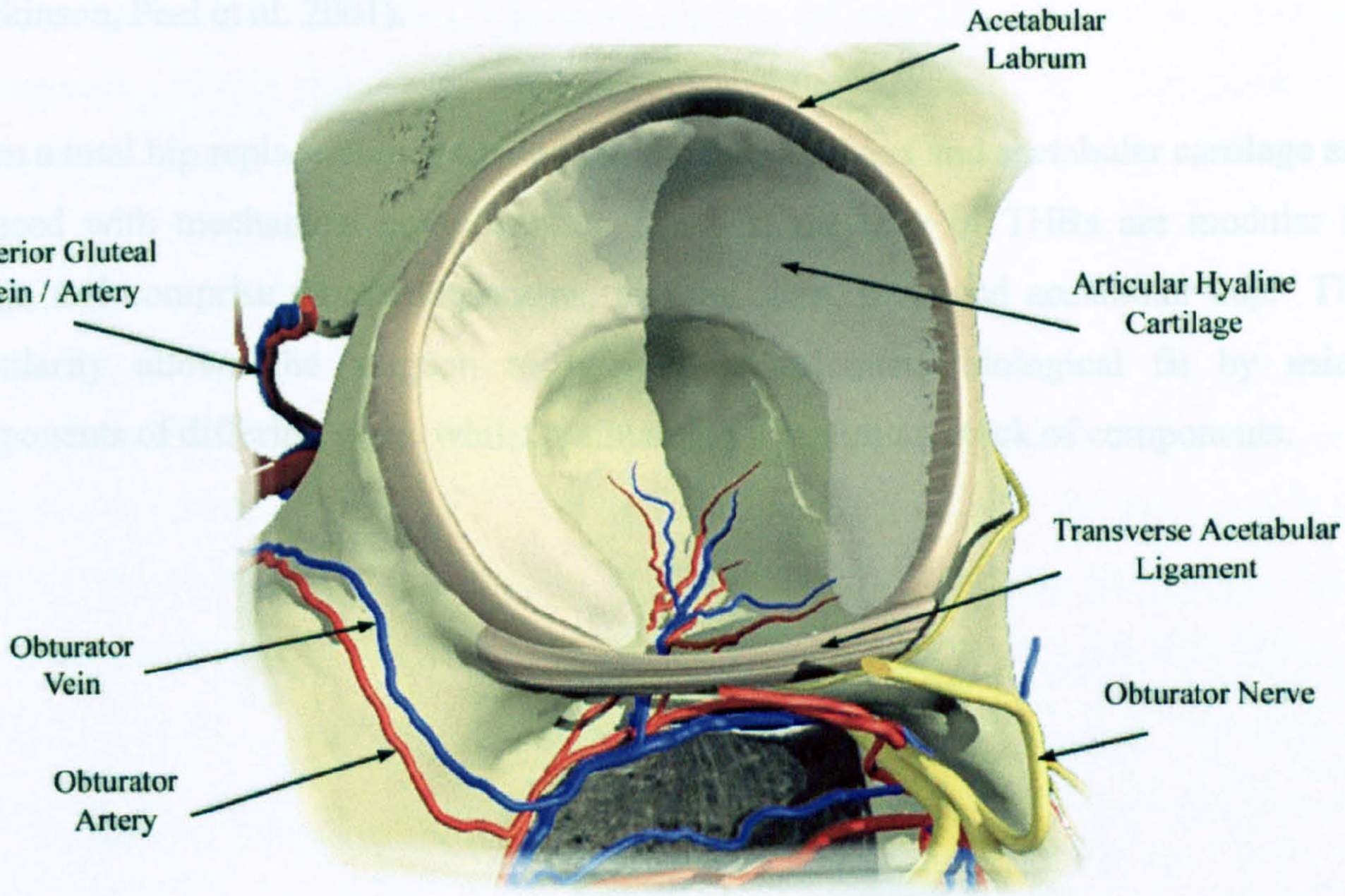

Fig. 2 Basic anatomy of the acetabular
(femoral head omitted)
Adapted from Primal Pictures (2003)

A painful hip can severely affect the patient's ability to lead a full active life, and pain when weight bearing is an early symptom of a degenerative hip joint. Degeneration of the hip joint such as osteoarthritis can occur with no previous history of injury to the hip joint. With osteoarthritis the hip joint simply "wears out". With other disorders such as avascular necrosis the femoral head actually dies due to loss of blood supply.

Around 8 million people in the UK suffer hip pain from a wide range of hip disorders, though osteoarthritis is the most common. For many, the most appropriate treatment will be a Total Hip Replacement (THR). Over 30,000 hip replacements are performed by the National Health Service (NHS) each year at a cost of £139 million. THR is a highly effective procedure, producing immediate and dramatic benefits in almost all cases (National Audit Office 2000). Globally, the number of THRs performed annually is less clear, with the number reported varying between 400,000 (Yildiz, Ha et al. 1998),

500,000 (Finerman, Dorey et al. 1998) 800,000 (Pendegrast 1997) and 1 million (Wilkinson, Peel et al. 2001).

When a total hip replacement is carried out the femoral head and acetabular cartilage are replaced with mechanical components. The vast majority of THRs are modular in design and comprise three components, femoral stem, head and acetabular cup. The modularity allows the surgeon to achieve an adequate biological fit by using components of differing sizes, whilst maintaining a minimum stock of components.

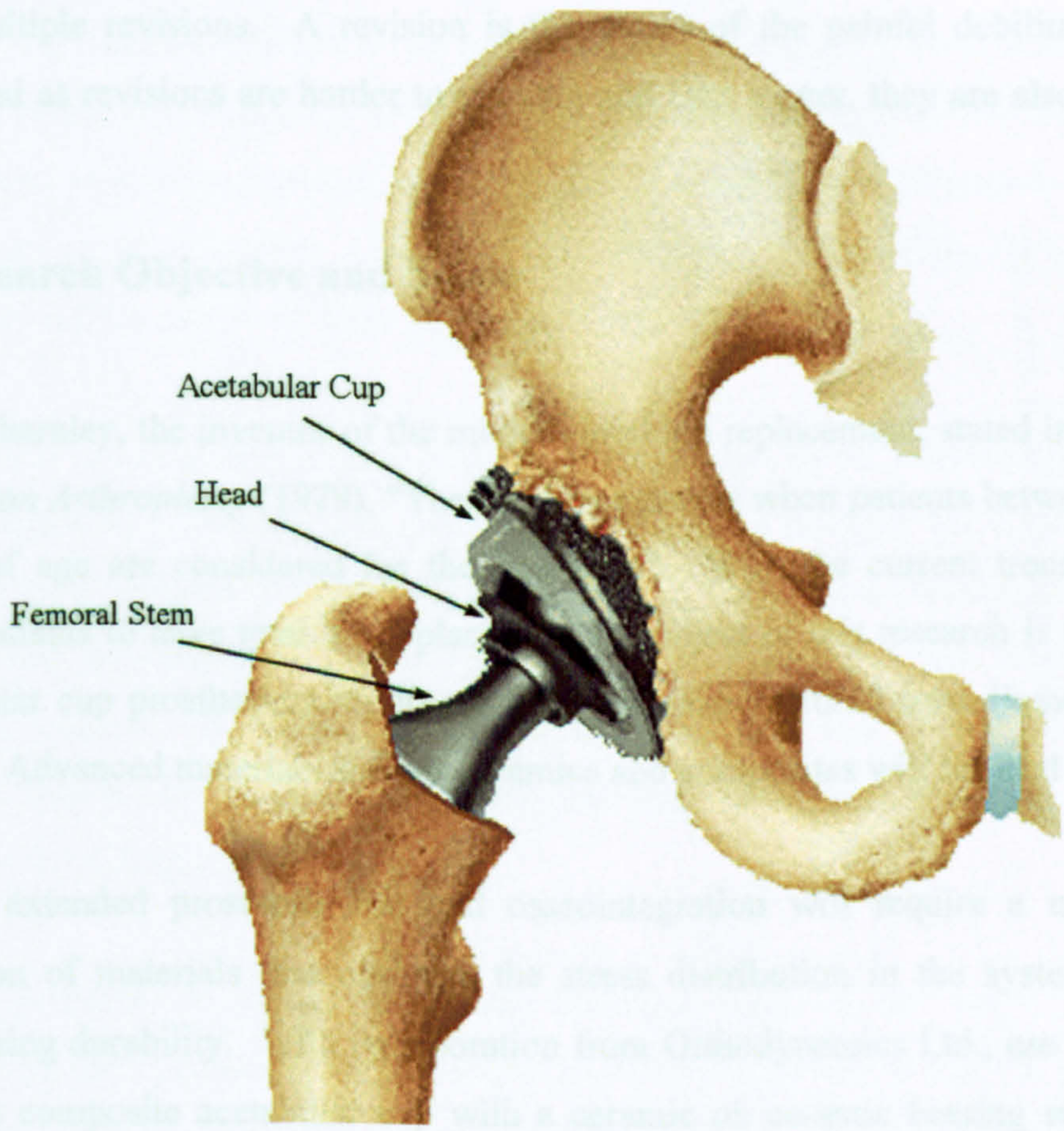

Fig. 3 General arrangement of components in Total Hip Replacement
Adapted from Medical Multimedia Group (1997)

The general arrangement of THR components varies very little (Fig. 3), but design and materials vary greatly. A UK survey carried out in 1994 (National Audit Office 2000) found that 62 different prostheses made by 19 companies were sold in the UK. Age,

lifestyle and surgeons' preference are the main influences on the type of prosthesis and method of primary fixation used. The most common primary fixations are cemented and uncemented. With a cemented fixation the bone is reamed out larger than prosthesis and epoxy cement is inserted to give a cement mantle around the prosthesis. Conversely, in an uncemented THR, the bone is reamed smaller than the prosthesis creating a 'press fit' when the prosthesis is introduced.

The average length of hospital stay in England for a primary THR is 11 days, but this varies greatly from 5 days to 30 days (National Audit Office 2000). Although some THRs achieve a ten to fifteen year survivorships, many do not. For this reason, patients require multiple revisions. A revision is the repeat of the painful debilitating THR process, and as revisions are harder to perform and take longer, they are also higher in cost.

1.2 Research Objective and Scope

Sir John Charnley, the inventor of the modern total hip replacement, stated in his book, *Low Friction Arthroplasty* (1979), "The challenge comes when patients between 45 and 50 years of age are considered for the operation". With the current trend for even younger patients to have total hip replacement the object of this research is to produce an acetabular cup prosthesis with an extended life manufactured from 'bone friendly' materials. Advanced materials such as ceramics and composites will be used to achieve this.

To attain extended prosthesis life and osseointegration will require a material or combination of materials that optimise the stress distribution in the system without compromising durability. With collaboration from Orthodynamics Ltd., use of a novel cementless composite acetabular cup with a ceramic on ceramic bearing surface was proposed to complement the existing carbon fibre reinforced stem, the "Bradley Femoral Stem HA Coated". The project also investigates limitations in current mechanical testing methods of the acetabular prosthesis and proposes a cheap, fast method that is closer to anatomical loading conditions. Fatigue test of the prosthesis was carried out using the new testing method and an S-N Curve produced. The final designs should last longer and perform better thus reducing the necessity for costly revisions later on in life.

1.3 Outline of Thesis

Chapter 1 presents the general background of total hip replacement and related biomechanics and introduces the current literature. This literature review examines factors contributing to acetabular cup failure or loosening and investigates the current state of the art with regard to prosthesis design, materials, fatigue of ceramics and mechanical testing. The Chapter summary places the many facets of the Literature Review in context for the successful design of a novel acetabular prosthesis.

The design and manufacture of a novel acetabular cup prosthesis is described in Chapter 2. Critical design specifications are identified from the literature review in Chapter 1 and combined with manufacturing constraints from the sponsor company to produce a minimum design specification. Chapter 2 also examines the materials, design features and range of motion analysis for the proposed acetabular prosthesis.

The Literature Review in Chapter 1 highlights the need to advance the mechanical testing methods of acetabular hip prosthesis. Chapter 3 presents the formulation of mechanical tests methods and the design of novel test rigs for the mechanical testing of acetabular hip prostheses. Chapter 3 continues by proposing a fast, repeatable and economical method of mechanically testing acetabular cup prostheses, and is particularly relevant for acetabular hip prostheses with ceramic bearing surfaces such as that proposed in Chapter 2.

Chapter 4 presents the experimental and analytical methodology employed in this research. The test specimens, their preparation and the procedures used in mechanical testing are described. The Finite Element Analysis (FEA) of the test specimens is also described, as are theories of strength and failure.

Results presented in Chapter 5 originate from finite element techniques, mechanical testing and manufacturing trials. The stress distribution in the acetabular and possible osseointegration advantages of the proposed prosthesis are explored using 2D FEA. 3D FEA is utilised in this section to predict the prosthesis' and test rig's ability to withstand mechanical loading. Mechanical testing ensures that the final iteration of the proposed

acetabular prosthesis and taper adaptors can withstand everyday loads encountered in-vivo; to produce an S/N curve for the proposed prosthesis; to uncover any weaknesses due to manufacturing processes; and to test the suitability of the proposed anatomically orientated testing methods.

Chapter 6 contains the discussion, whilst Chapter 7 outlines the conclusions, limitations and future work.

1.4 Literature Review

1.4.1 Background and Related Biomechanics

Surgeons and engineers have studied the human hip joint for hundreds of years for its amazing robustness. It can withstand many cycles of high loading. For example, jogging can exert a force of five and half times body weight (Bergmann 1993). The articular cartilage (bearing surface) within the joint has the ability to alter its thickness to maintain sphericity. Early work by Rushfeld et al. (1979) showed that articular cartilage could compensate by as much as 500μm for irregular bony foundations, keeping localised maximum deviations less than 150μm. It also showed that the pressure distribution of the acetabular cartilage is non-uniform with a maximum pressure of 6.8 MPa at a 1350 N load. Mann (2002) confirmed that these results were in agreement with other authors, for example with von Eisenhart et al. (1999), but failed to explain Hodge et al's. (1989) results showing maximum pressure loading of 18 MPa. Hodge et al's. maximum 18 MPa pressure was in fact encountered during the raising from a chair and not during normal gait as in most other studies.

The understanding of loads incurred in the acetabulum is extremely important for prosthesis design, because as with the articular cartilage, bone also has the ability to adapt to localised conditions. For this reason the hip joint should be considered as a structure rather than a continuous material; the bone is generally thought of as two types, cortical (compact) and trabecular (spongeous). The stiff cortical bone is a shell around the softer trabecular bone creating a 'sandwich' structure (Fig. 4).

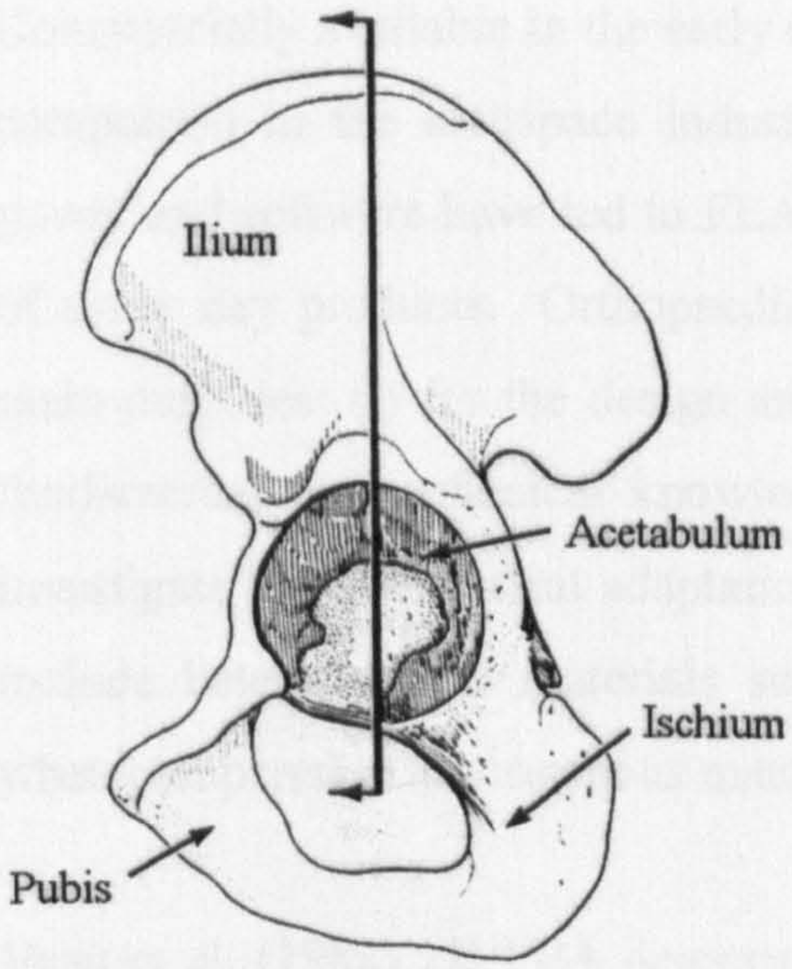

Direction of
Vasu et al. (1982) Slice

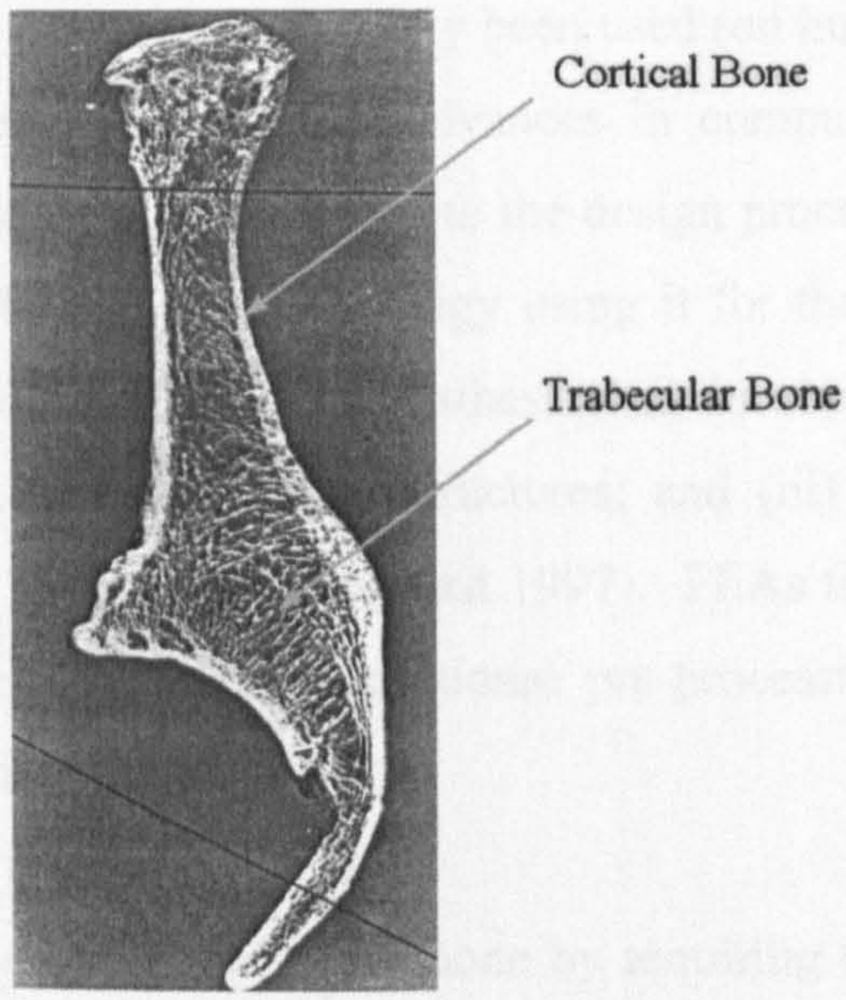

Roentgenogram of Slice Showing
Trabecular Orientation

Fig. 4 Direction and roentgenogram of Vasu et al. (1982)
2D slice through pelvis showing 'sandwich construction'

Adapted from Vasu et al. (1982)

The mechanical properties of both cortical and trabecular bone are dependent on the mechanical demands placed on them (Buckwater, Glimcher et al. 1995). The ultimate strength of cortical bone is in the range 100-150 MPa, whilst that of trabecular bone is in the 8-50 MPa range (Nordin and Frankel 2001). The variations are due to shape and structure, and, in general, it is not enough to describe the strength of bone by a single number due to the differences in mechanical behaviour. The ability of bone to remodel by altering its size shape and structure is summarised as Wolff's Law which states that the remodelling of bone is influenced and modulated by the mechanical stresses (Nordin and Frankel 2001).

Traditionally, interest existed in orthopaedic and orthopaedic-related sciences with respect to stress and strains in loaded bones, specifically concerning function i.e. Wolff's law. The mathematical tools available for stress analyses in classic mechanics were not very suitable for the highly irregular structural properties of bone (Huiskes and Chao 1983). The introduction of Finite Element Analysis (FEA) into orthopaedic-related sciences in the 70's was the logical next step, as FEA had the capability to

evaluate stresses in structures of complex shape, loading and material behaviour. Commercially available in the early 60's, FEA packages had mainly been used (on huge computers) in the aerospace industry by specialists. Recent advances in computer power and software have led to FEA being widely incorporated into the design process of every day products. Orthopaedics has embraced this technology using it for three main purposes: (i) for the design and pre-clinical analysis of prostheses; (ii) to obtain fundamental biomechanical knowledge about musculoskeletal structures; and (iii) to investigate time-dependent adaptation process in tissues (Pendegrast 1997). FEAs that include heterogeneous materials such as bone, do require additional pre-processing when compared to homogenous materials, such as steel.

Vasu et al. (1982) 2D FEA demonstrates the complex nature of bone by requiring the division of a simple 2D slice of the pelvis (Fig. 4) into five discrete regions each having different material properties (Fig. 5).

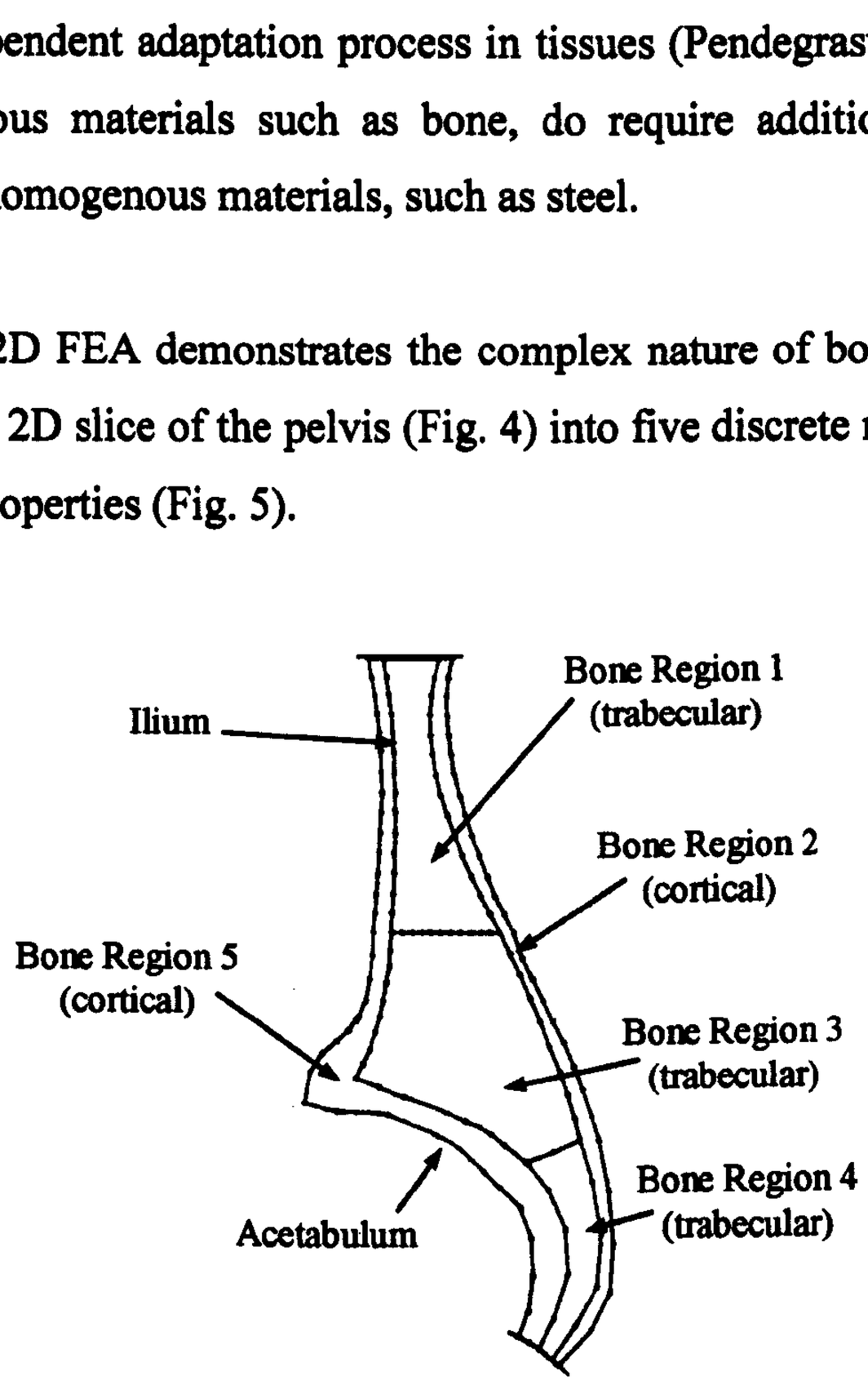

Fig. 5 Bone regions in Vasu's (1982) 2D FEA.
Adapted from Vasu et al (1982)

A finite element analysis by Rapperport et al. (1985) demonstrates an even greater number of bone regions (Fig. 6). The greater number of regions can be partly attributed to the orientation of the slice through the acetabulum. Vasu's (1982) section was selected as the section of high loading, whilst Rapperport's (1985) model seems

primarily to be selected to correspond with an axisymmetric model undertaken by Pedersen et al. (1982). Pedersen's (1982) choice of section was limited to the orientation shown in (Fig. 6), as it is the only position symmetrical enough to allow axisymmetric FEA modelling of the acetabulum.

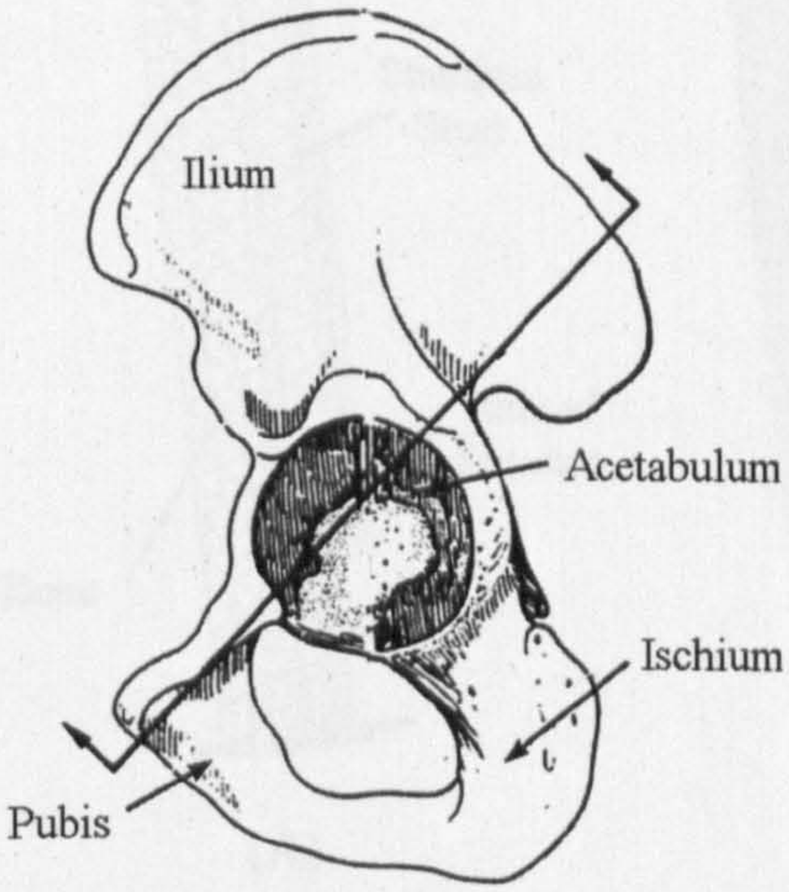

Direction of Rapperport et al. (1985) and Pedersen et al. (1982) Slice

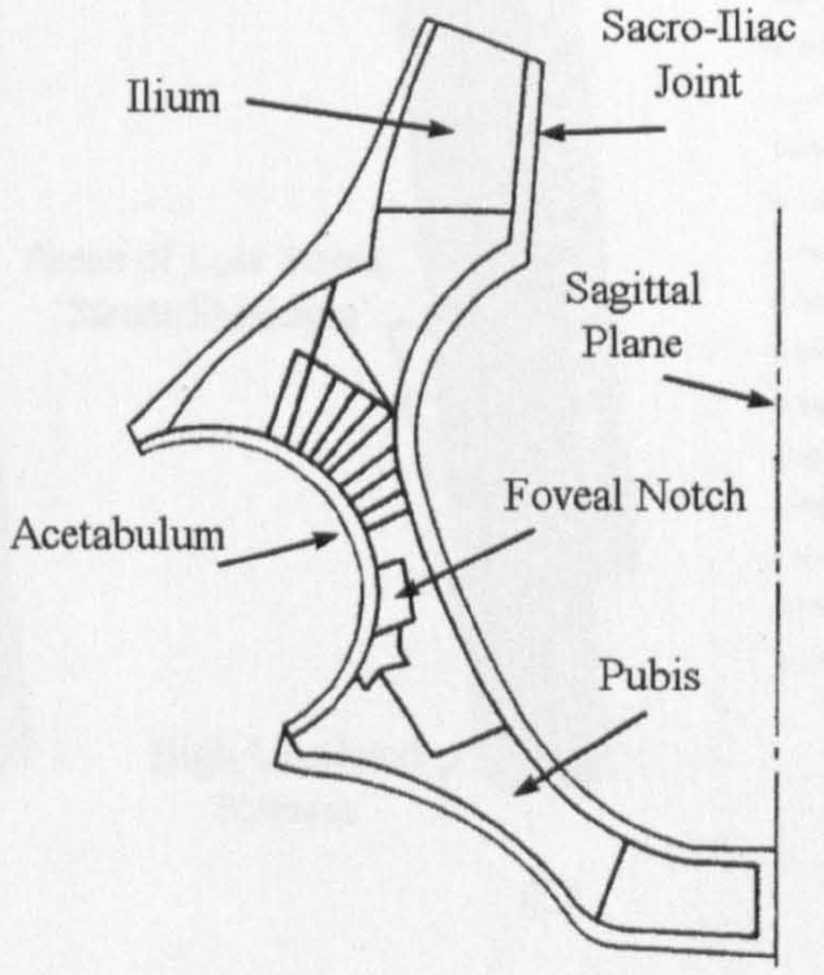

20 Discrete Regions of Bone in Rapperport et al. (1985) Slice

Fig. 6 Direction of Rapperport's (1985) and Pedrersen's (1982) slice through pelvis and Rapperport's (1985) bone regions

Adapted from Rapperport et al. (1985).

Vasu (1982) and Rapperport (1985) warn of the limitations of their 2D analysis due the out of plane stiffness that cannot be incorporated into 2D models. The strength of both studies is that they show that in comparison with bone morphology, density and orientation of bone corresponds to localised stresses. If for any reason these localised stresses are removed or transferred in another way, Wolff's Law would lead to bone remodelling and possible bone resorption. This is a continuing problem within prosthesis design and is due to the normally much stiffer prosthesis 'shielding' the bone from stress inducing loads (Fig. 7).

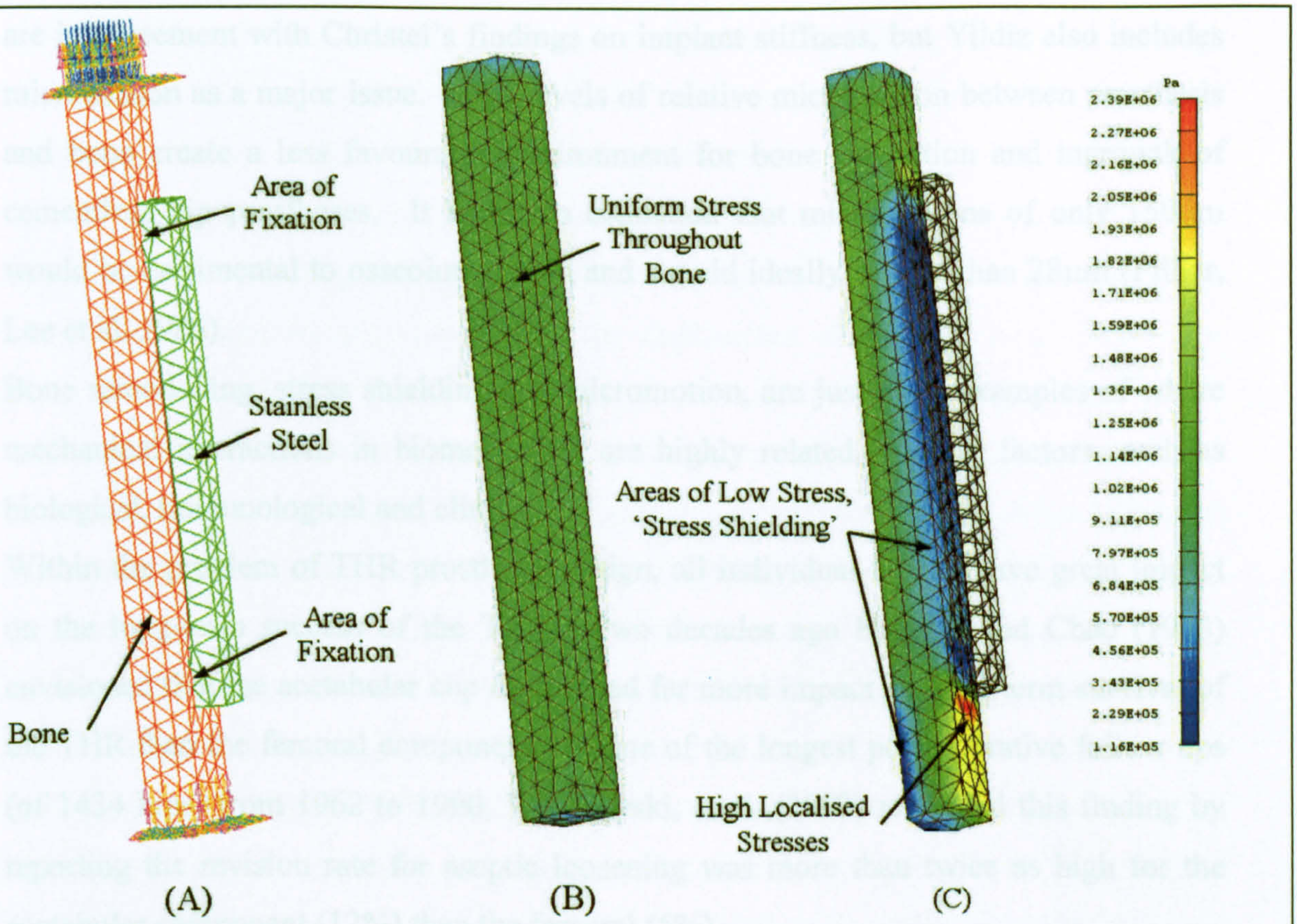

(A) Homogenous bone with a stainless steel support. Support fixated to the bone at its ends. The base of the bone is fixed with the top of the bone loaded axially in compression.

(B) Results of bone loaded without stainless steel support. Uniform stress through majority of bone.

(C) Results of bone loaded with stainless steel support. The support is shielding parts of the bone, reducing stresses by approximately 50%. The support is also inducing higher than normal stresses at its base.

Fig. 7 Simple FEA demonstrating stress shielding

THR requires the removal of the acetabular cartilage and in some cases, subchondral (cortical) bone (Jacob, Huggler et al. 1976; Carter, Vasu et al. 1982; Pedersen, Crowninshield et al. 1982). Therefore the stresses in the acetabulum are a direct result of the way the acetabular prosthesis transfers the load from the femoral head.

Matching bone and implant stiffnesses tends to decrease the detrimental effects of stress protection (Christel, Meunier et al. 1987). Other authors such as Yildiz, et al. (1998)

are in agreement with Christel's findings on implant stiffness, but Yildiz also includes micromotion as a major issue. High levels of relative micromotion between prosthesis and bone create a less favourable environment for bone apposition and ingrowth of cementless hip prostheses. It has been estimated that micromotions of only 150μm would be detrimental to osseointegration and should ideally be less than 28μm (Pilliar, Lee et al. 1986).

Bone remodelling, stress shielding and micromotion, are just three examples of where mechanical interactions in biomechanics are highly related to other factors, such as biological, immunological and clinical.

Within the problem of THR prosthesis design, all individual factors have great impact on the long-term success of the THR. Two decades ago Huiskes and Chao (1983) envisioned that the acetabular cup design had far more impact on long-term survival of the THR than the femoral component. In one of the longest post-operative follow ups (of 1434 hips) from 1962 to 1990, Wroblewski, et al. (2002) reiterated this finding by reporting the revision rate for aseptic loosening was more than twice as high for the acetabular component (12%) than the femoral (5%).

Aseptic loosening can be described as prosthesis loosening even though it is free of infection or septic material, and is widely accepted as a major cause of THR failure (Pedersen, Crowninshield et al. 1982; Rapperport, Carter et al. 1987; Massin, Shmidt et al. 1989; Morscher 1992; Wilkinson, Peel et al. 2001; Ornstein 2002). Whilst there is general agreement that aseptic loosening is the major reason for failure of THR, the pathological basis for aseptic loosening continues to be debated (Ornstein 2002).

Mjoberg (1997) postulates that loosening begins at an early stage due to either insufficient initial fixation or early loss of fixation. Other authors such as Ornstein (2002) suggest that the final explanation for aseptic loosening might be sought in a combination of multiple etiologic factors.

1.4.2 Factors Contributing to Acetabular Cup Failure or Loosening

1.4.2.1 Bone cement

Bone cement based on polymethylmethacrylate (PMMA) remains an important material for primary fixation of hip prosthesis, but its use in THR is not without problems. During polymerisation of the cement, a high level of heat is generated due to

exothermic reaction, especially with thicker mantles. The exposure of bone to high temperatures has led to incidences of bone necrosis and tissue damage, ultimately resulting in failure of the prosthetic fixation (Huiskes and Chao 1983; Dunne and Orr 2002). Mixing technique has a great impact on the porosity of the cement mantle. For example, vacuum mixing improves the fatigue strength by an order of magnitude, when compared to hand mixing, but causes the appearance of an occasional large pore (Murphy and Prendergast 2000). Residual stress, caused by the shrinkage of the cement during polymerisation when combined with cement mantle defects such as pores, has been shown to create cracks in the cement even before the patient stands after the operation (Huiskes 1980; Lennon and Prendergast 2002). These cracks are normally found to originate from defects such as pores at the interfaces depending on the direction of loading (McCormack and Prendergast 1999; McCormack, Prendergast et al. 1999; Lennon and Prendergast 2002).

Hernigou and Le Mouel (1999) studying voids in femoral cement mantle concluded that voids had no significant effect on loosening, or the THR's suvivorship in-vivo. Whilst Hernigou and Le Mouel propose several explanations as to why the voids have no effect, they fail to discuss what effect activity levels would have. It is possible that because of the relative old age of their patients (mean age 58), their activity levels would be lower and less strenuous than activity levels in younger patients. These lower activity levels may not induce stresses high enough around the voids to initiate cracks or fatigue failure.

Cement debris, such as cracks or micromotion, could travel to between the bearing surfaces causing extremely elevated amounts of wear (3rd-body wear) (Wang, Chopra et al. 2002).

1.4.2.2 Screw Acetabular Cup Prostheses

There are types of acetabular prosthesis that do not suffer from the problems involved with bone cement, one of which is the screwed cup. A variety of these are availible, but their common feature is that the cup is screwed into the acetabulum to achieve primary stability (Fig. 8).

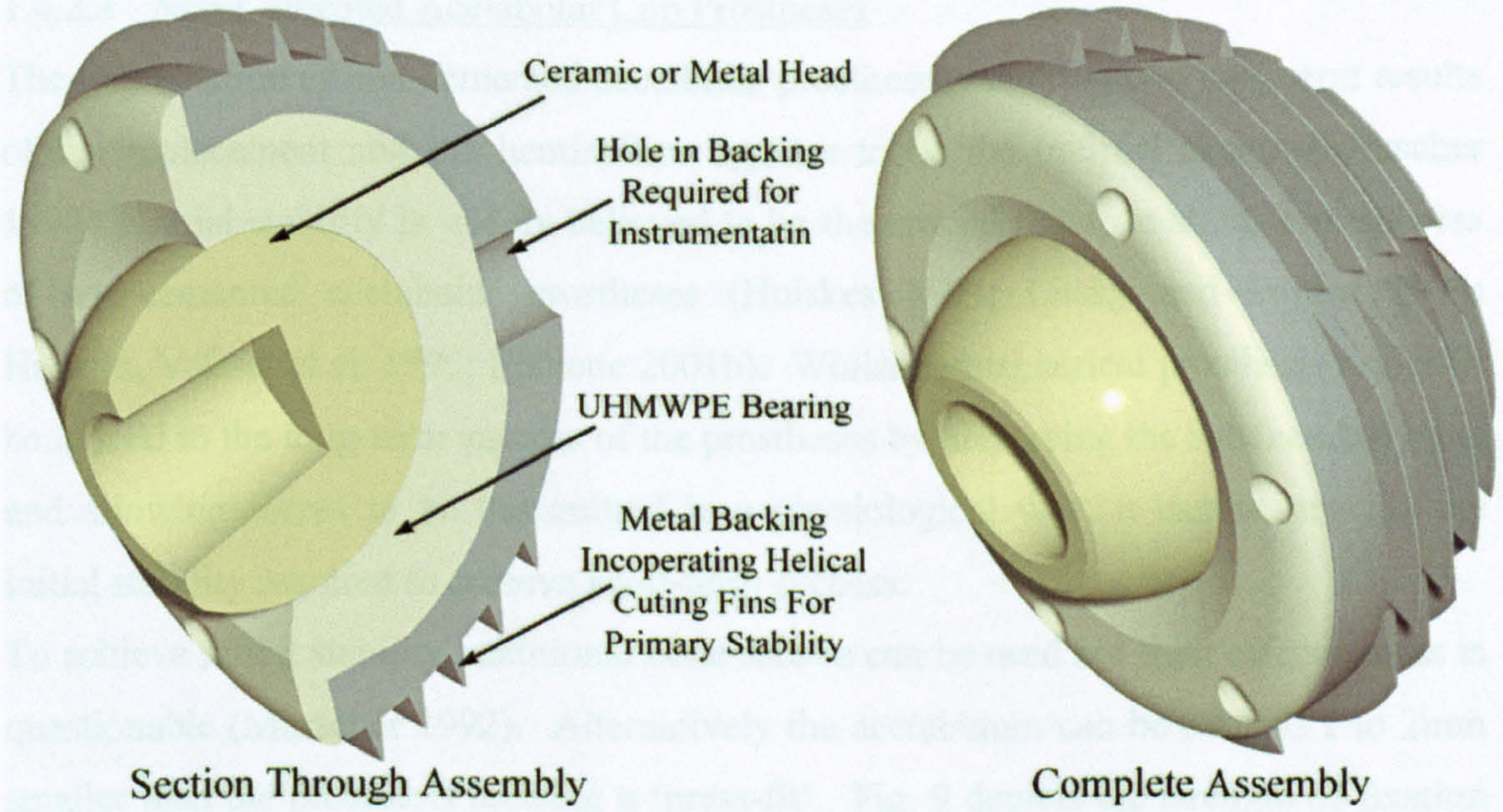

Fig. 8 Threaded metal backed UHMWPE acetabular cup and head

The screwed metal backing does however bring some totally new problems to the fore. Dalstra and Huiskes (1994) have found that in some cases pre-stresses approximated to the ultimate tensile strength of the surrounding cortical bone. These pre-stresses, generated during implantation and required to guarantee good initial stability, do not subsequently reduce by any significant amount. In fact the stresses would never probably drop below 91.5% of their initial value. These stress values will have significant influence on the way the body remodels that area (Wolff's law), and may even lead to fractures of the bone (Taylor and Tanner 1997). Despite many favourable reports describing their success, the use of threaded acetabular cups has fallen out of favour because of the growing number of reports of long-term fixation failure. Yahiro et al. (1995) concluded that the generalised use of threaded acetabular cups in THR should be abandoned, and indeed they have been in North America (Morscher 1992). Despite this, the use of threaded acetabular cup continues in the UK and Europe with reportedly encouraging mid-term results (Pandit, Hand et al. 1999; Epinette 2001b). However, Pandit et al.'s study can be criticised for the employment of a method for measuring cup migration that can only detect coarse position changes and therefore fails to detect any early signs of cup loosening or migration.

1.4.2.3 Non-Cemented Acetabular Cup Prostheses

The implantation of non-cemented acetabular prostheses may improve long-term results of hip replacement and the hemisphere appears to be the optimal design (Morscher 1992). Initial stability is widely believed to be the crucial factor to short-term success of non-cemented acetabular prostheses (Huiskes 1993; Litsky and Pophal 1994; Havelin, Vollset et al. 1995; Epinette 2001b). Whilst hemispherical prosthesis design is beneficial to the long-term success of the prostheses by preserving the subchondral bone and allowing forces to be transmitted in a physiological way, it cannot provide the initial stability required to achieve short-term success.

To achieve initial stability, additional bone screws can be used but their effectiveness is questionable (Morscher 1992). Alternatively the acetabulum can be reamed 1 to 2mm smaller than the prosthesis creating a 'press-fit'. Fig. 9 depicts the strength of fixation of a non-cemented press-fit implant to cancellous bone in experimental animals. Fixation increases rapidly during the first 2 weeks and then reaches a plateau, suggesting that there is an initial period of decreased stability with non-cemented implants when compared to cemented (Sumner and Galante 1992).

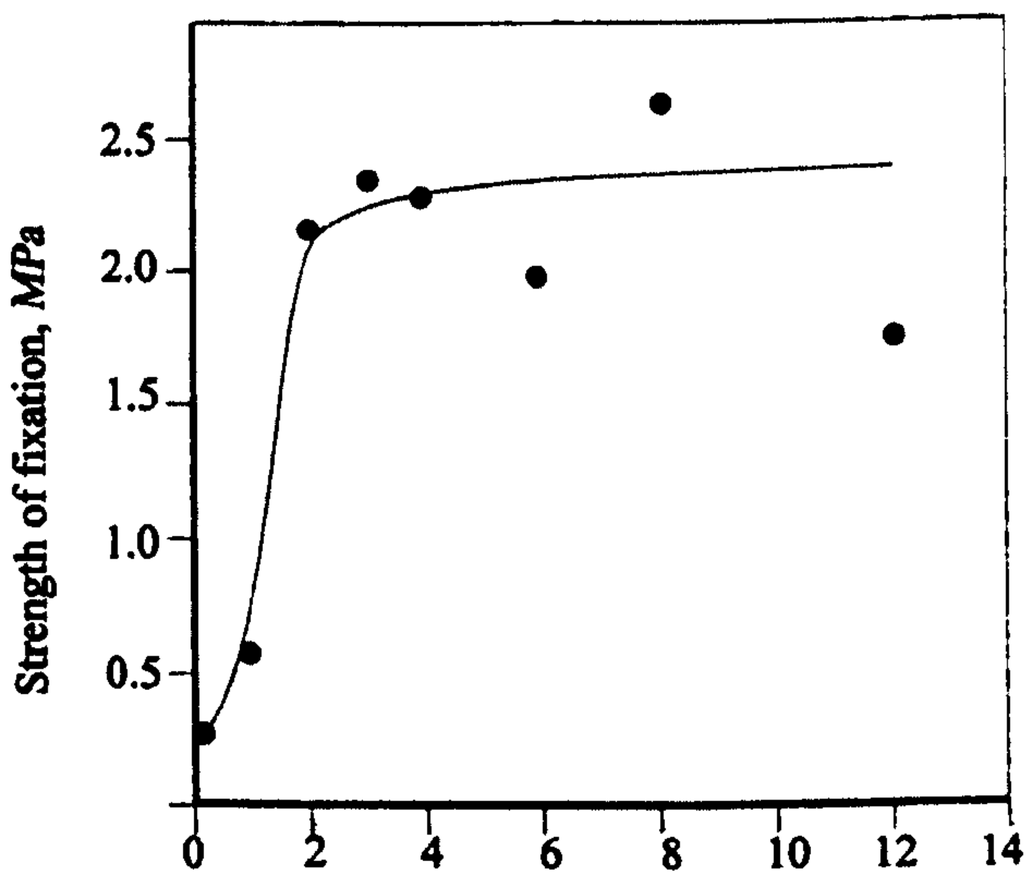

Fig. 9 Strength of non-cemented press-fit fixation over time
Adapted from Sumner and Galante (1992)

Typical of non-cemented THR is the failed-bonding scenario, which implies that in-growth or osseous integration does not occur due to gaps and relative motions at the implant-bone interface (Huiskes 1993). The use of coatings such as hydroxyapatite (HA) has been shown to encourage bone apposition (Bauer, Stulberg et al. 1993; Epinette 2001b), but no uncemented prosthesis approaches the initial stability of cups secured with PMMA (Litsky and Pophal 1994).

1.4.2.4 Ultra-High Molecular Weight Polyethylene (UHMWPE)

Ultra-high molecular weight polyethylene (UHMWPE) is the most common bearing material used in acetabular cup prosthesis (Walter 1992). The UHMWPE bearing is normally metal backed and is used in conjunction with femoral heads made from a variety of materials including metal and ceramic (Fig. 10).

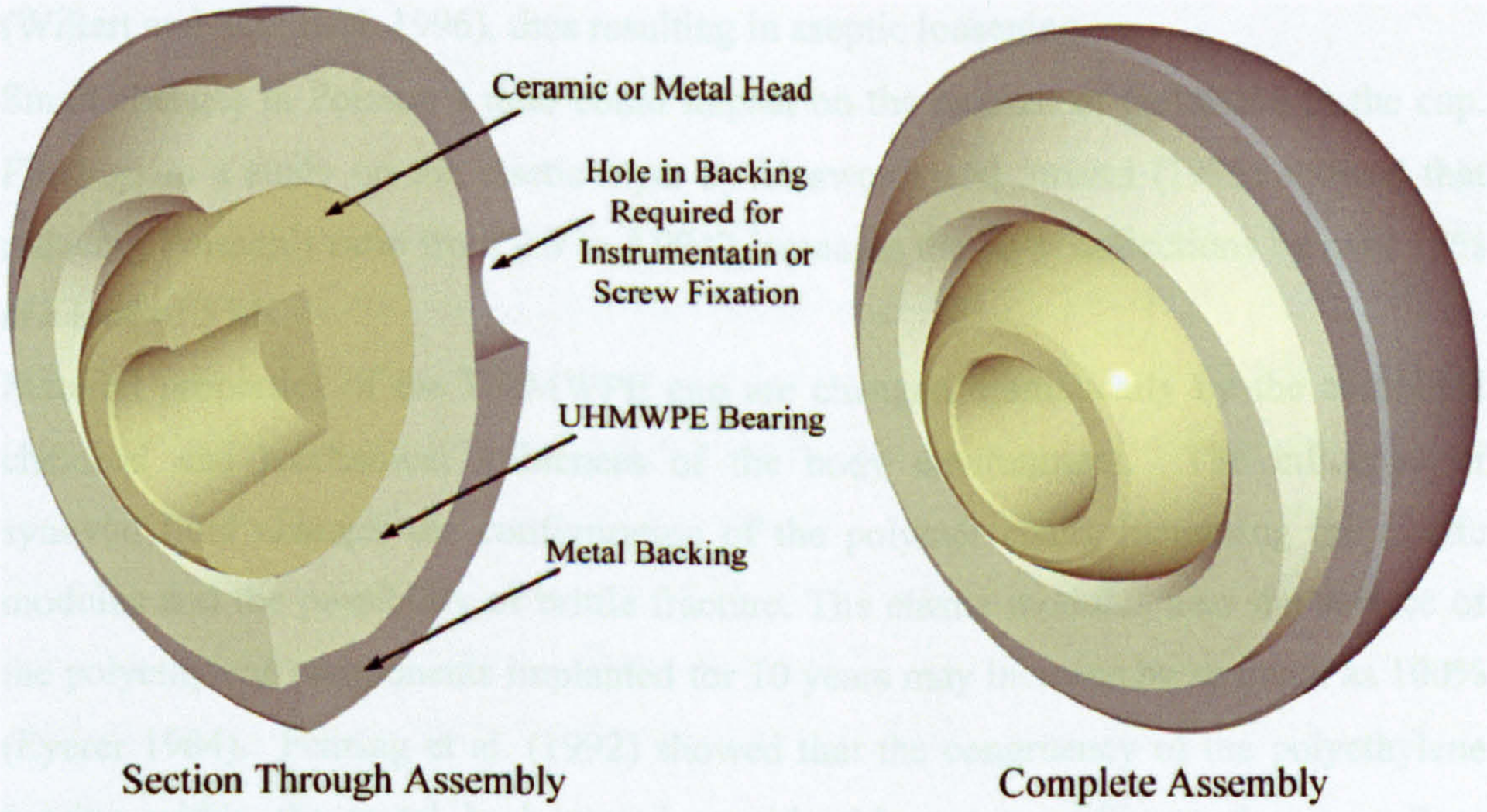

Fig. 10 Metal backed UHMWPE acetabular cup and head

The UHMWPE bearing can be penetrated at a rate as high as 0.5 mm/year by a femoral head within the first postoperative years. Wear rates diminish to 0.2 mm/year after 5 years with a metal femoral head. With the use of a ceramic femoral head, the penetration can be reduced to 0.1 mm/year (Zichner and Lindenfeld 1997). Engh and Culpepper (1997) highlighted the problem of polyethylene bearing wear and reported the radiographic appearance of progressive wear which, in their opinion was severe enough to cause the femoral head to completely penetrate the polyethylene bearing.

Their findings differ from the widely accepted view that aseptic prosthesis loosening is a major cause of THR failure (Pedersen, Crowninshield et al. 1982; Rapperport, Carter et al. 1987; Massin, Shmidt et al. 1989; Morscher 1992; Wilkinson, Peel et al. 2001; Ornstein 2002). Engh and Culpepper (1997) claim that polyethylene wear is their most frequent reason for reoperation. However this could be due to the young age of their patients (46.8 year mean age).

The biological response to wear debris of UHMPE has profound effects on local tissue and on fixation of the implant (Livermore, Ilstrup et al. 1990; Callaway, Flynn et al. 1995; Shaver, Brown et al. 1997). Wear particles create fibrous tissue which may spread unlimitedly in the joint capsule. The unlimited spread of this fibrous tissue can cause extensive resorption of the surrounding bone. The loss of bone surrounding the prosthesis also means the loss of bony anchors required for the fixation of the implant (Willert and Semlitsch 1996), thus resulting in aseptic loosening.

Small changes in Poisson's ratio could impact on the amount of deflection in the cup. Findings in a study on the elastic layer by Unsworth and Strozzi (1995) showed that reducing Poisson's ratio from 0.5 to 4.9942 increases the layer deflections by over 12% at a load of 5 kN.

Material properties of the UHMWPE cup are changed dramatically by the combined chemical and mechanical influences of the body environment. The influence of synovial fluid changes the configuration of the polymer chain, increasing the elastic modulus and the possibility of brittle fracture. The elastic modulus near the surface of the polyethylene components implanted for 10 years may increase by as much as 100% (Eyerer 1984). Fehring et al. (1992) showed that the congruency of the polyethylene bearing within the metal back varied considerably among different designs. Poor congruency results in unsupported polyethylene that may cause cold flow and higher stresses on loading that could increase wear (Kurtz, Gabriel et al. 1993). Bobyn, Tanzer et al.'s. (1994) study of metal backed UHMWPE cups supports Fehring et al.'s. (1992) earlier findings and reported the UHMWPE surface area that was actually supported by metal varied from 25% to 75% (percent contact) depending on cup design. It may be possible for any wear debris created by micromotion between the bearing and backing to travel easily to the bone and prosthesis interface by the instrumentation and fixation holes that are necessary in the metal backing (Fig. 10). One of the major drawbacks with this design is that the ceramic or metal heads have a far greater elastic modulus

than the UHMWPE. Consequently, the ceramic component acts as a rigid indenter to deform the liner, further increasing the possibility of micromotion and therefore wear debris. The continued development of UHMWPE has reduced wear rates by 90% by elevated levels of crosslinking of the polyethylene but only under ideal conditions. Various levels of crosslinking are achieved depending on the dose of irradiation. However in-vivo the problem of 3rd-body wear from particles such as bone cement still causes extremely high wear rates of the crosslinked UHMWPE (Wang, Chopra et al. 2002). The use of ceramic heads in conjunction with a UHMWPE cups can reduce wear rates by 50% compared to metal heads, but it seems logical to avoid bearing surfaces which generate debris which is potentially dangerous to the durability of the interface and stability of the prosthesis.

1.4.3 Composites and Ceramics as Biocompatible Materials

1.4.3.1 Ceramics

Ceramic on ceramic has been used in THR as bearing couple for over 30 years with varying degrees of success. They were first implanted in France by Pierre Boutin (1970) who used an alumina-on-alumina (Al_2O_3) wear couple with the initial aim of suppressing osteolysis related to polyethylene wear debris. An alumina-on-alumina bearing couple has many theoretical advantages. It not only eliminates polyethylene from the system but can also reduce wear by up to 3 orders of magnitude under 3rd body elevated wear conditions (Wang, Chopra et al. 2002). Under normal wear conditions an alumina-on-alumina couple exhibits extremely low linear wear when compared to other couples (Table 1).

Bearing couple	**Average linear wear rate**
Metal-on-UHMWPE	0.2mm per year
Alumina-on-UHMPE	0.1mm per year
Alumina-on-Alumina	0.001mm per year

Table 1 Linear wear rates for common bearing couples in THR
(Zichner and Lindenfeld 1997; Willmann 2000c)

Under severe 3rd body wear conditions such as particles of bone cement inclusion, no increase of wear was found in alumina-on-alumina couples (Wang, Chopra et al. 2002). This could be attributed to a specific tribological regime (fluid film) which is different to the one observed in metal-on-UHMWPE or ceramic-on-UHMWPE (Sedel, Bizot et al. 2000). Any wear debris created in an alumina couple is biocompatible and bioinert as it does not trigger a host immune reaction. Alumina ceramic being highly oxidised and thus inert, demonstrates a high biocompatibility in bulk or particulate forms (Christel 1992; Willmann 1998; Murray 1999; Sedel, Bizot et al. 2000).

Ceramic prostheses are still commonly associated with brittleness and fracture, and whilst this may have been true in the 1970's, modern ceramics have much improved toughness. However the early failures are still clouding objective judgements today. An extensive search of literature by Willmann and Heros (1998) included 35 studies and tried to quantify the incidence of ceramic failure. Willmann and Heros (1998) were pleased to report that the incidence of fracture in later-day ceramic components was quite low. Improvements since 1985 have led to an alumina material that has a much reduced grain size, lower porosity and fewer micro-cracks and inclusions, all of which have led to a greater increase in toughness and burst strength of the material. Medical-grade alumina is standardized today according to ISO 6474 and ASTM F 603 and is based on high purity alumina (BSI 1994). Thus the estimated fracture rate of about 1 in 300 cases in 1974, has decreased to less than 1 in 20,000 cases in contemporary designs (Epinette 2001a). Material fracture of the alumina components occurs less frequently than the fractures of polyethylene sockets and bone cement observed in conventional prosthesis. Mittelmeir and Heisel (1992) evaluated this in their revision cases and it is now generally believed that alumina prosthesis fracture is no longer an issue (Epinette 2001a; D'Antonio 2002).

With mechanical failures no longer an issue for ceramics, attention has returned to the major cause of ceramic cup failure: aseptic loosening (Nizard and Sedel 1992; Willmann 1998; Bizot, Banallec et al. 2000; Gardelin, Seminario et al. 2000; Gualtieri, Calderoni et al. 2000; Scheller, Claus et al. 2000; Bierbaum, Barsoum et al. 2001; Park, Han et al. 2001). Most of the long and middle term failures have been attributed to aseptic loosening (Bizot, Banallec et al. 2000) with the most probable reason being implant stiffness (Bizot, Banallec et al. 2000; Gardelin, Seminario et al. 2000; Gualtieri, Calderoni et al. 2000; Mendes, Said et al. 2000; Pitto, Schwämmlein et al. 2000;

Epinette 2001a; Park, Han et al. 2001). In-vitro analysis showed a 50 times higher stiffness of modular cups with ceramic than UHMWPE (Pitto, Schwämmlein et al. 2000). This higher stiffness could impair primary stability and cause stress-shielding and negative remodelling (Wolf's law) with the outcome of cup loosening, migration, or both.

Three general alumina cup designs have been used: monolithic cups, monoblock cups and metal cups with ceramic or polyethylene liners (Table 2).

Cup Design	**Important characteristic**	**Evaluation**
Monolithic	Made from alumina ceramics only - cementless fixation - cemented	Used in early 1970's. Osseointegration not satisfactory. High revision rates.
Monoblock	Metal thread on a ceramic liner, pre-assembled by the manufacturer.	Used in the late 1980's. Osseointegration not satisfactory. High revision rates.
Modular cups with ceramic liners (inserts)	Metal shell. The surgeon may insert either a ceramic or polyethylene liner.	Today's concept, introduced in the mid 1980's Used in more than 50 acetabular cups. Excellent wear rates. Success is limited by the stiffness of the prosthesis as a whole, possibly causing loosening.

Table 2 Ceramic cup designs used in THR

Adapted from Willmann (2000b)

Recent developments with modular cups have created a 'sandwich' concept. As with most modular cups there is a metal shell but a ceramic bearing is integrated into an UHMWPE inlay (Fig. 11).

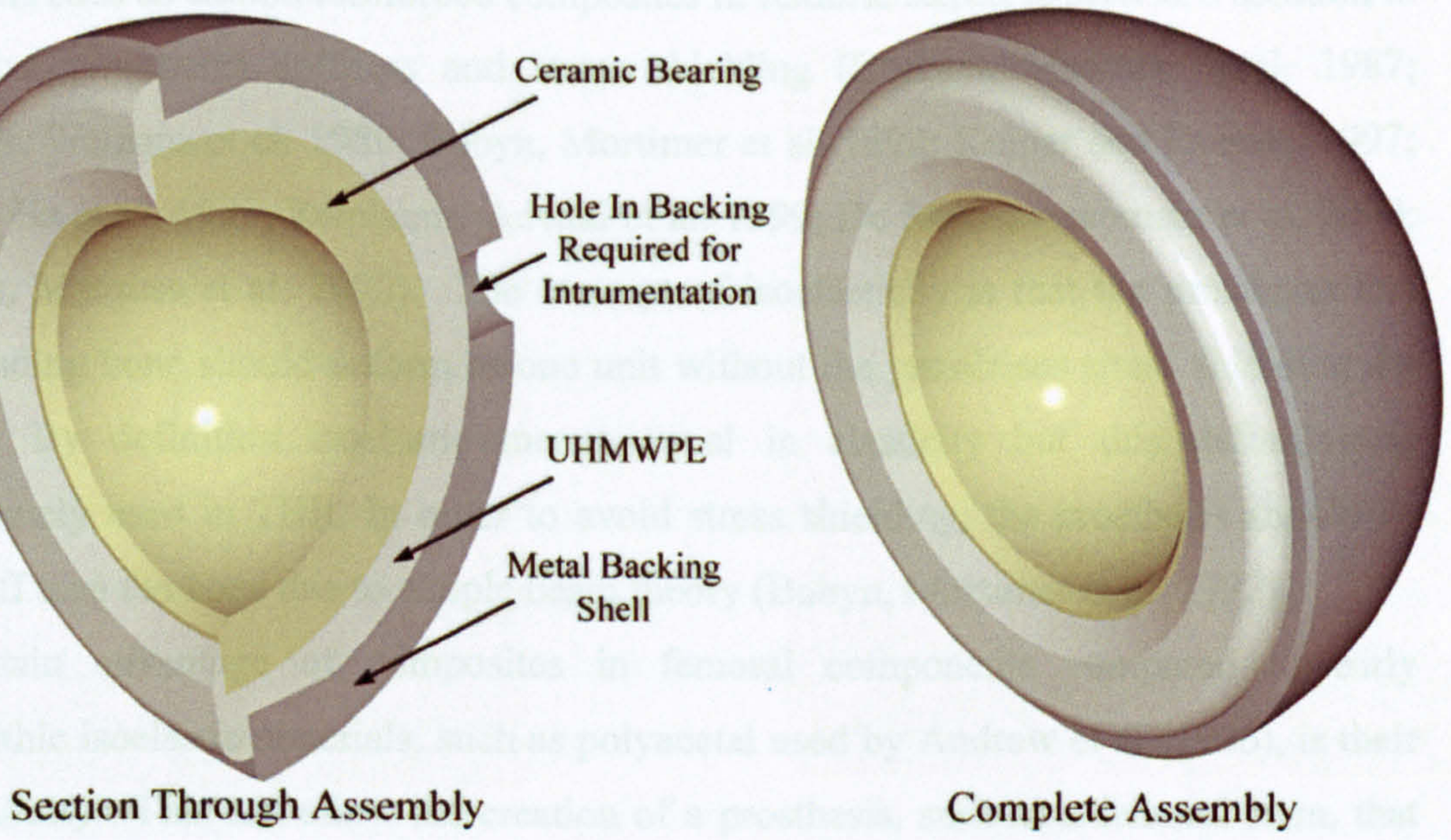

Fig. 11 Metal backed ceramic cup with UHMWPE inlay

The UHMWPE inlay reduces the stiffness of the joint couple significantly but returns the problems inherent with UHMWPE to the system. Whilst early clinical results (24-65 months) do not indicate any UHMWPE particle induced osteolysis, long-term follow up data is required (Park, Han et al. 2001).

Seen by many as a promising solution to young active patients, 150,000 alumina-on-alumina THR's have been undertaken; mainly in Europe. Current ceramic designs seem the most appropriate for young, active functional demanding patients, but the success is limited by the stiffness of the prosthesis as a whole, possibly causing loosening.

1.4.3.2 Composites

The main applications for composites in THR are ceramic-ceramic type, such as alumina-zirconia, which are being investigated for bearing couples, and carbon reinforced composites used in femoral stems. The next generation of composite ceramics will create tougher and better wearing characteristics than alumina (Willmann 2000a; Willmann 2000c). These characteristics allow the reduction in bearing size without compromising the prostheses strength and are necessary for the use of ceramics in smaller THR's, such as children and the Japanese market. The use of isoelastic

materials such as carbon reinforced composites in femoral stems, is seen as a solution to excessive prostheses stiffness and stress shielding (Christel, Meunier et al. 1987; Huiskes, Weinans et al. 1989; Bobyn, Mortimer et al. 1992; Kuiper and Huiskes 1997; Yildiz, Ha et al. 1998; Reinhardt, Advani et al. 1999; De Santis, Ambrosio et al. 2000; Simoes, Marques et al. 2000). The concept of isoelasticity is that the prosthesis and surrounding bone should deform as one unit without the prostheses stress shielding the bone. By definition isoelastic means equal in elasticity but this definition is inaccurately used in THR. In order to avoid stress shielding, the prosthesis should be less stiff than the bone due to simple beam theory (Bobyn, Mortimer et al. 1992).

The main advantage of composites in femoral components compared to early monolithic isoelastic materials, such as polyacetal used by Andrew et al (1986), is their 'tune-ability'. This can allow the creation of a prosthesis, such as a femoral stem, that has varying stiffness along its length to suit the local bone stresses (De Santis, Ambrosio et al. 2000). To alter prosthesis stiffness there are only two variables, the elastic modulus (E) and the second moment of area (I). Geometrical variations (I) are limited by the dimensions of the surrounding bone therefore mainly variations in elastic modulus (E) affect the stiffness (Taylor 1998). Whilst it is possible to alter the prosthesis stiffness locally it is very difficult to obtain a very highly differentiated elastic modulus within the structure and hence some composite femoral stems still require a metallic core (Simoes, Marques et al. 2000).

Many manufacturing processes exist for the manufacture of composites, but for use in THR, normally woven, braided or chopped fibres are incorporated within a matrix (Fig. 12).

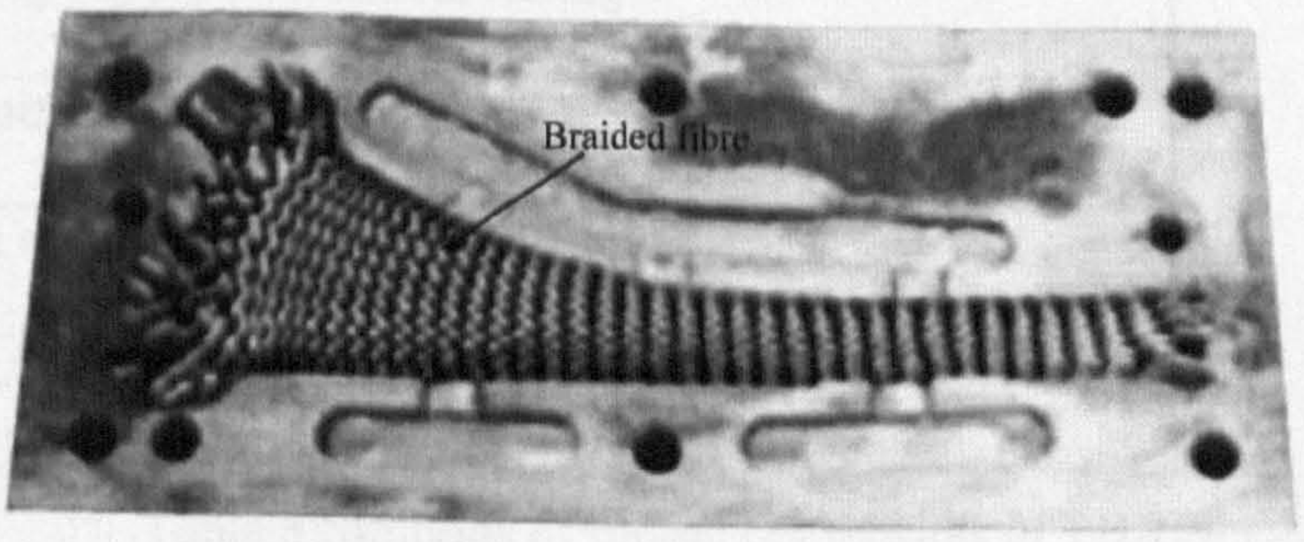

Fig. 12 Example of braided fibre pre-forms inside half of the mould

(de Oliveira Simoes and Marques 2001)

Matrix and fibre reinforcement options are extensive but for biomedical applications such as THR, biocompatibility with fatigue and sterilisation resistance are three major examples of design criteria that are paramount. Carbon fibres are the most used reinforcement for biomedical structural applications (de Oliveira Simoes and Marques 2001). An important reason for this is that the addition of carbon fibres to a matrix does not compromise the biocompatibility as a whole (Williams 2001).

Choice of matrix for the composite in THR applications is wide, but polymers being investigated mainly include polysulfone, polyethylene, polyethermide, liquid crystalline polymer and polyetheretherketone (Magee, Weinstein et al. 1988; Shirandami and Esat 1990; Akay and Aslan 1996; Kettunen, Makela et al. 2001).

The polyetheretherketone (PEEK) polymer and PEEK carbon fibre reinforced composite are rapidly replacing glass, stainless steel and other materials in the biomedical industries. PEEK's excellent resistance to the damaging effects of sterilisation processes, coupled with the tune-ability of its mechanical properties are highly desirable factors. For example PEEK reinforced with carbon fibres can be tailored to have an elastic modulus in the range of 1GPa to 170GPa (Chang, Perez et al. 1990).

The tuning of the flexural modulus can achieve both global and local stiffness variations in a PEEK carbon fibre composite (Table 3).

Tuning method	**Outcome**
Local change of ply direction	Local tuning
Complete Change of ply direction	Global tuning
Change of number of ply's	Local tuning
Change matrix and/or fibre material	Global tuning
Change matrix/fibre volume fraction	Global tuning

Table 3 Methods of tuning composites in THR

Whilst all the signs look promising for isoelastic prosthesis, clinically the outcome is not so clear-cut. It is generally agreed that reduced modulus prosthesis would avoid stress shielding (Bobyn, Mortimer et al. 1992; Glassman, Crowninshield et al. 2001).

To avoid the cancelling monolithic properties of bone cement, the obvious choice for primary fixation is a pressfit. With press fit fixation comes other problems, not least the additional interface stresses imposed (Huiskes, Weinans et al. 1989; Levenston, Beaupré et al. 1993; Kuiper and Huiskes 1997; Taylor 1998; Yildiz, Chang et al. 1998; Simoes, Marques et al. 2000). Adam et al.'s. (2002) recent clinical study of carbon fibre femoral components showed 92% aseptic loosening in 47 hips. This disastrous result is in complete opposition to the early clinical trial of Andrew et al.'s. (1986) isoelastic stem where 92% of patients were satisfied and their 3rd generation stem had zero instances of loosening (48 hips). Taylor's (1998) analytical study also predicted poor performance for pressfit stems and suggested that the use of a controlled stiffness implant offered no advantages over conventional designs. Taylor (1998) attributes the poor performance of pressfit stems to trabecular bone stresses above the 4MPa failure threshold but neglects to describe fully the bone regions of his model. Andrew et al.'s. (1986) early success could be due to their realisation of the importance of immediate mechanical stability by removing all trabecular bone. In conclusion, Adam et al. (2002) reported that they were not achieving the primary stability required and attributed the failure to a badly designed stem shape and poor surface properties coupled with limited prosthesis sizes.

Whilst a limited number of composite THRs are now in clinical trials, the majority of these components are femoral with traditional metal backed acetabular cups. The advantages of a reduced modulus acetabular component have been widely overlooked with only one trial incorporating a monolithic reduced modulus acetabular cup (Andrew, Flanagan et al. 1986). Difficulties in manufacture, particularly incorporating a bearing surface to the cup, are likely reasons for limited reported research into this area.

1.4.4 Mechanical Testing Standards Used In Total Hip Replacement

An anomaly within the highly regulated field of hip prosthesis design is the absence of mechanical testing standards for acetabular cups. The majority of previous mechanical test standards in this area have addressed the femoral stem, ceramic heads or wear of the articulating surfaces with only passing reference to the acetabular cup. There are many standards both in the UK (BSI), and internationally (ISO) for femoral components and

indeed the harmonised BSI/ISO standard ISO 7206 comprises 10 parts (BSI 1998-2002). Whilst parts of ISO 7206 have been withdrawn and replaced, for example by ISO 14242, other regulatory bodies such as the U.S. Food and Drug Agency (FDA) still refer to the withdrawn parts of the ISO 7206 standard (BSI 1992; FDA 1995b; BSI 2002).

Raimondi and Pietrabissa (1999) examined the different testing conditions possible within the ISO 7206 standard and reported that ISO 7206 will give experimental data of reasonable accuracy. They did however highlight the standard's inadequacies e.g. the standard did not specify the minimum thickness of the embedding medium. Whilst Raimondi and Pietrabissa (1999) found ISO 7206 to give reasonable fatigue results for similar stems, Cristofolini and Viceconti (1999) propose a testing protocol for *femoral stems* that enables differences between implants to be detected. The strength of Cristofolini and Viceconti's (1999) test is the underlying minimum requirements that the protocol achieved:

1. It should replicate in vitro the relevant physiological situation and actions.
2. It should be repeatable and reproducible.
3. It should be designed so as to enable differences between implants to be detected.

Testing and material standards for alumina femoral heads are also in existence (BSI 1992; BSI 1994; FDA 1995b) and manufacturers adapt these standards for acetabular prosthesis containing alumina bearing surfaces. The major limitation of the heads UCS test (ISO 7206-5) is that it is an axial test. Whilst being the most mechanically demanding orientation for femoral heads containing a taper, the axial test is not necessarily suitable for use with acetabular components (Fig. 13).

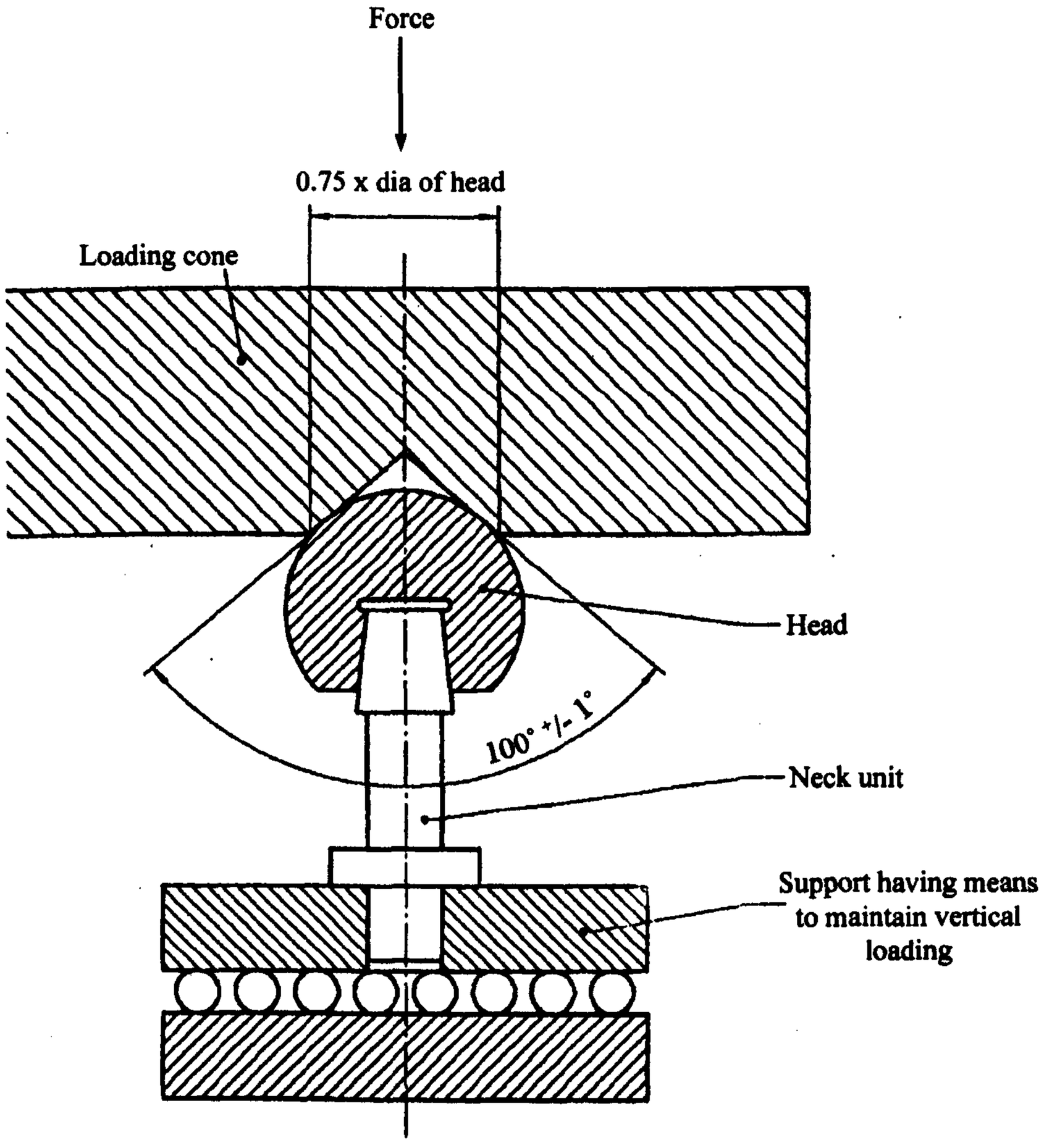

Fig. 13 Axial testing of head and neck region of stemmed femoral component

Adapted from ISO 7206-5

Of particular importance in the testing of acetabular cups incorporating alumina ceramics, which are inherently brittle, are variations in test rig stiffness, which could greatly influence test results.

The reported research into acetabular cup testing is extremely limited with only guidelines from the FDA being specific to the acetabular prosthesis (FDA 1995a). The ad hoc bastardisation of the femoral standards for use with acetabular cups leaves specific requirements open to interpretation. A specific example of this is the orientation of the acetabular cup, which was not anatomically described by any femoral standard until a wear-test standard in 2002 (BSI 2002). Cristofolini and Viceconti (1999)

encountered similar 'interpretation' problems when researching load transfer across the hip and concluded that data could not easily be compared between authors.

Further research into the creation of acetabular prosthesis testing protocols is required, paying particular attention to the use of ceramic on ceramic bearing surfaces and the three underlying requirements discussed by Cristofolini and Viceconti (1999).

1.4.5 Fatigue Failure of Alumina Ceramic

Fatigue failure is generally thought of as a phenomenon by which a material can fail at a stress lower than static strength if the load is applied repeatedly (Norman, Cubitt et al. 1995). Whilst this definition accurately describes the work carried out in this thesis and the term 'fatigue' will be used exclusively to describe this 'cyclic mechanical fatigue', it should be noted that ceramics have several processes of fatigue failure, and that cyclic mechanical fatigue is only one specific field. Other specific fatigue fields within ceramics include:

- Thermal Fatigue – Where the induced stresses and strains find their origins in thermal contraction or expansion.
- Static Fatigue – Also known as 'stress corrosion', it is the behaviour of a material under constant load.
- Dynamic Fatigue – Tests where load or strain is increased at a constant rate (Roebben, Steen et al. 1996).

Due to the microstructure of ceramics they were traditionally considered to be immune to fatigue damage under cyclic loading and any crack advance was attributed to environmentally assisted growth (static fatigue) integrated over the loading cycle (Gilbert, Petrany et al. 1995; Chevalier, Olagnon et al. 1999). Ceramics are known to be sensitive to defects where cracks can initiate. Unlike ductile materials, fatigue cracks in ceramics do not appear to initiate naturally. Rather, crack initiation is invariably associated with some pre-existing defect (Zheng, Yan et al. 1999; Ritchie, Gilbert et al. 2000).

The first evidence of cyclic fatigue effects in ceramics were reported by Dauskardt et al. (1987). It is now widely believed that the major mechanism of fatigue in ceramics is

degradation of crack-tip shielding bridging grains (Vekinis, Ashby et al. 1990; Guiu, Li et al. 1991; Hu and Mai 1992; Dauskardt 1993b; Dauskardt 1993a; Kishimoto, Ueno et al. 1994; Gilbert and Ritchie 1997; Chevalier, Olagnon et al. 1999; Ritchie, Gilbert et al. 2000) (Fig. 14). These bridging grains contribute to ceramics' so-called resistance curve or R-curve, which increase the fracture toughness as a crack penetrates the material under monotonic load (Roebben, Steen et al. 1996).

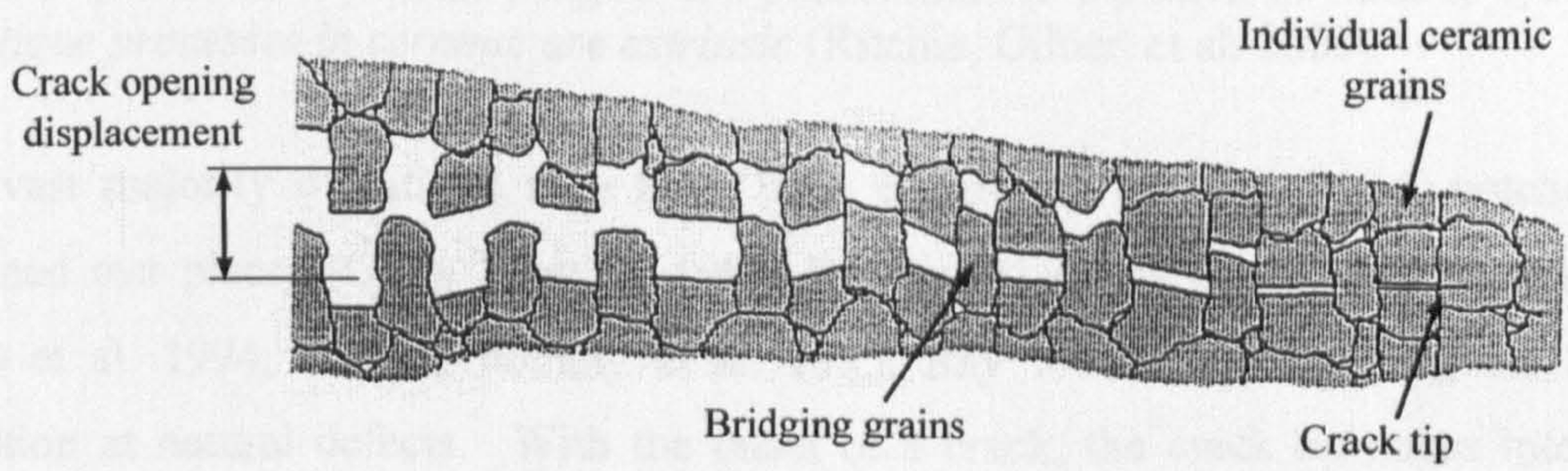

Fig. 14 Grain bridges in the wake of a growing crack

Adapted from Vekinis et al (1990)

The *R*-curve increase in fracture toughness is created by stresses between the bridging grain and matrix, shielding the crack tip. Grain bridging of alumina ceramic can be extensive, as reported by Dauskardt (1993b), with bridging zones extended 10mm and more behind the crack tip.

For fatigue-crack propagation of a single crack, there are two possible classes of fatigue mechanism:

> *Intrinsic mechanisms where, as in metals, crack advance results from damage process in the crack-tip region, which are unique to cyclic loading and extrinsic, where the crack-advance mechanism ahead of the crack tip is identical to that for monotonic loading, but the unloading cycle promotes accelerated crack growth by degrading crack tip shielding e.g. grain bridging, behind the tip. Where as the cyclic processes in metal fatigue are predominately intrinsic in nature, cyclic fatigue processes in ceramic are extrinsic* (Ritchie, Gilbert et al. 2000).

The vast majority of fatigue tests have been undertaken on precracked, notched or indented test pieces (Guiu, Li et al. 1991; Dauskardt, James et al. 1992; Kishimoto, Ueno et al. 1994; Gilbert, Petrany et al. 1995; Ray 1998), thus omitting the crack initiation at natural defects. With the onset of a crack, the crack tip stress intensity factor is defined as:

$$K = Y\sigma\sqrt{a},$$

where Y is the crack shape parameter, σ is the applied stress and a is the crack length. When a brittle material is loaded, cracks grow either catastrophically, subcritically, or not at all. If the threshold for subcritical crack growth, K_{th}, is not exceeded by K then the crack will not grow. If the initial crack length a_0 is sufficiently large or the stress sufficiently high to cause K to be higher than K_{th} the crack grows slowly prior to catastrophic failure, often according to the empirical slow crack growth (SCG) power law:

$$\frac{da}{dt} = AK^n,$$

where A and n are constants. The crack grows to a critical length a_c when the stress intensity factor at the tip reaches the fracture toughness value, K_c, of the material upon which catastrophic crack growth occurs. The development of high toughness materials has revealed that K_c is not a material parameter and the so-called R-curve effect reflects an increase of the fracture toughness as the crack penetrates the material. The rate the fracture toughness increases depends on the microstructure of the ceramic, on specimen geometry, on initial crack length and on the loading system. The degradation of the R-

curve effect due to cyclic loading is the major factor in causing the material to fail at lower stress levels (fatigue). Several authors have proposed specific mechanisms to qualitatively explain the enhanced *R*-curve toughness. The mechanism of all of these proposed toughening mechanisms can be characterised by a stress intensity factor K_i The sum of the K_i values equals K_s which has to be subtracted from the applied K to obtain the effective stress intensity factor experienced by the crack tip, K_{tip} under cyclic loading:

$$K_{tip} = K - K_s$$

Crack tip shielding explains both SCG rate and an enhanced toughness since it is K_{tip} that has to equal K_{th} or K_c before subcritical or catastrophic crack growth occurs (Roebben, Steen et al. 1996).

Chevalier et al. (1999), suggests that a single curve would be obtained for both static and cyclic loading when plotting the crack velocity versus the local crack tip stress intensity factor. This means that the same propagation mechanism, stress corrosion, occurs at the crack tip, and the difference between static and cyclic fatigue only lies on the toughening degradation. However, new bridges must be established with every fatigue crack growth increment and the total crack shielding effect is restored for mechanical equilibrium. In practice, fatigue crack growth and frictional degradation of bridges occur concurrently during cyclic fatigue (Hu and Mai 1992).

First generation biological grade alumina ceramics from the 1970's used in THR had a high incidence of fracture (3%-5%), the large grain size of the material was a strong contributing factor to failure. Continued gains in density, grain size refinement and mechanical properties, has led to nearly a 45% improvement in mechanical strength (Willmann and Heros 1998). The compressive strength depends strongly on the grain size. The strength decreases from 5000 N mm^{-2} to about 2000 N mm^{-2} when the grain size increases from 2μm to 30μm (Dörre and Dawihl 1980).

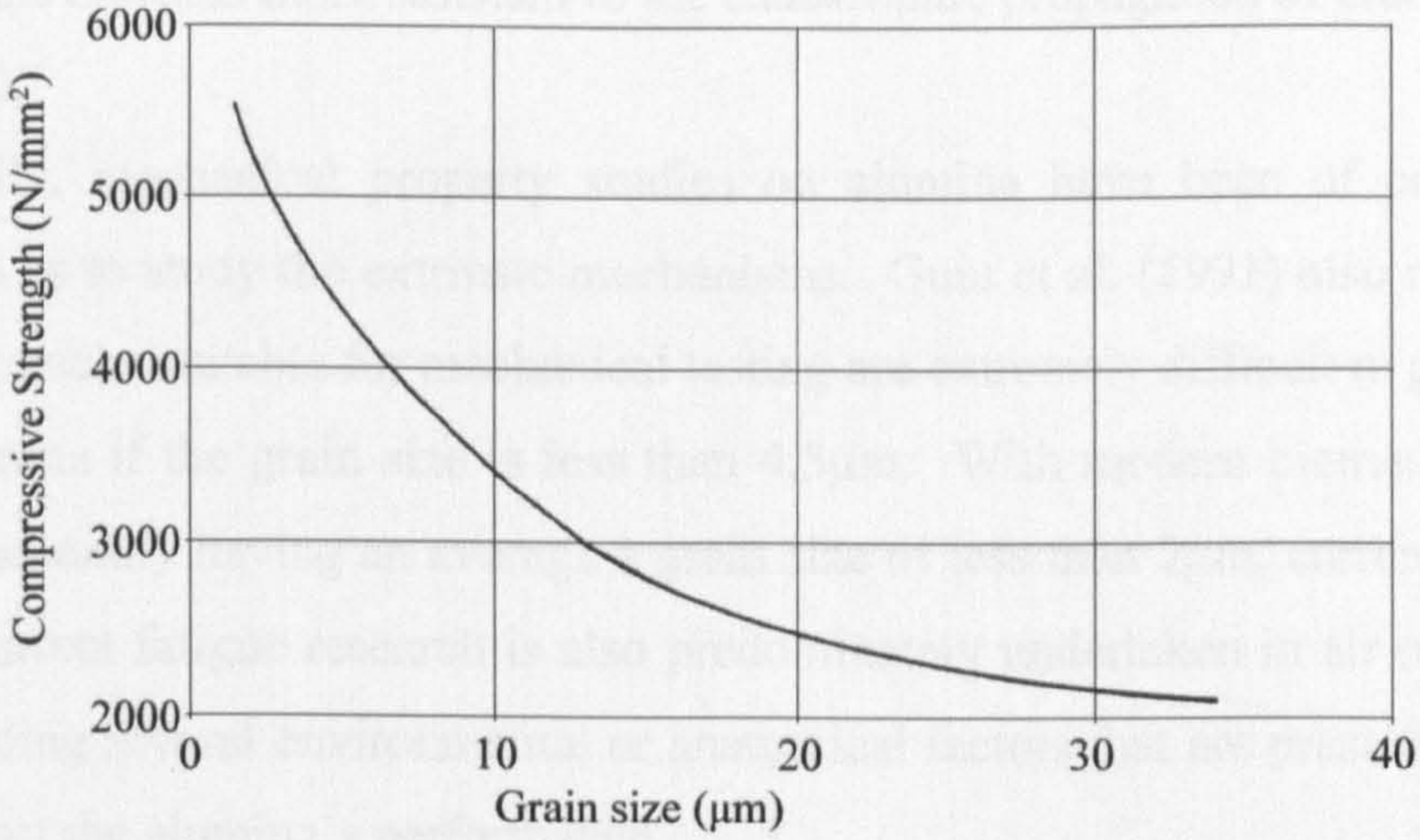

Fig. 15 Compressive strength of high density alumina ceramics versus medium grain size

Adapted from Dörre and Dawihl (1980)

The majority of alumina ceramics now used in THR have a grain size of less than 2μm, and this gives the strength required to meet the ISO specification (Fig. 16). The reduction of grain size does however mean the lessening of the beneficial R-curve behaviour and bridging effect that are more pronounced in course-grained material.

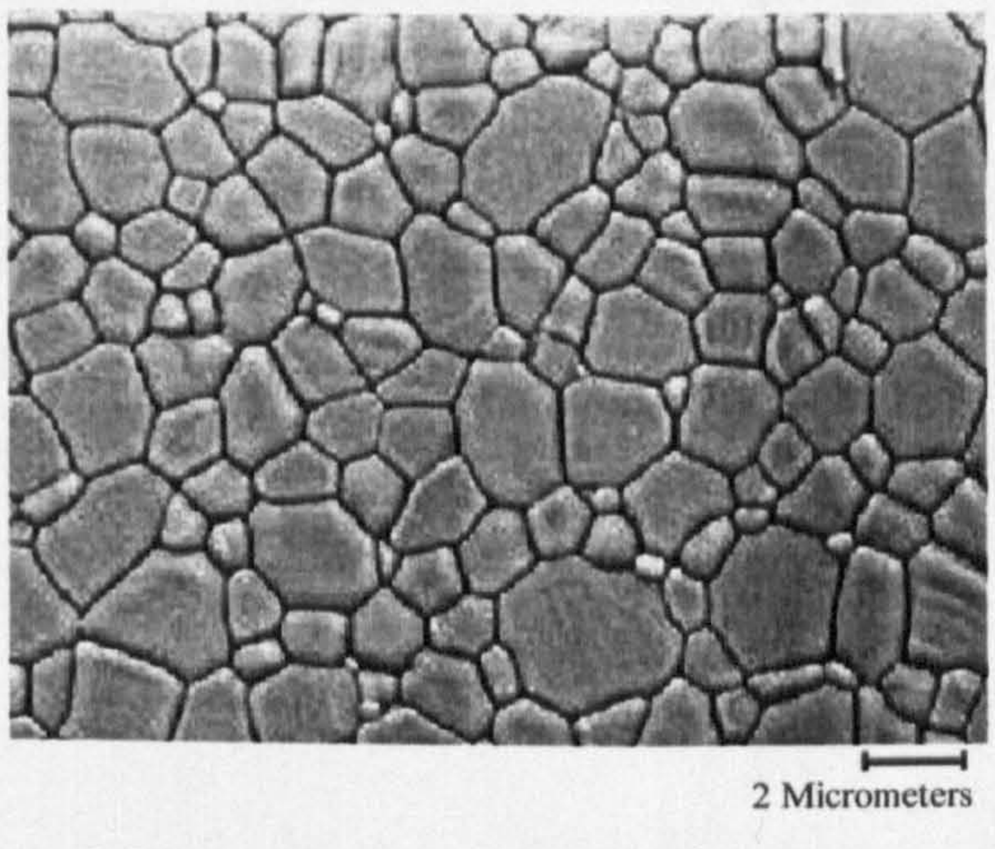

Fig. 16 A micrograph highlighting the fine grain structure of modern alumina (Vitox Alumina with average grain size of 1.2 μm. Magnification x4380)

Adapted from Morgan Matroc Ltd. (2000)

The crack propagation threshold is much higher in coarse grained alumina (Kishimoto, Ueno et al. 1994), with larger grains providing stronger, more effective crack bridging,

rendering the material more resistant to the catastrophic propagation of cracks (Guiu, Li et al. 1991).

Traditionally, mechanical property studies on alumina have been of coarse-grained alumina so as to study the extrinsic mechanisms. Guiu et al. (1991) also noted the fact that stable cracks suitable for mechanical testing are extremely difficult to grow in high-purity alumina if the grain size is less than 4.5μm. With modern biomedical alumina ceramics generally having an average a grain size of less than 2μm, current literature is scarce. Current fatigue research is also predominately undertaken in air or other gases thus excluding several environmental or anatomical factors that are present in THR that could impact the alumina's performance.

Krainess and Knapp (1978) investigated the influence of aging alumina in Ringer's solution, which is commonly used for the in vitro simulation of bodily fluids in THR. They reported Ringer's solution could reduce mechanical strength. Moist environments are also known to accelerate cyclic crack growth rates in most ceramics (Ritchie, Dauskardt et al. 1990) by contributing to the process of stress corrosion (or static fatigue) (Dauskardt 1993b). The use of ceramics in a liquid environment can also affect crack growth by hydrodynamic pressure trapped in the wake of the fatigue crack. Under some conditions, the crack faces in the near tip region may move in opposite directions to the rest of the crack (i.e. closing while the rest of the crack faces are opening) (Yi, Dill et al. 1997; Yi, Cox et al. 1999).

Research into fatigue failure of fine-grained alumina is lacking with no known publications regarding the fatigue of a complete anatomically orientated alumina acetabular cup prosthesis in Ringer's solution which is proposed by the author.

1.5 Summary

It is now accepted that THR is an extremely effective procedure, improving the quality of life for millions of patients worldwide. Ironically however it has become the victim of its own success. Originally intended for older patients, THR is now being used increasingly on younger, much more active patients who require prostheses that can last longer and endure a much more active lifestyle without the need for revision. Design goals have advanced from simply alleviating pain and discomfort for elderly patients, to returning young active patients to more physically demanding life styles, including sports activities. As a result, the primary cause of THR failure in younger patients is aseptic loosening; more specifically, the loosening is twice as likely to be in the acetabular cup than the femoral stem (Wroblewski, Siney et al. 2002). The cause of aseptic loosening is still fiercely debated, but the final explanation might be sought in a combination of multiple etiologic factors including, prosthesis stiffness, particulate reaction and stress shielding. Traditional titanium alloy prosthesis and UHMWPE bearing surfaces all suffer from these damaging factors. Efforts must be concentrated on developing an acetabular cup that minimises or eradicates these factors whilst improving performance and increasing prosthesis life. Proposed in this study is an acetabular cup that consists of an alumina ceramic bearing incorporated into a reduced stiffness carbon reinforced composite backing (Fig. 17).

Alumina ceramic has been used as a bearing couple since the 1970's and its mechanical properties have been greatly improved over this time. Much work has been undertaken demonstrating alumina's superior wear resistance and biocompatibility compared to other materials used in THR, such as UHMWPE. Currently, there is little understanding of fatigue failure of alumina when used in hip prostheses and indeed until recently ceramics were not thought to suffer from fatigue failure. This is reflected in both US and European testing standards with the total absence of any standards regarding acetabular prosthesis testing. Extensive effort must be concentrated on developing suitable testing methods that can create anatomically orientated fatigue failures for future research.

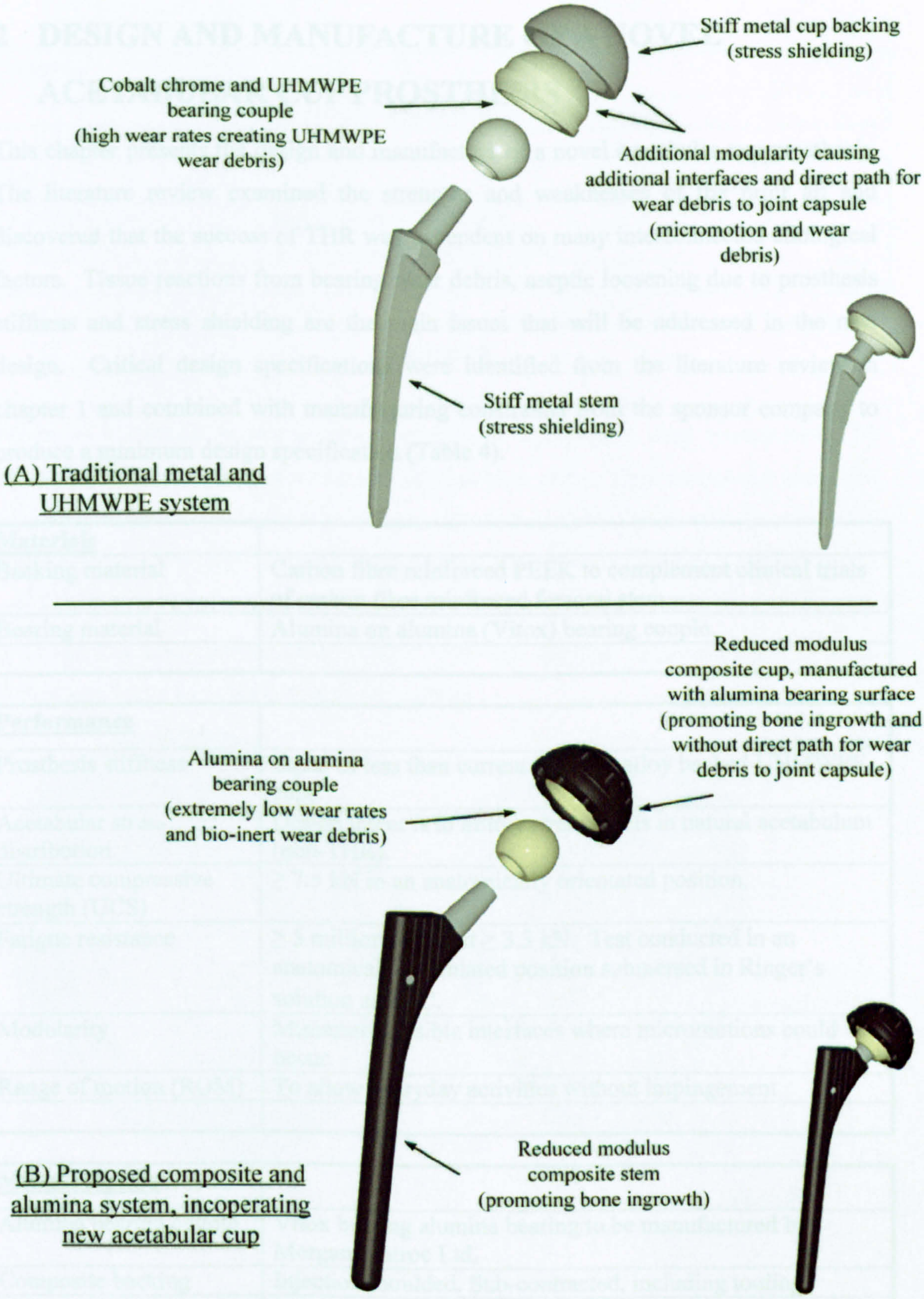

Fig. 17 Comparison of traditional THR prostheses (A), with proposed composite prostheses (B)

2 DESIGN AND MANUFACTURE OF A NOVEL ACETABULAR CUP PROSTHESIS

This chapter presents the design and manufacture of a novel acetabular cup prosthesis. The literature review examined the strengths and weaknesses of the prior art and discovered that the success of THR was dependent on many interconnected etiological factors. Tissue reactions from bearing wear debris, aseptic loosening due to prosthesis stiffness and stress shielding are the main issues that will be addressed in the new design. Critical design specifications were identified from the literature review in chapter 1 and combined with manufacturing constraints from the sponsor company to produce a minimum design specification (Table 4).

Materials	
Backing material	Carbon fibre reinforced PEEK to complement clinical trials of carbon fibre reinforced femoral stem.
Bearing material	Alumina on alumina (Vitox) bearing couple.

Performance	
Prosthesis stiffness	Equal or less than current titanium alloy backed UHMWPE cups.
Acetabular stress distribution	Design intent is to mimic stress levels in natural acetabulum (non-THR)
Ultimate compressive strength (UCS)	$\geq$ 7.5 kN in an anatomically orientated position.
Fatigue resistance	$\geq$ 5 million cycles at $\geq$ 3.3 kN. Test conducted in an anatomically orientated position submersed in Ringer's solution at 37°C.
Modularity	Minimum possible interfaces where micromotions could occur.
Range of motion (ROM)	To allow everyday activities without impingement

Manufacturing	
Alumina bearing couple	Vitox bearing alumina bearing to be manufactured by Morgan Matroc Ltd.
Composite backing	Injection moulded. Sub-contracted, including tooling.
Sizing and finishing	In house.

Quantity	
	50-100 per manufacturing run.

Size	
Prosthesis size	46mm-64mm diameters.
Bearing size	To suit 28mm diameter head

Table 4 Critical design specifications identified from literature review and company constraints

All novel acetabular prosthesis manufactured for this project were manufactured by injection moulding and consist of a reduced modulus carbon fibre reinforced composite backing (PEEK 450CA30) and an alumina on alumina hot isostatically pressed (HIP) bearing couple (Vitox®). Bespoke Vitox® cups were manufactured by Morgan Matroc and incorporated into the PEEK injection moulding trials (Fig. 18). At this time no literature has been located describing any similar process incorporating a ceramic component into a composite injection moulding.

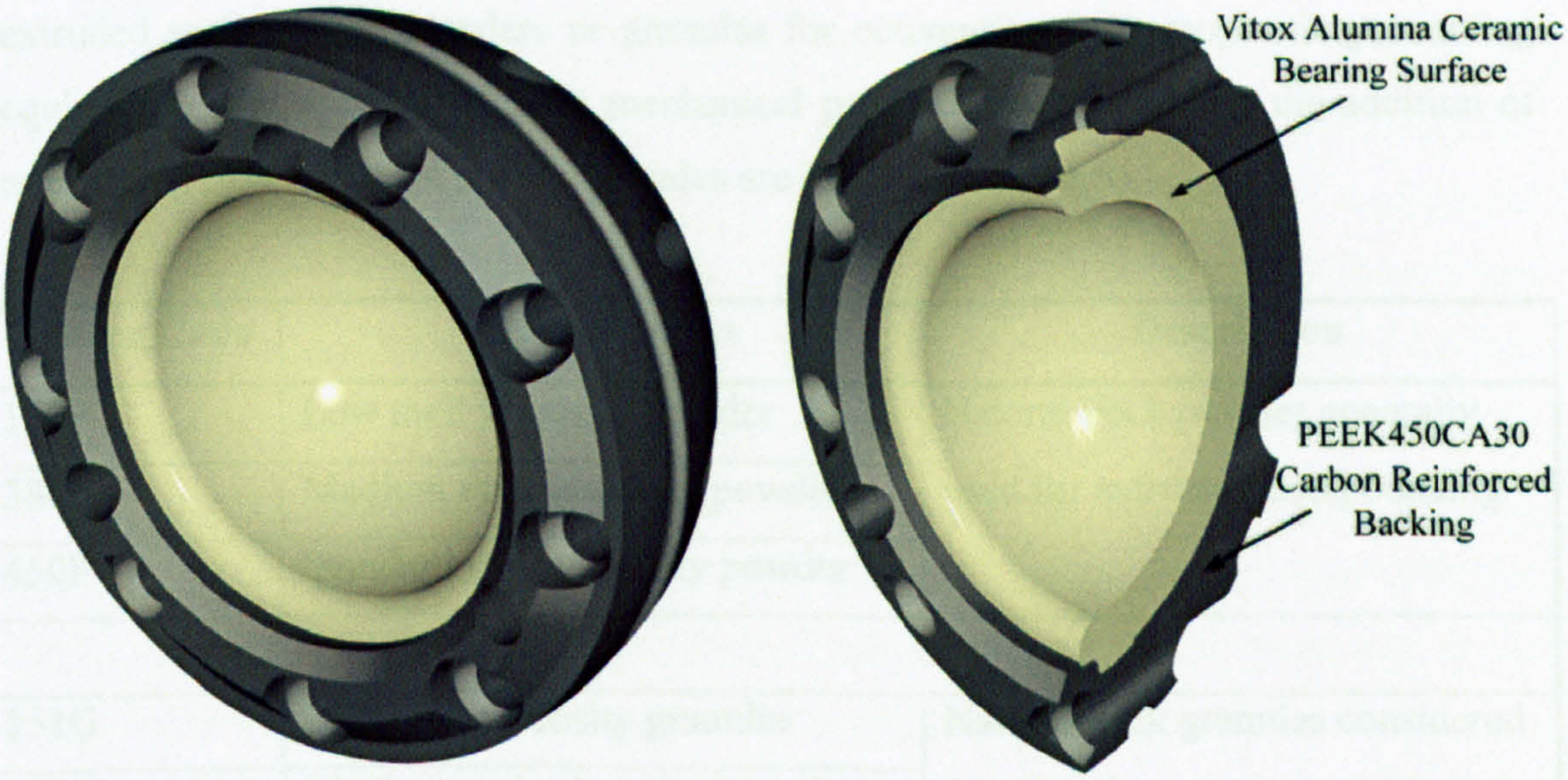

Fig. 18 Novel composite / ceramic acetabular hip prosthesis (50mm)

2.1 Material Properties

The urgent need to produce reduced stiffness acetabular prostheses was described in the Literature Review in Chapter 1. The proposed combination of Vitox alumina ceramic bearing couple and carbon fibre reinforced PEEK materials will combine the excellent tribological properties of the Vitox ceramic with the reduced modulus (compared to metal prostheses) of the carbon fibre reinforced PEEK. The well-proven Vitox ceramic bearing couple gives exceptional wear performance with very little bioinert wear debris, whilst the reduced modulus of carbon fibre reinforced PEEK will minimise stress shielding and promote bone ingrowth. Justification of the material selection can be found in Section 5.1 page 70.

2.1.1 Properties of PEEK and Carbon Fibre Reinforced PEEK

Polyetheretherketone solely manufactured by Victrex® and sold under the trade name PEEK is widely regarded as the highest performance thermoplastic material currently available. PEEK is supplied in many stock forms and mechanical properties including extruded sections and powders or granules for conventional thermoplastic processing equipment. Tailoring of PEEK's mechanical properties is possible by the addition of reinforcing fibres; several standard grades are available (Table 5).

Victrex Code	Characteristics	Description
150P	Low melt viscosity powder	Natural Peek powder generally used for extrusion compounding
380P	Medium melt viscosity powder	
450P	Standard melt viscosity powder	
151G	Low melt viscosity granules	Natural Peek granules considered as general purpose extrusion and injection moulding grades
381G	Medium melt viscosity granules	
450G	Standard melt viscosity granules	
150GL30	Low melt viscosity granules	30% glass fibre reinforced PEEK granules
450GL30	Standard melt viscosity granules	

150CA30	Low melt viscosity granules	30% carbon fibre reinforced PEEK granules
450CA30	Standard melt viscosity granules	
150FC30	Low melt viscosity granules	Special tribological grade PEEK, 10% graphite, 10% PTFE, 10% carbon fibre
450FC30	Standard melt viscosity granules	

Table 5 Standard Grades of PEEK™

Well-publicised product liability cases in the Unites States of America resulted in raw material manufactures, such as DuPont and Dow Chemical, being unwilling to supply materials to the medical device sector (Williams 2001). Although legislation in the United States now gives raw material suppliers some protection and supplies are returning, Victrex® will not supply PEEK for implantable devices such as hip prosthesis. Whilst Victrex's® unwillingness to expose itself to litigation is understandable, there are numerous studies and clinical trials that show the biocompatibility of PEEK and carbon fibre reinforced PEEK™ (Scotchford 2001; Williams 2001). The supply of PEEK is now becoming less problematical as Victrex® now manufacture an unfilled PEEK, namely PEEK OPTIMA LT that is available for implantable devices. Not surprisingly this material has exactly the same mechanical properties as the original unfilled PEEK. Recent correspondence with Victrex® has also shown that reinforced grades will also be available for use in implantable devices (Cartwright 2003). The PEEK family of materials offers many desirable qualities for use in hip prosthesis: biocompatibility, radiotranslucency, sterilizability, long-term stability, fatigue performance and bone-like stiffness (Invibio Biomaterial Solutions 2003). The ability to adjust PEEK's elastic modulus to that close to bone, allows the design of a reduced stiffness implant whilst maintaining a strength exceeding the original bone (Fig. 19). Traditional metallic prosthesis have stiffnesses orders of magnitude higher than the surrounding bone, therefore they are not able to transfer loads sympathetically and thus cause stress shielding (1.4.1 Background and Related Biomechanics).

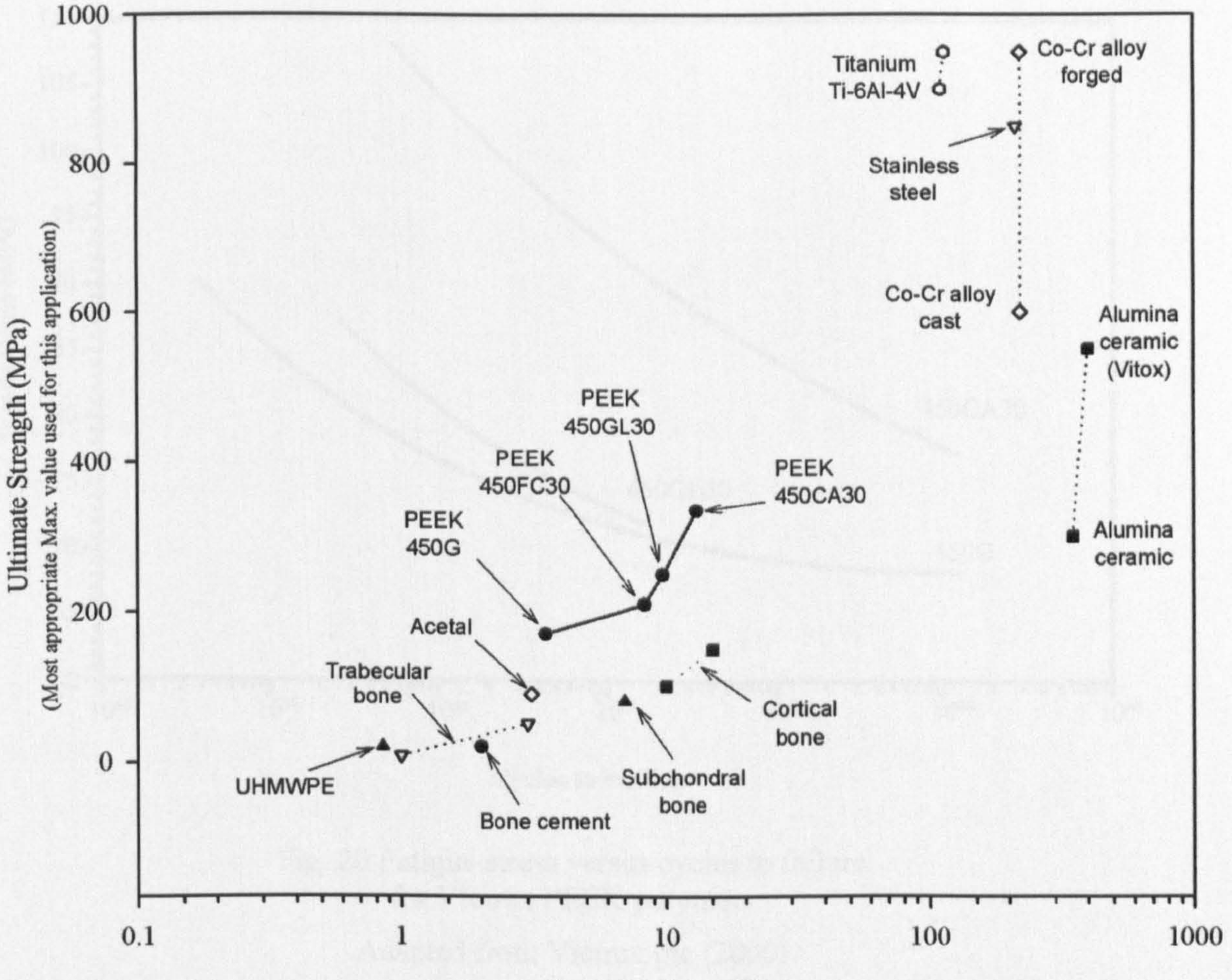

Fig. 19 Flexural modulus and ultimate strength of materials discussed (Pedersen, Crowninshield et al. 1982; Huiskes and Chao 1983; Rapperport, Carter et al. 1985; Huiskes 1987; Prendergrast, Monaghan et al. 1989; Victrex plc 2000; Nordin and Frankel 2001; Matweb 2003a)

THR's endure fatigue-inducing loads in everyday activities such as walking and stair climbing. The number of cycles annually can be close to a million for walking and at loads many times body weight (Bergmann 1993; Paul 1999). PEEK's excellent fatigue resistance is further enhanced by both glass and carbon fibre reinforcement (Fig. 20) and outperforms many thermoplastic matrices containing the same reinforcement (Victrex plc 2000).

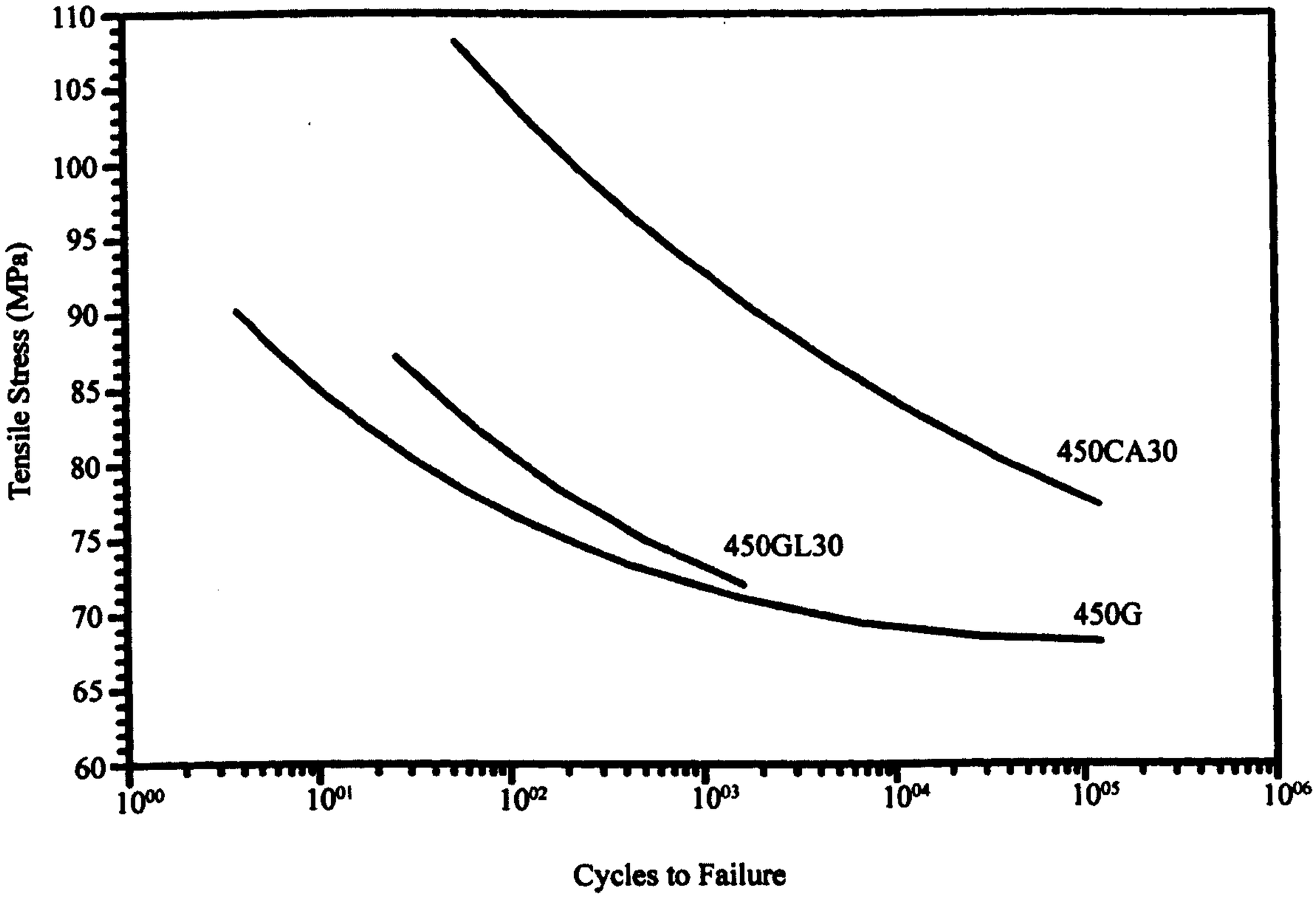

Fig. 20 Fatigue stress versus cycles to failure
for Victrex PEEK polymers
Adapted from Victrex plc (2000)

PEEK femoral prostheses can promote bone ingrowth and improved bone mineral density especially when hydroxyapatite (HA) coated (Orthodynamics Ltd 2003). HA is mainly known for its special ability to contact bone tissue and to form chemical bonding with natural bone. An inorganic constituent of bone, HA's limitations in mechanical properties have only allowed non-loaded applications in its bulk form. The deposition of HA coatings has permitted the exploitation of its bioactive properties in structural applications, such as THR. Coatings have commonly been applied by plasma-spraying technique, but there are problems associated with this method (Stoch, Brozek et al. 2003). One considerable problem of the plasma spraying technique, especially when used with PEEK composites, is that of the high temperatures involved which can damage the composite (Fig. 21).

Melted acetabular prosthesis caused by incorrect plasma spraying of HA coating (prosthesis manufactured from PEEK).

HA coating correctly applied by plasma spraying (prosthesis manufactured from PEEK).

Fig. 21 Examples of correctly and incorrectly applied HA coating

Other improved methods of HA deposition on carbon materials, such as electrochemical, are being investigated, (Stoch, Brozek et al. 2003). This requires temperatures of only 60°C for deposition, but requires a further procedure at 425°C, which is in excess of PEEK's melting temperature. Recent development in the PEEK material itself may lead to the elimination of the problems inherent with HA coating. Laboratory experiments by Abu Bakar et al. (2003) have introduced HA to the PEEK and carbon reinforced composite itself. If this material should become commercially available it may allow the manufacture of PEEK composite prostheses with the benefits of HA 'built in', making the need for coating unnecessary.

2.1.2 Properties of Vitox Alumina Ceramic

High purity alumina ceramics have been used for approximately 30 years in THR. Mechanical strength properties have increased during the last two decades by the introduction of high purity chemically derived submicron alumina powders as well as by improved processing technologies. Clean room technologies and hot isostatic pressing (HIP) have resulted in major improvements with respect to material properties (Burger and Richter 2000). These continued gains have led to nearly a 45% improvement of mechanical strength (Willmann and Heros 1998). Vitox is a 99.9% pure alumina ceramic and is manufactured by Morgan Matroc from the purest biograde

material available (Morgan Matroc). The material exceeds the ISO and ASTM standards as set out in 'specification for ceramic materials based on high purity alumina'(ASTM; BSI 1994) in both material properties and composition (Table 6).

Property	Vitox (Morgan Matroc)	Biolox (CeramTec)	ISO 6474	ASTM F603-00
Bending Strength (MPa)	380-550	580	≥ 250	≥ 400
Density (kg/m^3)	3960	3980	≥ 3940	≥ 3940
Wear Resistance (mm^3) (In accordance with ISO 6474)	--	0.001	≥ 0.1 [a]	--
Average Grain Size (μm)	1.2	< 2	≤ 4.5	≤ 4.5
Hardness	19.3 GPa, 0.5 kg load	2000 HV	--	18 GPa, 1 kg load
Fracture Toughness (MPa-$m^{1/2}$)	4-6	--	--	--
Modulus of Elasticity (GPa)	400	380	--	--
Compressive Yield Strength (MPa)	2600	--	--	--
Al_2O_3	> 99.9	--	≥ 99.5	≥ 99.5
SiO_2	< 0.002	--	≤ 0.1	≤ 0.1
Fe_2O_3	< 0.001	--		
CaO	--	--		
Na_2O	< 0.002	--		
MgO	0.05	--	≤ 0.3	≤ 0.5
[a] This test applies only if articulation of ceramic on ceramic is intended.				

Table 6 Comparison of Vitox Alumina against international standards and other manufacturers

From (ASTM; BSI 1994; Morgan Matroc Ltd. 2000; CeramTec 2003; Matweb 2003b)

Components are initially manufactured in the 'green state' by computer numerically controlled (CNC) machines prior to firing. Firing is undertaken at high-pressure known as hot isostatic pressed (HIP). Final finishing on critical dimension is undertaken by

grinding to tolerances greater than 0.025mm and sphericity of 0.015mm. Dimensional inspection is undertaken by state of the art computerised three-dimensional measuring machines (CMM) to ensure the highest quality control.

2.2 Design Features

The new acetabular cup prostheses are designed so that all sizes can be CNC machined from generic 65mm diameter injection mouldings that incorporate the alumina bearing (Fig. 22). The benefits of this method are threefold; firstly, the reduction of injection moulding tooling costs, as only one injection mould tool is required to manufacture the complete product range; secondly, the CNC machining of all sizes of components from generic mouldings allows a reduced inventory of sizes to be kept; and thirdly, custom sizes and shapes can easily and cheaply be produced if required.

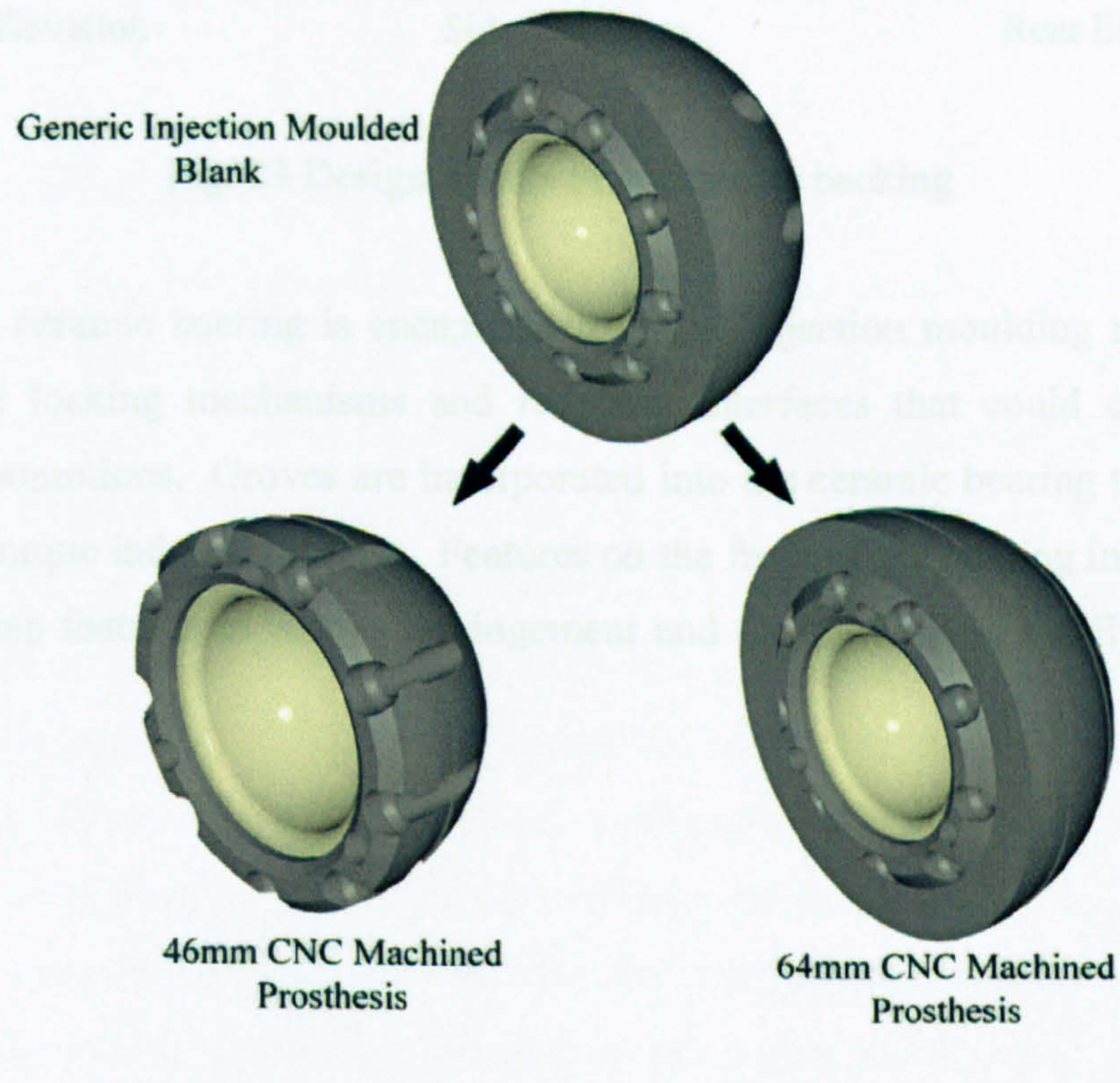

Fig. 22 Generic injection moulded blank and finish machined prostheses

Primarily designed for a pressfit into the acetabulum, a ring of 9 counter bored holes allows the use of bone screws should additional initial fixation be required. In addition to these 9 holes, a further 3 threaded holes are also situated on the front of the cup for instrumentation. On the rear of the cup blind holes are created during injection moulding to further reduce the prosthesis stiffness, provide anchorage for bone ingrowth

and reduce material costs. Whilst the overall size and shape of the prosthesis is being CNC machined, two groves are also machined into the diameter to aid fixation upon bone ingrowth (Fig. 23).

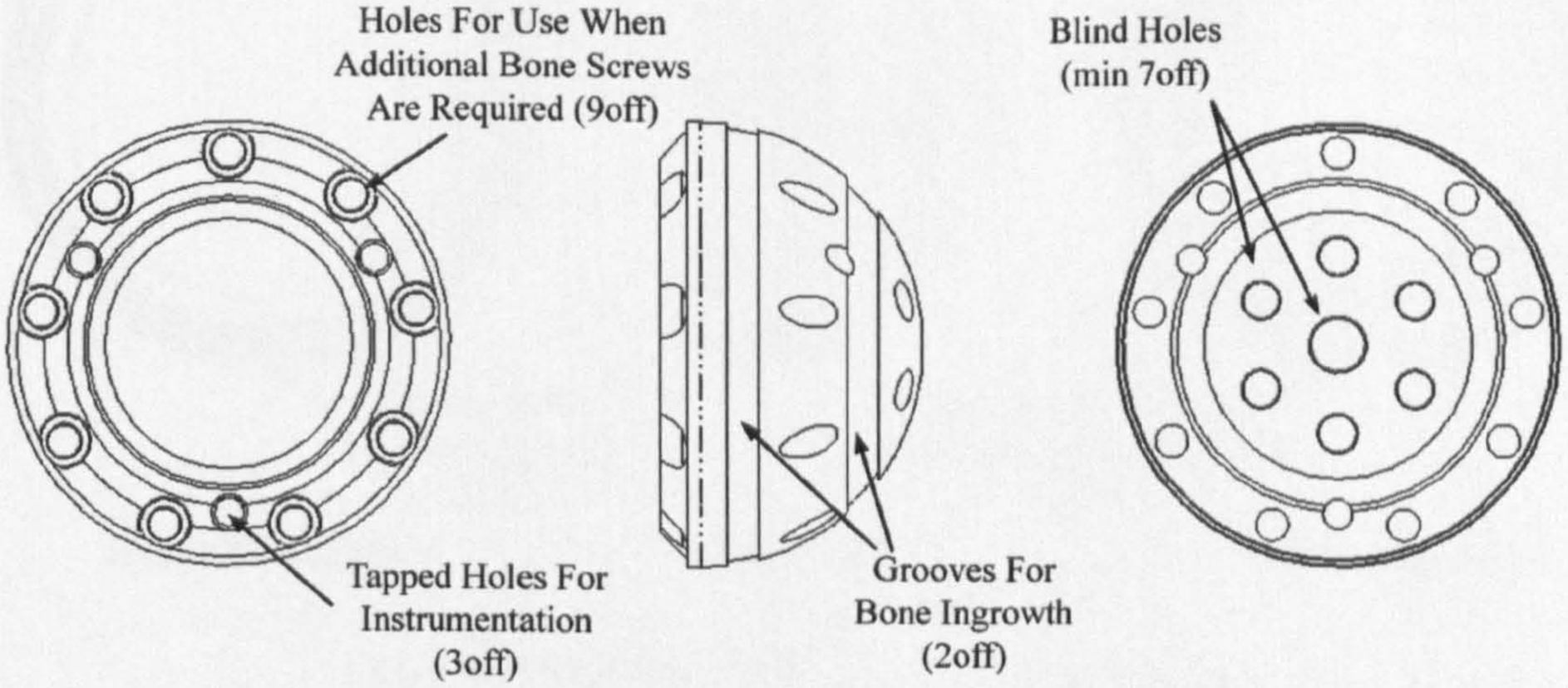

Fig. 23 Design details of composite backing

The alumina ceramic bearing is encapsulated during injection moulding removing the necessity for locking mechanisms and reducing interfaces that could cause debris-creating micromotions. Groves are incorporated into the ceramic bearing to resist axial pullout and torque induced rotation. Features on the front of the bearing include a large radius and step features to reduce impingement and fix the bearing axially (Fig. 24 & Fig. 25)

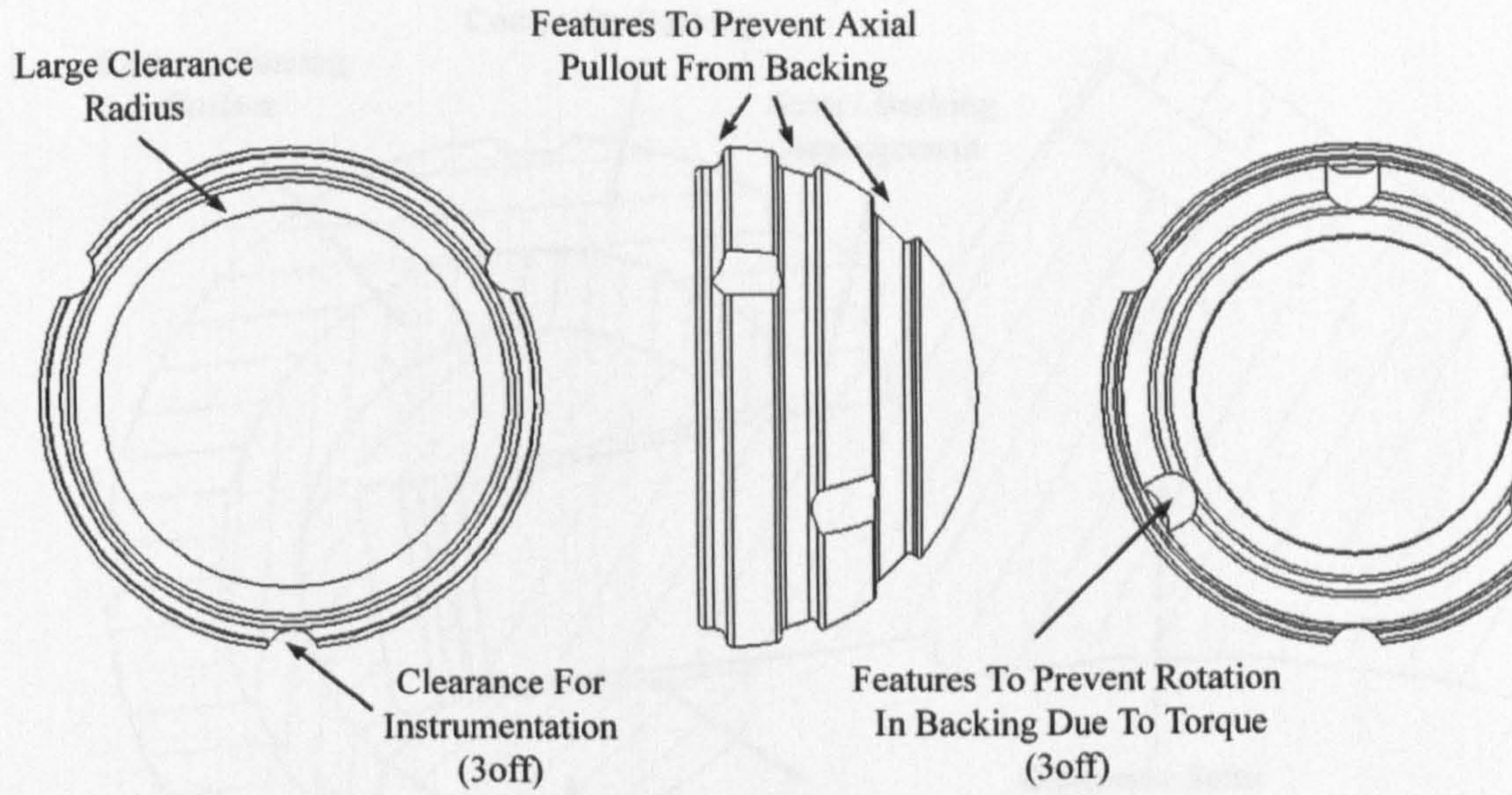

Fig. 24 Design details of Vitox alumina bearing

2.3 Range of Motion (ROM)

The design of the new acetabular cup prosthesis was coupled with the existing Orthodynamics' composite femoral stem and alumina head. This configuration is the proposed THR system in which the new acetabular cup will be used (Fig. 17 part B page 33). Limitations in the range of motion (ROM) of THR can lead to impingement which may result in dislocation or damage to the ceramic components. Impingement is defined as contact between the femoral neck and the rim of acetabular cup or insert (Bader, Steinhauser et al. 2000). Critically for the patient, poor ROM during everyday activities that require large ranges of motion, such as the tying of a shoelace, could lead to impingement causing dislocation of the head from the cup. Historically impingement of ceramic components frequently resulted in cracking or chipping. Under ideal prostheses orientation, no impingement of this new system should occur during normal activities, but full ROM is extremely sensitive to the orientation in which the surgeon places the acetabular cup (Bader, Steinhauser et al. 2000; D'Lima, Urquhart et al. 2000). For this reason additional precautions were taken to ensure that no stem to ceramic impingement could occur and that any impingement would be stem to composite, thus avoiding possible damage to the comparatively brittle ceramic (Fig. 25).

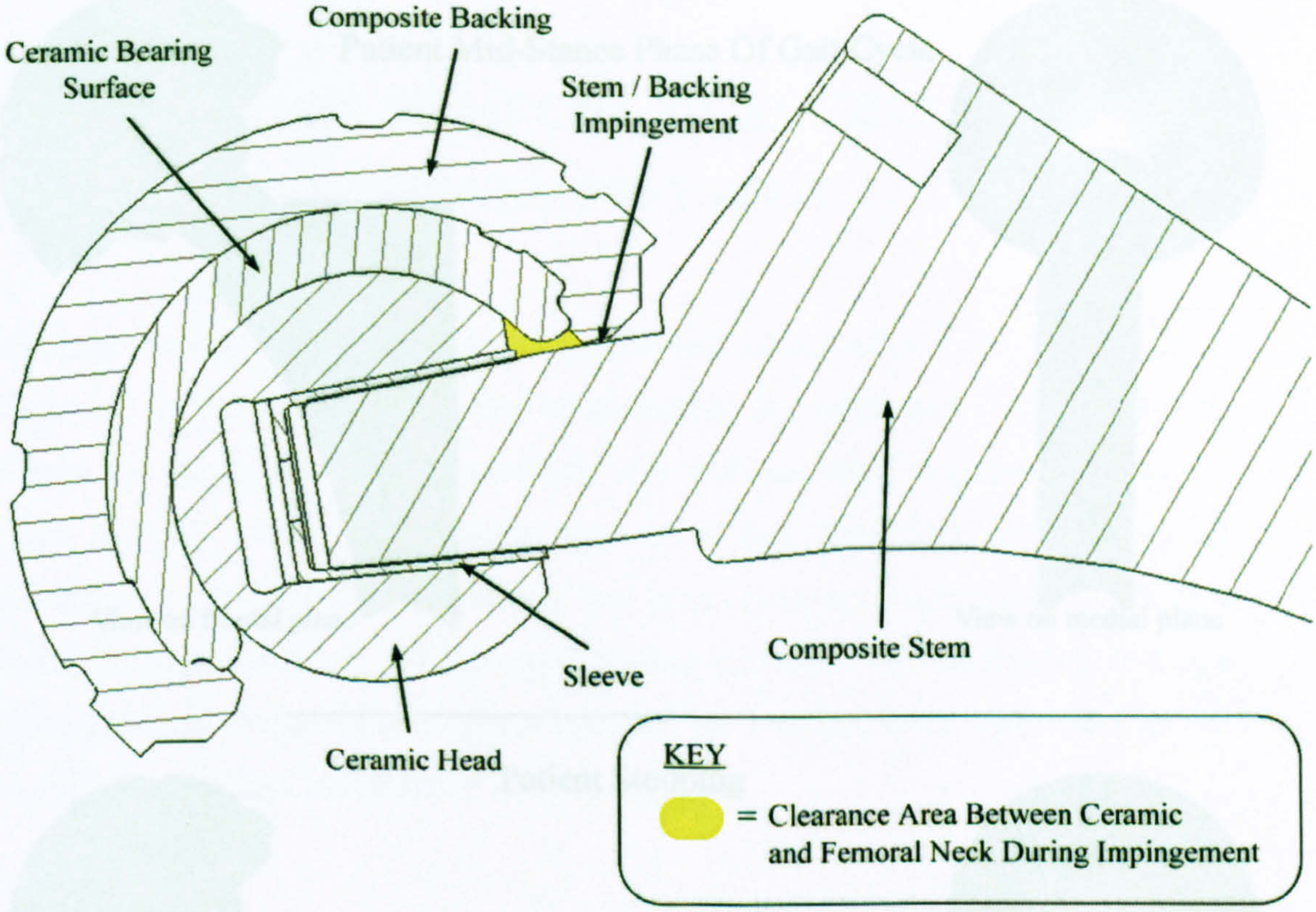

Fig. 25 Planar section through proposed THR system showing impingement and ceramic clearance

ROM tests for the more demanding of everyday activities were carried out as described by D'Lima et al (2000) based on anatomical orientations by Johnston and Smidt (1970). The new THR system was modelled using Pro Engineer (Parametric Technology, Waltham, Massachsetts), a parametric computer-assisted-design program. Example images of the results are displayed in Fig. 26 and these examples demonstrate the ease in which this new system can achieve these demanding activities whilst leaving many additional degrees of movement until impingement.

The new system's ROM exceeds both Johnston and Smidt's (1970) 'ideal' range of motion and D'Lima et al.'s (2000) 'Excellent' range of motion proposals. The full ROM results with anatomical descriptions can be found in Appendix 1.

Patient Mid-Stance Phase Of Gait Cycle

View on frontal plane

View on medial plane

Patient Stooping

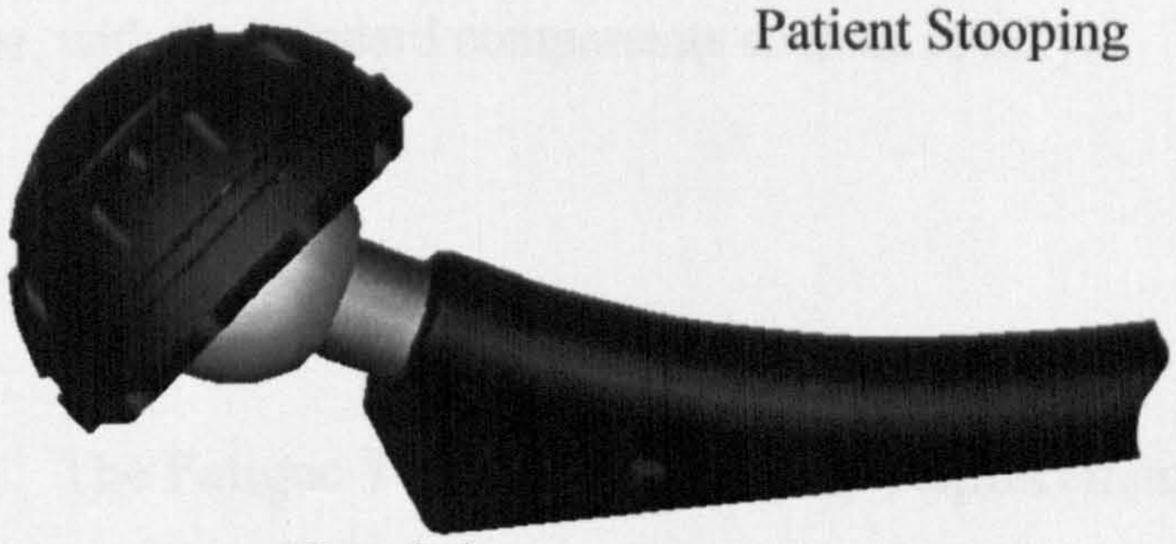

View on frontal plane

View on medial plane

Patient Tying Shoe Lace

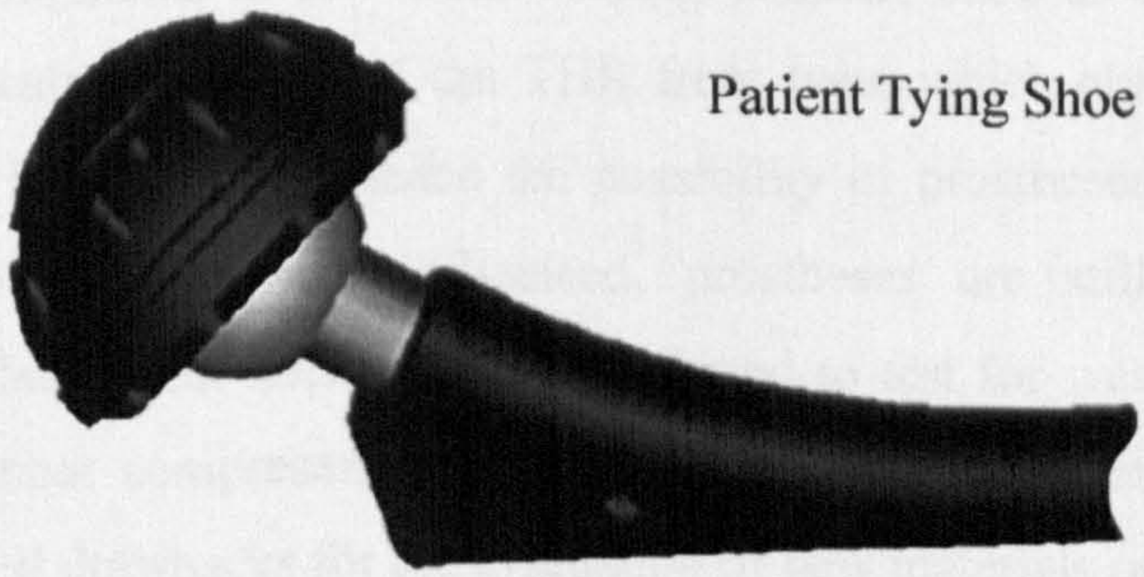

View on frontal plane

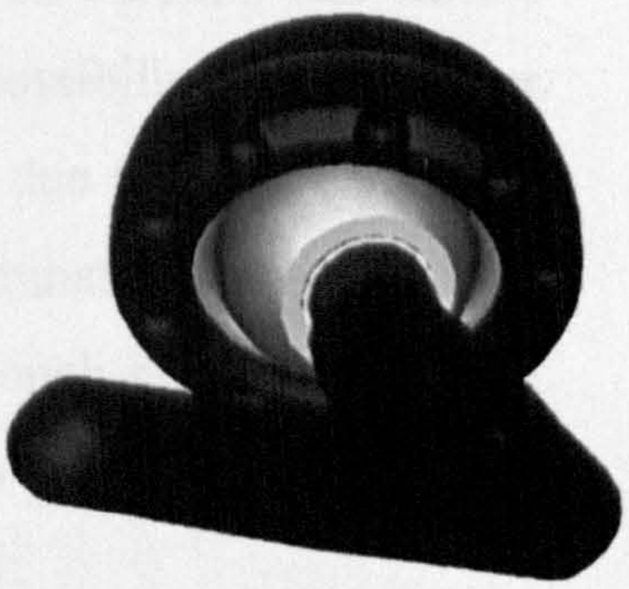

View on medial plane

Fig. 26 Position of stem during everyday activities (impingement checks)

3 FORMULATION OF MECHANICAL TEST METHODS AND DESIGN OF NOVEL TEST RIGS

This chapter presents the formulation of mechanical tests methods and the design of novel test rigs for the mechanical testing of acetabular hip prostheses. The urgent need to advance the mechanical testing methods of acetabular cups was described in the Literature Review 1.4.4. This chapter proposes a fast, repeatable and economical method of mechanically testing acetabular cup prostheses, and is particularly relevant for acetabular hip prostheses with ceramic bearing surfaces. All mechanical test rigs were designed and manufactured by the author. All test rigs were assembled by the author, with the standard components sourced locally.

3.1 Fatigue Test Rig

3.1.1 The Fatigue Testing Of Total Hip Replacements

Historically, mechanical testing of THR systems has been biased towards the wear of the articulating couple due to the high frequency of this type of mechanical failure. Developments in low wear bearing couples, such as ceramic on ceramic can almost eradicate the failure of the THR from wear which gives the possibility of far greater time in service and hence the possibility of prostheses failure due to fatigue. Whilst THR materials have advanced, prostheses are still predominately tested in hip simulators that were primarily designed to test for wear. Although hip simulators are the most comprehensive method of mechanically testing hip prostheses, they have several drawbacks for the evaluation of new materials or designs:

1. Hip simulators are expensive pieces of specialist machinery that can only be used for the testing of hip prostheses. Prices are in excess of £80,000
2. They are slow, with a typical speed of 1Hz, therefore a test replicating 20 years of use would take in excess of 33 weeks to complete. Traditional THR materials would have probably long worn out before a simulated 20 years; therefore the speed of the testing was less important.

The slow speed of the hip simulator is limited mainly by the range of motion and the required load profile, as described in ISO 14242-1 (BSI 2002) and shown below (Fig. 27). Full explanation of the terms found in the key can found in Appendix A1.1).

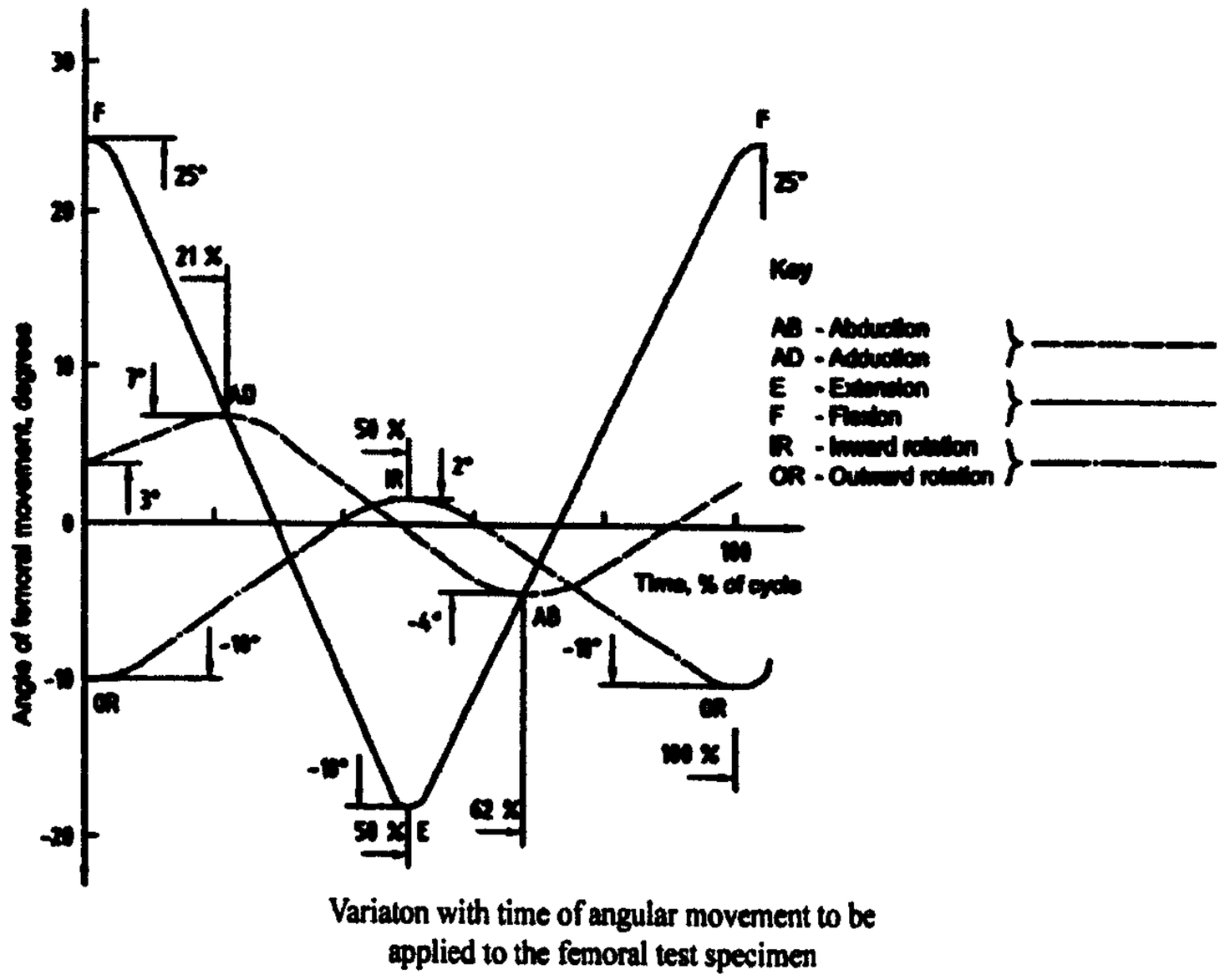

Variaton with time of angular movement to be applied to the femoral test specimen

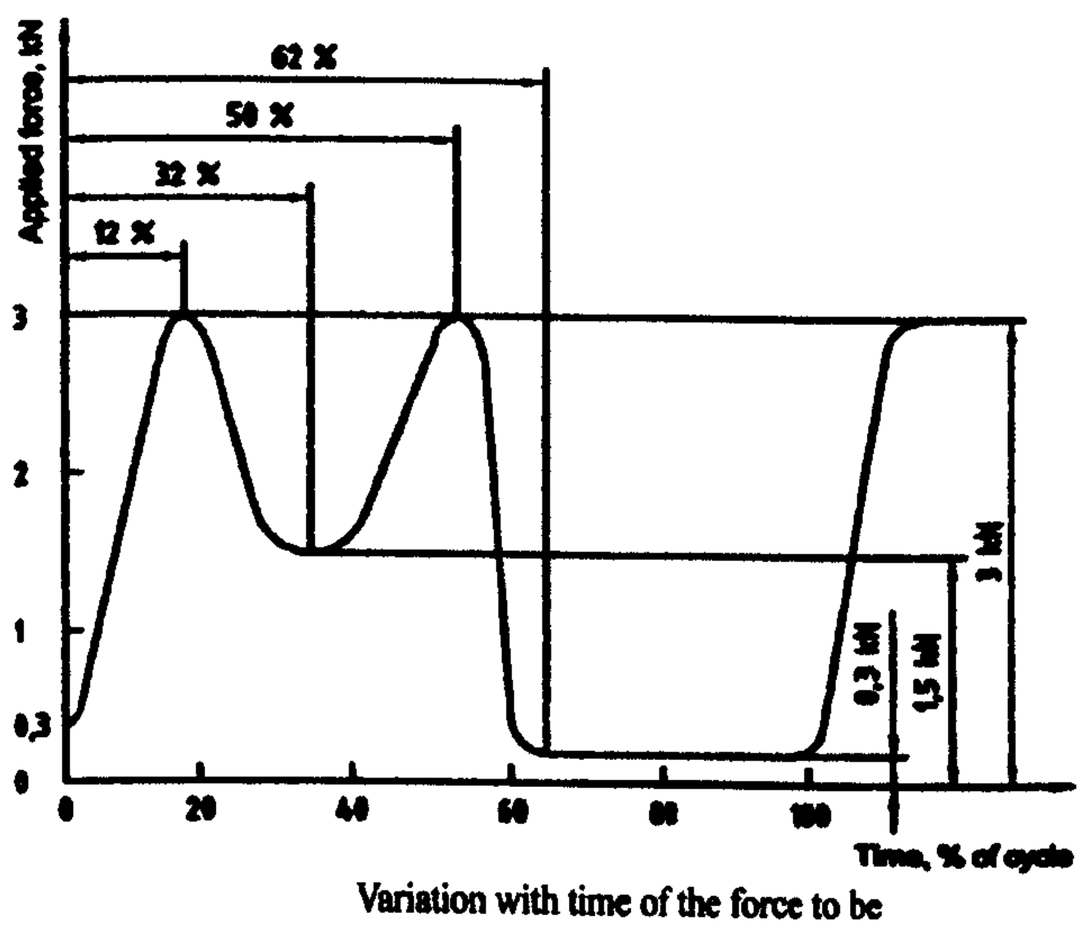

Variation with time of the force to be applied along the loading axis

Fig. 27 Angular movements and load profile required by ISO14242-1for hip simulators

Adapted from BSI (2002)

The plots in Fig. 27 describe the angular position required for the 3 axes of movement and the single axis of loading required to simulate walking. For the rapid evaluation of a new design's susceptibility to fatigue failure, due to the extended life now made possible with modern ceramics, the author designed a new single axis fatigue test rig.

3.1.2 Design Of Fatigue Test Rig

Major issues with current testing, as described in the Literature Review (1.4.4 Mechanical Testing Standards Used In Total Hip Replacement), were addressed in the design of this novel fatigue test rig. The fatigue rig created the ability to produce relatively quick fatigue damaged acetabular cup prosthesis for investigation of fatigue cracks, as described in the Literature Review (1.4.5 Fatigue Failure of Alumina Ceramic). Designed to complement the slow but comprehensive hip simulators tests, this test and rig allows fast repeatable fatigue testing using common single axis testing machines that can be found in most material laboratories. This section outlines the whole fatigue testing system. The general assembly drawing for the test rig and engineering drawings for all parts manufactured in house are listed in Appendix 2. The complete fatigue testing system can be seen in Fig. 29 including an enlarged image of the novel fatigue testing rig.

The acetabular component is embedded into the test rig using Devcon WR-2 putty (ITW Devcon, Northants, UK) and gives an anatomical testing position of 45° degrees for the acetabular cup with 10° of femoral abduction. The femoral head and taper adaptor are mounted on a titanium alloy taper. The use of a titanium alloy taper instead of a complete femoral stem allows confidence that tests can be repeated accurately with regard to position and stiffness by eliminating the variables inherent when using a complete stem. The mounting of a complete stem, when carried out in accordance with ISO 7206-4 (BSI 1998-2002), can allow several variables that can change position or stiffness of the test. The set-up for mounting femoral stems can be seen in Fig. 28 and variables include the Young's modulus of the mounting material; variation of stiffness due to bubbles in the mounting material; and variation of mounting material height, changing the bending moment.

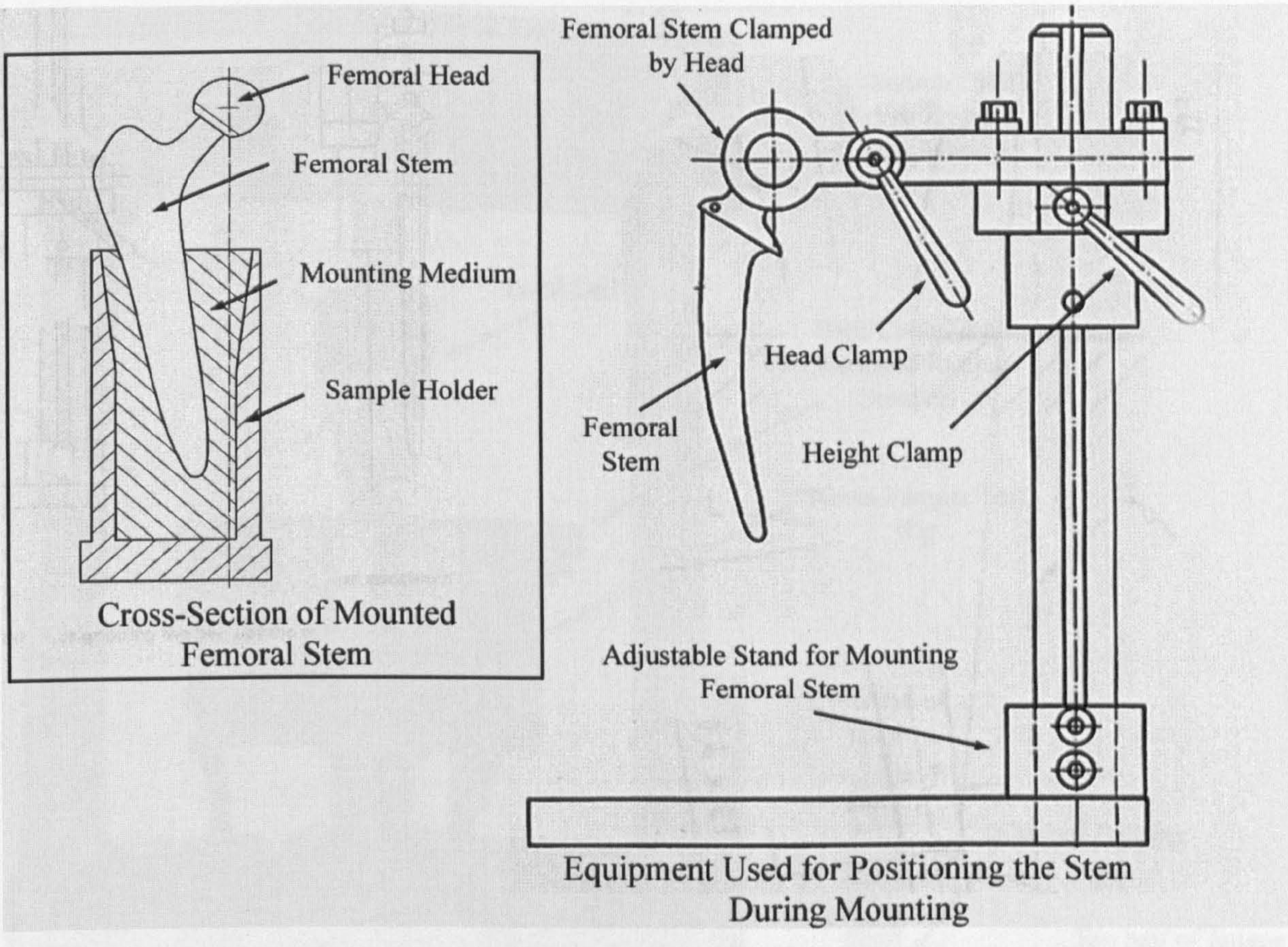

Fig. 28 General mounting arrangement of the femoral stem for fatigue testing and cross-section of mounted femoral stem (insert)
Adapted from ISO 7206-4 (BSI 1998-2002)

The use of a titanium alloy taper allows the direct comparison between the results of differing acetabular cups, and the testing of these cups to higher loads than possible if using a complete femoral stem. The harsh corrosive environmental conditions experienced by THR components in-vivo, are simulated with the use of a constantly aerated Ringer's solution at 37° C. Load is applied with a sinusoidal waveform by an Instron 8872 servo hydraulic test machine (Instron Ltd. Buckinghamshire, UK).

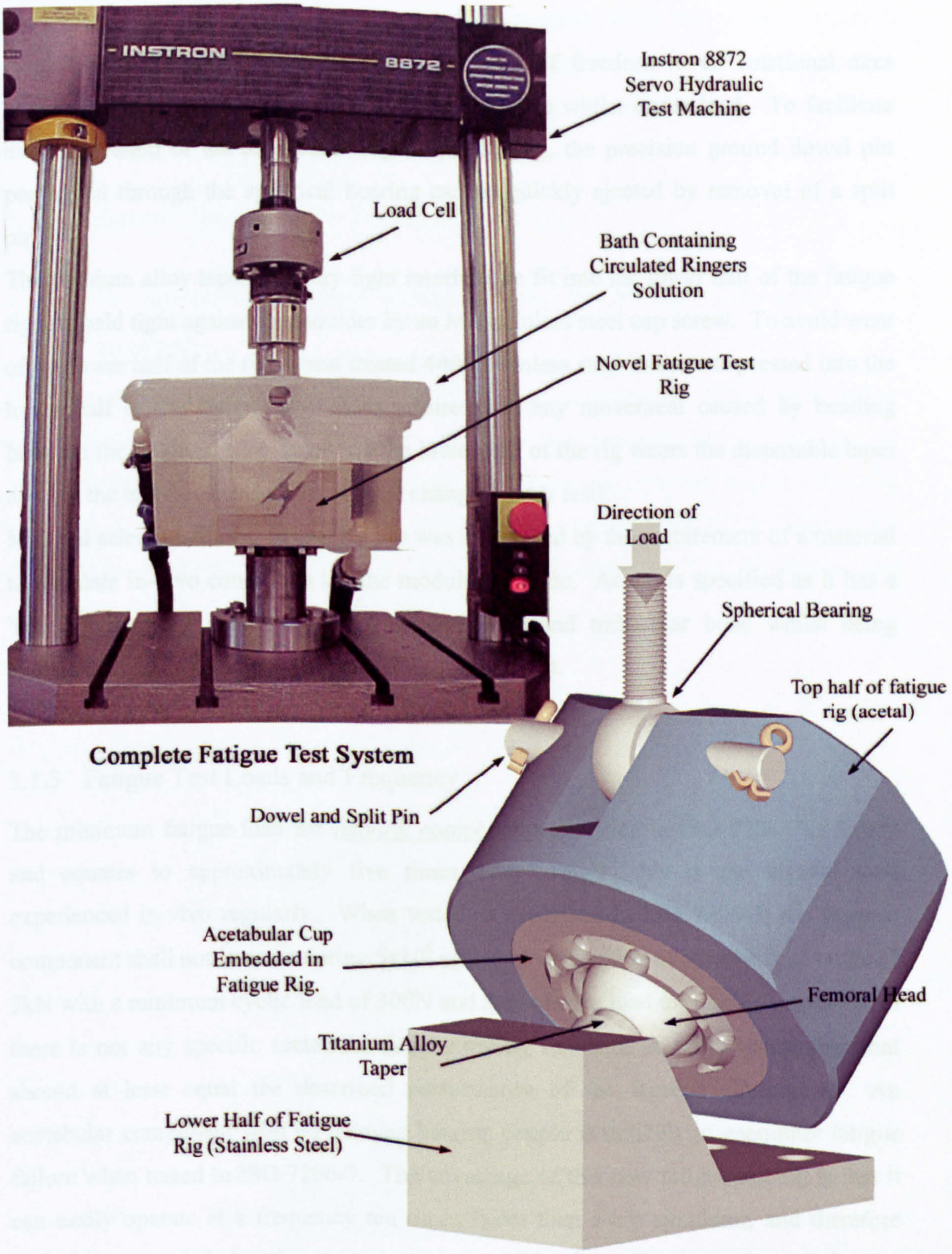

Complete Fatigue Test System

Novel Fatigue Test Rig

Fig. 29 Proposed fatigue test system and enlarged image of test fatigue rig

A stainless-steel spherical bearing gives degrees of freedom in all rotational axes allowing the bearing couple to be self-aligning, even whilst under load. To facilitate easy inspection of the acetabular cup during testing, the precision ground dowel pin positioned through the spherical bearing can be quickly ejected by removal of a split pin.

The titanium alloy taper is a very light interference fit into the lower half of the fatigue rig and held tight against its shoulder by an M6 stainless steel cap screw. To avoid wear of the lower half of the rig, a heat treated 440C stainless steel insert was pressed into the lower half of the fatigue rig. This ensures that any movement caused by bending between the titanium alloy taper and the lower half of the rig wears the disposable taper and not the test rig (titanium alloy taper changed every test).

Material selection for the fatigue rig top was influenced by the requirement of a material to simulate in-vivo conditions i.e. the modulus of bone. Acetal is specified as it has a Young's modulus between that of cortical bone and trabecular bone whilst being chemically inert and fatigue resistant (Fig. 19 page 38).

3.1.3 Fatigue Test Loads and Frequency

The minimum fatigue load for femoral components specified in ISO 7206-7 is 3.3kN and equates to approximately five times body weight, this is the highest load experienced in-vivo regularly. When tested as described in ISO 7206-7, the femoral component shall not fracture during $5x10^6$ cycles of application of a cyclic load range of 3kN with a minimum cyclic load of 300N and a maximum load of 3.3kN. Logically, as there is not any specific acetabular fatigue testing standard, an acetabular component should at least equal the described performance of the femoral component. An acetabular component with an alumina bearing couple is unlikely to encounter fatigue failure when tested to ISO 7206-7. The advantage of this new fatigue test rig is that it can easily operate at a frequency ten times faster than a hip simulator, and therefore undertake extended duration tests in an acceptable time. The extension of the test duration is also beneficial if current expectations of THR are to be fulfilled, as the current duration of $5x10^6$ cycles only equates to 5 years of walking. Other benefits of the new fatigue test rig is the ability to run tests at loads far greater than loads

experienced in-vivo, and beyond the load limits possible when testing incorporates a femoral stem. Fatigue testing at these elevated loads and frequencies makes it possible to gain a full understanding of an acetabular cup's fatigue performance, and the creation of a S/N curve.

3.2 Ultimate Compressive Strength Test Rig

3.2.1 The Ultimate Compressive Strength Testing of Ceramic Acetabular Prostheses

The ultimate compressive strength (UCS) of acetabular components, like fatigue testing of acetabular components, is without any specific testing standard. For the UCS testing of acetabular cups with ceramic bearing surfaces, anecdotal evidence suggests that the majority of UCS testing has been an adaptation of a withdrawn ISO standard (ISO 7206-5), as described in a 1995 U.S. FDA guidance document. Fig. 30 outlines the orientation of the original unmodified ISO 7206-5 test.

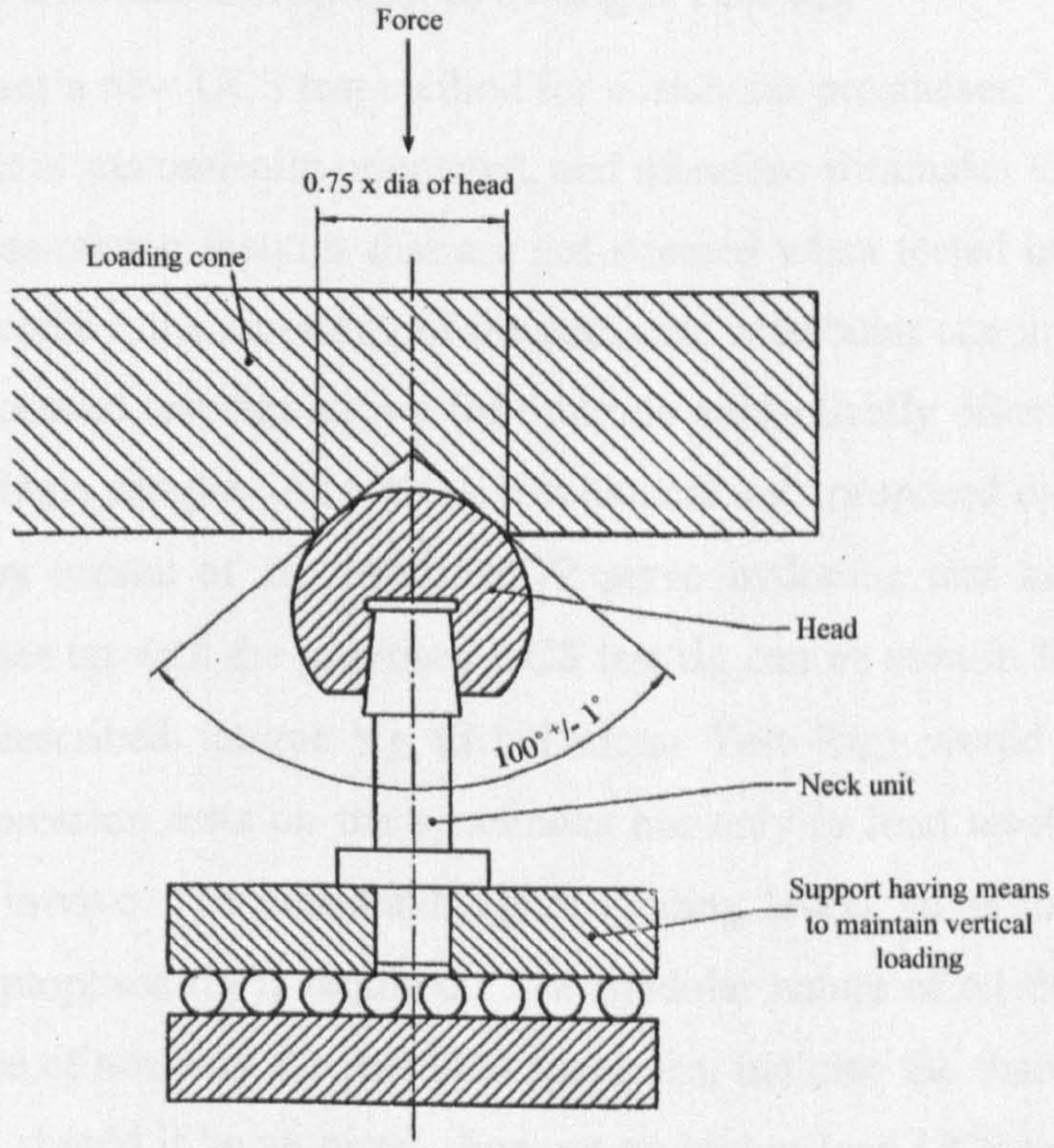

Fig. 30 Axial testing of head and neck region of stemmed femoral component

Adapted from ISO 7206-5

Further adaptation of the FDA standard (FDA 1995b) for use with acetabular components, is the replacement of the loading cone with the acetabular cup. The major limitation of this FDA/ISO adapted test is that it is an axial test. Whilst axial loading is the most mechanically demanding orientation for femoral heads containing a taper, when adapted for use with acetabular components, it may not be. The following points highlight the shortfalls of testing ceramic acetabular cup prostheses in this manner:

1. Axial loading of the acetabular cup prosthesis is not experienced in-vivo, and therefore a UCS result in this orientation is of little or no use
2. Loading the acetabular cup axially may not reveal stress-raising features that would be apparent when loaded in an anatomical orientation
3. The lack of a specimen mounting procedure leads to missed opportunities in data collection i.e. undertaking a UCS test after a fatigue test.

3.2.2 Design of Ultimate Compressive Strength Test Rig

The author proposes a new UCS test method for acetabular prostheses. Importantly the proposed UCS test is anatomically orientated, and therefore eliminates the possibility of not revealing stress-raising features that are not stressed when tested in the traditional axial method. Secondly, the mounting of the complete acetabular cup in a mount that is common to all proposed test rigs allows for multiple anatomically orientated tests to be undertaken on a single sample. As with all mechanical tests proposed by the author, the load is applied by means of an Instron 8872 servo hydraulic test machine and the complete system set up with the proposed UCS test rig can be seen in Fig. 31 page 55. The previously described fatigue rig (3.1 Fatigue Test Rig) would be capable of undertaking compression tests on the specimens but only to load levels several times that experienced in-vivo. To withstand higher loading levels, so as to obtain the full UCS results, the proposed rig is required. The modular nature of all the proposed test rigs allows the use of not only the mounted specimen, but also the titanium alloy taper and femoral head should it be required. For use on higher load UCS tests, a one-piece cobalt chrome head and taper is proposed to avoid ceramic head failure prior to test completion.

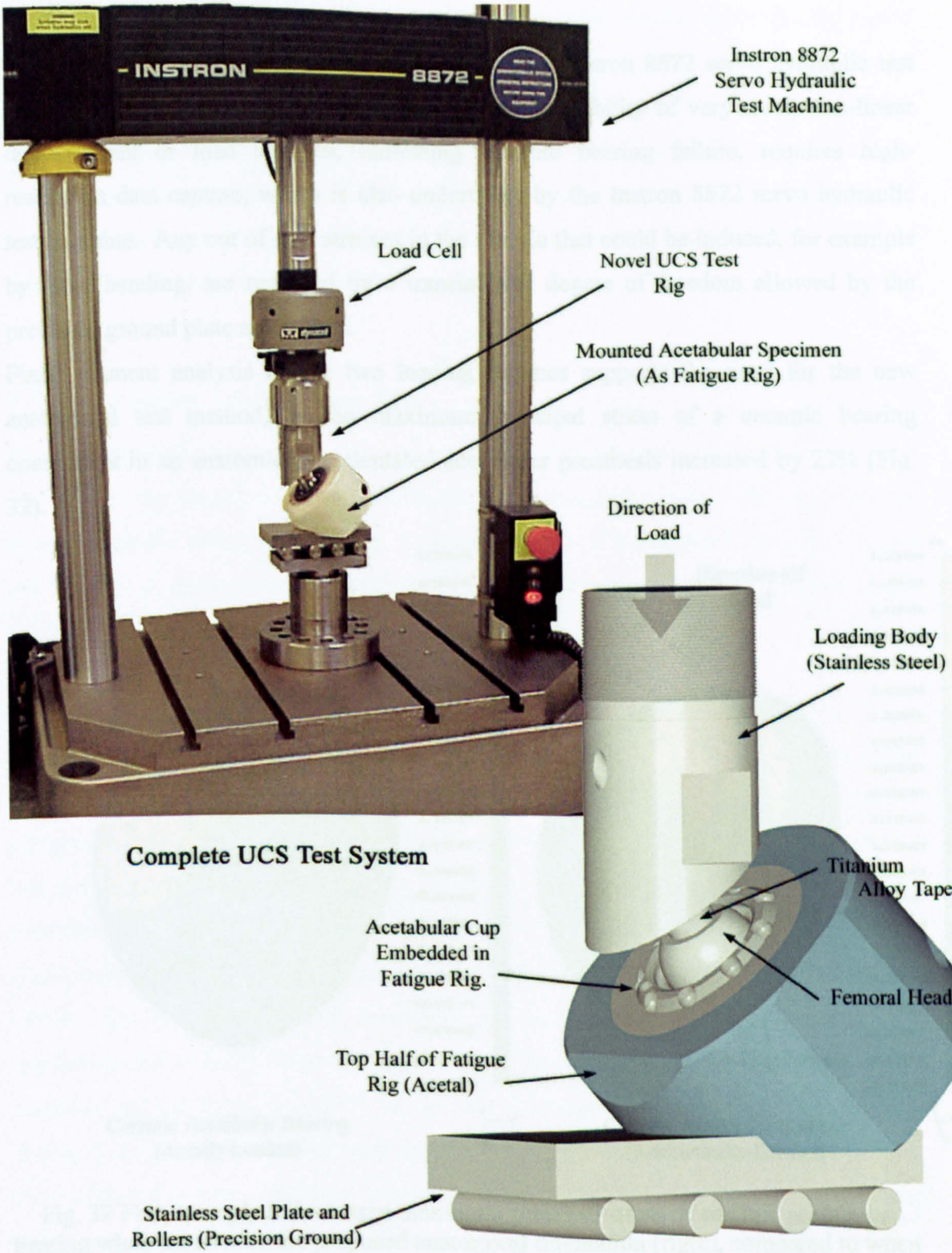

Complete UCS Test System

Novel UCS Test Rig

Fig. 31 Proposed UCS test system and enlarged image of UCS rig

Loading of the specimen is computer controlled by Instron 8872 servo hydraulic test machine, with either load or stroke control. The possibility of very small non-linear displacement or load changes, indicating ceramic bearing failure, requires high-resolution data capture, which is also undertaken by the Instron 8872 servo hydraulic test machine. Any out of axis stresses in the sample that could be induced, for example by taper bending, are removed by a translational degree of freedom allowed by the precision ground plate and rollers.

Finite element analysis of the two loading regimes supports the need for the new anatomical test method, as the maximum principal stress of a ceramic bearing component in an anatomically orientated acetabular prosthesis increased by 22% (Fig. 32).

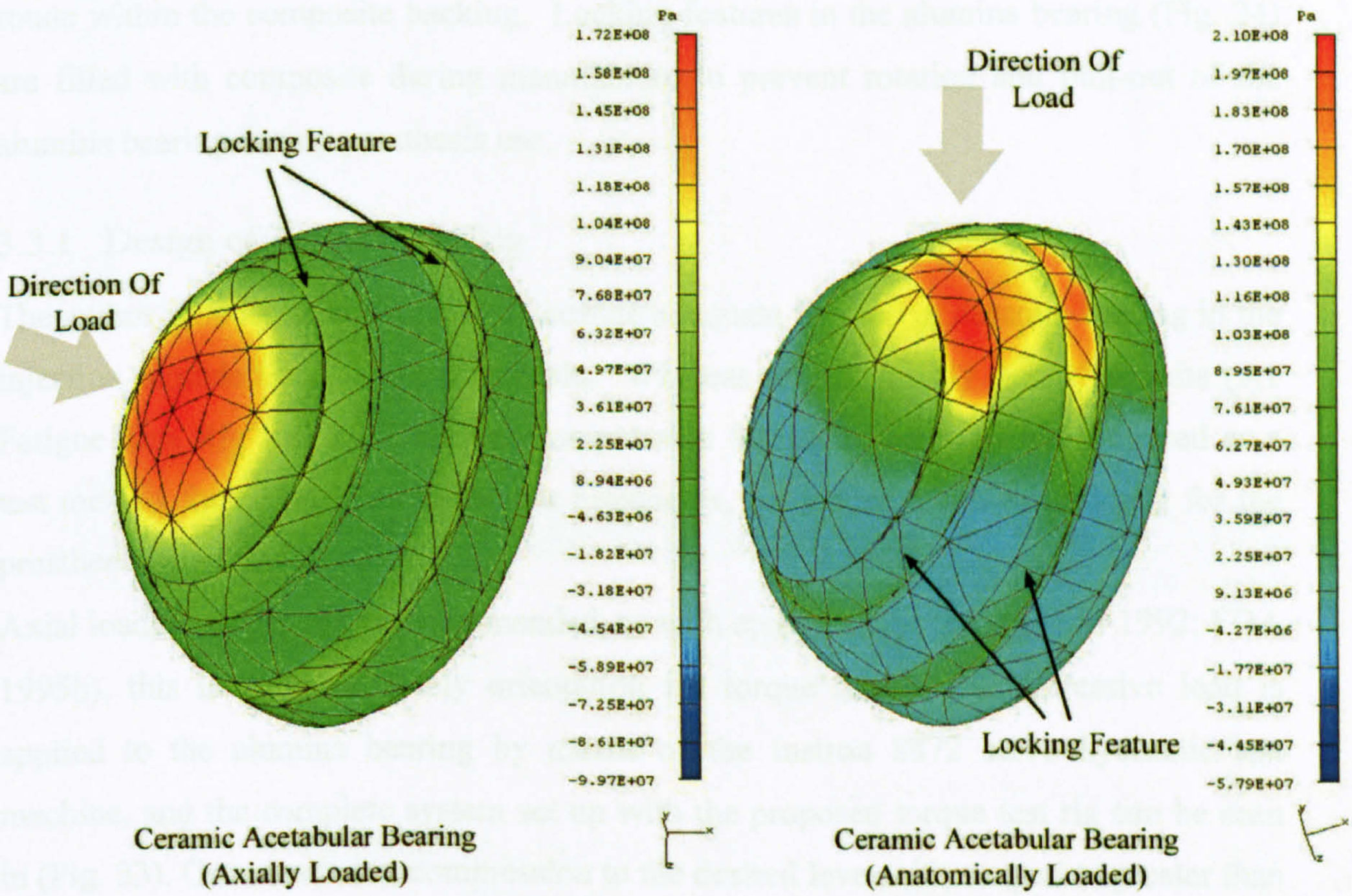

Fig. 32 FEA example of increased maximum principal stress of ceramic acetabular bearing when tested with the proposed anatomical orientation (right), compared to when tested axially (left)

Increases in maximum principal stress, such as in Fig. 32, are particularly significant with ceramics such as alumina, as they are between 4 and 12 times weaker in tension than compression. Had only axial UCS testing of this component been undertaken the

consequences of the higher stresses in the component, when loaded anatomically, would not have become apparent until implantation in-vivo. Testing of the component, whether actual or FEA, in the proposed anatomical orientation highlights, in this case, the locking feature as a stress raiser. Adoption of the proposed UCS test would ensure that any stress-raising features off the central axis, such as the locking feature, would be identified prior to manufacture (if using FEA) or at the very least during mechanical testing, and certainly prior to implantation in-vivo.

3.3 Maximum Torque Test Rig

The novel manufacturing method for the proposed acetabular prosthesis (Chapter 2 page 34) requires the formulation of a mechanical test to ensure the alumina bearing does not rotate within the composite backing. Locking features in the alumina bearing (Fig. 24) are filled with composite during manufacture to prevent rotation and pull-out of the alumina bearing during prosthesis use.

3.3.1 Design of Torque Test Rig

The author proposes a new test to determine adequate fixation of ceramic bearing in the injection moulded acetabular prosthesis. Whereas the previously described tests (3.1 Fatigue Test Rig and 3.2 Ultimate Compressive Strength Test Rig) are proposed as a test method for all types of acetabular prostheses, the torque test is specifically for the prosthesis proposed by the author.

Axial loading of the cup is recommended, as with ceramic head testing (BSI 1992; FDA 1995b), this is the most likely orientation for torque failure. Compressive load is applied to the alumina bearing by means of the Instron 8872 servo hydraulic test machine, and the complete system set up with the proposed torque test rig can be seen in (Fig. 33). Once loaded in compression to the desired level, either equal to greater than those achieved in-vivo, rotational movement of the head can be applied by means of the torque gauge. Adequate fixation of the alumina acetabular bearing is demonstrated if there is rotation of the torque gauge without movement of the acetabular-bearing. Observation of the torque required to overcome friction can also be recorded. Failure of the ceramic acetabular-bearing to withstand the torque applied, results in the bearing rotating within the backing. The failure torque can be recorded from the torque gauge.

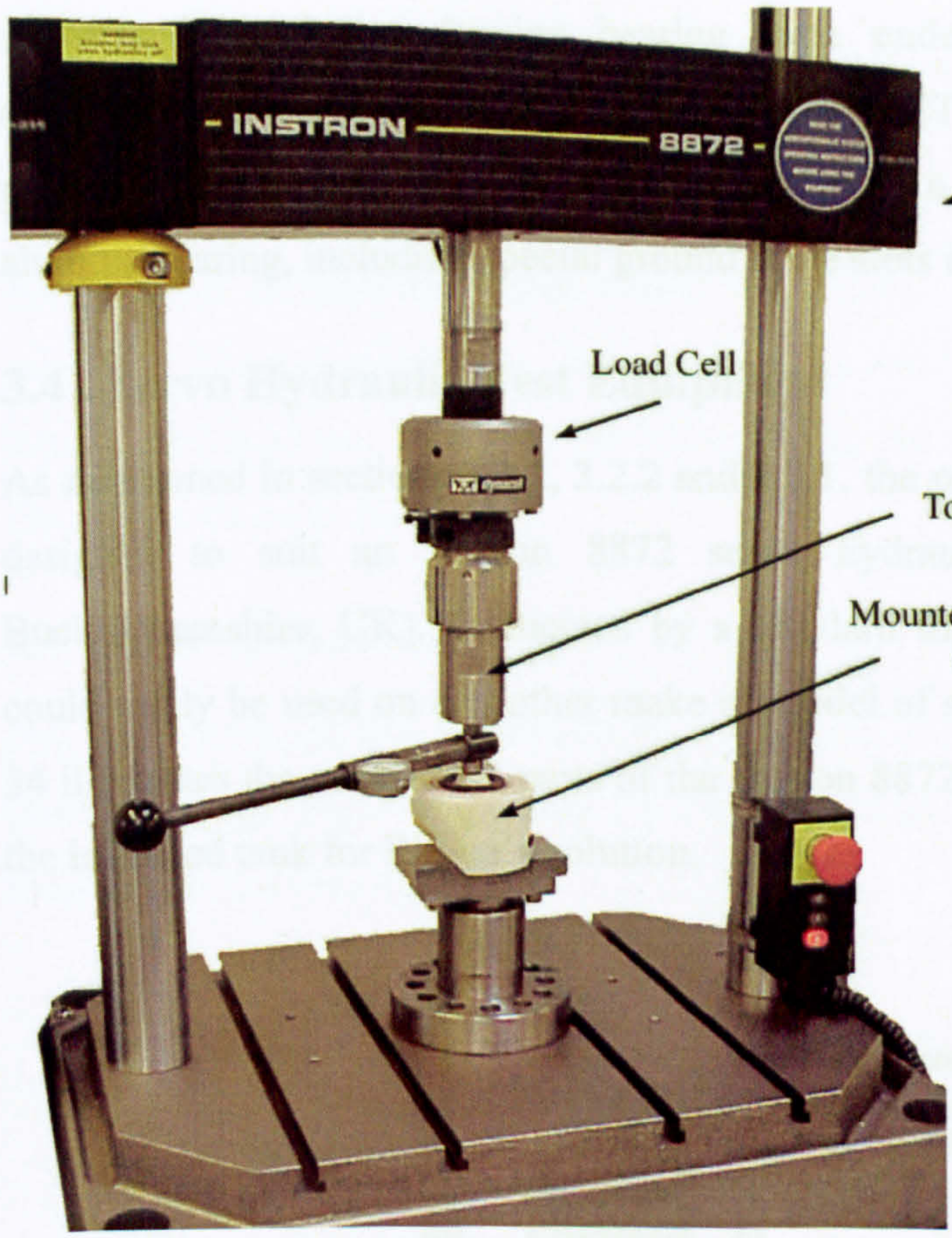

Complete Fatigue Test System

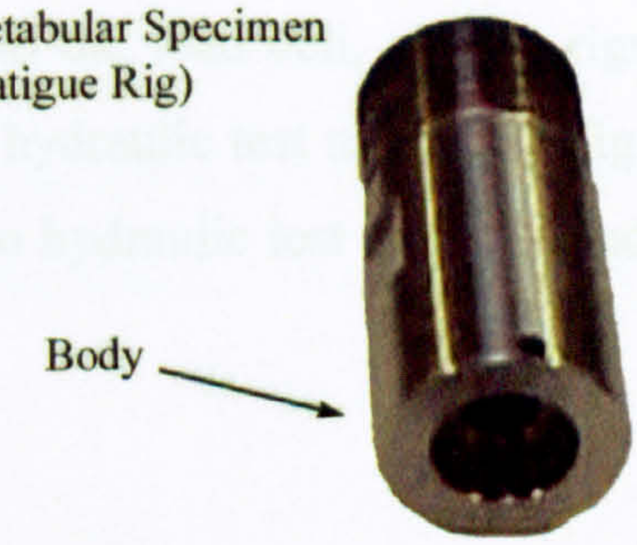

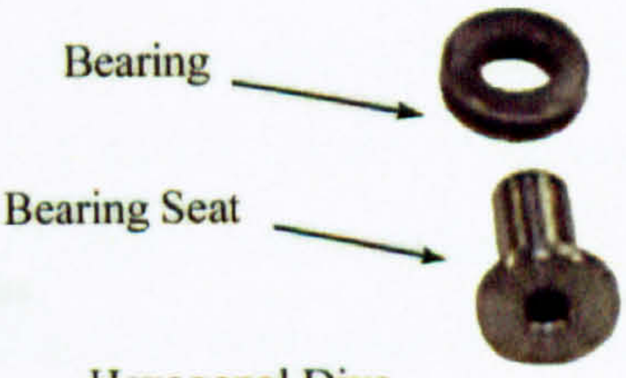

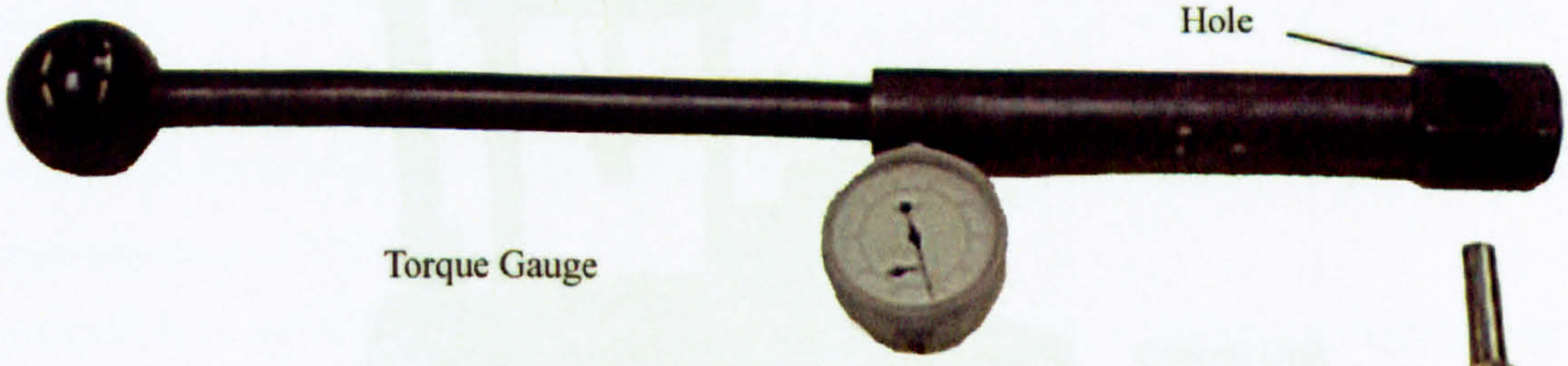

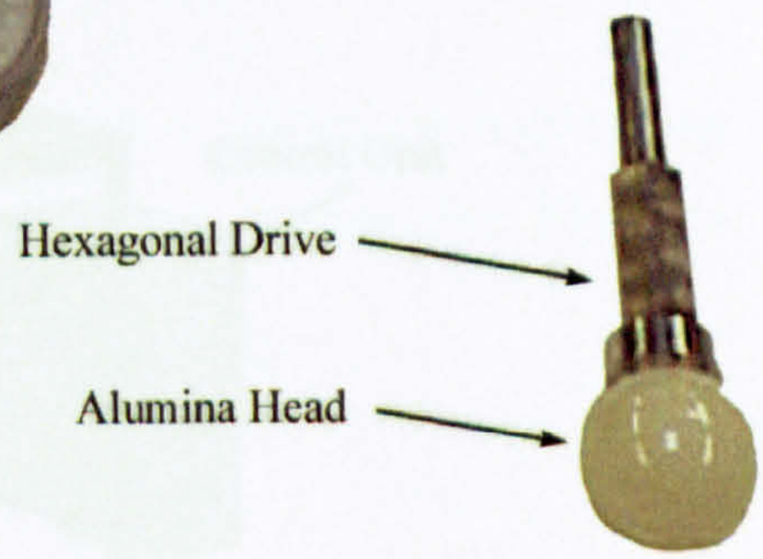

Exploded View Of Torque Rig Components

Fig. 33 Proposed torque test system and exploded view of torque rig

The modular nature all the proposed test rigs allows torque testing to be carried out both prior and post fatigue or UCS testing and also in an anatomical orientation. The ability

to undertake torque-testing post UCS and fatigue test, allows retrieval of data and an understanding of the alumina bearing even under worse case, 'failed bearing', conditions. Should an ultimate failure torque (UFT) of the acetabular prosthesis be required the alumina head can be replaced with a number of drive options to the alumina bearing, including special ground drive slots in the ceramic cup.

3.4 Servo Hydraulic Test Equipment

As mentioned in sections 3.1.2, 3.2.2 and 3.3.1, the proposed mechanical test rigs were designed to suit an Instron 8872 servo hydraulic test machine (Instron Ltd. Buckinghamshire, UK). Connected by a standard thread to the load cell, all test rigs could easily be used on any other make or model of servo hydraulic test machine. Fig. 34 illustrates the component parts of the Instron 8872 servo hydraulic test machine and the insulated tank for Ringer's solution.

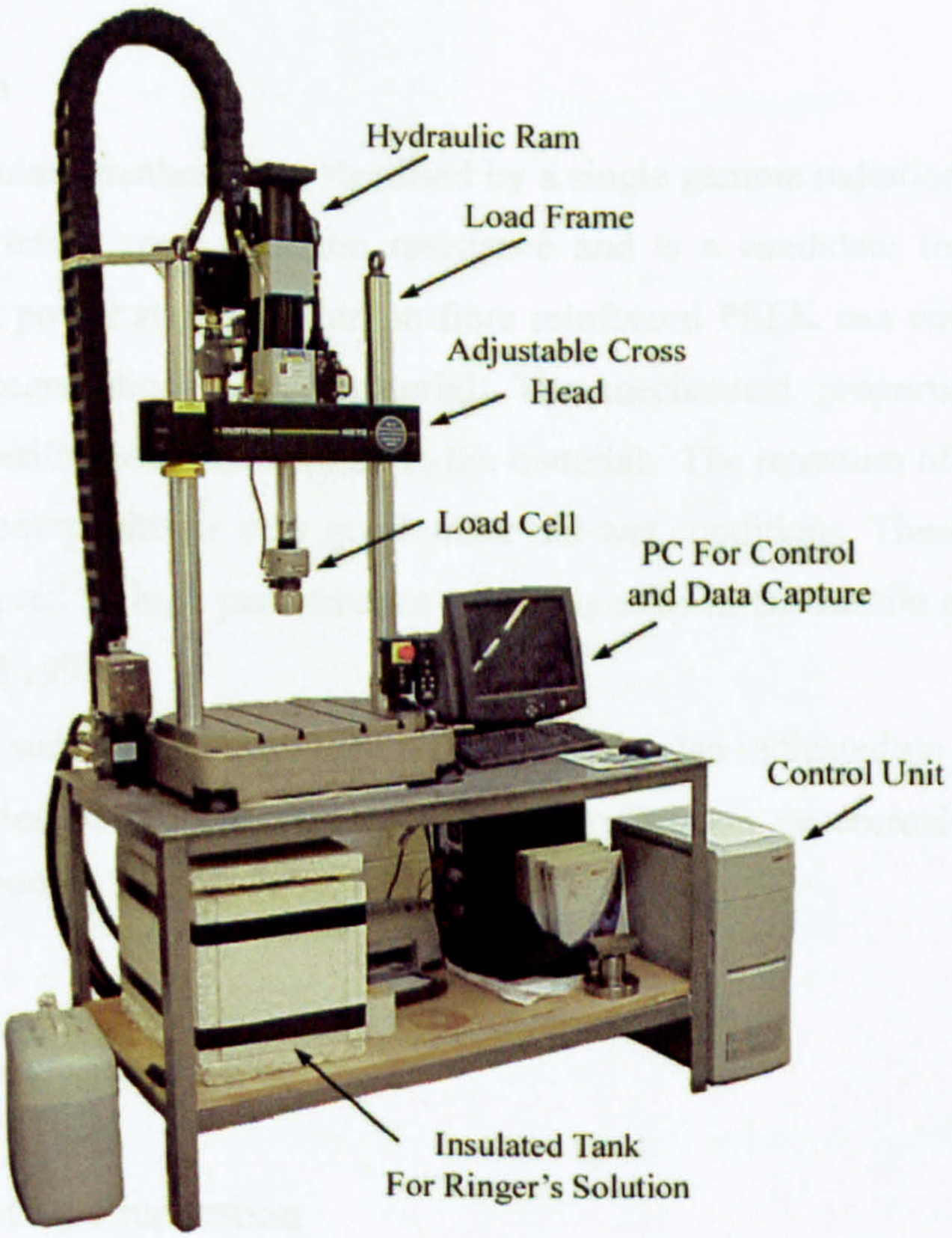

Fig. 34 Component parts of the Instron 8872 servo hydraulic test machine and the insulated tank for Ringer's solution

4 EXPERIMENTAL AND ANALYTICAL METHODOLOGY

This chapter presents the experimental and analytical methodology employed in this research. The test specimens, their preparation and the procedures used in mechanical testing are described. The FEA modelling of the test specimens is also described, as are theories of strength and failure.

4.1 Test Specimens

Finished acetabular cup prostheses in a range of sizes were supplied by Orthodynamics (Section 2 page 34) for mechanical testing in a 'ready for implantation' form, including sterilisation and packaging.

4.1.1 Sterilisation

The finished acetabular prostheses are sterilised by a single gamma radiation dose of 25 - 35 kGy. PEEK has a good radiation resistance and is a candidate for insulating materials in nuclear power stations. Carbon fibre reinforced PEEK can withstand 25 - 35 kGy without degradation to the material. The mechanical properties are also unaffected by the sterilisation dose applied to the material. The retention of mechanical properties of these composites is very good under hot-wet conditions. These composite materials can be served as high performance materials even in the hostile environment (Orthodynamics Ltd 1998).

Investigation of the stability of Vitox high purity alumina also indicated no degradation in material properties when subjected to gamma sterilisation or corrosive Ringer's solution (Murray 1999).

4.2 Specimen Preparation

4.2.1 Acetabular Cup Preparation

Sterilised acetabular cups were received for testing in sealed packaging ready for implantation or testing, and therefore only required mounting for mechanical tests. All

proposed mechanical tests could be carried out on the mounted specimen. A hemispherical cavity with a diameter 4mm larger than the test specimen was machined into the acetal mount. The specimen and acetal mount were then axially aligned on a vertical milling machine. The specimen was held by dummy instrumentation and the mount was held in a rotary table (Fig. 35). The orientation of the specimen was set using the rotary table. The vertical milling machine's quill was set at a depth that creates a 2mm cavity around the specimen. Finally the specimen was set into the mount using Devcon WR-2 putty (ITW Devcon, Northants, UK) and allowed to set.

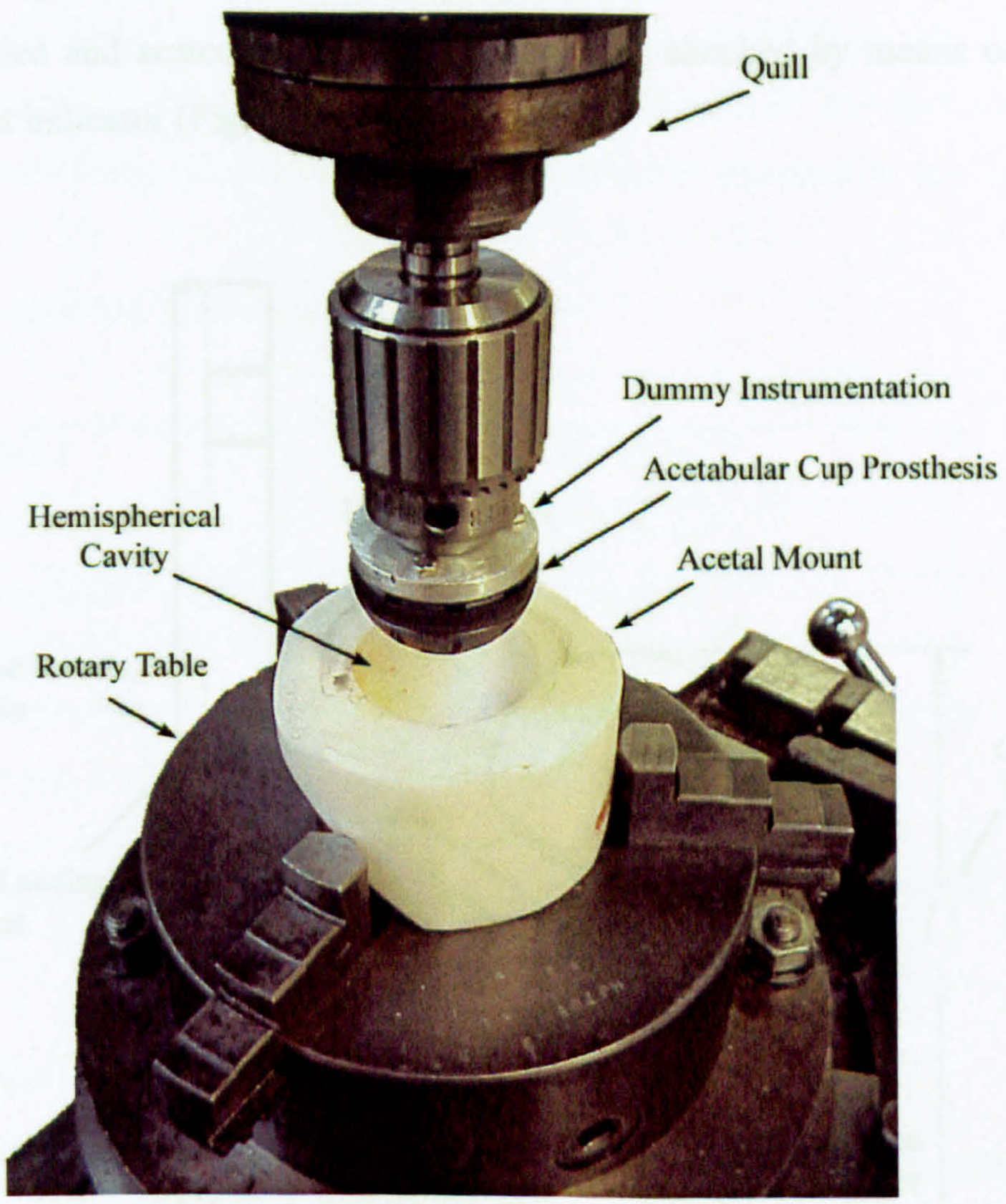

Fig. 35 Mounting of acetabular cup prosthesis for mechanical testing

(Image prior to application of mounting putty and setting of depth)

4.2.2 Head and Taper Preparation Required for Fatigue Test

To ensure the correct seating of the head, taper adaptor and taper, these components were assembled and axially loaded. This not only seated the components but insured the assembly could withstand the load that it would be subjected to during fatigue tests. The load for seating was applied as described in ISO 7206-5, as seen in Fig. 30 (page 53).

It is impossible to manufacture these components to produce perfect test alignment when assembled and fitted to the fatigue test rig due to manufacturing tolerances. To achieve test alignment, the titanium alloy taper was left oversize and finished machined once assembled and seated. Correct alignment was checked by means of slip gauges and a dial test indicator (Fig. 36).

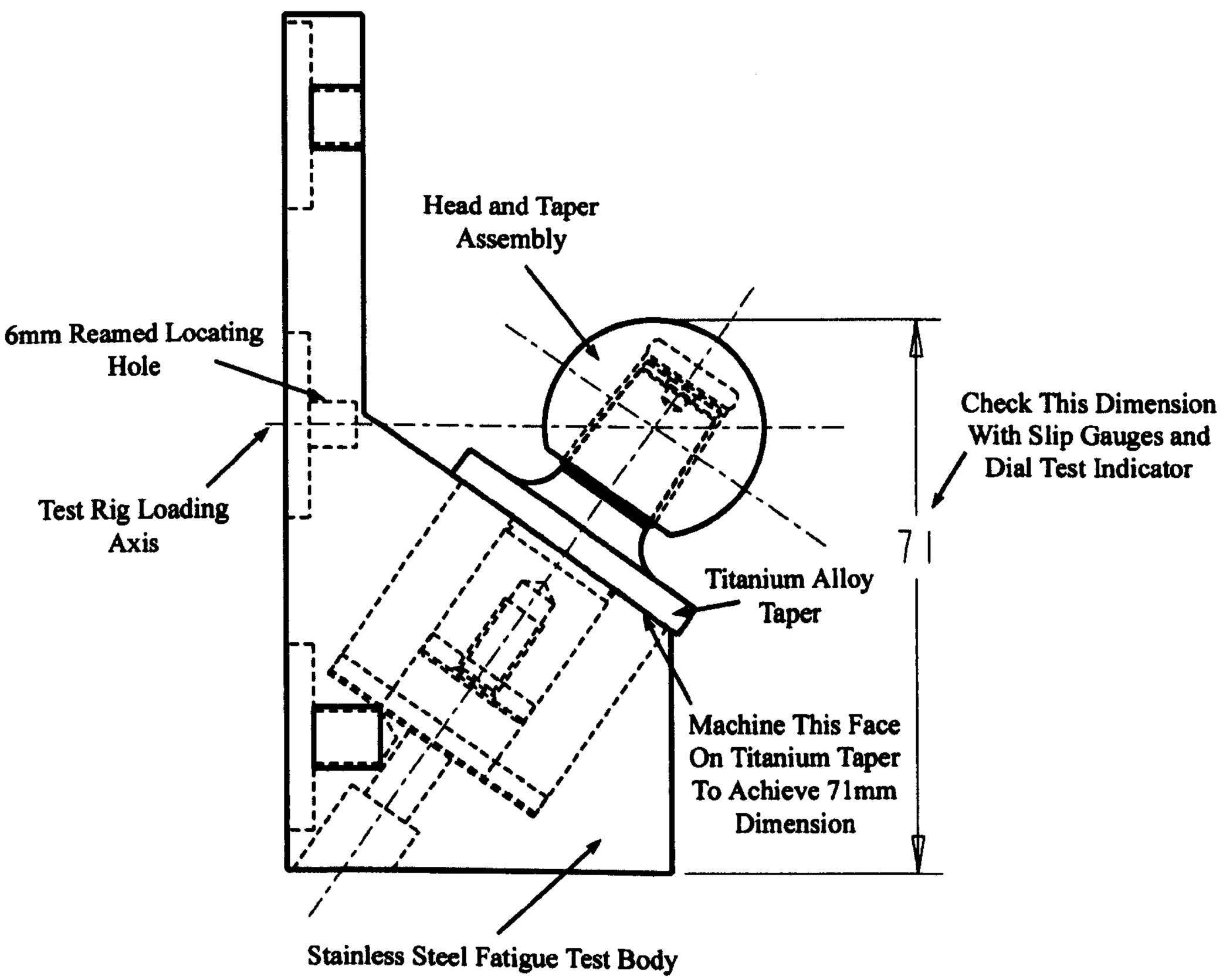

Fig. 36 Engineering drawing for final fitting of taper/head assembly

To achieve alignment, simple trigonometry was used to calculate the amount of material to be removed from the titanium alloy taper. Due to the notch sensitivity of titanium alloy, care was taken in machining the taper. Any undercutting of the titanium alloy taper would make the taper highly likely to fail during fatigue testing.

4.3 Test Environment

To simulate the corrosive nature of bodily fluids, the fatigue testing was undertaken in an aerated bath of Ringer's solution (Fig. 29 page 51). The sample was submerged in a small bath of Ringer's solution at a temperature of 37°C. An electric pump continuously circulated the heated Ringer's solution from a 20 litre insulated tank to the small bath containing the test sample. The solution returned to the main tank by gravity.

The Ringer's solution consists of:

Deionised Water	20 Litres
Sodium Chloride	172 grams
Calcium Chloride Hexahydrate	6.4 grams
Potassium Chloride	6 grams

Table 7 Constituent parts of Ringer's solution

Any loss during testing due to evaporation was replenished with deionised water.

4.4 Mechanical Testing Procedures

The modularity of the proposed mechanical test rigs allowed multiple tests to be carried out on a single mounted sample. An example of the many benefits of this modularity is the ability to run a fatigue test followed an UCS test to determine what effect, if any, the cyclic loading had on the sample's UCS. This section describes the procedure proposed for each type of mechanical test. A simple sinusoidal waveform was used for the loading of the specimen, but advanced load and velocity profiles to simulate activities such as stumbling and falling were possible via LabVIEW software (National Instruments, Newbury, UK).

4.4.1 Fatigue Test Procedure

1. If not mounted from a previous test, mount the acetabular prosthesis for testing (4.2.1page 60).
2. Place the mounted acetabular prosthesis in Ringer's solution for a minimum of 24 hours to acclimatise (4.3 page 63).
3. Fit the femoral head to the titanium alloy tapers and axially load to seat the head (4.2.2 page 62).
4. Assemble the mounted specimen to the fatigue rig using new ground dowel and split pins (Fig. 29 page 51).
5. Under load control, load the specimen at a rate of 0.1 kN/sec to the required fatigue load. This loading ensures all components are fully seated and that the specimen would not fail under static loading.
6. Unload the specimen and start the fatigue test at the required sinusoidal load and R value.
7. Observe stroke and load values. Upon any anomalous values of the load or stroke, suspend the test, remove the test sample and physically inspect bearing surfaces for failure using dye-penetrant.
8. Suspend the test, remove the test sample and physically inspect bearing surfaces for failure every 1.5 million cycles using dye-penetrant.
9. Replace the precision ground dowel holding the mounted sample every 6 million cycles so as to avoid fatigue failure of this component.
10. Run test to failure of the mounted component or until the desired number of cycles is achieved.

4.4.2 Ultimate Compressive Strength Test Procedure

1. If not mounted from a previous test, mount the acetabular prosthesis for testing (4.2.1page 60).
2. Assemble femoral head in the UCS test rig. To avoid possible alumina head failure when UCS test is to failure, use cobalt-chrome or high nitrogen stainless

steel head assembly. If UCS testing with an alumina head is required, fit the alumina head to the titanium alloy tapers and axially load to seat the head (4.2.2 page 62).

3. Install mounted acetabular cup on roller base and align with top of UCS rig (Fig. 31 page 55).
4. Lightly seat femoral head in acetabular cup by lowering the servo-hydraulic ram.
5. Load the acetabular cup at the desired rate until either acetabular cup failure or the desired UCS load is achieved. Check for failure using dye-penetrant.

4.4.3 Torque Test Procedure

1. If not mounted from a previous test, mount the acetabular prosthesis for testing (4.2.1page 60).
2. Assemble the desired femoral head onto the torque rig and axially load to seat the head (Fig. 33 page 58 and 4.2.2 page 62).
3. Install mounted acetabular cup on fixed base and align with top of torque rig (Fig. 33 page 58).
4. Lightly seat femoral head in acetabular cup by lowering the servo-hydraulic ram.
5. Load the acetabular cup to the desired axial load and hold.
6. Rotate the torque gauge, note at what torque either head or alumina bearing rotation occurs.
7. Test failure is defined as rotation of the alumina cup within the composite backing.

4.5 Fatigue Crack Microscopy Study

4.5.1 Acetabular Prosthesis Preparation For Microscopic Study

The hemispherical shape of the acetabular prosthesis alumina bearing creates difficulties in examining the surface. Difficulties arise due to the small radius of the bearing surface, making it impossible for the objective lens to get close to the damaged area without impinging. To resolve this problem the sample was sectioned to allow access to the damaged area.

The sample was removed from the acetal mount by means of the central 8mm axis hole (Appendix A2.2 page 138). Sectioning was carried out on an Accutom 5 precision cut-off machine with a 330CA diamond coated blade (Struers Ltd. Glasgow, UK) and is shown in Appendix 3.

Advice was sought from Struers Ltd. (Glasgow, UK) on the best procedure for cutting the novel combination of hard alumina bearing and tough carbon reinforced PEEK backing. Their recommendations are shown in Table 8.

Cut-off Wheel:	330CA	Force:	High
Speed:	3000 rpm	Rotation:	Oscillation
Feed:	0.035 mm/sec	Oscillation Angle:	10°

Table 8 Accutom 5 parameters for sample sectioning

Test samples that show a large amount of cracks from testing and prior to sectioning may be vacuum impregnated with Epofix (Struers Ltd. Glasgow, UK). Vacuum impregnation of the sample prevents the possibility of further damage from the sectioning procedure.

4.5.2 Optical Microscopy

Microscopic inspection was conducted on an Olympus BX60 Microscope with the advantage of videotext overlay Appendix 3. The microscope with videotext overlay (shown in Appendix 3) enables measurement of surface features under examination but with the disadvantage of low magnification (maximum 1000x).

4.6 Mechanical Failure Criteria

Since it is impractical to test every material with every combination of stresses, failure theories were developed based on the material's performance during a tensile test. These theories are not derivable laws, but tend to be unifying accounts of experimental data (Adams and Askenazi 1999). These 'classic' failure theories or criteria allow the determination of failure with complex stress states that are typical in engineering components. Sometimes one of these theories is modified empirically in order to obtain better agreement with experimental data (Juvinall and Marshek 2000). Table 9 displays a selection of classic failure criteria and shows the same criteria can often be known by several names.

Maximum Stress Criterion or Maximum Normal Stress Theory or Rankine Criterion
Maximum Shear Stress Theory or Tresca's Theory or Guest's Law
Maximum-Distortion-Energy-Theory or Maximum-Octahedral-Shear-Stress Theory or Von Mises-Hencky Theory
Coulomb-Mohr Theory
Modified Mohr Theory

Table 9 Examples of classic failure criteria

Not all failure criteria are suited to all materials and are normally separated for use with ductile and brittle materials. The figure below (Fig. 37) shows comparison of three ductile failure theories (left) and three brittle failure theories (right)

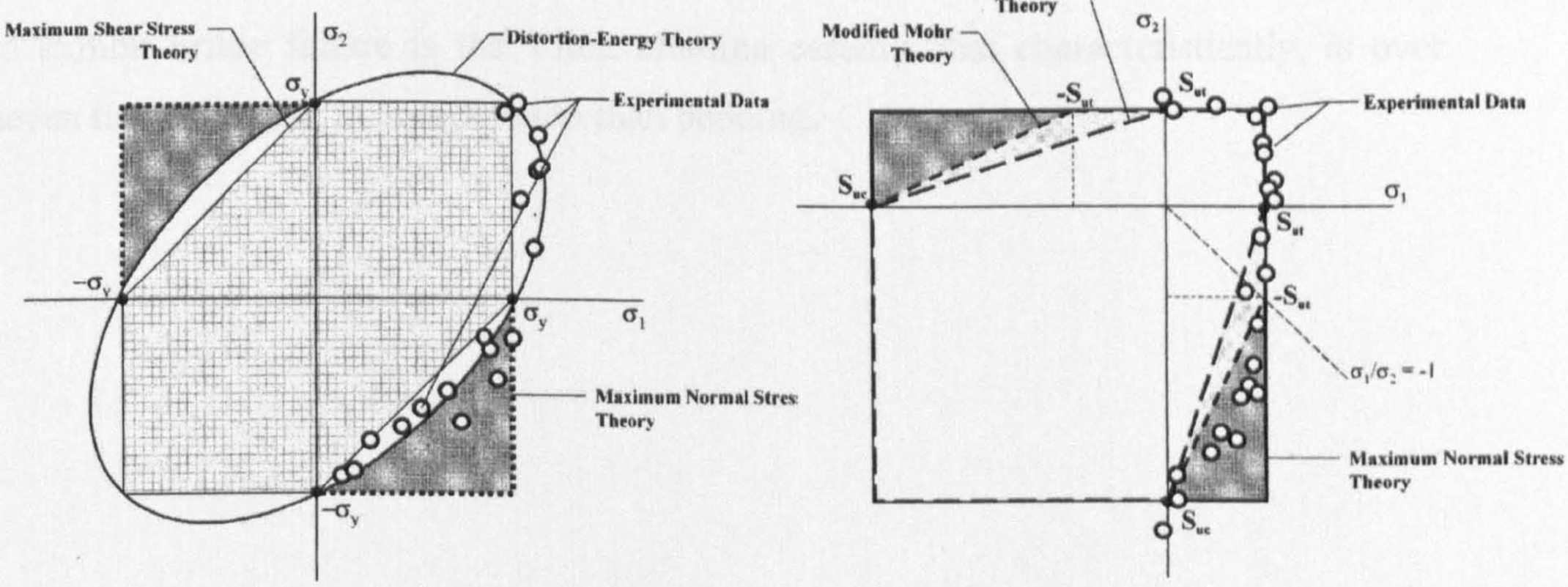

Fig. 37 Ductile failure theories (left),
brittle failure theories (right)
(Adams and Askenazi 1999)

Ductile failure is characterised by slow crack or void propagation after significant plastic deformation. Von Mises-Hencky (Distortion energy) theory is probably the most widely used ductile theory and has the best match with experimental data (Adams and Askenazi 1999). The Von Mises-Hencky stresses are available in the majority of FEA packages and the non-directional nature allows quick interpretation of the results. The stress quantity is calculated from Equation 4-1 and failure occurs when the Von Mises stress is greater or equal to the materials yield strength

$$\sigma_{vm} = \left[\frac{(\sigma_1 - \sigma_2)^2 + (\sigma_2 - \sigma_3)^2 + (\sigma_1 - \sigma_3)^2}{2} \right]^{1/2}$$

Equation 4-1

Von Mises-Hencky will be used in this study to describe materials that exhibit ductile failure.

Brittle failure is generally characterised by the lack of plastic deformation before fracture and usually much greater strength in compression than tension. Maximum normal stress theory will be used in this study, mainly due to its simplicity but also as this theory correlates reasonably well with test data for brittle fractures (Juvinall and

Marshek 2000). Brittle failure occurs when the normal stress is greater or equal to the ultimate compressive or ultimate tensile strength. The only material in this study likely to exhibit brittle failure is the Vitox alumina ceramic that characteristically, is over seven times stronger in compression than bending.

5 EXPERIMENTAL RESULTS

5.1 Proving of Conceptual Design Using Finite Element Analysis

This section deals with proving that the proposed concept is viable for human implantation and that the design offers improvement over the current state of the art. Finite Element Analysis was used to compare the stress distribution in the subchondral bone adjacent to prostheses. FEAs were undertaken on two designs and five combinations of materials. FEA of the natural hip was also included as a benchmark for the stress distributions.

5.1.1 Introduction

Finite element analysis of THR and the surrounding bone has been undertaken since the 70's (see Section 1.4.1 page 6). The majority of early work concentrated on the femur and femoral prosthesis, which lends itself better to two-dimensional FEA (2D FEA). Whilst 2D FEA and Axisymmetric FEA have been undertaken incorporating the acetabulum, it is widely recognised that these models are limited by their inability to accurately represent anatomic loading and structure of the acetabulum and pelvis (for example Dalstra and Huiskes 1995). A 2D model cannot account for the out-of-plane part of the acetabular wall and will therefore be too flexible. The opposite is true for an axisymmetric model due to the required assumption of a 360 degree acetabular wall (Rapperport, Carter et al. 1987; Dalstra and Huiskes 1995; Dalstra, Huiskes et al. 1995). The pelvis is a complex three-dimensional structure with multiple muscle attachments and interactions with other skeletal structures. The pelvic bone has evolved into a very efficient 'sandwich' structure, which is well able to carry forces that are multiple that of body weight. Quantative accuracy, even with 3D models, can never be assured because of anthropometric differences between patients. Ignoring anthropometric differences, but considering how many potential sources of errors are present in such a complex model, experimental validation is always recommended (Bernakiewicz and Viceconti 1999; Viceconti, Muccini et al. 1999). Very few authors have created 3D models including the complex loading and geometry required to quantitatively determine the stress distributions in a rigorous manner and validated them with mechanical testing.

Dalstra and Huiskes et al. (1995; 1995) have produced complex 3D models that have incorporated model validation, but 3D models are not suited to parametric studies due their complex nature. The production of accurate 3D models is becoming easier due to advances in technologies such as 3D, Computer Tomography (CT) and Dual-Energy X-Ray Absorptiometry (DEXA) scanners, but validation using cadavers is outside the scope of this study.

A 2D parametric FEA study was undertaken by the author to compare the stress distribution in the acetabulum of the proposed composite and ceramic cup with other prostheses and the natural hip. A 2D FEA has the advantage that a much finer mesh can be created economically, proving basic concepts before more elaborate and expensive 3D analyses are pursued. These admittedly simple models offer insight into the effect prosthesis design and material selection have on stress distribution in the subchondral bone and pelvis. These stress values will have significant influence on the way the body remodels that area and therefore the impact on the long-term survival of the THR (Wolff's law, see section 1.4.1). Although there are many significant factors involved in the biological response, this study addresses only those that are stress related. Whilst the study was predominately parametric in nature, loads and boundary conditions were applied in a manner that could give semi-quantative results.

5.1.2 Method

The finite element models of the acetabulum were based on the 2D FEA models of several authors (Pedersen, Crowninshield et al. 1982; Vasu, Carter et al. 1982; Rapperport, Carter et al. 1985; Rapperport, Carter et al. 1987; Levenston, Beaupré et al. 1993). The geometry for the model was generated from a 4mm slice cut normal to the acetabulum through the pubis and ilium. The 2D slice, shown in Fig. 38 is subsequently modelled with 12 regions to account for the varying material properties of the hip. Material regions were assumed isotropic, and their Young's modulus and Poisson's ratio are displayed in Table 10.

Boundary conditions are similar to the deformable boundary conditions described by Rapperport et al. (1985) and more accurately reflect natural boundary conditions than rigid boundary conditions. The pubic symphsis was allowed to displace in the sagittal plane whilst the sacroiliac joint was free to displace only in the plane of the joint. The extreme margin of the ilium was rigidly fixed (see Fig. 38).

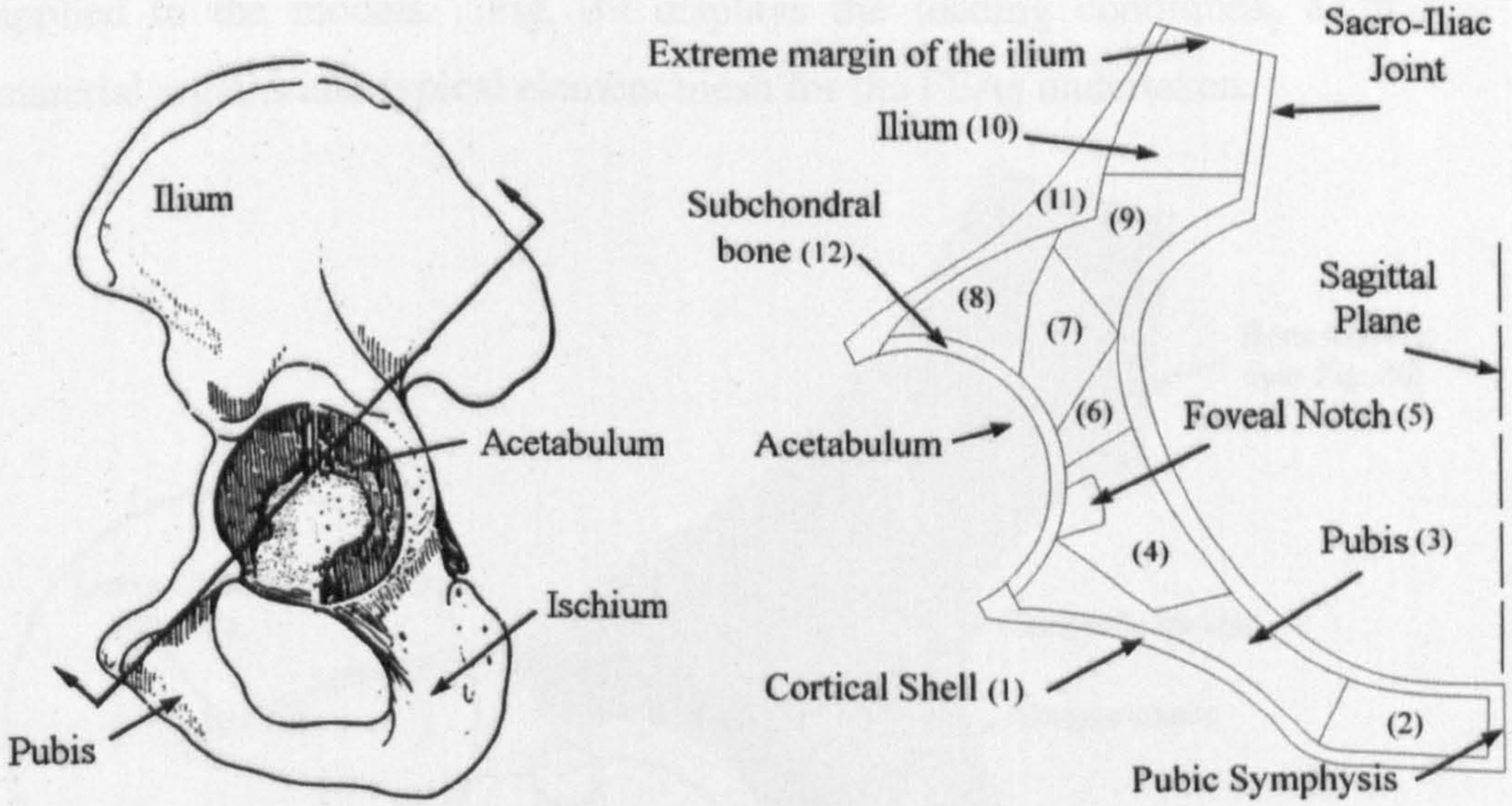

Orientation of the FEA model slice
Adapted from Rapperport et al. (1987)

Material property regions for use in the FEA Models

Fig. 38 Orientation and material property regions for FEA models

Material/Region	Young's Modulus (MPa)	Poisson's Ratio	Material/Region	Young's Modulus (MPa)	Poisson's Ratio
Cortical Bone (1)	1100	0.3	Cortical Bone (11)	1100	0.3
Cancellous Bone (2)	80	0.2	Subchondral Bone (12)	700	0.3
Cancellous Bone (3)	400	0.2			
Cancellous Bone (4)	300	0.2	PEEK 450CA30	13000	0.44
Foveal Notch (5)	200	0.2	PEEK (Unfilled)	3500	0.4
Cancellous Bone (6)	400	0.2	Vitox (Alumina)	400000	0.23
Cancellous Bone (7)	500	0.2	Ti-6Al-4V (Grade 5)	113800	0.342
Cancellous Bone (8)	600	0.2	UHMWPE	850	0.3
Cancellous Bone (9)	450	0.2	Cartilage	15	0.45
Cancellous Bone (10)	80	0.2			

Table 10 Mechanical properties of materials used in FEA

The loading was applied to the modelled proximal part of the femur or the femoral component and boundary conditions were imposed that would allow displacement only along the direction of loading. Loading in this manner, well away from the acetabular prosthesis's interface with the subchondral bone, allows the stresses in this area to be well calculated. The load at an angle of 20° medial of vertical represents typical early phase loading during walking. The load magnitude of 89.9N was determined to be anatomically correct for similar boundary condition by Vasu et al. (1982) and was

applied to the models. Fig. 39 displays the loading conditions, additional model material regions and typical element mesh for the FEAs undertaken.

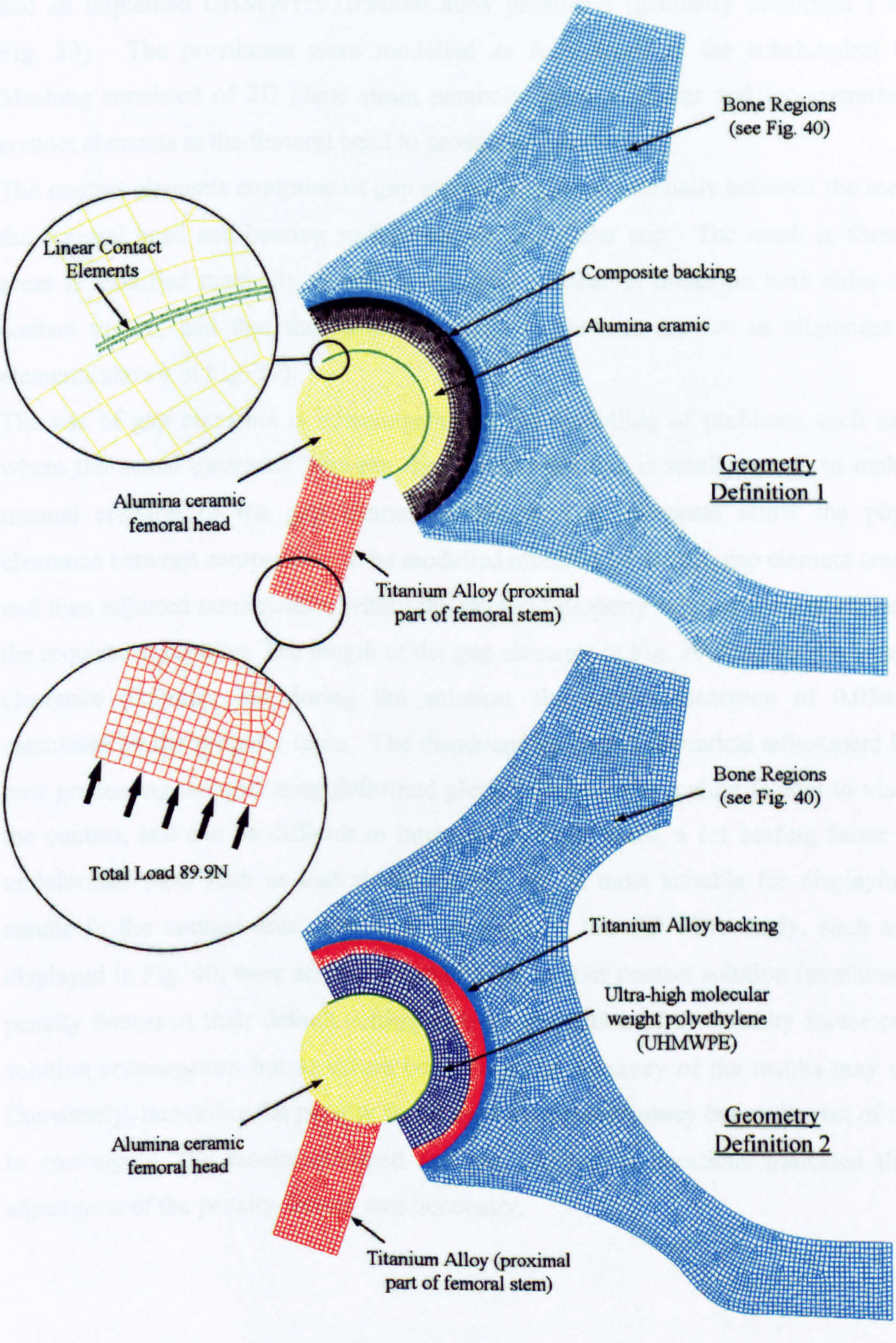

Fig. 39 Loading, contact elements and meshes used in 2D FEA

The geometries modelled simulated the proposed alumina/PEEK prosthesis implanted and an implanted UHMWPE/Titanium alloy prosthesis (geometry definition 1 and 2 Fig. 39). The prostheses were modelled as fully fixed to the subchondral bone. Meshing consisted of 2D plane strain parabolic brick elements and incorporated 101 contact elements at the femoral head to prosthesis interface.

The contact elements comprise of gap elements inserted manually between the mesh of the femoral head and bearing surface on the acetabular cup. The mesh in these two areas is modified manually to ensure an equal number of nodes on both sides of the contact region, and that the surface normals at these nodes are in alignment (gap elements shown in Fig. 39).

The use of gap elements is advantageous in the modelling of problems such as this, where the actual clearance between the two components is small enough to make the manual creation of the gap elements difficult. Gap elements allow the physical clearance between components to be modelled much larger (to aid gap element creation) and then adjusted numerically, within the physical property table of the gap element, to the required separation. The length of the gap elements in Fig. 39 displays this increased clearance (0.5mm), but during the solution, the correct clearance of 0.05mm is calculated by the property table. The disadvantage of this numerical adjustment is that post processing incorporating deformed plots requires large scaling factors to visualise the contact, and can be difficult to interpret. In these cases, a 1:1 scaling factor or an undeformed plot, such as that shown in Fig. 40, is most suitable for displaying the results in the contact area. The final solutions in this 2D FEA study, such as that displayed in Fig. 40, were achieved within three or four contact solution iterations, with penalty factors at their default setting of ten. Reduction of the penalty factor can aid solution convergence, but at values below one the accuracy of the results may suffer. Conversely, increasing the penalty factor may increase accuracy but at the risk of failing to converge. The results obtained and the number of iterations indicated that no adjustment of the penalty factors was necessary.

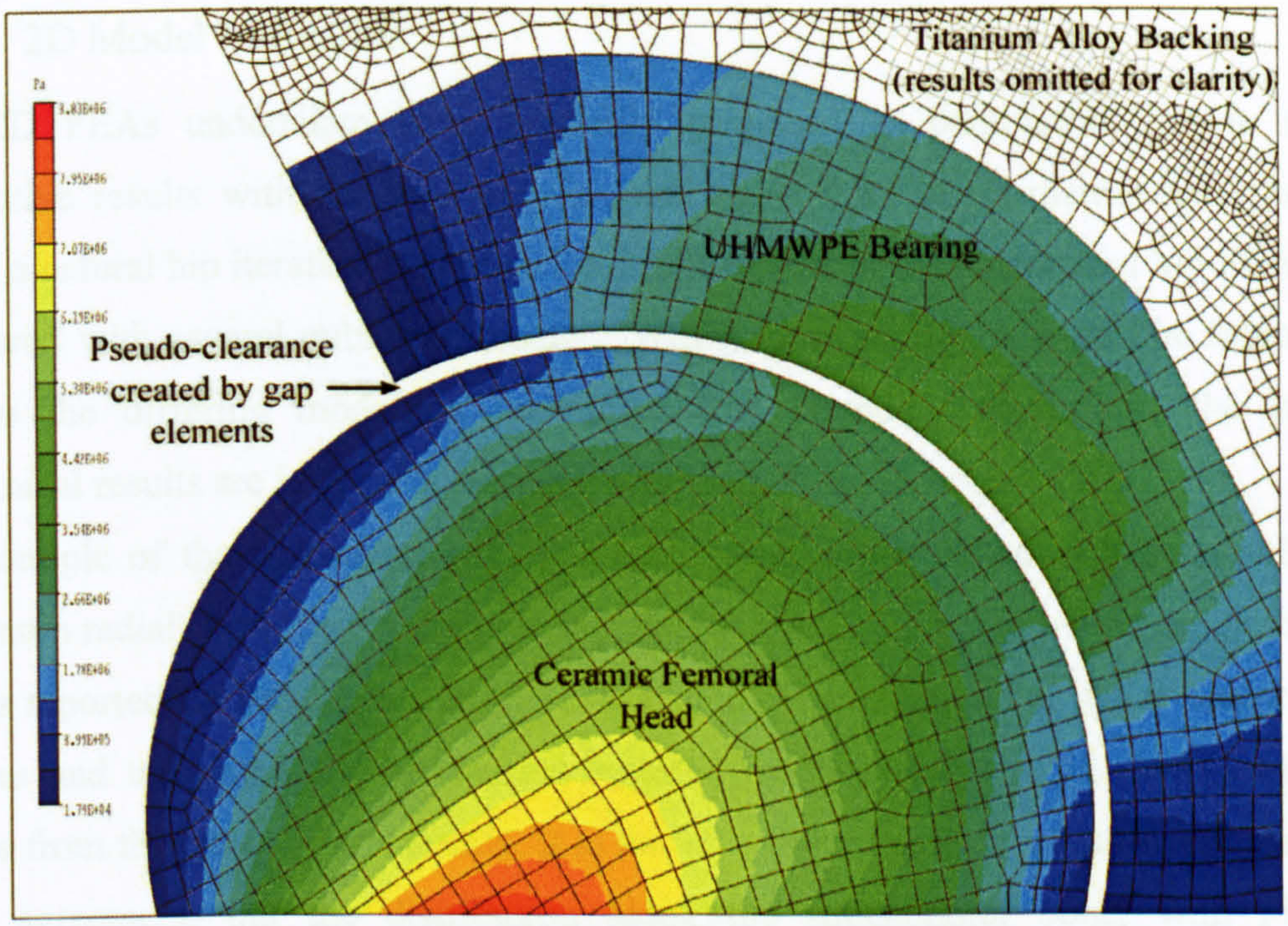

Fig. 40 Example undeformed Von Mises stress plot of contact region

The contact, evident by the stress distributions in the two components (Fig. 40), ensures that the applied load is accurately transferred to the acetabular cup and therefore to the area of interest in this study; the bone/prosthesis interface.

Further material iterations of the two FEA models (Fig. 39) gave an additional four simulations, including a natural hip and other common prostheses (Table 11).

Prosthesis or Model type	Geometry definition used (see Fig. 38)	Prosthesis backing material	Prosthesis bearing material	Femoral head material	Material of proximal femoral region	Number of parabolic brick elements	Number of contact elements
Composite/Ceramic (Proposed)	Def. 1	PEEK 450CA30	Vitox Alumina	Vitox Alumina	Ti-6Al-4V	12201	101
Titanium alloy/UHMWPE	Def. 2	Ti-6Al-4V	UHMWPE	Vitox Alumina	Ti-6Al-4V	11158	101
Natural Hip	Def. 1	Cartilage		Cortical bone	Cortical bone	12201	101
Titanium alloy/Ceramic	Def. 2	Ti-6Al-4V	Vitox Alumina	Vitox Alumina	Ti-6Al-4V	11158	101
Solid Ceramic	Def. 1	Vitox Alumina		Vitox Alumina	Ti-6Al-4V	12201	101
Unfilled Peek/Ceramic	Def. 1	Unfilled PEEK	Vitox Alumina	Vitox Alumina	Ti-6Al-4V	12201	101

Table 11 FEA iterations and mesh details

5.1.3 2D Model Validation

The 2D FEAs undertaken were primarily proposed as parametric, but to obtain qualitative results with previous authors, and 'base line' stress distributions for this study, a natural hip iteration was modelled. The results of the anatomical hip FEA were compared with several published results. Whilst an exact match would be impossible due to the differing modelling techniques and boundary conditions, the study's anatomical results are in good agreement with the published work.

An example of the agreement with published work is displayed in Fig. 41 with the maximum radial compressive stress in the natural hip model being within ten percent of results reported by Rapperport et al. (1987). Fig. 41 compares the radial compressive stresses and tangential tensile stresses reported by Rapperport et al. (1987) with the results from this study. Importantly, it is not only the magnitude of the stress that is in close agreement, but the distribution along the subchondral bone, with Fig. 41 displaying similar stress distribution to that of Rapperport et al. (1987).

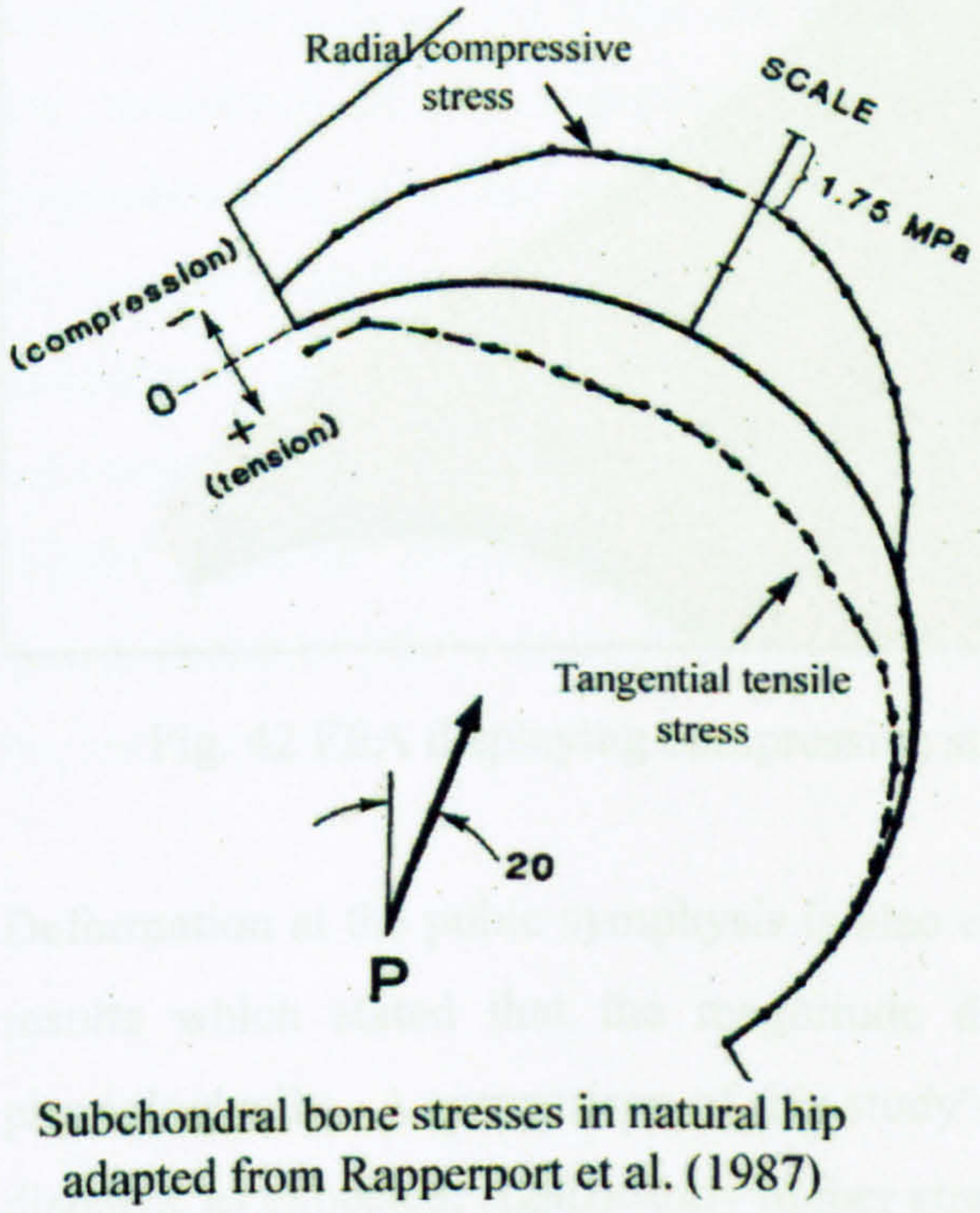

Subchondral bone stresses in natural hip adapted from Rapperport et al. (1987)

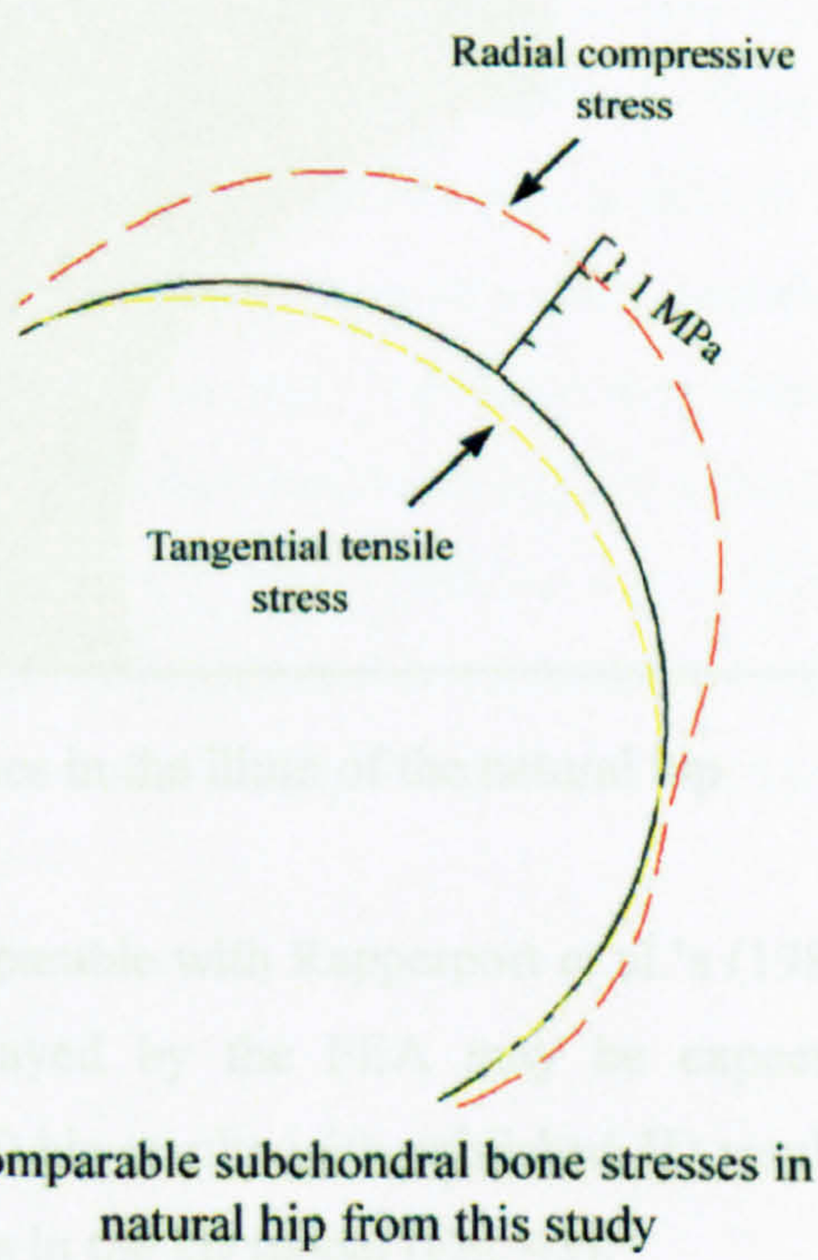

Comparable subchondral bone stresses in natural hip from this study

Fig. 41 FEA results of the stress distributions in the natural acetabulum

The results from this study also exhibited similar stress characteristics in the ilium to those of Rapperport et al.'s earlier work (Rapperport, Carter et al. 1985) and are displayed in Fig. 42 which shows the high compressive stresses transferred to the ilium cortical shell, where the majority of the load is known to be transferred to (Dalstra and Huiskes 1995).

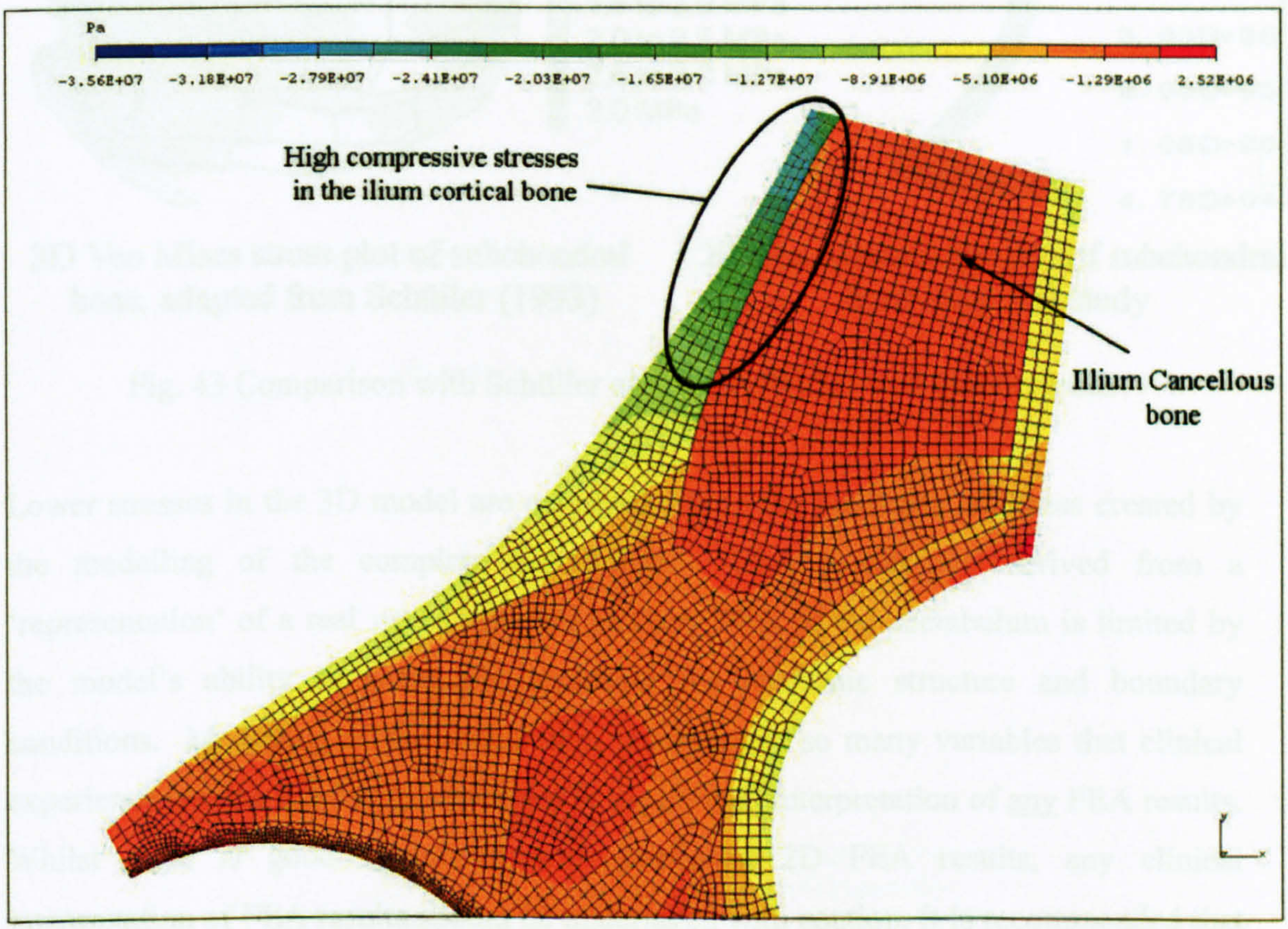

Fig. 42 FEA displaying compressive stresses in the ilium of the natural hip

Deformation at the pubic symphysis is also comparable with Rapperport et al.'s (1985) results which stated that the magnitude displayed by the FEA may be expected physiologically. A comparison of this study's 2D hip results with published 3D results, displays, as expected, significantly higher stresses in the 2D model (Fig. 43).

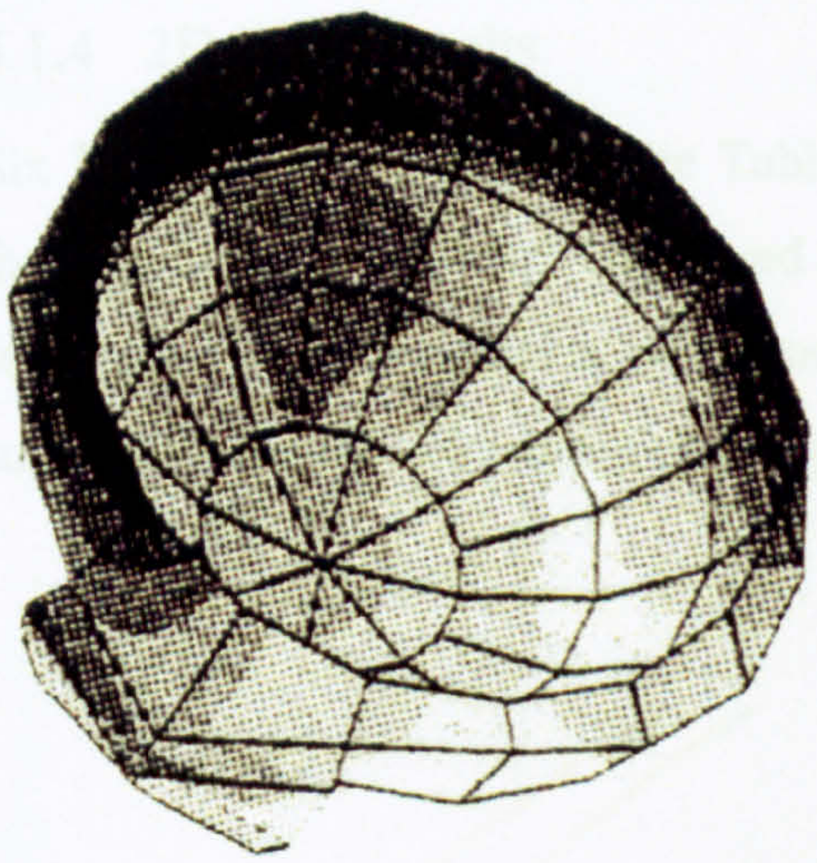

3D Von Mises stress plot of subchondral bone, adapted from Schüller (1993)

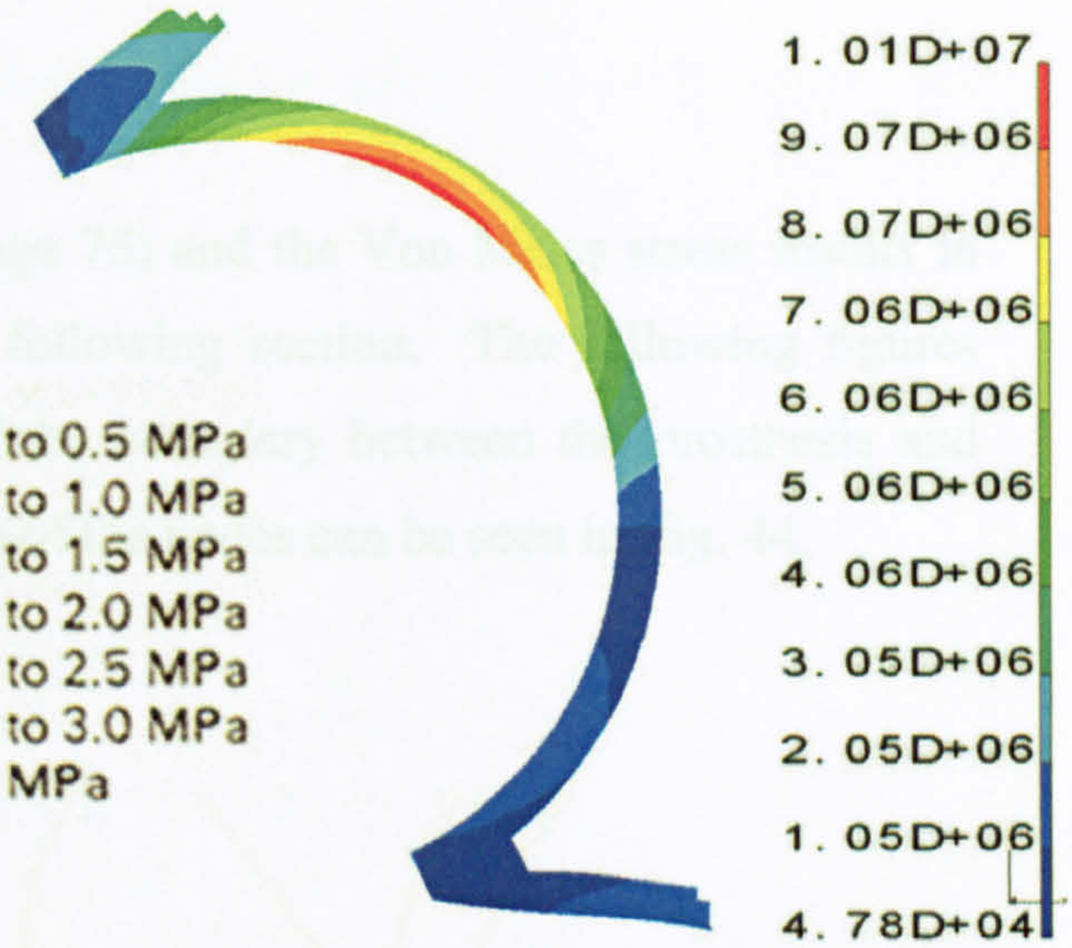

2D Von Mises sress plot of subchondral bone from this study

Fig. 43 Comparison with Schüller et al's. (1993) 3D Von Mises results

Lower stresses in the 3D model are expected due to the additional stiffness created by the modelling of the complete acetabulum. FEA results are derived from a 'representation' of a real world problem and any FEA of the acetabulum is limited by the model's ability to accurately represent the anatomic structure and boundary conditions. Modelling of the acetabulum incorporates so many variables that clinical experience may be extremely important in the clinical interpretation of any FEA results. Whilst there is good agreement with published 2D FEA results, any clinical interpretation of FEA results should be undertaken with caution. It is recommended that the results presented here should be viewed as a parametric study as originally intended.

5.1.4 2D FEA Results

Six FEAs were undertaken (see Table 11 page 75) and the Von Mises stress results in the subchondral bone are displayed in the following section. The following figures represent Von Mises stress at the nodes of the boundary between the prosthesis and subchondral bone. The approximate position of the nodes can be seen in Fig. 44.

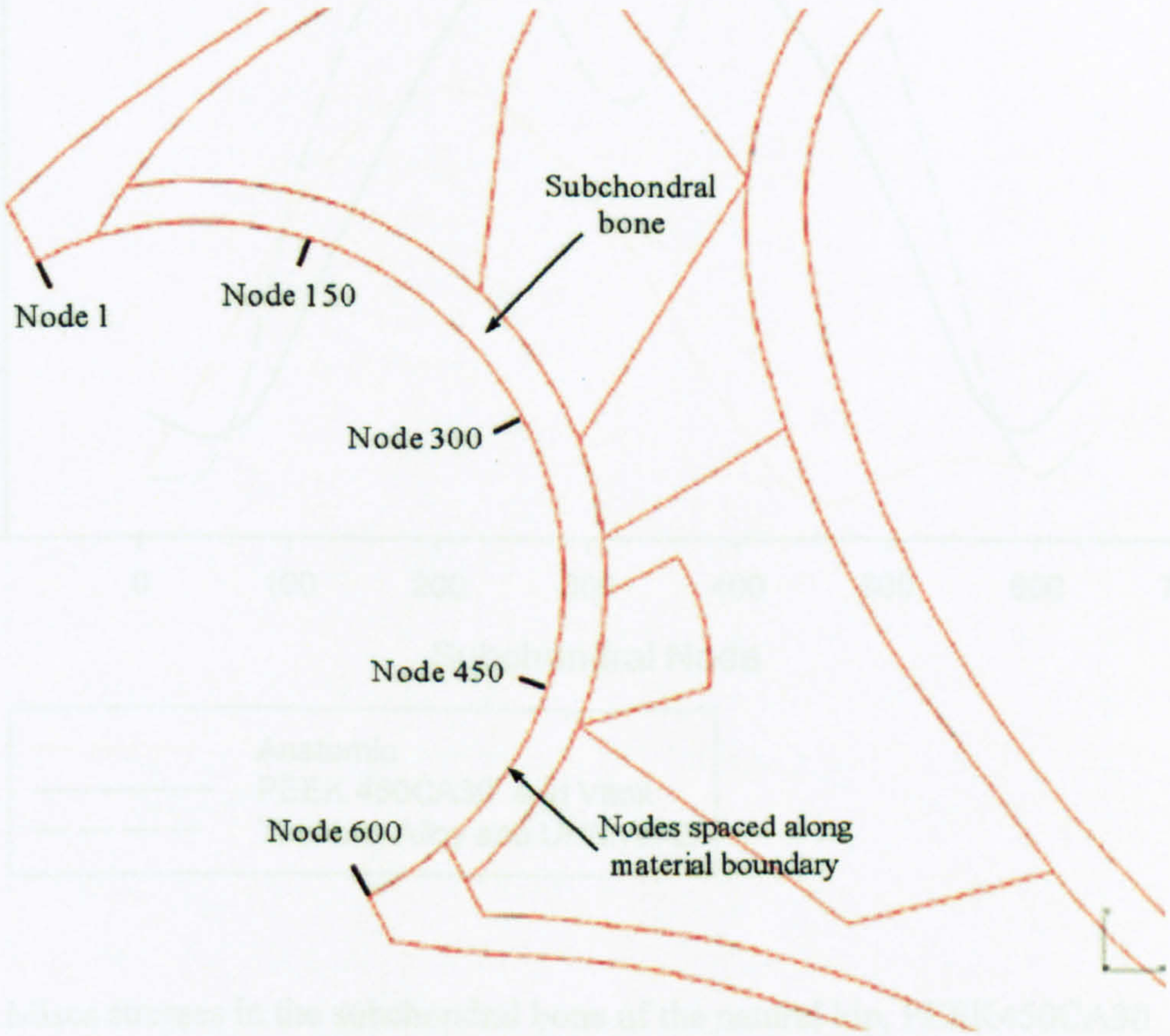

Fig. 44 Approximate position of nodes at prosthesis to subchondral bone interface

Results for the implanted PEEK450CA30/Vitox, Titanium alloy/UHMWPE prostheses and the natural hip are displayed in Fig. 45.

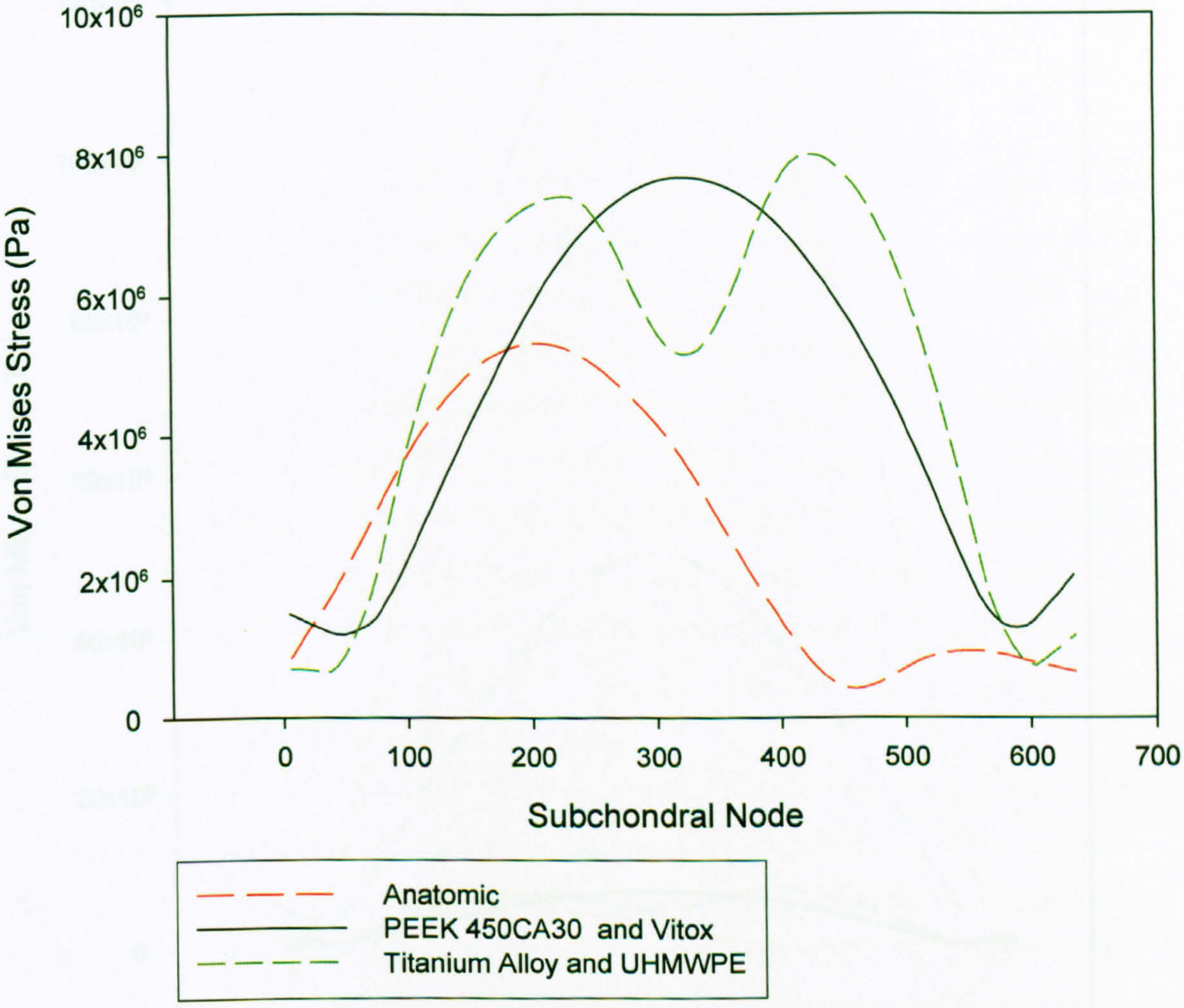

Fig. 45 Von Mises stresses in the subchondral bone of the natural hip, PEEK450CA30 backed and Vitox prosthesis and Titanium alloy backed and UHMWPE prosthesis

The PEEK 450CA30 backed Vitox prosthesis proposed by the author creates slightly less Von Mises stress in the subchondral bone than the traditional titanium alloy backed UHMWPE prosthesis, and over 40% more than the natural hip (Fig. 45). Using the same FEA meshes as displayed in Fig. 39, but changing the materials, allowed comparisons with other prostheses types that incorporate a ceramic bearing couple. A solid Vitox prosthesis and a titanium alloy backed prosthesis with a Vitox liner were simulated and the results are displayed in Fig. 46

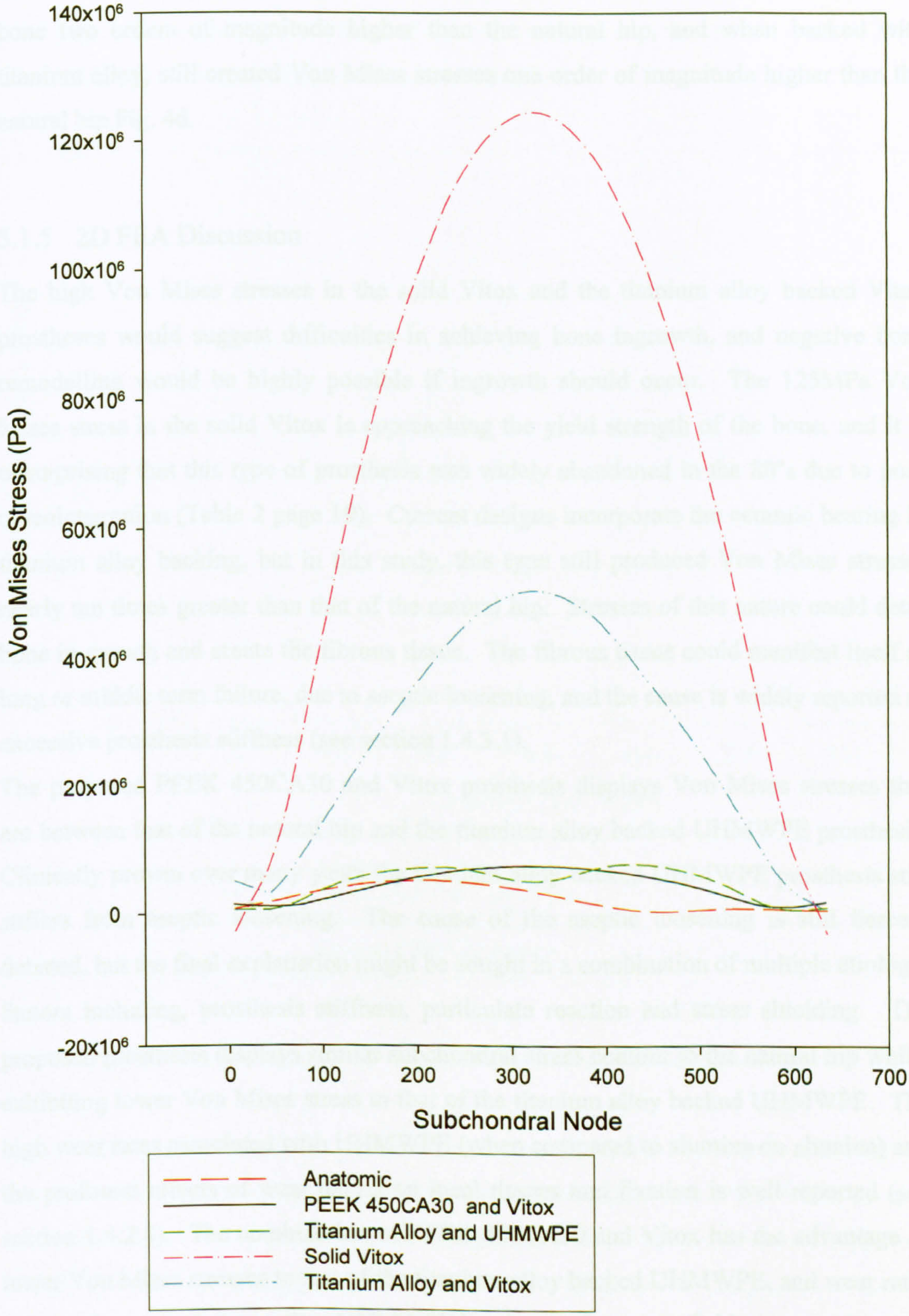

Fig. 46 Von Mises stresses in the subchondral bone of Titanium alloy backed and Vitox prosthesis, solid Vitox prosthesis and prostheses / natural hip from Fig. 45

Simulation of the solid Vitox prosthesis created Von Mises stresses in the subchondral bone two orders of magnitude higher than the natural hip, and when backed with titanium alloy, still created Von Mises stresses one order of magnitude higher than the natural hip Fig. 46.

5.1.5 2D FEA Discussion

The high Von Mises stresses in the solid Vitox and the titanium alloy backed Vitox prostheses would suggest difficulties in achieving bone ingrowth, and negative bone remodelling would be highly possible if ingrowth should occur. The 125MPa Von Mises stress in the solid Vitox is approaching the yield strength of the bone, and it is unsurprising that this type of prosthesis was widely abandoned in the 80's due to poor osseointegration (Table 2 page 19). Current designs incorporate the ceramic bearing in titanium alloy backing, but in this study, this type still produced Von Mises stresses nearly ten times greater than that of the natural hip. Stresses of this nature could deter bone in growth and create the fibrous tissue. The fibrous tissue could manifest itself as long or middle term failure, due to aseptic loosening, and the cause is widely reported as excessive prosthesis stiffness (see section 1.4.3.1).

The proposed PEEK 450CA30 and Vitox prosthesis displays Von Mises stresses that are between that of the natural hip and the titanium alloy backed UHMWPE prosthesis. Clinically proven over many years the titanium alloy backed UHMWPE prosthesis still suffers from aseptic loosening. The cause of the aseptic loosening is still fiercely debated, but the final explanation might be sought in a combination of multiple etiologic factors including, prosthesis stiffness, particulate reaction and stress shielding. The proposed prosthesis displays similar subchondral stress contour to the natural hip whilst exhibiting lower Von Mises stress to that of the titanium alloy backed UHMWPE. The high wear rates associated with UHMWPE (when compared to alumina on alumina) and the profound effects of wear debris on local tissues and fixation is well reported (see section 1.4.2.4). The combination of PEEK 450CA30 and Vitox has the advantage of lower Von Mises stresses to that of the titanium alloy backed UHMWPE, and wear rates orders of magnitude lower than UHMWPE bearing surfaces (see Table 1 page 17). Any alumina wear debris that is created is bioinert and the Von Mises stress in the subchondral bone caused by the PEEK 450CA30 and Vitox prosthesis could be further

reduced by the modification of the volume fraction of the PEEK composite (see Section 2.1.1 page 36). An example of this is shown in Fig. 47, where the use of unfilled PEEK has created Von Mises stresses less than the natural hip.

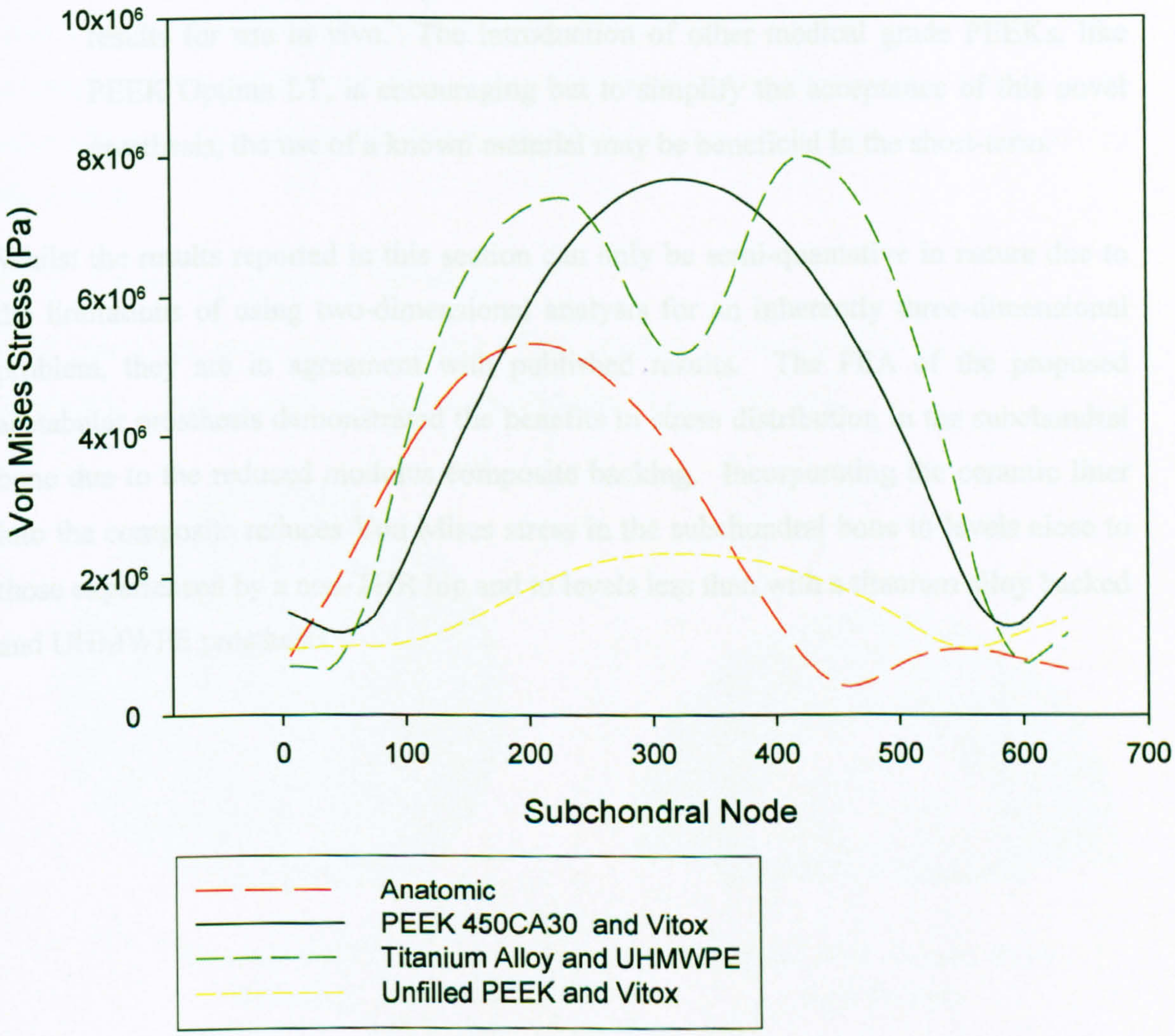

Fig. 47 Further reduced Von Mises stresses by the use of unfilled PEEK

Fig. 47 displays the excellent 'tune-ability' of the prosthesis that can be achieved by altering the volume fraction of the PEEK composite. Although the Von Mises stresses in the PEEK 450CA30 and Vitox prosthesis are lower than the titanium alloy and UHMWPE prosthesis, slightly lowering the stiffness further by adding holes to the composite backing may be beneficial to osseointegration.

This further lowering of the stiffness could easily be achieved by the 'tuning' of the composite, but the addition of the holes had several benefits:

1. The holes would act as additional features for fixation during osseointegration.
2. Although being comparatively new to THR, PEEK 450CA30 does have good results for use in vivo. The introduction of other medical grade PEEKs, like PEEK Optima LT, is encouraging but to simplify the acceptance of this novel prosthesis, the use of a known material may be beneficial in the short-term.

Whilst the results reported in this section can only be semi-quantative in nature due to the limitations of using two-dimensional analysis for an inherently three-dimensional problem, they are in agreement with published results. The FEA of the proposed acetabular prosthesis demonstrated the benefits in stress distribution in the subchondral bone due to the reduced modulus composite backing. Incorporating the ceramic liner into the composite reduces Von Mises stress in the subchondral bone to levels close to those experienced by a non-THR hip and to levels less than with a titanium alloy backed and UHMWPE prosthesis.

5.2 Design and Manufacture Iterations

This section deals with iterations in the acetabular cup prosthesis that proved necessary from early results, namely, moulding trials, mechanical testing or FEA results. Early mechanical testing of the complete system also exposed considerable problems with the taper adaptor. This was an existing Orthodynamic's component that was to be used in the system.

5.2.1 Composite Backing Iterations

CNC machining along with sectioning of the prosthesis revealed voids in the composite backing that were created during the injection moulding (Fig. 48).

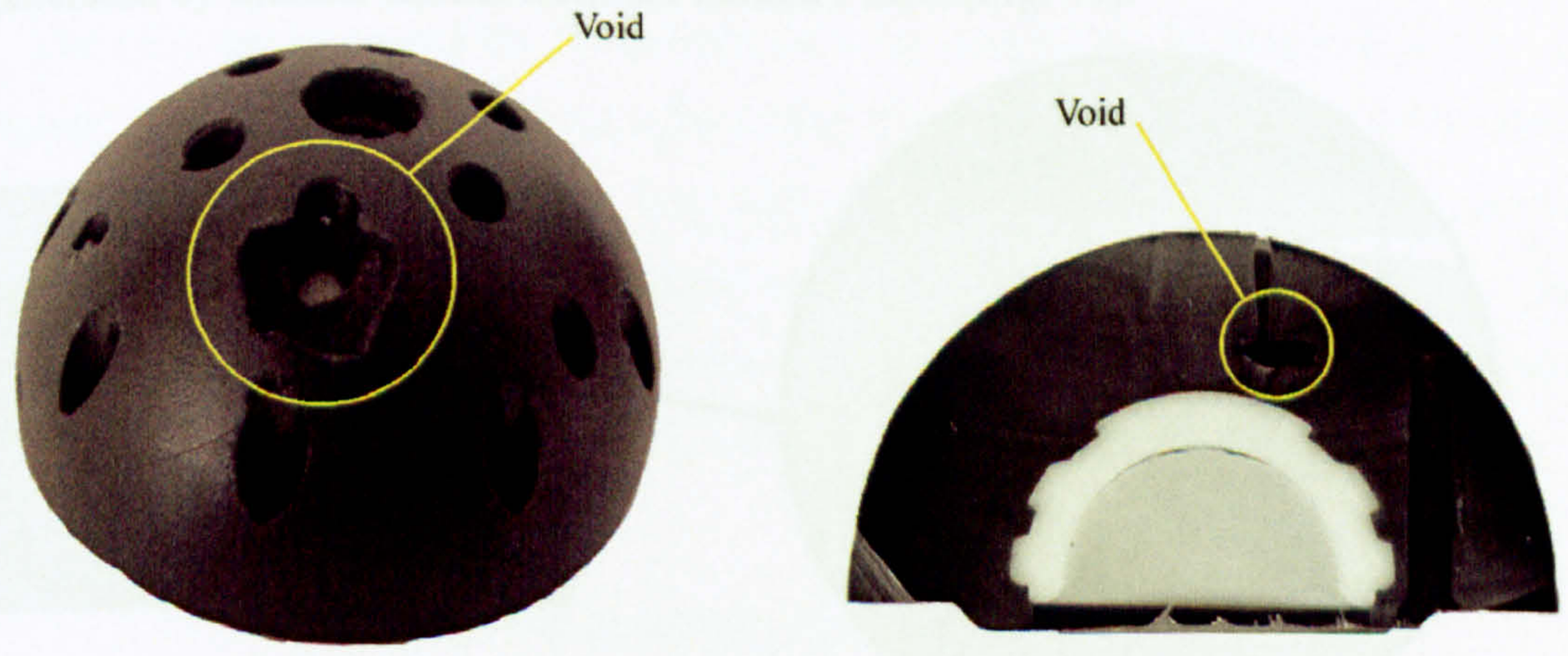

External Void In Moulding

Internal Void Around Blind Hole Feature

Fig. 48 Voids in injection moulding

The injection moulding gate was repositioned and three pins on the rear of the prosthesis near the gate were removed to improve the flow of the PEEK450CA30 during moulding. Further injection moulding trials were undertaken to optimise injection moulding settings to ensure the moulding fills completely (Table 12).

Injection Moulding Settings	Value
Temperature of PEEK	290°C
Mould Temperature	185°C
Pressure	1050 bar

Table 12 Optimised injection moulding settings

5.2.2 Alumina Bearing Iterations

Initial injection moulding runs incorporating the alumina bearing resulted in the appearance of small cracks in the alumina bearing. Investigations revealed the cracks to be generated by thermal shocks from the molten PEEK (Fig. 49).

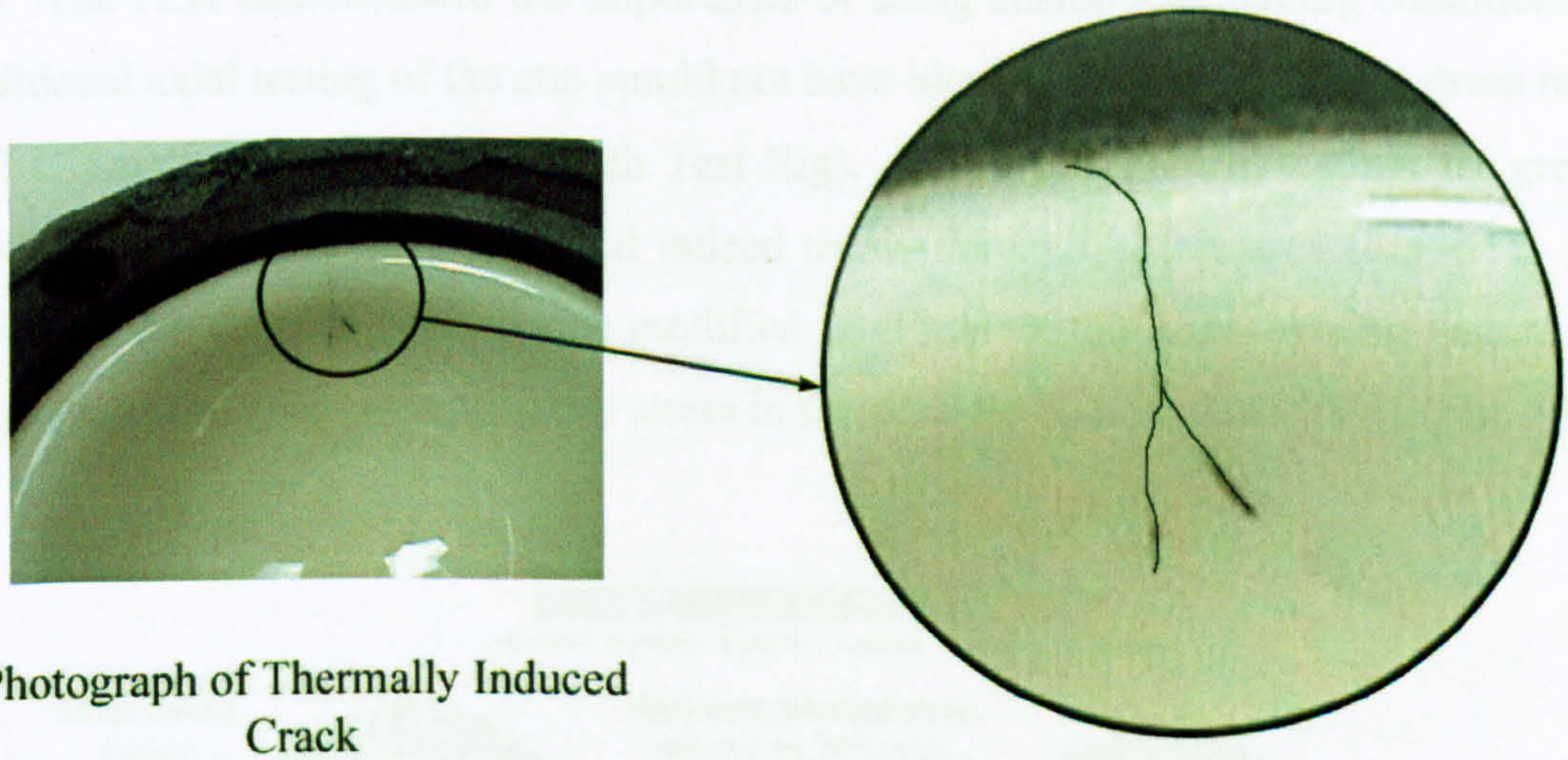

Photograph of Thermally Induced Crack

Close Up View of Crack (Computer Enhanced)

Fig. 49 Images of thermally induced crack in ceramic bearing

Consultation with the ceramic bearing manufactures (Morgan Matroc) determined that a temperature difference of greater than 180°C could cause cracking in the ceramic. The solution to the thermal stresses was pre-heating of the ceramic bearings to 160°C before placement in the mould (mould temp. of 185°C) to ensure a temperature difference of less than 180°C upon filling with PEEK at 290°C. Additional dwell times for the opening and closing of the mould were incorporated to reduce the temperature difference further.

Mechanical interlocking of the PEEK backing and alumina bearing is achieved by the ingress of PEEK during injection moulding into specially designed features in the alumina. Shrinkage of the composite during cooling may enhance this mechanical locking further, and the coefficients of thermal expansion are shown in Table 13.

Material	Linear 20°C	Linear 100°C	Linear 250°C	Linear 1000°C
PEEK 450CA30	14µm/m-°C	14µm/m-°C	30µm/m-°C	----------
Vitox	8.9µm/m-°C	8.9µm/m-°C	8.9µm/m-°C	8.9µm/m-°C

Table 13 Coefficients of thermal expansion for selected prosthesis materials

FEA of the new acetabular prosthesis found that, when loaded anatomically, a locking feature in the alumina cup lay on the line of loading thus creating a stress raiser (Fig. 50). The FEA demonstrated the importance of using anatomical loading conditions, as traditional axial testing of the cup would not have identified this feature as a stress raiser (3.2 Ultimate Compressive Strength Test Rig). Severe mechanical testing, far greater than loads experienced in-vivo, did indeed create damage in this area (Fig. 51). The design of the ceramic bearing was modified to eliminate this stress-raising feature and thus reduce the maximum principal stress in the ceramic by a predicted 24% (Fig. 50).

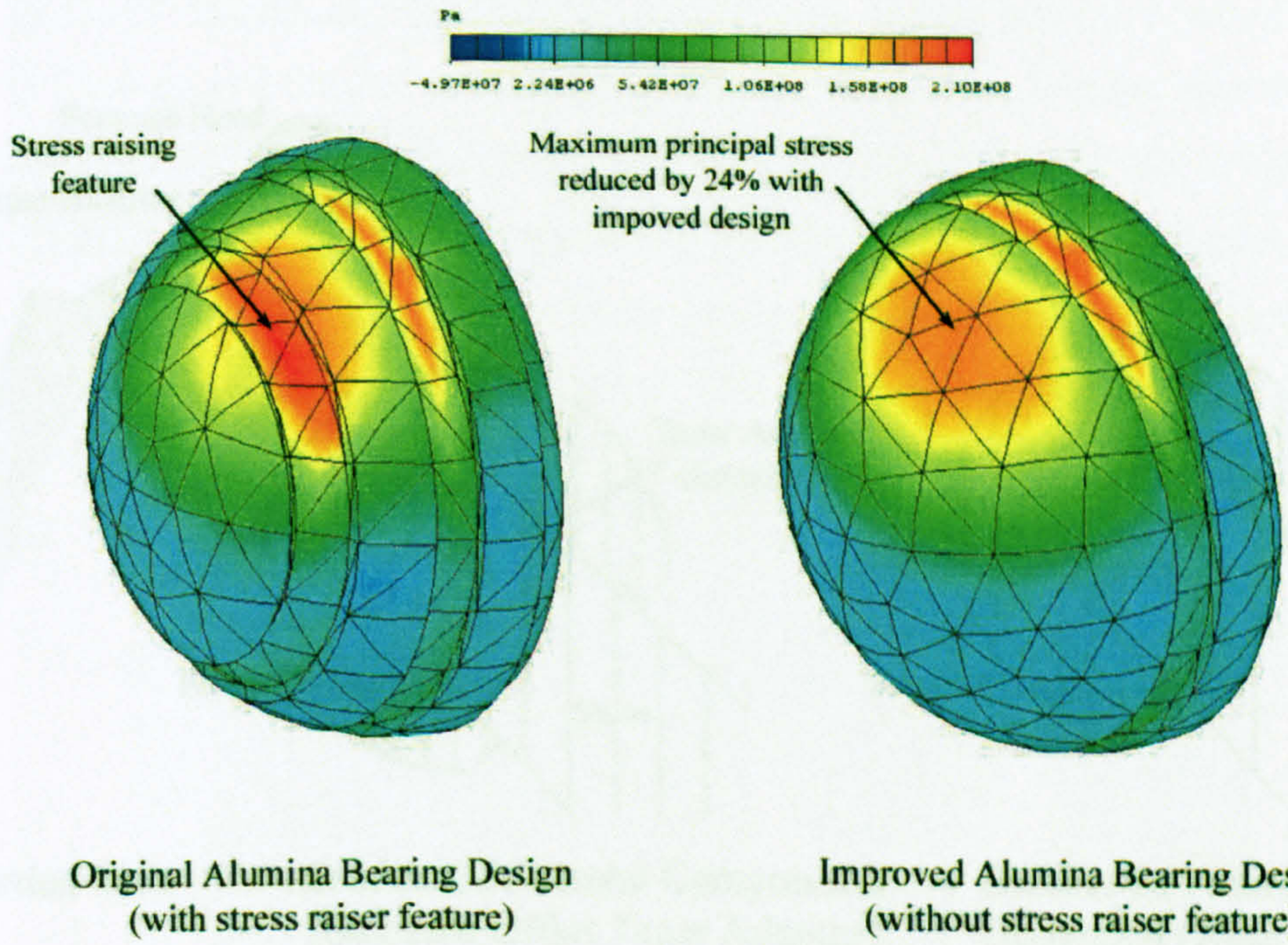

Fig. 50 FEA's of alumina bearing iteration

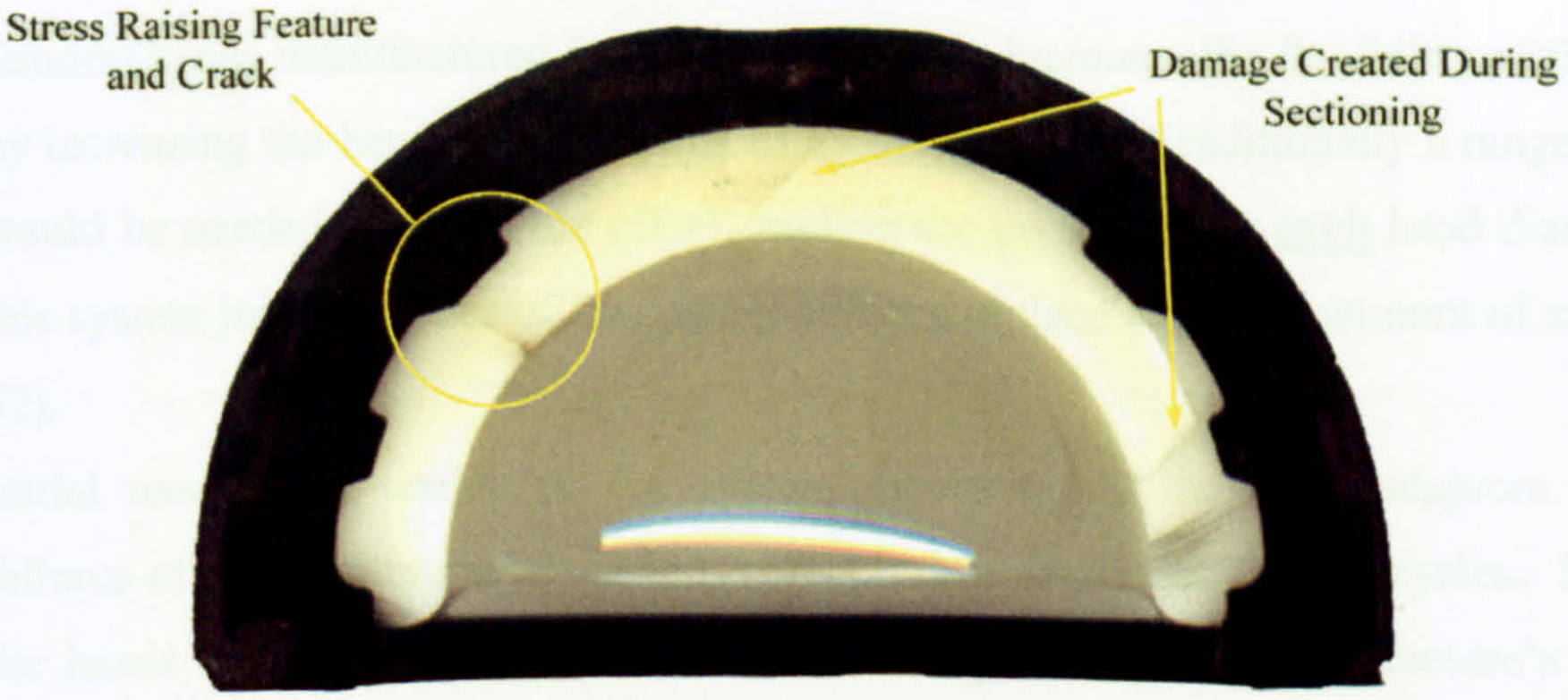

Fig. 51 Sectioned prosthesis showing crack due to stress raising feature

5.2.3 Taper Offset Adaptor Redesign

The most common method of attaching the femoral prosthesis to the head is by means of a locking taper fit. The absence of standardisation has led to over 100 different taper designs (Cales and Stefani 1998). The use of Orthodesign's taper adaptor was initially proposed for this new THR system, which allowed the connection of differing proprietary taper designs (Fig. 52).

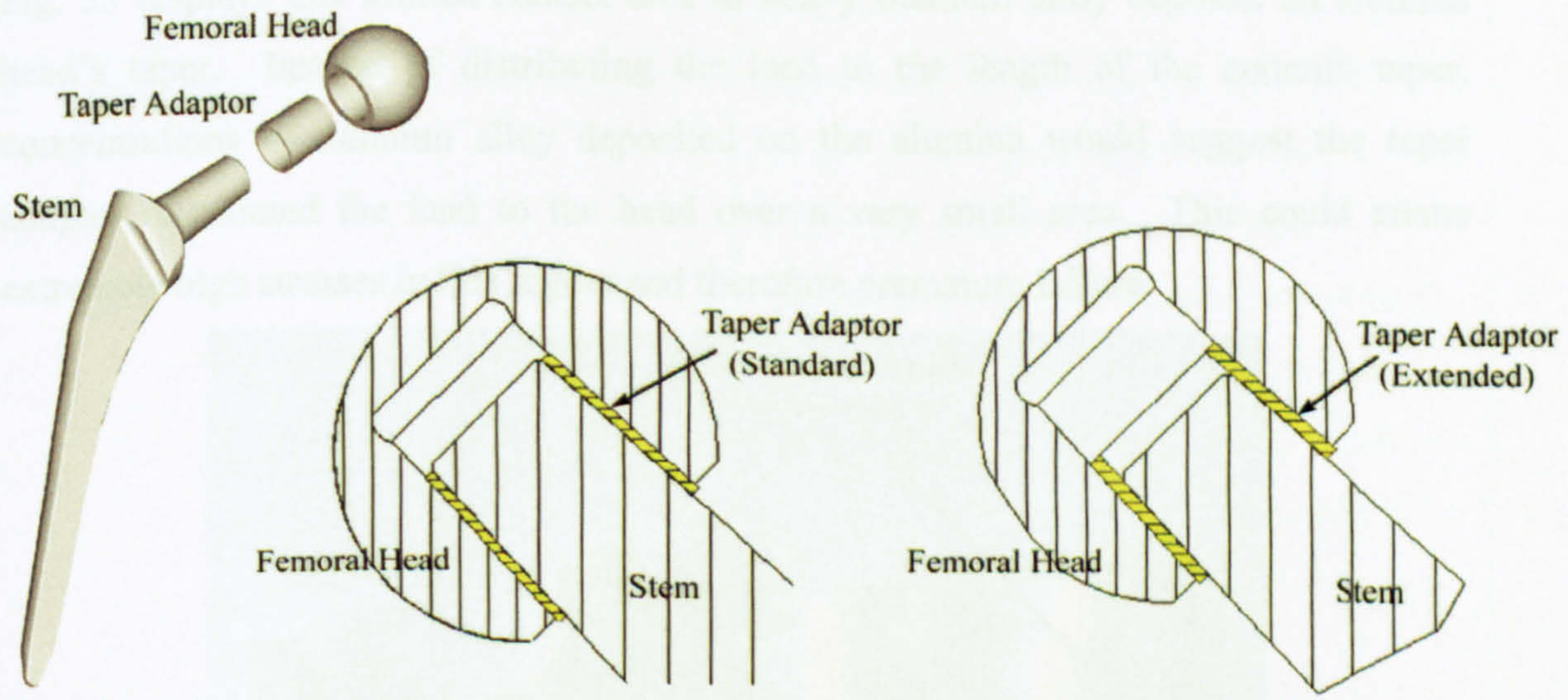

Exploded View

Section Of Femoral Components
(Standard Offset Taper Adaptor)

Section Of Femoral Components
(Extended Offset Taper Adaptor)

Fig. 52 Orthodynamics original taper adaptors

This design of taper adaptor has been used successfully for approximately 10 years with femoral heads manufactured from zirconia; it also increases the flexibility of the system by increasing the head offset if required by the surgeon. Traditionally a range of heads would be needed to adjust the offset, tripling the inventory for **each** head diameter. In this system just two types of inexpensive sleeve replace this huge amount of stock (Fig. 52).

Initial mechanical testing of the system incorporating the taper adaptors produced failures of the alumina heads at unacceptably low loads and fatigue cycles. Failure of the heads at loads as low as 7.5 kN was unexpected as the manufacture's literature describes failure at loads as high as 95.8 kN (axially loaded).

Such early failure of the alumina head was of great concern, particularly to the manufacturer (Morgan Matroc) who has distributed many thousands of this standard part. Also at this time anecdotal evidence of a surgeon using these adaptors, but mixing Alumina and Zirconia heads came to light. The result of using the taper adaptor with alumina heads in-vivo was the same as experienced in initial testing; catastrophic head failure.

5.2.3.1 Alumina Head and Taper Adaptor Study

Inspection of a failed head revealed evidence of very limited taper to head contact area. Fig. 53 displays this limited contact area as heavy titanium alloy deposits on alumina head's taper. Instead of distributing the load to the length of the ceramic taper, concentrations of titanium alloy deposited on the alumina would suggest the taper adaptor distributed the load to the head over a very small area. This could create extremely high stresses in this region and therefore premature failure.

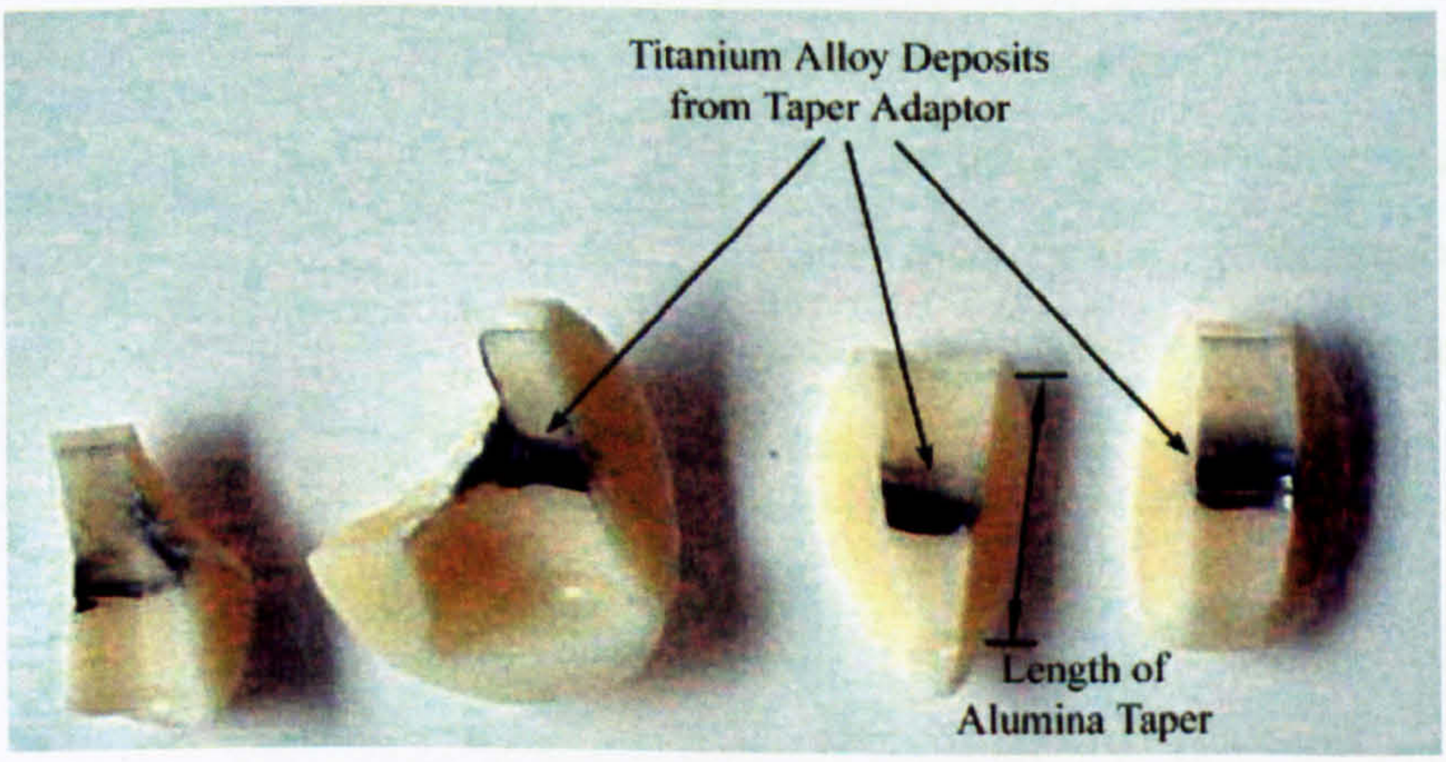

Fig. 53 Pieces of failed head showing limited taper contact area

Geometrical analysis of taper adaptors was undertaken using Zeiss Scanware three-dimensional Coordinate Measuring Machine (3D CMM) and Taylor Hobsen Tally Surf. Photographs of this equipment and typical outputs can be seen in Appendix 4.

The taper adaptors analysed consisted of two, sub-contractor manufactured, standard offset adaptors on which heads had failed during mechanical testing (Adaptors A and B). A random sample of four adaptors that were manufactured in-house by Orthodynamics was also analysed. These four consisted of two standard offset adaptors (Adaptors C and D) and two extended offset adaptors (Adaptors E and F).

The premature failure of the alumina heads appeared to be caused by the taper adaptor having several manufacturing problems compounded with an underlying design flaw. Full details of the geometric analysis can be found in Appendix 4 and a summary of the results is shown below in Table 14.

Problem Discovered	**Comment**
Incorrect tolerance of internal taper	Both internal and external taper angles used a –2' and +0' tolerance. For the sleeve to perform correctly the internal taper angle should have a –0' and +2' tolerance.
Insufficient straightness of external taper	Straightness of the external taper is critical for the correct loading of the ceramic head. Whilst the greatest deviation from straightness was only 2.1μm (acceptable) the profile was not. Profiles recorded from the tally surf indicated that the sleeve would load the head in an unacceptable '3 point bend', creating high stresses in the head.

Inability to manufacture to required tolerance	The mean error for both the internal and external tapers were unacceptable, with a mean error of +0°2'24" for the external taper and +0°3'13" for the internal taper.
Incorrect taper angle in CNC code	The trigonometry required in the CNC code to machine the tapers on the sleeve was incorrect giving an error of +0°2'24" on the external angle and +0°3'13" on the internal angle. The area of CNC code that was incorrect may well have been due to 'tweaking' to give a perceived better fit on the inspection head.
Unsuitable manufacturing method	The external profile was created in a single cut with the tool used for parting of the component. Work-piece deflection and tool wear would account for dimensional and geometric errors of the external taper when machined in this manner.

Table 14 Results of taper adaptor study

In response to the results from the analysis of the original tapers (Table 14), the author designed a new family of tapers suitable for use with alumina heads (Fig. 54). Two significant changes to the original design were made:

1. A 'bucket bottom' was made which allowed the transfer of load to the head along the complete length of the head's taper whilst adding to the component's stiffness during machining, thus allowing better dimensional stability.
2. Most significantly, the angle tolerances on the inner and outer tapers were changed to ensure correct loading of the head throughout the tolerance range.

In addition to these two design changes, tighter production controls were introduced to achieve manufacturing tolerances.

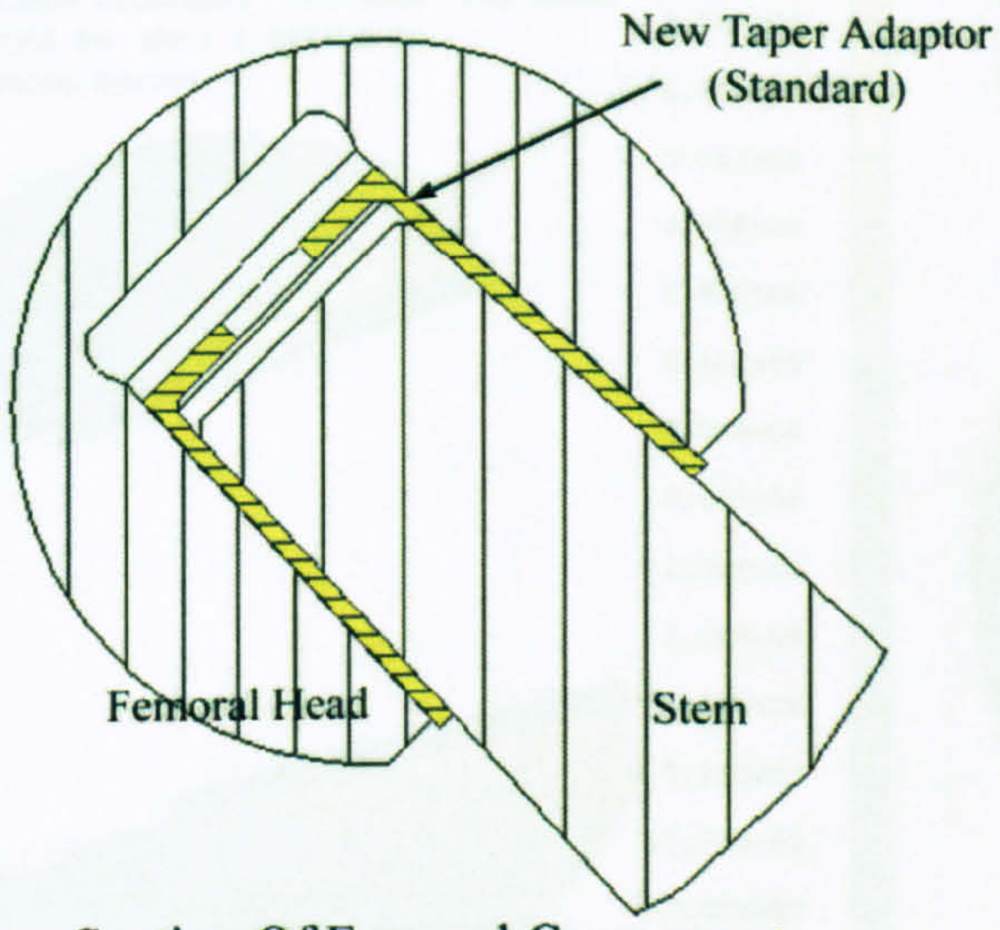

Section Of Femoral Components
(New Standard Offset Taper Adaptor)

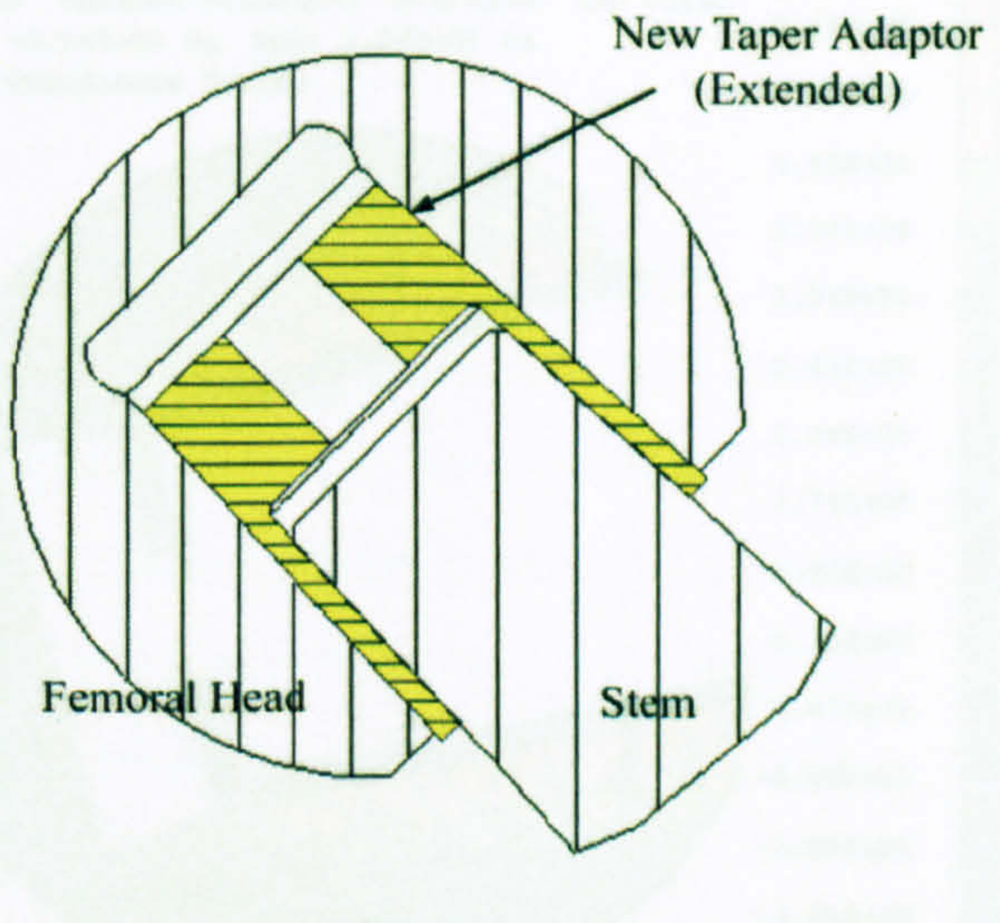

Section Of Femoral Components
(New Extended Offset Taper Adaptor)

Fig. 54 New design taper adaptors

Comparison FEAs of the new design and original design taper adaptors were undertaken with axial loading. Three-dimensional models of the head and taper were created using the data obtained from geometric study for the original tapers and mid limit for the new tapers. Meshing comprised parabolic tetrahedrals with linear contact elements modelled between the head and external sleeve taper surfaces. Load was applied to the internal sleeve surface whilst a polar area of the head was fully restrained.

Analysis of the original standard offset adaptor (Adaptor C) and the new design standard offset adaptor revealed a 34% decrease in maximum principal stress in the new design (Fig. 55).

Analysis of the original extended offset adaptor (Adaptor F) and the new design extended offset adaptor revealed a 22% decrease in maximum principal stress in the new design (Fig. 56).

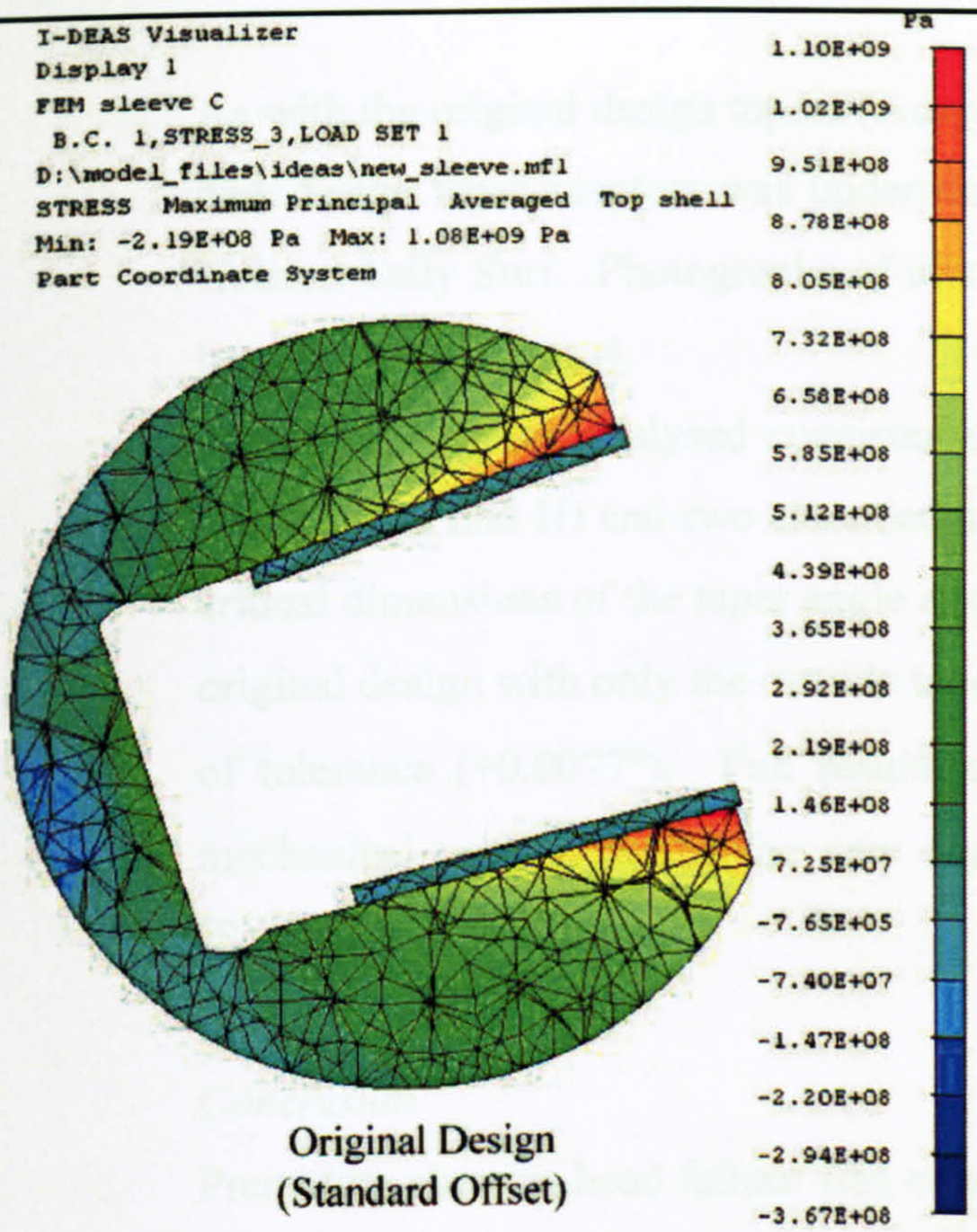

Fig. 55 FEA comparison of original design and new design standard offset tapers

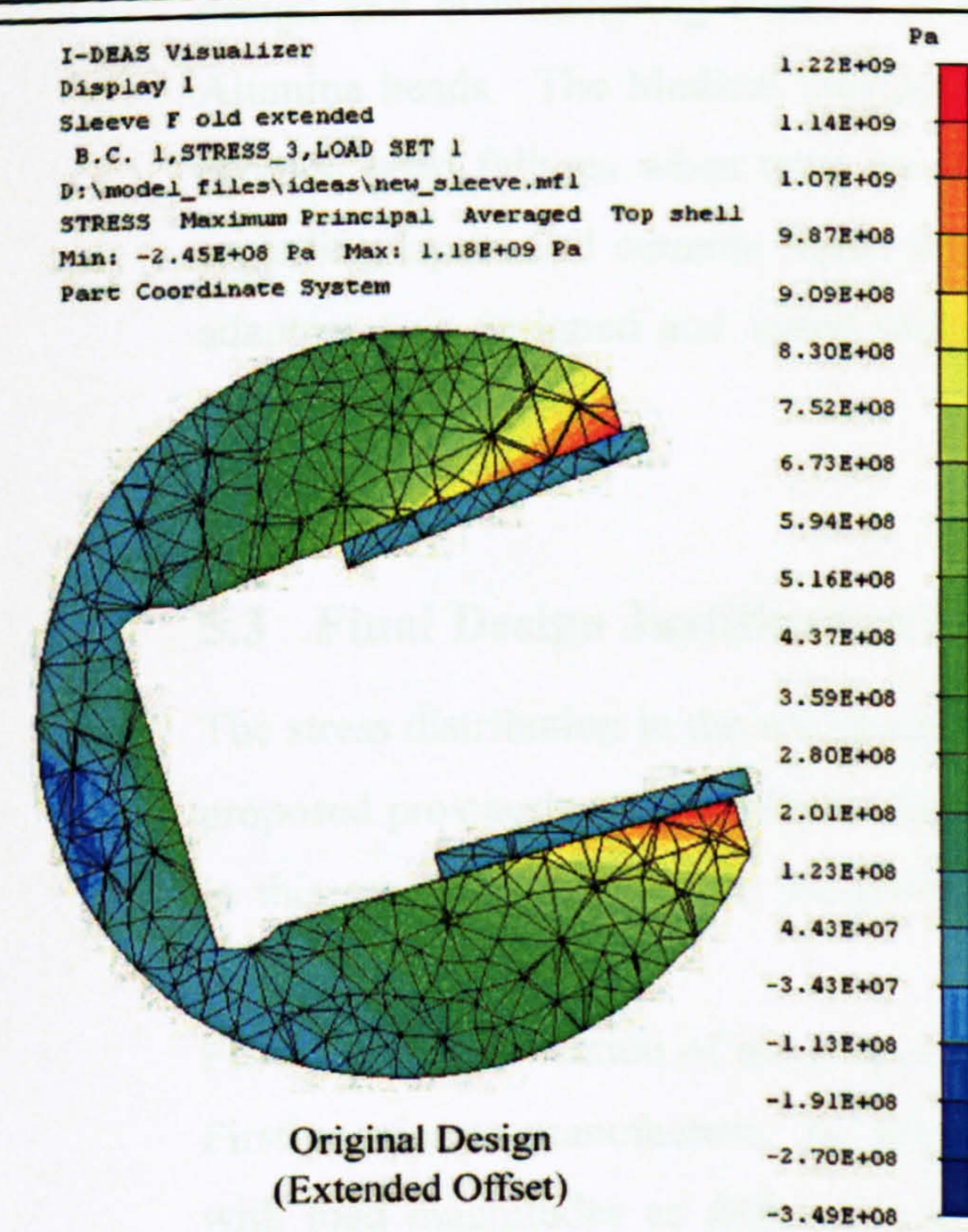

Fig. 56 FEA comparison of original design and new design standard extended tapers

As with the original design tapers (Adaptors A,B,C,D,E,F) a geometrical analysis of the new design taper adaptors was undertaken using Zeiss Scanware 3D CMM and Taylor Hobsen Tally Surf. Photographs of this equipment, typical outputs and full results can be seen in Appendix 4.

The taper adaptors analysed consisted of two, standard offset adaptors of new design (Adaptors G and H) and two extended adaptors of new design (Adaptors I and J). The critical dimensions of the taper angle and taper straightness were vastly improved on the original design with only the outside taper angle on the new extended sleeve slightly out of tolerance (+0.0077°). Full results can be found in Appendix 4. All subsequent mechanical tests involving the new design of the taper did not produce head failure (Section 5.3.1).

Conclusion

Premature alumina head failure was experienced both during mechanical testing and in-vivo whilst using the original design taper adaptors. Analysis discovered that both the design and manufacturing method of the original taper adaptor were unsuitable for Alumina heads. The Medical Devices Agency was duly notified to the possibility of ceramic head failures when used on incorrect tapers and they issued a safety notice regarding tapers and ceramic heads in general (Appendix 4). A new family of taper adaptors was designed and tested without any instance of catastrophic alumina head failure.

5.3 Final Design Justification Using 3D Finite Element Analysis

The stress distribution in the acetabular and possible osseointegration advantages of the proposed prosthesis were explored using 2D FEA in Section 5.1. 3D FEA was utilised in this section to predict the prosthesis and test rig's ability to withstand mechanical loading.

FEA design justification of the proposed acetabular cup was undertaken in two phases. Firstly, prior to manufacture, the designs were modelled as three-dimensional FEAs with load magnitudes as defined in the design specification. Crucial in minimising tooling and mechanical testing costs, this initial phase assessed the design and materials ability to withstand mechanical loading. This phase also ensured that the proposed test

rig could withstand the loads endured in typical mechanical tests (see Section 3.1 and 3.2 for test details). The second phase was to load the FEA model to a magnitude determined during ultimate compressive strength (UCS) testing that caused prosthesis failure. Agreement of this second phase of FEA with mechanical testing gives confidence that any subsequent modification to the design can be accurately modelled using FEA.

5.3.1 Modelling Technique

The load orientation and boundary conditions for the FEA models were determined from the UCS and fatigue tests (see Sections 3.1 and 3.2). This anatomically correct orientation was simplified using symmetry and boundary conditions to considerably reduce modelling and solution times (Fig. 57)

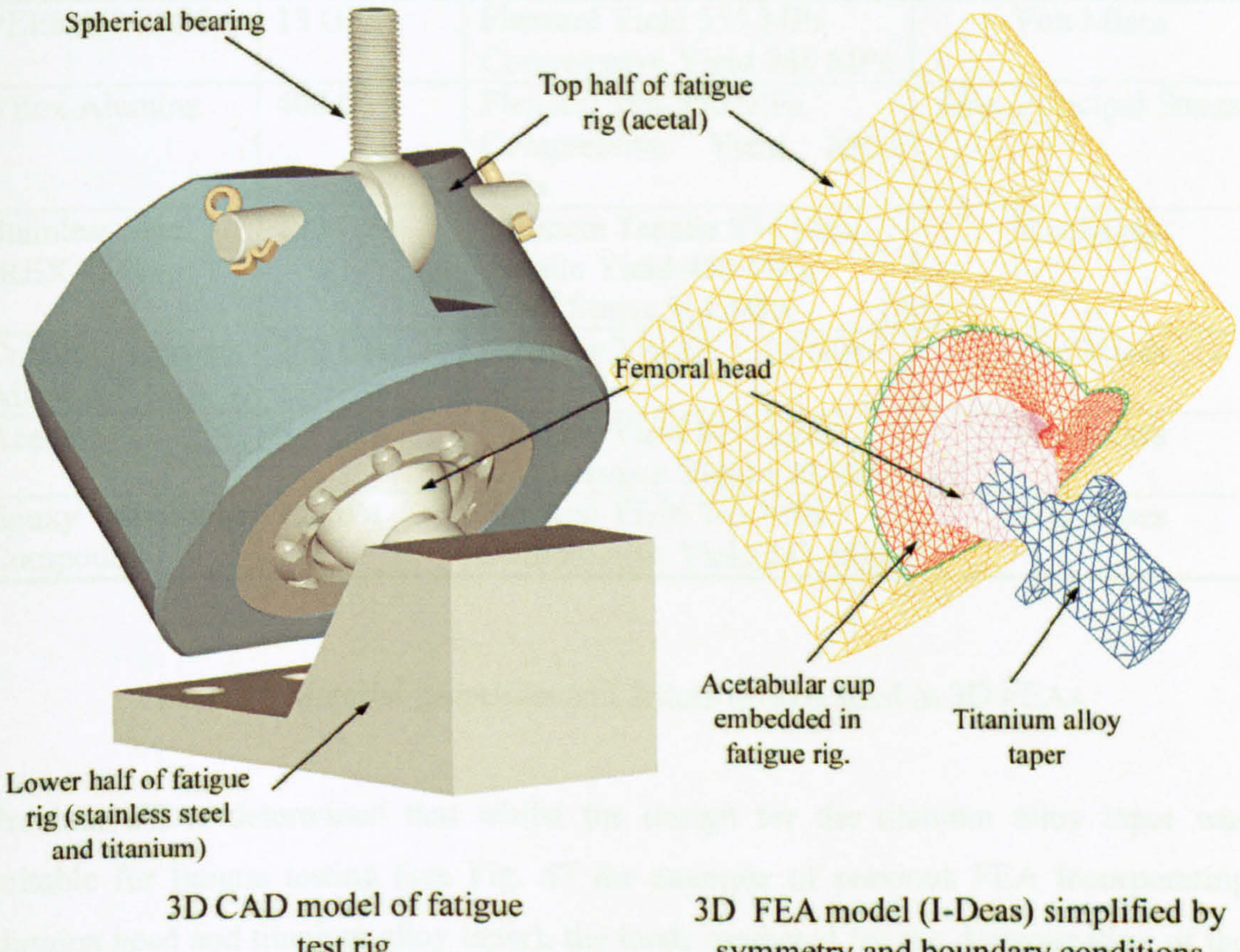

Fig. 57 Full 3D CAD model and simplified FEA of fatigue test (I-Deas)

The FEAs were originally undertaken using I-Deas software version 9. Assumptions that relatively small displacements at the femoral head to cup contact area would allow

a faster, more economical, linear solution were made. These initial FEAs revealed, that whilst the displacements were comparatively small, rotation of the head in the cup due to the taper bending would require a non-linear contact solution. The undertaking of a non-linear solution is extremely computer intensive, with solutions possibly taking many hours or days, and requires advanced, robust software. Final non-linear FEAs (displayed in this section) were undertaken using ANSYS Workbench 8. The ANSYS software incorporates a very robust and stable solver with advanced tools for solution convergence. The failure criteria used in the FEAs to predict failure are dependent on material properties and were explored in Section 4.6. The criteria and material locations used in the 3D FEAs are displayed below in Table 15 and Fig. 58.

Material	Youngs Modulus	Material Strength	Failure Criteria
PEEK450CA30	13 GPa	Flexural Yield 355 MPa Compressive Yield 240 MPa	Von Mises
Vitox Alumina	400 GPa	Flexural 380-550 MPa Compressive Yield 2600 MPa	Max-Principal Stress
Stainless Steel (REX 734)	193 GPa	Ultimate Tensile 874 MPa Tensile Yield 450 MPa Proof Stress 514 MPa	Von Mises
Cobalt Chrome Alloy	200 GPa	Ultimate Tensile 1308 MPa	Von Mises
Acetal	3.1 GPa	Flexural Yield 89.6 MPa Compressive Yield 110 MPa	Von Mises
Epoxy Moulding Compound	15 GPa	Flexural Yield 345 MPa Compressive Yield 241 MPa	Von Mises

Table 15 Material properties and failure criteria used in 3D FEAs

Previous FEAs determined that whilst the design for the titanium alloy taper was suitable for fatigue testing (see Fig. 57 for example of previous FEA incorporating alumina head and titanium alloy taper), the loads predicted for the determination of the ultimate compressive strength would be greater than the yield strength of the taper. A strengthened one-piece head and taper was manufactured and used in all of the final ANSYS FEAs. The use of the one-piece head and taper in the FEA models allows the

loading of both the fatigue and UCS tests to be undertaken by the changing of boundary conditions only.

The final ANSYS FEAs included fully detailed CAD geometry, such as the prosthesis's hole features (Fig. 58). Final converged meshes and convergence details can be seen in the following results sections.

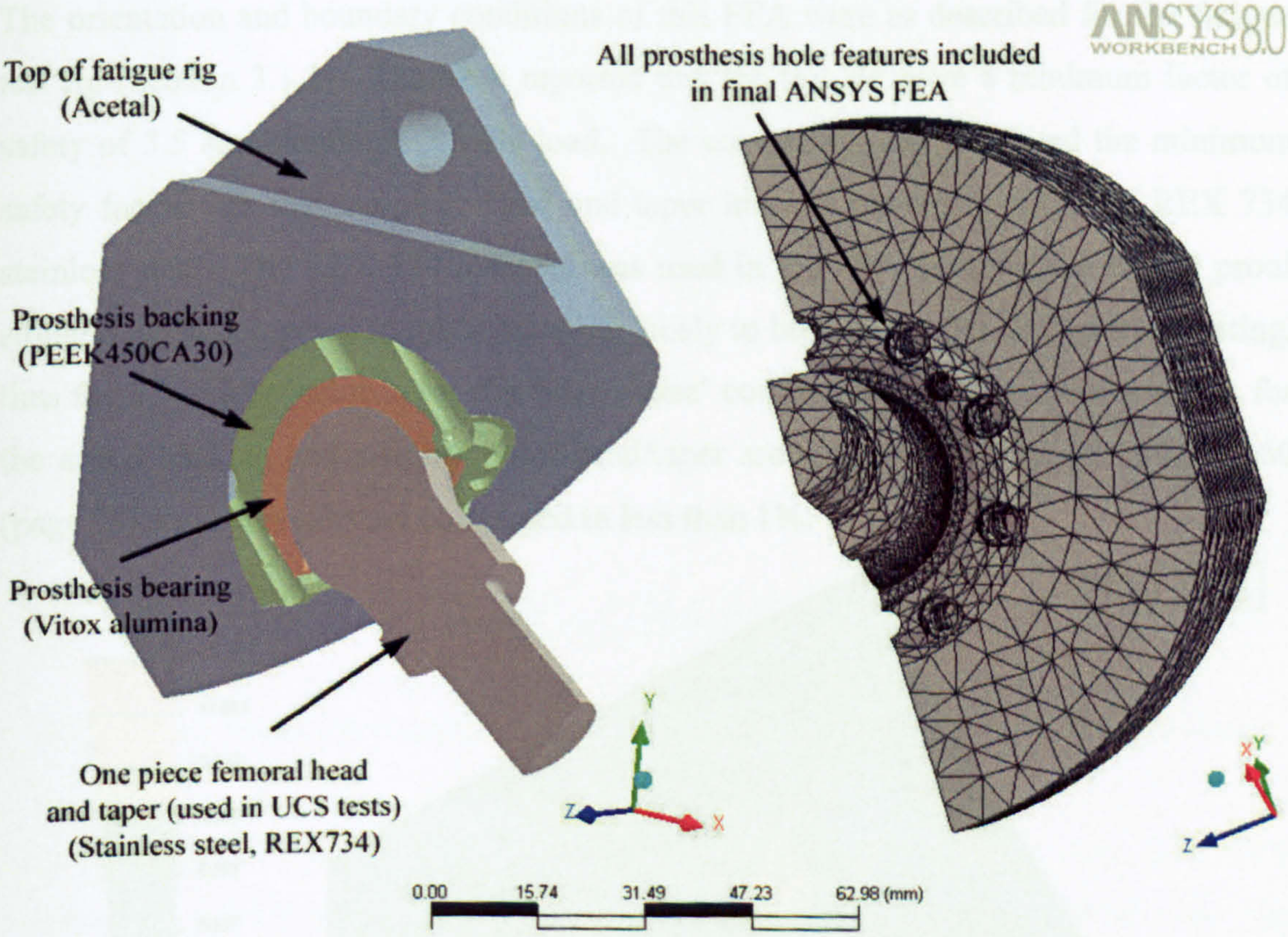

Fig. 58 Two views of final 3D ANSYS FEA model, displaying overall configuration, materials used and unconverged mesh

5.3.2 Results of FEA at 7.5 kN Load (Phase 1, Pre-manufacture)

The high tooling and manufacturing costs of the proposed prosthesis made it imperative that the prosthesis and test rig design iterations were undertaken at the modelling stage of the project. Pre-manufacture FEAs were crucial to the design of the prosthesis and test rigs. Failure of the prosthesis at anatomical loads or damage caused by test rig

failure would have been unacceptable at the mechanical testing stage due to the aforementioned costs. This FEA ensured that both the test rig and the prosthesis would not fail the mechanical tests required to progress the project to clinical trials. A load of 7.5 kN was specified in the design specification (Table 4 page 35). This load is double the load required for the BSI fatigue test (see Section 1.4.4 page 23) and greater than any load commonly experienced in-vivo.

The orientation and boundary conditions of this FEA were as described for the fatigue test rig (Section 3.1.2). The FEA reported that the test rig gave a minimum factor of safety of 3.5 at a simulated 7.5 kN load. The component that exhibited the minimum safety factor was the one-piece head and taper initially manufactured from REX 734 stainless steel. The REX 734 material was used in the FEA as it has the lowest proof strength when compared to other materials likely to be used for the taper during testing, thus the 3.5 safety factor is for the 'worst case' configuration. Von Mises stresses for the acetal backing and stainless steel head/taper are displayed in Fig. 59 and Fig. 60 (page 98) and the results are converged to less than 1%.

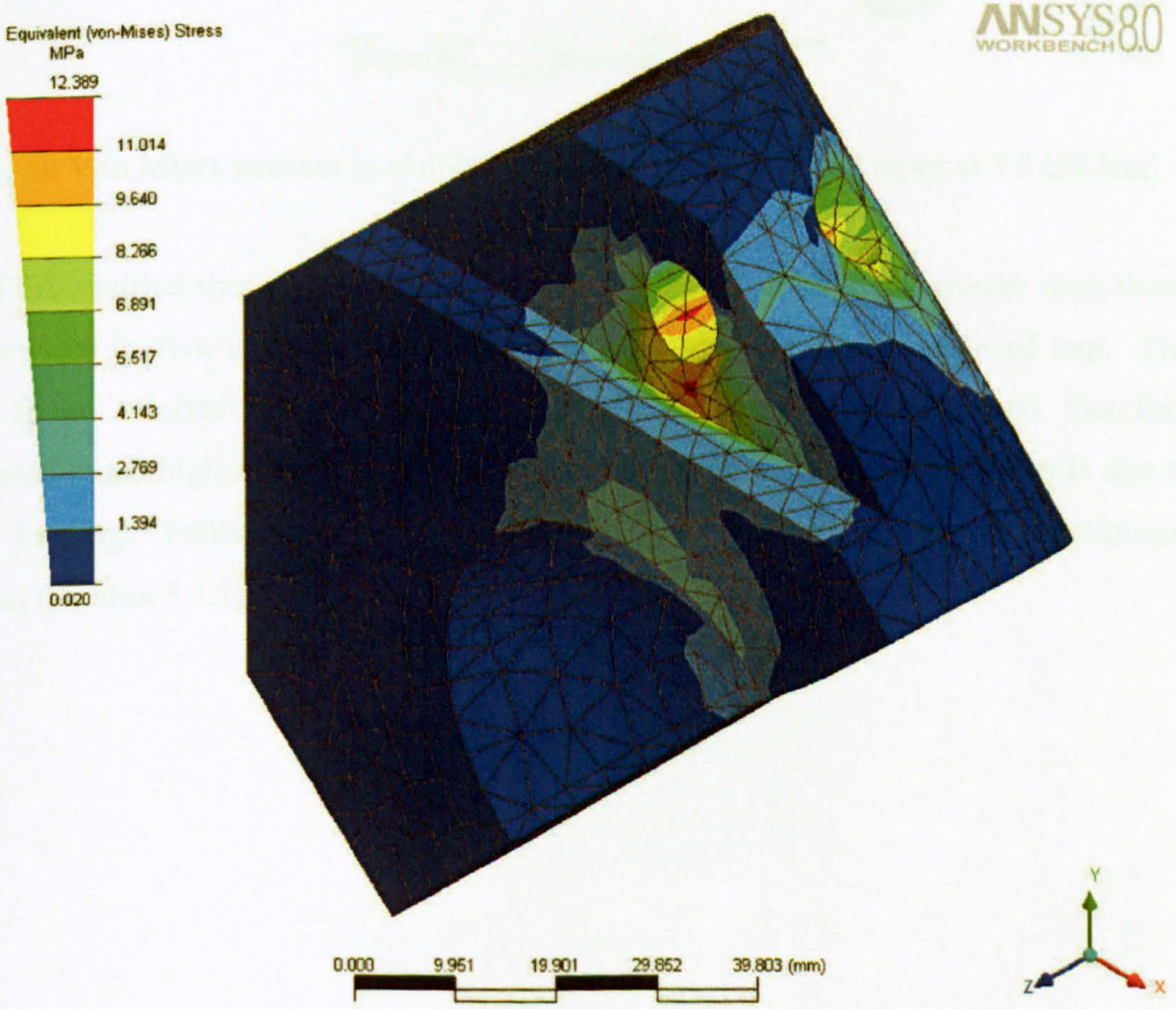

Fig. 59 Von Mises stresses in acetal test rig at 7.5 kN load

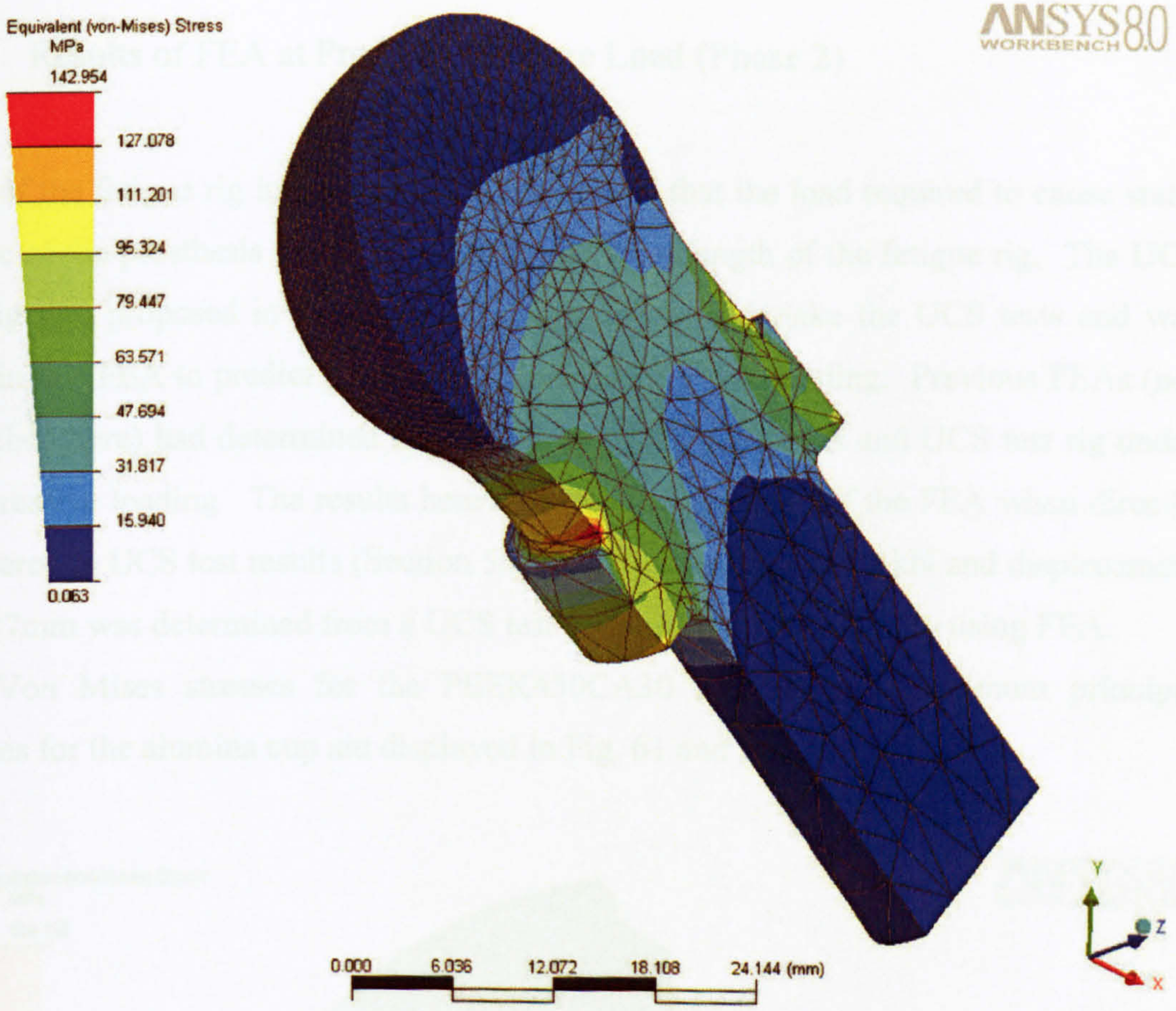

Fig. 60 Von Mises stresses in stainless steel one piece head and taper at 7.5 kN load

The FEA verified that the fatigue testing rig could withstand loads greater than those encountered in-vivo and was suitable for the fatigue testing of the proposed cup. The FEA found minimal stresses in the proposed acetabular prosthesis and therefore predicted much higher loads would be required to cause failure of the prosthesis due to static loading. Failure stresses in the prosthesis are explored fully in the following section (Section 5.3.3)

5.3.3 Results of FEA at Prosthesis Failure Load (Phase 2)

FEA of the fatigue rig in Section 5.3.2 determined that the load required to cause static failure of the prosthesis would be in excess of the strength of the fatigue rig. The UCS test rig was proposed in Section 3.2.2 (page 54) to undertake the UCS tests and was used in this FEA to predict prosthesis failure due to static loading. Previous FEAs (not described here) had determined the suitability of the prosthesis and UCS test rig under compressive loading. The results here focus on the accuracy of the FEA when directly compared to UCS test results (Section 5.4.1). A failure load of 22 kN and displacement of 0.37mm was determined from a UCS test and modelled accordingly using FEA.
The Von Mises stresses for the PEEK450CA30 backing and maximum principal stresses for the alumina cup are displayed in Fig. 61 and Fig. 62

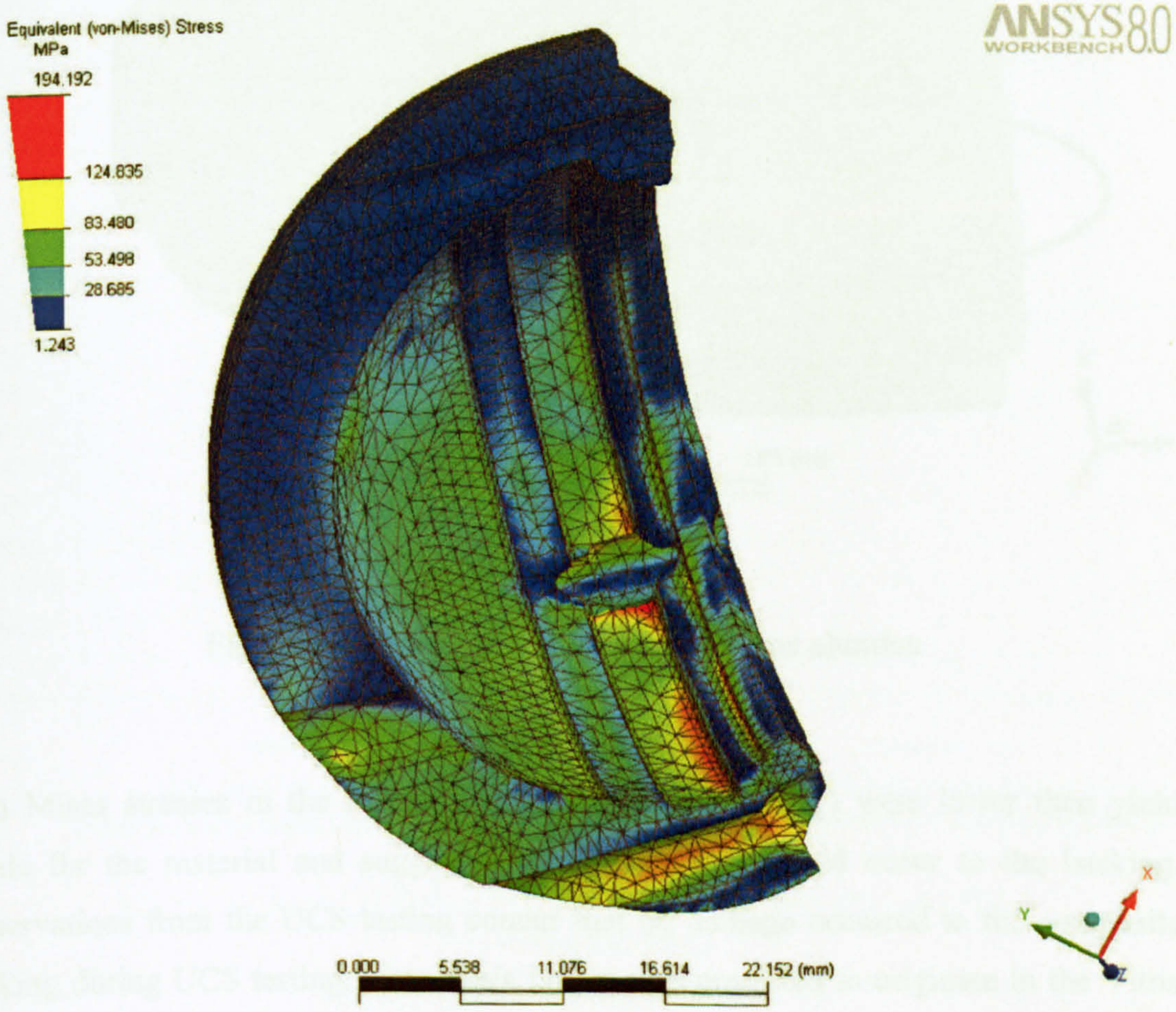

Fig. 61 Von Mises stresses of prosthesis backing
at failure load of 22 kN

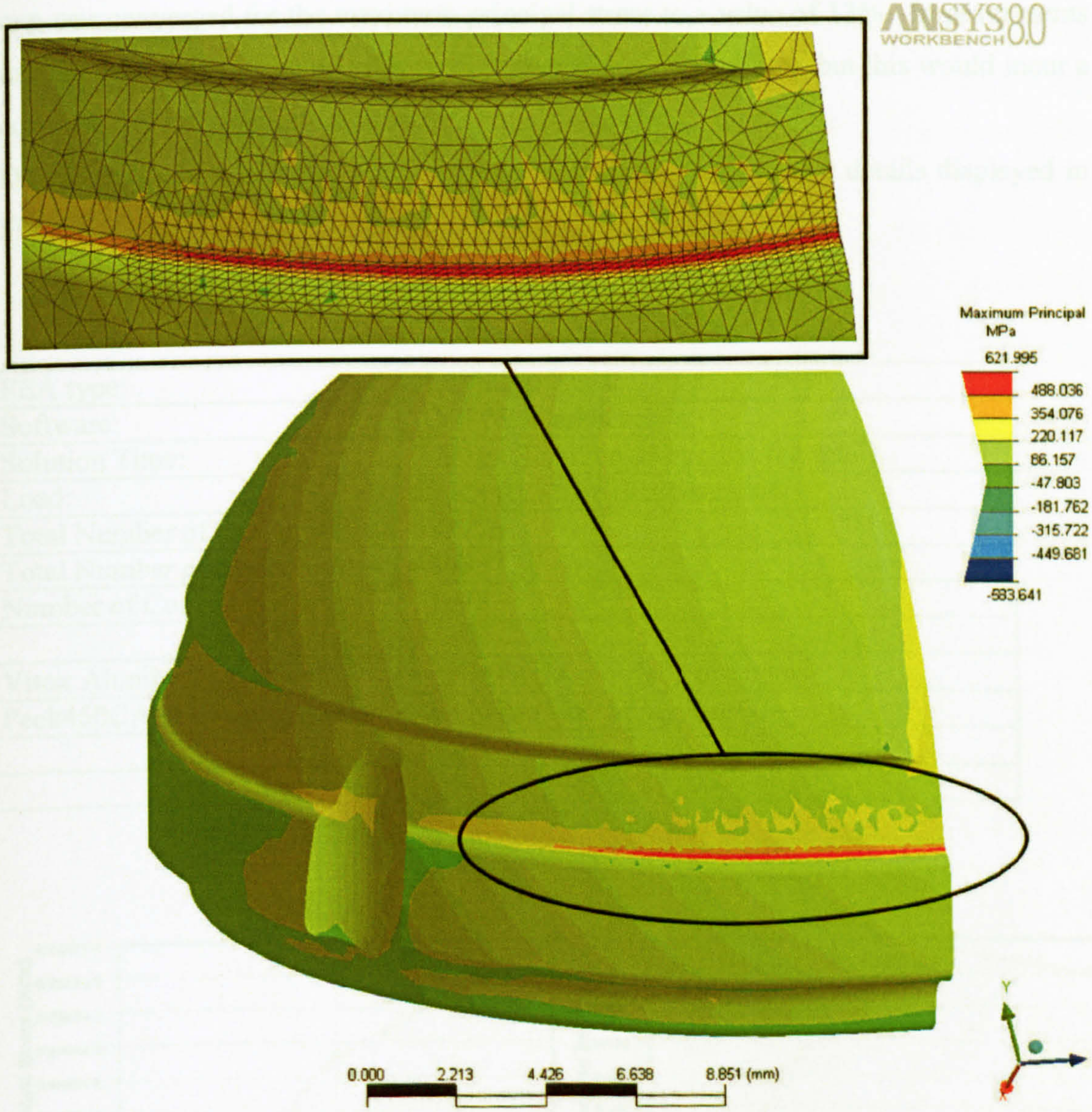

Fig. 62 Maximum principal stress of Vitox alumina cup at failure load of 22 kN

Von Mises stresses in the PEEK450CA30 backing (Fig. 61) were lower than yield levels for the material and suggested that no damage would occur to the backing. Observations from the UCS testing concur that no damage occurred to the composite backing during UCS testing. Prosthesis failure was predicted to originate in the Vitox alumina cup and is in agreement with the mechanical testing. Maximum principal stresses in the Vitox alumina of 622 MPa are 13% greater than the 550 MPa flexural

strength, suggesting an FEA accuracy of within 13%. The mesh in the Vitox alumina cup was converged for the maximum principal stress to a value of 13%. Improvements in FEA accuracy may be possible with further mesh convergence, but this would incur a considerably longer solution time.

Details of the FEA are displayed in Table 16 with the convergence details displayed in Fig. 63.

FEA type:	Non-linear
Software:	ANSYS Workbench 8
Solution Time:	7 hours (final iteration only, not total)
Load:	22 kN (0.37mm displacement)
Total Number of Elements:	385776
Total Number of Nodes	480937
Number of Contact elements:	51678
Vitox Alumina Cup Stress	622 MPa (Max Principal Stress)
Peek450CA30 Backing Stress	195 MPa (Von Mises Stress)

Table 16 Details of ultimate compressive strength FEA

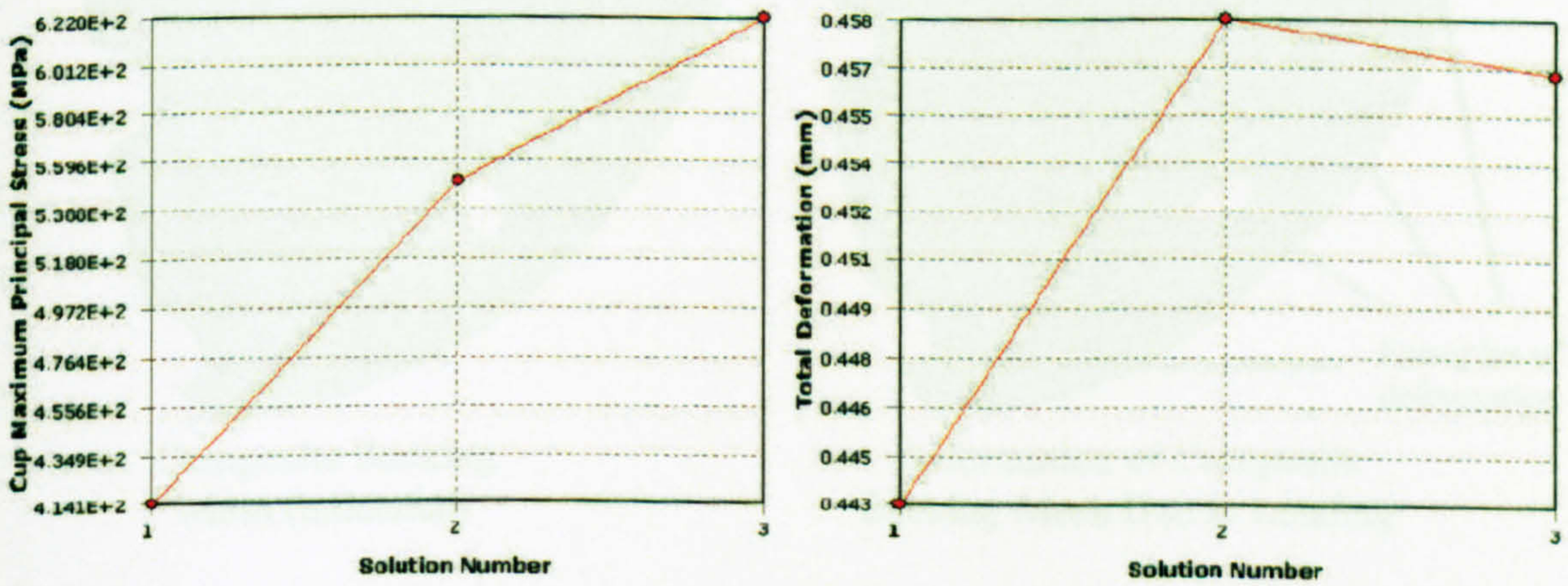

Alumina Cup Convergence
(Max Principal Stress Converged to 12%)

Total Deformation Convergence
(Displacement Converged to 0.4%)

Fig. 63 Mesh convergence of ultimate compressive strength FEA
(Vitox alumina cup)

5.3.4 Discussion of 3D FEA Results

The FEAs undertaken, as part of the iterative design process, were fundamental in achieving the clinical trial stage with the minimum of tooling and mechanical testing costs. Particularly useful in the design of the mechanical test rigs the FEAs gave confidence prior to mechanical testing of the suitability of the design and materials used. Manual calculations of the prosthesis would have been limited due to the complexity of the geometry and number of materials involved. An example of the FEA complexity can be seen in Fig. 64 that displays the deformation of the prosthesis composite backing.

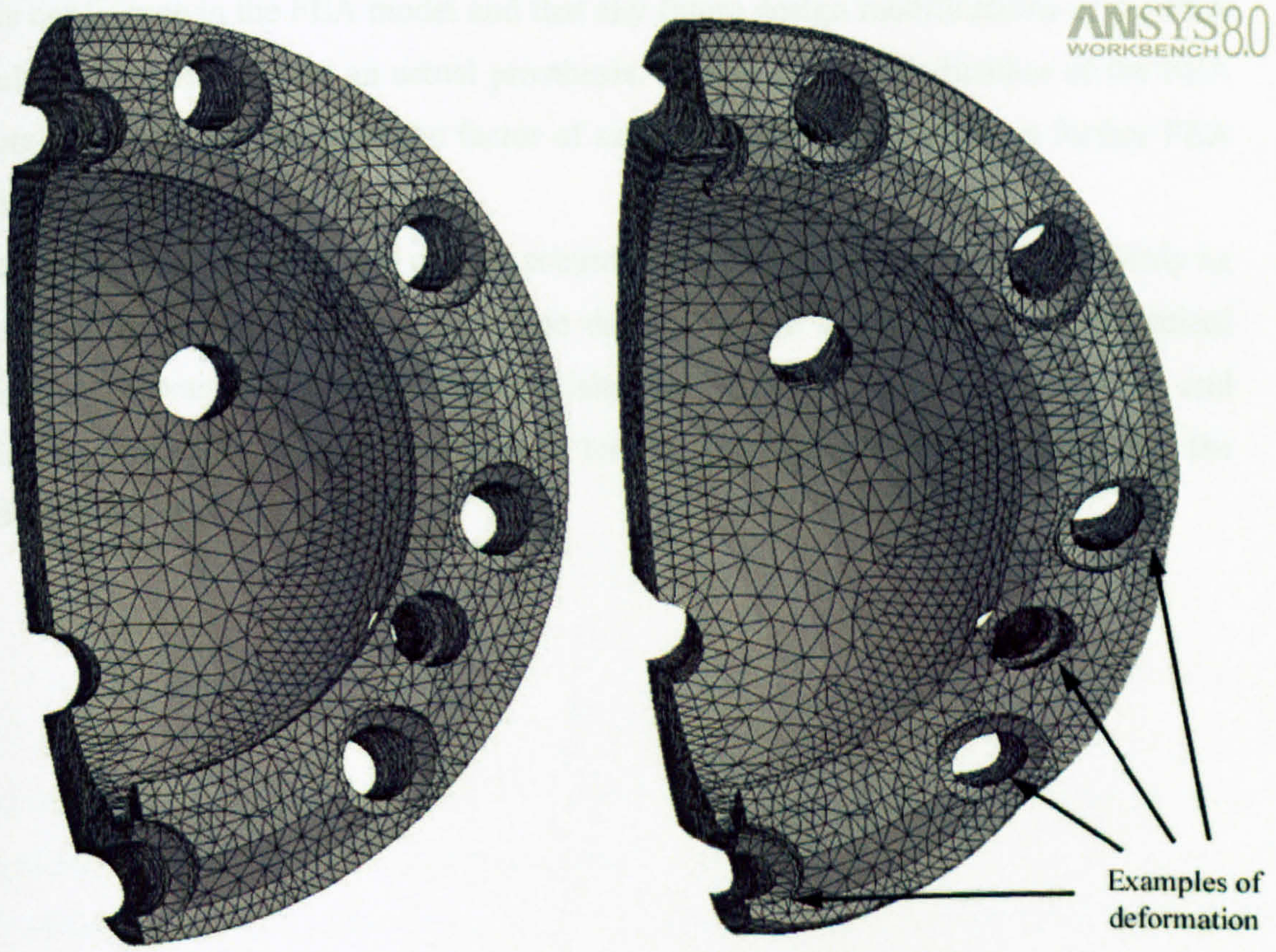

Composite Backing Mesh (unloaded)

Deformation of Composite Backing Mesh Due to Loading

Fig. 64 Complexity of ultimate compressive stress FEA demonstrated by composite backing deformation

(deformation scaled to aid visualisation)

Two types of FEA methodology were undertaken in this section; namely predictive engineering and failure verification. Predictive engineering was used in Phase 1 and allowed the analysis to drive the choice of geometries and materials to be used in the

prosthesis and test rigs design. The predictive analysis determined that whilst the fatigue rig could geometrically undertake the UCS testing, neither the spherical bearing nor titanium alloy/alumina taper combination could withstand the predicted UCS loads, and a separate UCS rig was required. This methodology has the greatest impact on minimising cost and improving the quality of the design (Adams and Askenazi 1999).

The second phase was failure verification, and represents the most rigid use of structural FEA (Adams and Askenazi 1999). Correlating FEA data to a prosthesis that had failed during UCS mechanical testing required careful interpretation of the boundary conditions and minimum assumptions of material properties. This failure verification gives confidence in the FEA model and that any future design modifications in the FEA should accurately simulate an actual prosthesis. It also gives an indication of the FEA accuracy and should influence the factor of safety adopted when based on further FEA models.

As with all FEA, the results are only as accurate as the data provided and should only be used as a tool to improve the prosthesis design; not as a substitute for mechanical testing. FEA was ideally suited to minimising the iterations between manufacture and testing, considerably reducing tooling and testing costs without 'over-engineering' the product or test rigs.

5.4 Mechanical Testing

This section presents the results of mechanical tests, as described in Section 4 page 60. The purpose of the mechanical testing is to ensure that the final iteration of the proposed acetabular prosthesis and taper adaptors can withstand everyday loads encountered in-vivo; to produce an S/N curve for the proposed prosthesis; to uncover any weaknesses due to manufacturing processes; and to test the suitability of the proposed anatomically orientated testing methods.

Ensuring that the final iteration of the proposed acetabular prosthesis could withstand everyday loads encountered in-vivo was the primary aim for the mechanical testing. If the mechanical test results were acceptable, the proposed cup could then be recommended for clinical trials.

All acetabular prostheses used in mechanical testing were in a finished, 'ready for implantation' state. This requires that all prostheses were packaged and sterilised. Prior to mechanical testing, the samples were mounted in the acetal testing mount (as described in Section 4.2.1 page 60). All fatigue tests incorporated the new design of taper adaptors proposed in Section 5.2.3.

5.4.1 Ultimate Compressive Strength Results

Mounted acetabular prostheses were positioned in the UCS test rig (Fig. 31 page 55) in accordance with the UCS test procedure detailed in Section 4.4.2 page 64 and loaded until failure. Load, displacement and time were recorded for use in post test analysis. High data-capture rates (>100 Hz) for the load and displacement are imperative as failure of the ceramic is not always immediately obvious from the real-time visual display (examples of data capture analysis shown in Appendix A5.1). An audible 'crack' at initial ceramic cup failure is also common, but not guaranteed in all failures.

Initially four UCS tests were undertaken, and additional UCS data was obtained from two fatigue tests. This was possible as prior to fatigue testing, the load was ramped to the maximum load encountered during the test. This ensured that all components in the

test were seated correctly and that the prosthesis could withstand the required load statically before dynamic loading.

Unexpectedly two specimens (specimen 01360 and 01360-HA) failed during this initial ramping of a fatigue test. The results of the UCS tests (
Fig. 65) show that whilst these two specimens failed at loads greater than the loads required for ISO 7206 (fatigue load of femoral stems), they failed below an acceptable level for this project and were investigated in Section 5.4.4 page 114.

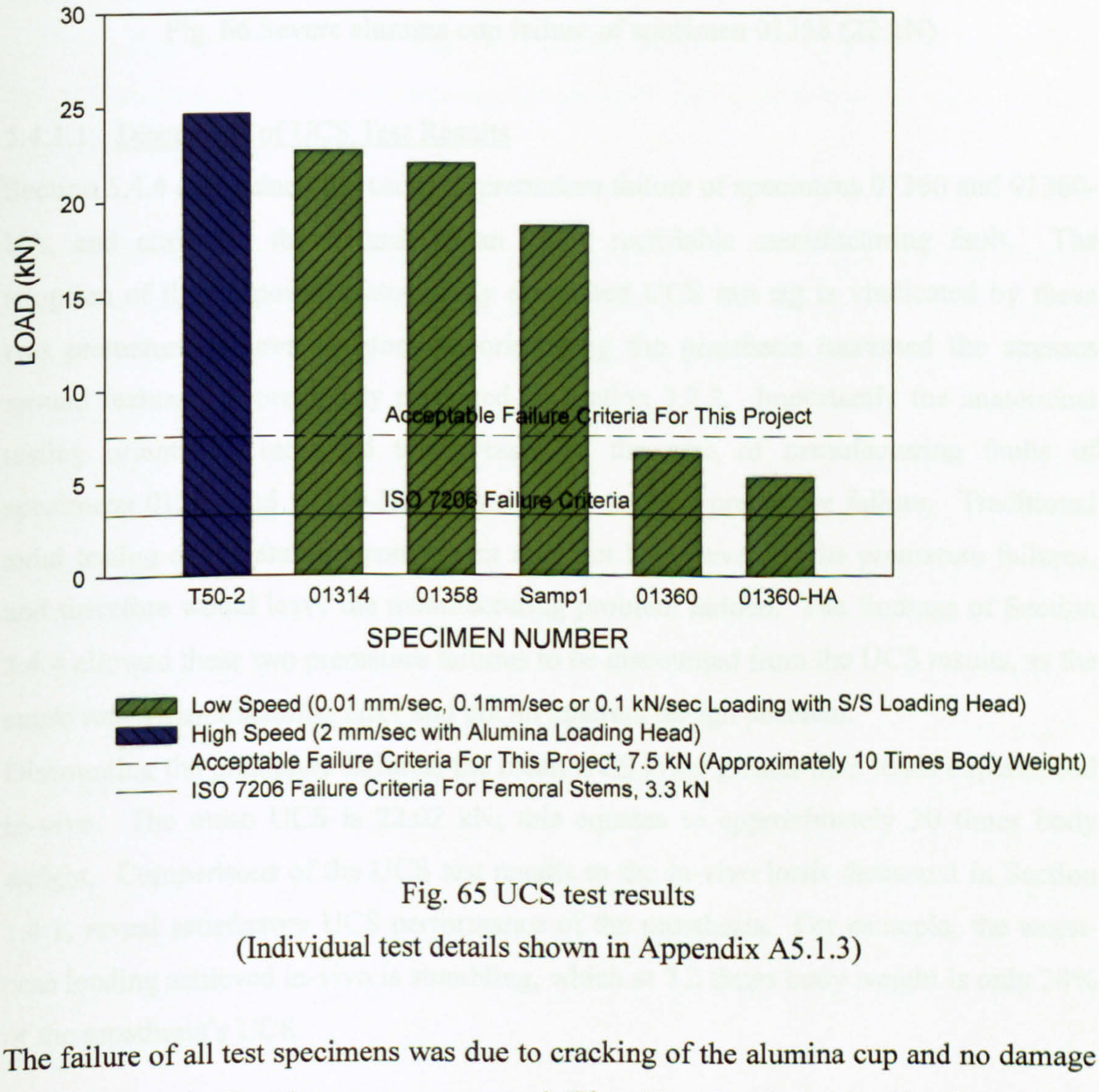

Fig. 65 UCS test results

(Individual test details shown in Appendix A5.1.3)

The failure of all test specimens was due to cracking of the alumina cup and no damage of the composite backing was encountered (Fig. 66). Continued loading beyond the UCS limits of the alumina, resulted in the destruction of the alumina but failed to cause any visual damage to the composite backing even at loads of in excess of 40 kN.

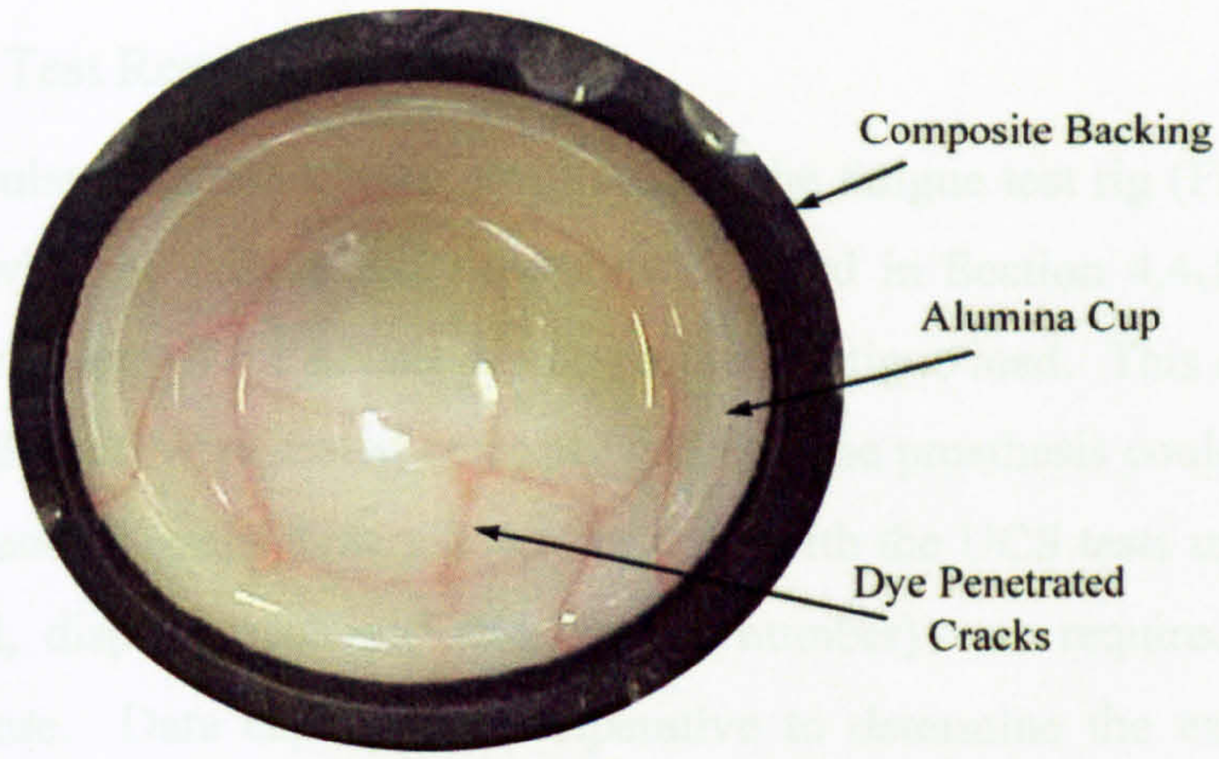

Fig. 66 Severe alumina cup failure of specimen 01358 (22 kN)

5.4.1.1 Discussion of UCS Test Results

Section 5.4.4 determined the cause of premature failure of specimens 01360 and 01360-HA, and attributed the failures to an easily rectifiable manufacturing fault. The adoption of the proposed anatomically orientated UCS test rig is vindicated by these two premature failures. Anatomical orientating the prosthesis increased the stresses around features, as previously predicted in Section 3.2.2. Importantly the anatomical testing orientation increased the stresses in the area of manufacturing faults of specimens 01360 and 01360-HA, contributing to their premature failure. Traditional axial testing of the alumina component may not have revealed the premature failures, and therefore would leave the manufacturing problem hidden. The findings of Section 5.4.4 allowed these two premature failures to be discounted from the UCS results, as the cause was a manufacturing error and not an inherent design problem.

Discounting the premature failures, the mean UCS is far greater than loads experienced in-vivo. The mean UCS is 22.02 kN; this equates to approximately 30 times body weight. Comparisons of the UCS test results to the in-vivo loads discussed in Section 1.4.1, reveal satisfactory UCS performance of the prosthesis. For example, the worst-case loading achieved in-vivo is stumbling, which at 7.2 times body weight is only 24% of the prosthesis's UCS.

5.4.2 Fatigue Test Results

Mounted acetabular prostheses were positioned in the fatigue test rig (Fig. 29 page 51) in accordance with the fatigue test procedure detailed in Section 4.4.1 page 64, and loaded statically at rate of 0.1 kN/sec to the required fatigue load. This ensured that all components in the test were seated correctly and that the prosthesis could withstand the required load statically prior dynamic loading. As with the UCS tests undertaken, data capture of load, displacement and time (cycle number) was required for post test analysis of failure. Data capture was imperative to determine the exact number of cycles before failure, as failure of the ceramic was not immediately obvious from the real time displays (examples of data capture analysis shown in Appendix A5.2). Upon visual discovery of failure, the data capture allowed determination of the exact cycle at which the failure occurred.

The fatigue results shown in Fig. 67 display two phases of the fatigue testing; ensuring minimum fatigue requirements are met for advancement to clinical trials; and the determination of the prosthesis fatigue life. With the primary aim of the mechanical testing being to evaluate the prosthesis suitability for progression onto clinical trials, the initial fatigue tests were undertaken solely to ensure that fatigue resistance exceeded that set out in ISO 7206-7. The first sample was halted at 5 million cycles, which exceeds the fatigue resistance required in ISO 7206-7 for femoral stems. The subsequent two tests were halted after exceeding double the number of cycles, at twice the load, of that required in ISO 7206-7 for femoral stems. The fatigue results shown in Fig. 67 depict these initial tests by squares with arrows. Due to the very limited number of prostheses for testing, further fatigue tests on these samples were undertaken to establish the loading level that fatigue failure begins. The results from these additional tests are omitted from Fig. 67 due to the multilevel loading, but the full test history for each specimen can be found in Appendix A5.2.5. Whilst not being included in the results, the additional tests allowed the baseline loads to be formulated for use in the determination of the prosthesis fatigue life.

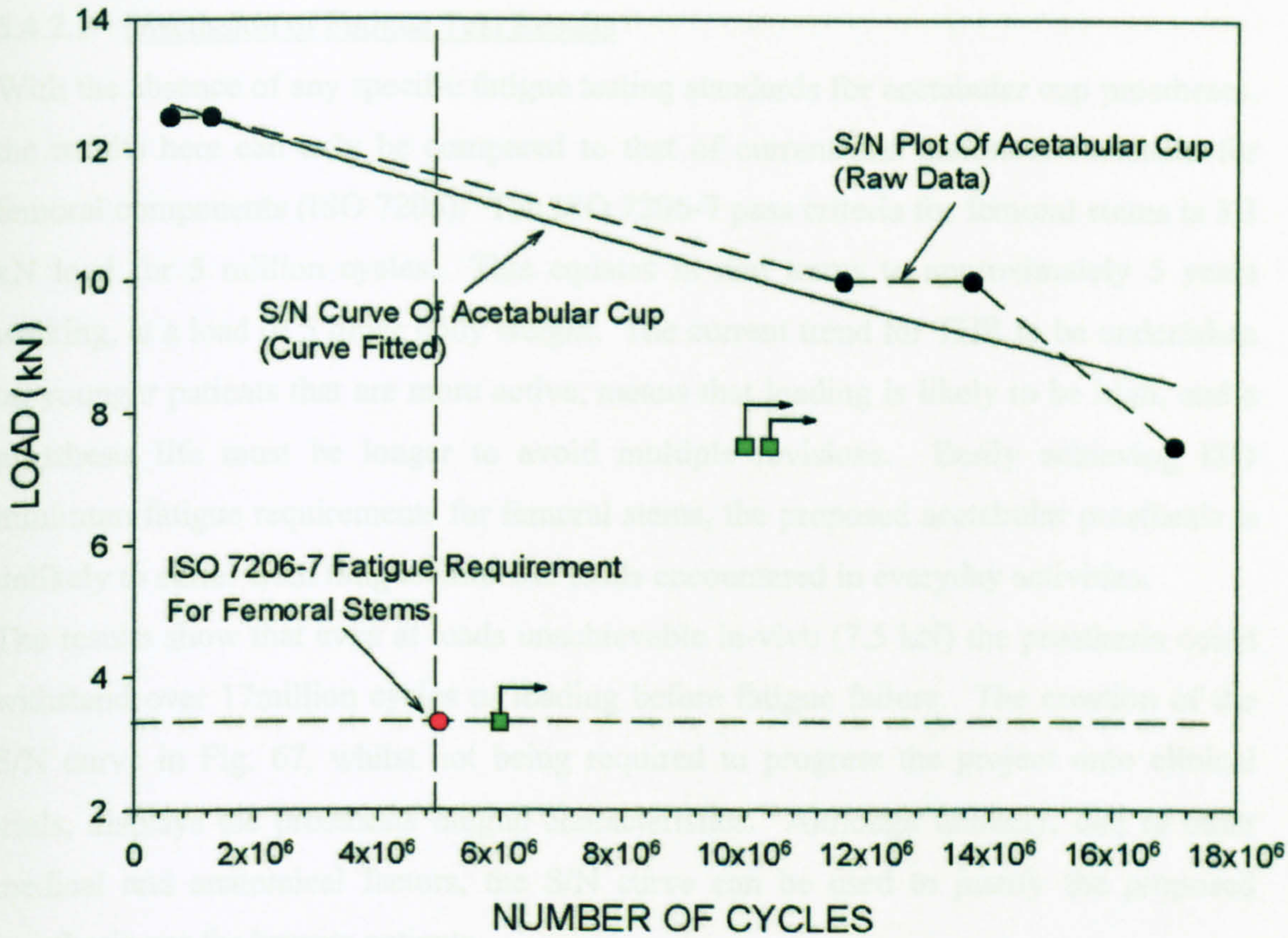

Fig. 67 Fatigue test results

(Individual test details shown in Appendix A5.2.5)

The second phase of fatigue testing was to determine the prosthesis fatigue life and these results are indicated in Fig. 67 by filled circles. These fatigue tests were left to run until fatigue failure occurred. In all cases fatigue failure occurred in the alumina cup without any visible damage to the composite backing.

All fatigue testing incorporated the new design of femoral head to femoral stem taper adaptor (Fig. 54 page 92). Unlike the incorporation of the original taper adaptor into mechanical testing, which caused catastrophic failure of the alumina femoral head (Section 5.2.3 page 88), no alumina femoral head failure occurred when the new design of taper adaptor was incorporated into the mechanical testing.

5.4.2.1 Discussion of Fatigue Test Results

With the absence of any specific fatigue testing standards for acetabular cup prostheses, the results here can only be compared to that of current and historical standards for femoral components (ISO 7206). The ISO 7206-7 pass criteria for femoral stems is 3.3 kN load for 5 million cycles. This equates in real terms to approximately 5 years walking, at a load of 5 times body weight. The current trend for THR to be undertaken on younger patients that are more active, means that loading is likely to be high, and a prosthesis life must be longer to avoid multiple revisions. Easily achieving ISO minimum fatigue requirements for femoral stems, the proposed acetabular prosthesis is unlikely to suffer from fatigue failure at loads encountered in everyday activities.

The results show that even at loads unachievable in-vivo (7.5 kN) the prosthesis could withstand over 17million cycles of loading before fatigue failure. The creation of the S/N curve in Fig. 67, whilst not being required to progress the project onto clinical trials, displays the prosthesis fatigue characteristics. Although unlikely, due to other medical and anatomical factors, the S/N curve can be used to justify the proposed prosthesis use for heavier patients.

ISO 7206-7 criteria was used for the original design of the fatigue rig and therefore extended test durations required the replacement of the dowel pin every 6 million cycles. Creation of the S/N curve required multiple, long test durations at even higher loading, and a casualty of this loading regime was the base of the fatigue rig. The failure of the base can be seen in Appendix A5.2.6. A heavy-duty version was subsequently built to withstand higher loads and longer test duration, this can be seen compared to the standard duty rig in Appendix A5.2.7. Several other fatigue rig modifications were made at this time and are listed below (also displayed in Appendix A5.2.7)

1. The specification of the hardened stainless steel insert (Appendix A2.4) was changed from 440C to 630 (17-4 PH) to give better corrosion resistance
2. The acetal specimen backing was enlarged to allow the use of a larger capacity spherical bearing and dowel pin.

The use of the proposed test rigs enabled fast, cheap and repeatable fatigue failures in the alumina cup. Replacement of the femoral component with the new fatigue test rig gives a repeatability of rig stiffness that has the ability to be 'tuned' to the desired stiffness. Operating at a frequency ten times faster than a hip-simulator, the proposed fatigue test method gives the opportunity for possible future research into the mechanics of fatigue failure of alumina bearing couples in THR.

5.4.3 Torque Test Results

Mounted acetabular prostheses were positioned in the torque test rig (Fig. 33 page 58) in accordance with the torque test procedure detailed in Section 4.4.3 page 65 and loaded statically to 3.3 kN and 7.5 kN. The torque required to rotate the alumina head at each of these loads was recorded and can be seen in Fig. 68. Test failure is defined as rotation of the alumina cup within the composite backing.

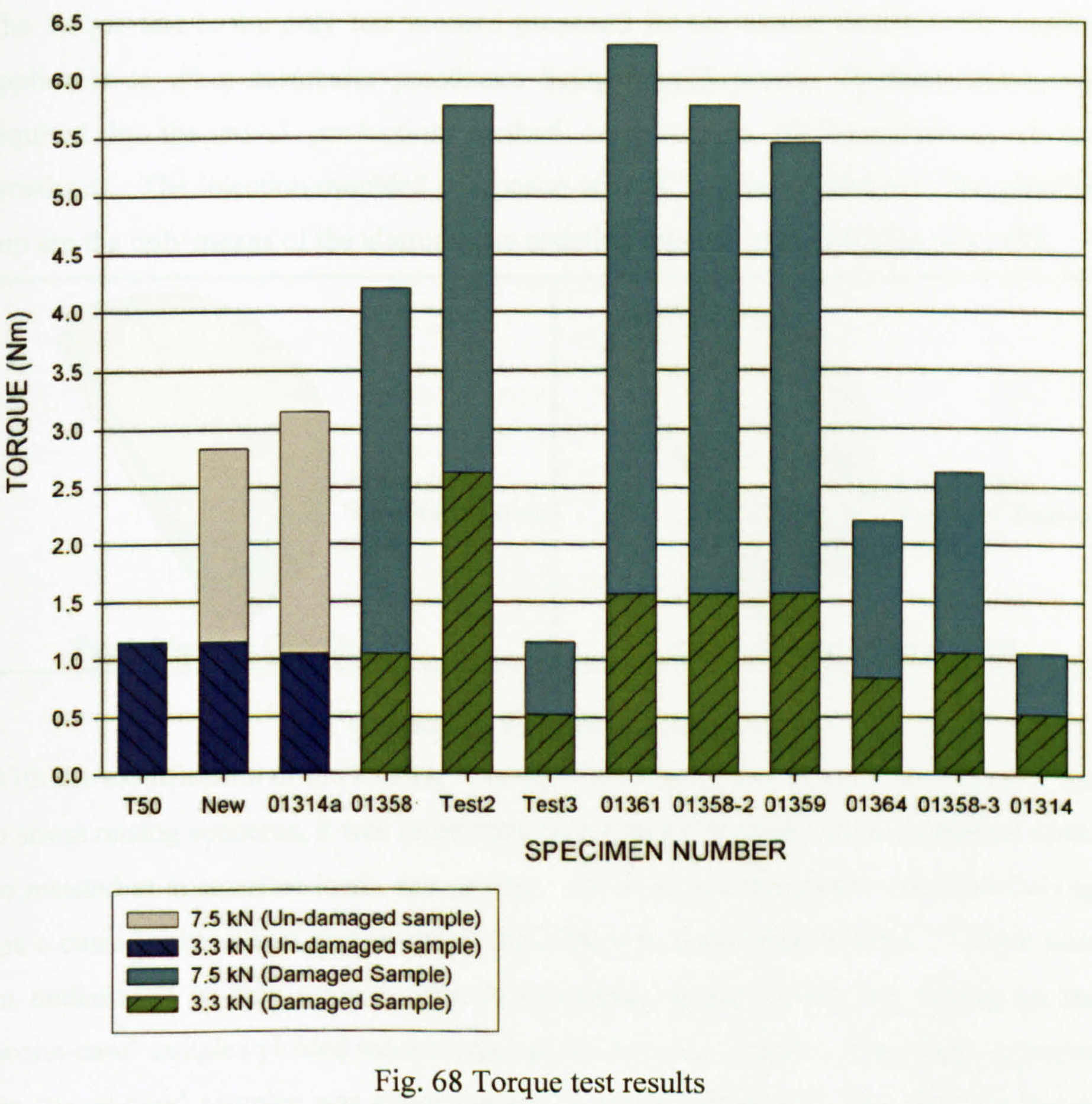

Fig. 68 Torque test results

Initial torque tests, on new or undamaged prosthesis, determined that very little torque was required to rotate the head whilst under axial load. These test are depicted in Fig. 68 by blue\grey bars and had a zero failure. Due to the success of these initial results, following torque tests would be undertaken in a 'worst-case' scenario. This worst-case

testing entails torque testing to be undertaken after UCS or fatigue testing had caused damage to the alumina cup. Full details of specific torque tests and severity of damage prior to torque testing can be found in Appendix A5.3. Highly damaged alumina cups managed to retain their integrity under torsional loading and there were zero incidences of alumina cup rotation.

5.4.3.1 Discussion of Torque Test Results

The torque test is the only test method proposed by the author that it is not readily applicable to other acetabular prostheses being manufactured. Its formulation was required by the novel production method employed in the manufacture of this prosthesis. The injection-moulded composite around 'keyway' features in the alumina cup are the only means of the alumina cup resisting rotation in the backing (Fig. 69).

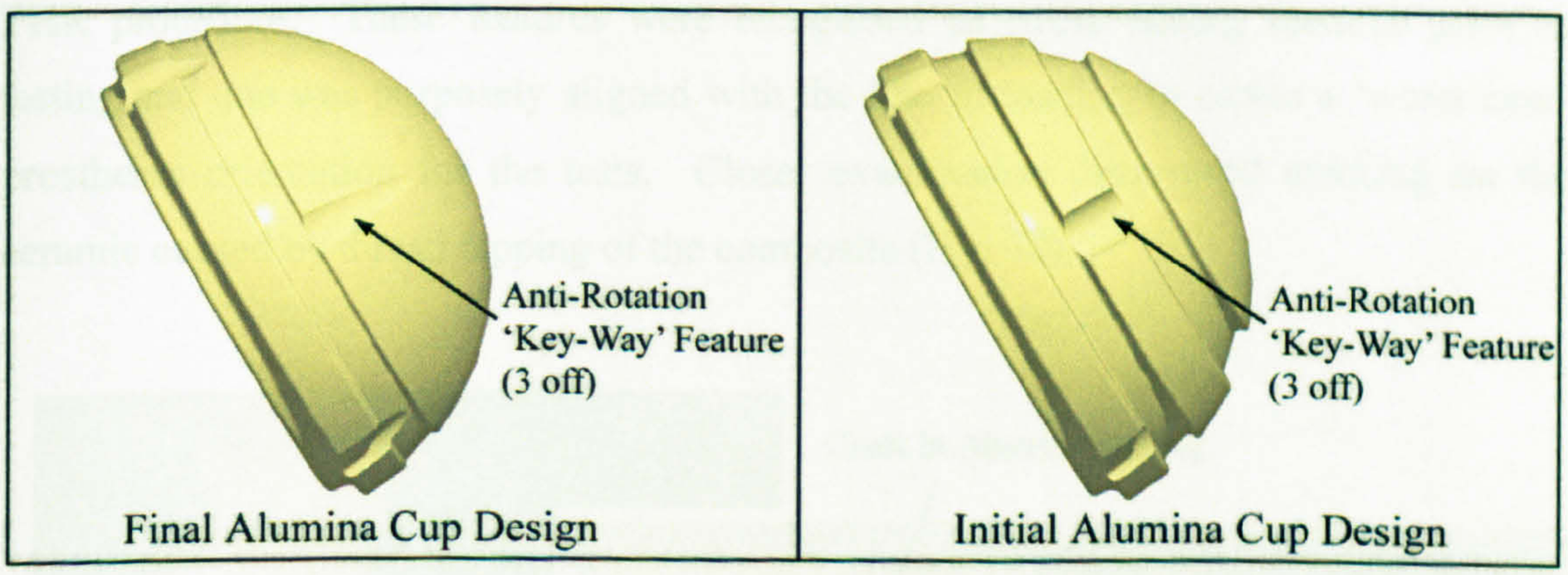

Fig. 69 Locking features in alumina cup

With the modification of the locking 'key-way' features (Section 5.2.2 and Fig. 69), due to stress raising concerns, it was imperative to determine that alumina cup rotation could be resisted at anatomical loads and greater. As expected, damage to the alumina cup has a considerable effect on the torque required to turn the femoral head. Torque tests on undamaged or new samples yielded consistent torque values, but testing on the 'worst-case' samples yielded inconsistent results between samples. The results between the 'worst-case' samples was either greater, or more surprisingly, less than the torque required to turn the undamaged samples. A possible explanation for the reduction in torque required would be damage to the cup creating a 'high' spot, thus reducing the contact area and creating point loading.

The success of the alumina cup to resist rotation even when severely damaged from prior UCS testing alleviated all fears of alumina cup rotation within the composite

backing. The test results indicate that no alumina cup fixation problems should arise when the prosthesis is implanted in-vivo.

5.4.4 Investigation of Abnormal Failure Loads and Proposed Solution

The Mechanical testing discovered several failure anomalies of the alumina cup at unexpectedly low loadings (

Fig. 65). Whilst the failure anomalies were at loads higher than that required for ISO 7206 (femoral stem standard), this unpredictability of failure is unacceptable for use as an implanted prosthesis. A study was undertaken to determine the cause of these anomalies and propose a solution.

Visual inspection of the prostheses failing at low loading, not unexpectedly, found crack initiation at one of the three tapped hole features used for instrumentation during the THR procedure. These features were recognised as stress raising features prior to testing and one was purposely aligned with the line of loading to create a 'worst case' prostheses orientation for the tests. Closer examination discovered marking on the ceramic caused by thread tapping of the composite (Fig. 70).

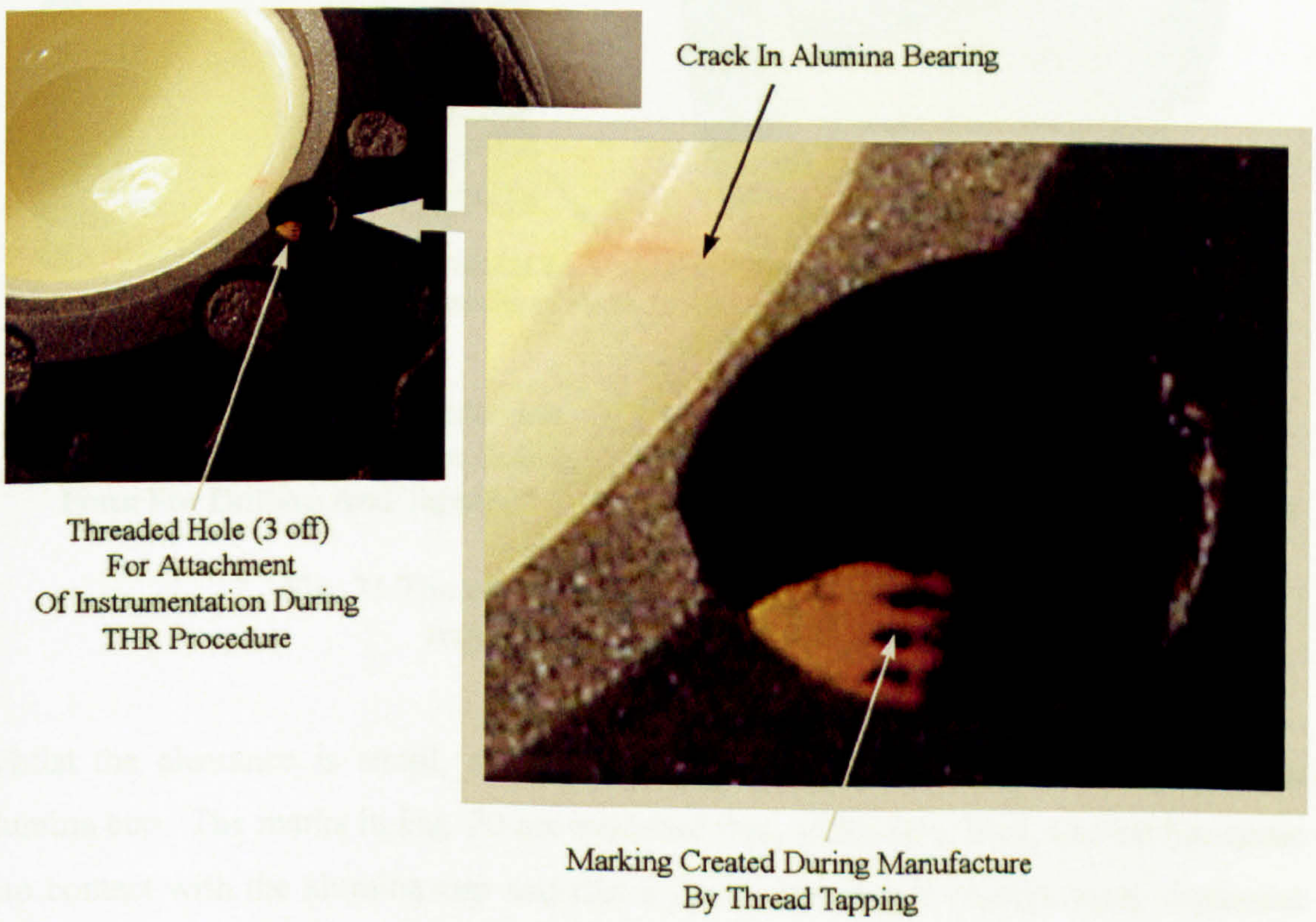

Fig. 70 Marking of alumina backing caused during manufacture

The injection moulding process creates the rough forms of these features by the use of tapered pins, and final sizing of the hole and thread tapping was carried out manually (Fig. 71). Manually drilling and tapping the prosthesis currently involves aligning the drill and tap with the axis of the hole formed by the injection moulding pins by eye.

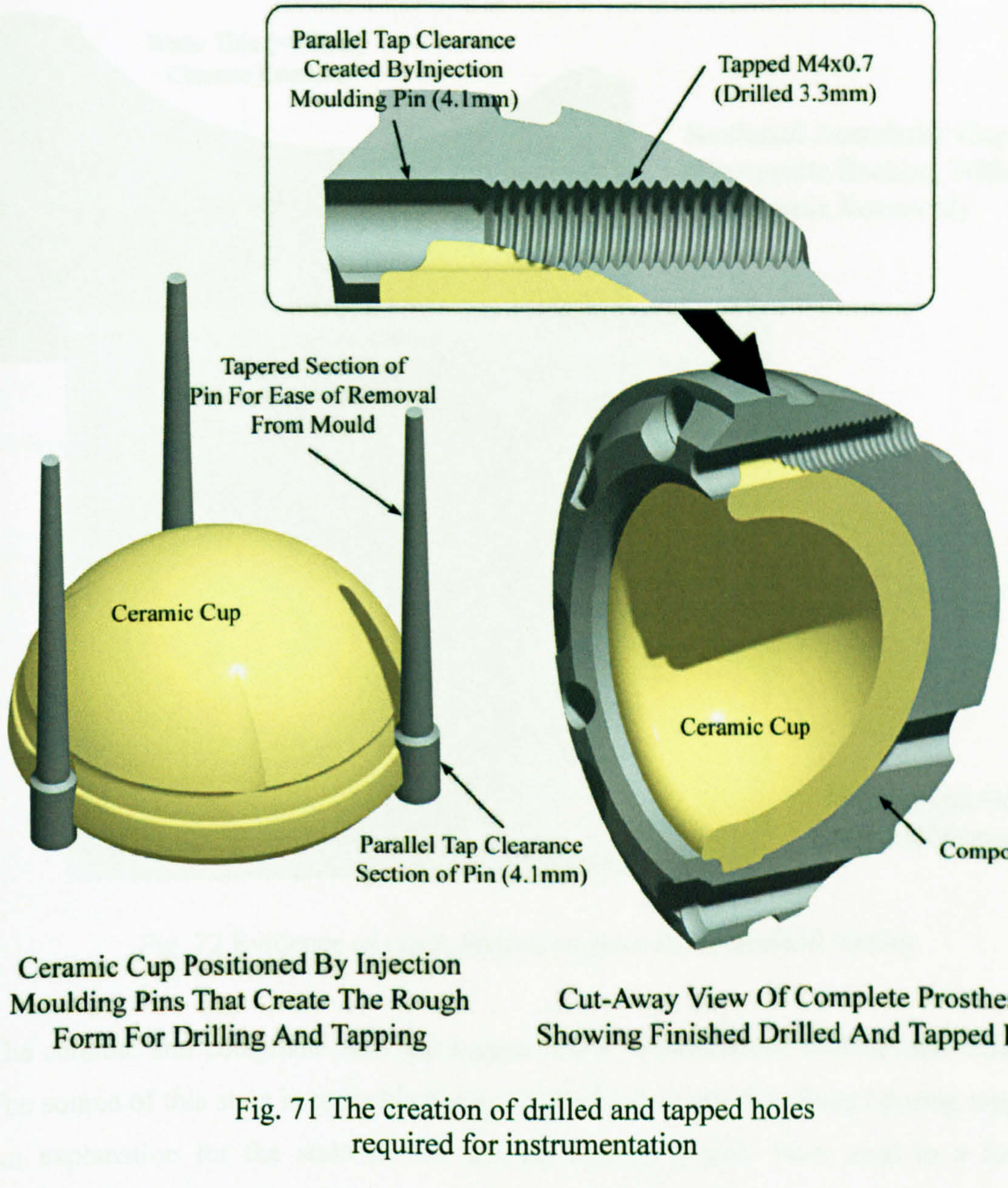

Ceramic Cup Positioned By Injection Moulding Pins That Create The Rough Form For Drilling And Tapping

Cut-Away View Of Complete Prosthesis Showing Finished Drilled And Tapped Hole

Fig. 71 The creation of drilled and tapped holes required for instrumentation

Whilst the clearance is small, at no time should either the drill or tap contact the alumina cup. The marks in Fig. 70 are evidence that, at the very least, the tap has come into contact with the alumina cup and that a jig or fixture that insures axial alignment would have been beneficial for these two manufacturing operations.

The sample was sectioned to investigate the possibility of damage to the alumina cup from this contact. Upon removal of the alumina cup, a very thin wafer of alumina was discovered that was detached (Fig. 72).

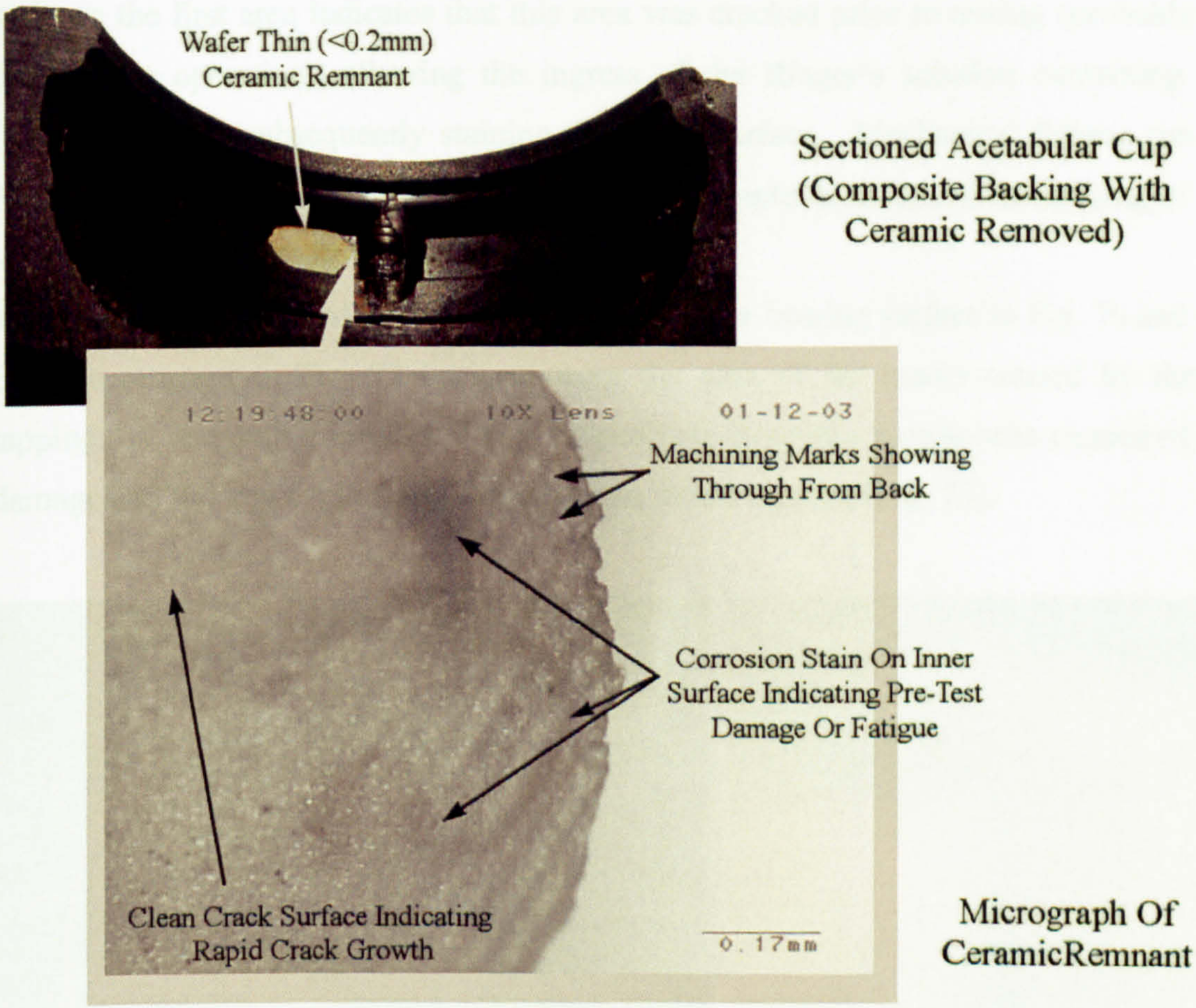

Fig. 72 Evidence of crack formation prior to mechanical testing

The ceramic and composite near the tapped holes suffered from considerable staining. The source of this stain is probably ferrous material that was introduced during tapping. An explanation for the stain is that the tap had previously been used in a ferrous material and deposited the debris during tapping of the composite, quickly corroding in the Ringer's solution. Wear of the tap in the tough composite, and therefore the deposition of high-speed steel particles in the area, could be a contributing factor to the source of the ferrous material creating the stain.

The presence of this corrosion stain, whilst clearly undesirable for clinical implantation, was of benefit in analysing the damage to the alumina cup. The micrograph in Fig. 72 displays two distinct areas on the fracture side of the wafer remnant. The first area displays a corrosion stain and the second area displays a clean fracture surface. The stain on the first area indicates that this area was cracked prior to testing (probably by the tapping operation), allowing the ingress of the Ringer's solution containing the ferrous material, subsequently staining the crack surface. Mechanical fatigue can be dismissed as the cause of this initial crack as this sample failed on initial ramping of the load and not during fatigue testing.

The large crack, coloured red by dye penetrant, on the bearing surface in Fig. 70 and the ceramic remnant in Fig. 72 initiated from the area of the marks caused by thread tapping. A remaining, lower stressed, tapped hole from this sample was examined for damage and showed evidence of damage from thread tapping (Fig. 73).

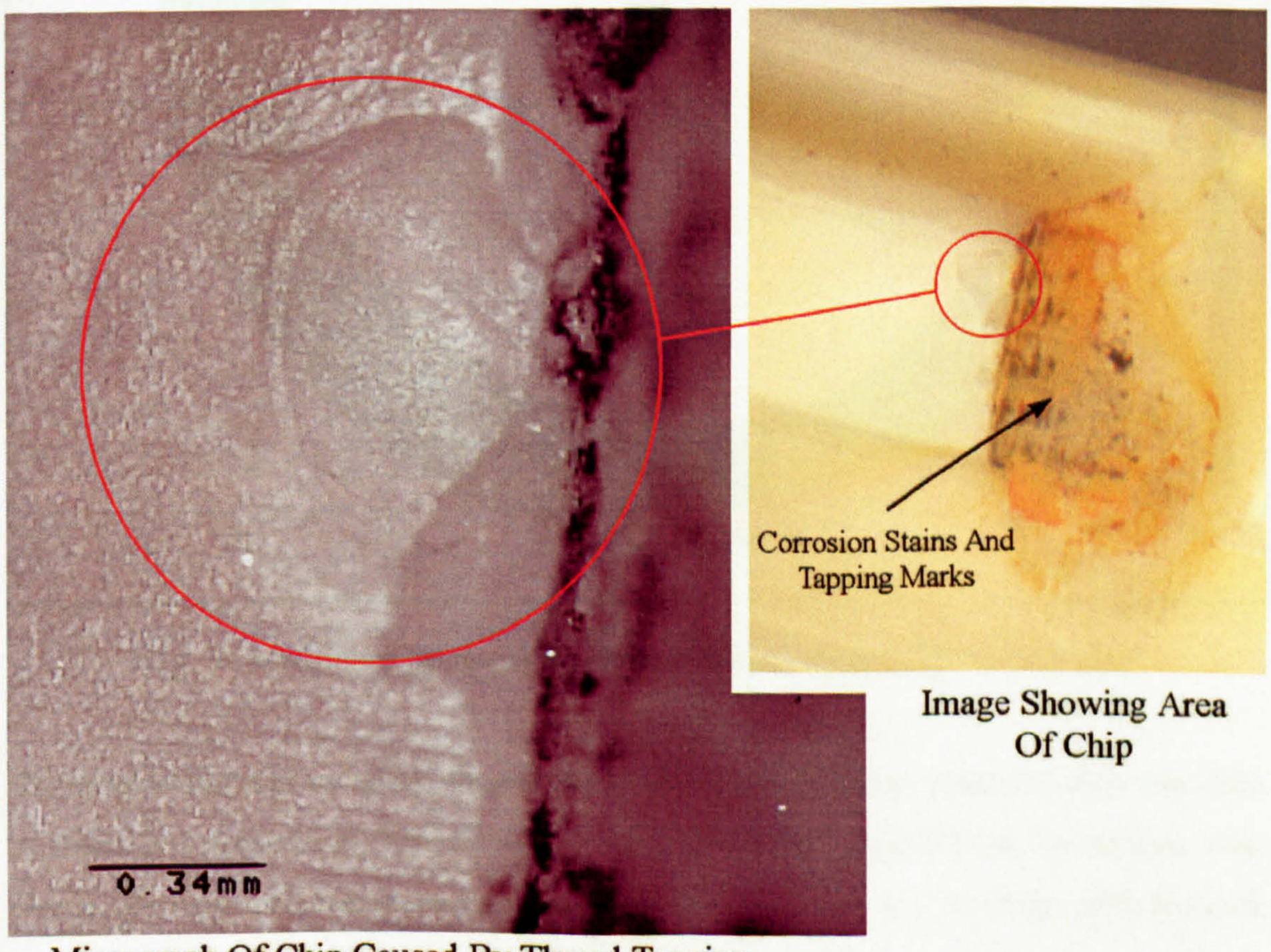

Micrograph Of Chip Caused By Thread Tapping During Manufacture

Image Showing Area Of Chip

Fig. 73 Evidence of ceramic damage from thread tapping

Any damage to the alumina ceramic prior to mechanical testing will severely limit the load bearing ability of the cup due to its low fracture toughness. With the fracture toughness of the Vitox alumina cups at 4 $MPa(m)^{1/2}$ any damage will have a catastrophic effect.

A three-dimensional FEA of the UCS test had previously been undertaken (Section 5.3) with the simulation results in close agreement the majority of mechanical testing. A two-dimensional slice of the alumina cup through the FEA, at a load of 22kN, reveals bending causing a maximum principal stress in the alumina of 370MPa (Fig. 74).

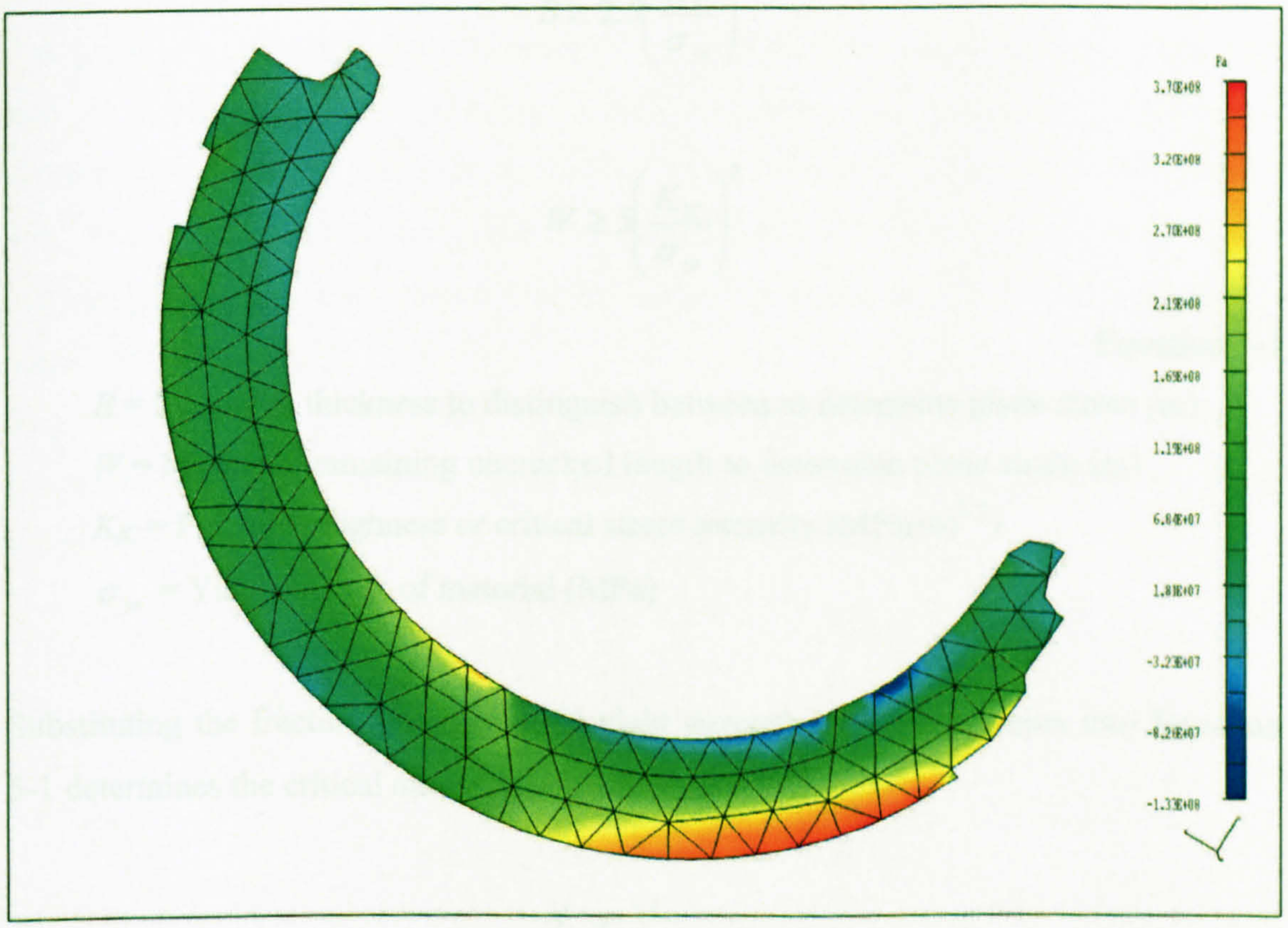

Fig. 74 Maximum principal stress in alumina cup at 22kN failure load

Characteristically of ceramic, alumina fails in tension at values approximately one fifth of those in compression, with failure in bending at only 380MPa on the tension side. Using this data, basic fracture mechanics could be applied to determine critical crack length.

5.4.4.1 Determination of Plane stress or Plane strain behaviour

The accuracy with which K_{IC} describes the fracture behaviour depends on how well the stress intensity factor characterises the conditions of stress and strain immediately ahead of the crack tip (Ewalds and Wanhill 1984). Minimum specimen sizes to ensure nominal plane strain behaviour have been established by considerable experimental studies. Examples to determine the minimum specimen thickness (B) and remaining uncracked length (W) are displayed below (Equation 5-1).

$$B \geq 2.5\left(\frac{K_{IC}}{\sigma_{ys}}\right)^2$$

$$W \geq 5\left(\frac{K_{IC}}{\sigma_{ys}}\right)^2$$

Equation 5-1

B = Minimum thickness to distinguish between to determine plane strain (m)

W = Minimum remaining uncracked length to determine plane strain (m)

K_{IC} = Fracture toughness or critical stress intensity ($MPa(m)^{1/2}$)

σ_{ys} = Yield strength of material (MPa)

Substituting the fracture toughness and yield strength of Vitox alumina into Equation 5-1 determines the critical dimensions to allow use of K_{IC}.

$$B \geq 2.5\left(\frac{4}{380}\right)^2 = 2.7*10^{-4}\text{m}$$

$$W \geq 5\left(\frac{4}{380}\right)^2 = 5.5*10^{-4}\text{m}$$

Equation 5-2

The material is thicker than $2.7*10^{-4}$m and the remaining uncracked length would be greater than $5.5*10^{-4}$m, therefore plane strain applies.

5.4.4.2 Determination of crack length to cause failure (22kN Load)

The numerical solution for stress intensity is shown below (Equation 5-3):

$$K_I = C\sigma\sqrt{\pi a}$$

Equation 5-3

K_I= Stress intensity (MPa(m)$^{1/2}$)

C = Geometry correction factor

σ =Stress applied to material (MPa)

a = Critical crack length (m)

The geometry correction factor is required due to the effect on the crack tip stress field and the finite size of the specimen. Crack dimension and position are required for accurate calculation of geometry correction factors. A number of common solutions are available for use without this crack data (Ewalds and Wanhill 1984) and the value of 1.12 will be used for the value of C in the following equations. This value represents a small single edge crack.

The rearrangement of Equation 5-3 and the substitution for known Vitox material properties and stress values obtained from FEA (see Fig. 74) gives the critical crack length at 22kN (Equation 5-4).

$$a_c = \frac{1}{\pi}\left(\frac{K_{IC}}{\sigma C}\right)^2 \qquad a_c = \frac{1}{\pi}\left(\frac{4}{370*1.12}\right)^2 = 2.97*10^{-5}\text{m}$$

Critical crack length is 0.0297mm

Equation 5-4

a_c = Critical crack length (m)

K_{IC} = Fracture toughness or critical stress intensity (MPa(m)$^{1/2}$)

σ_{ys} = Yield strength of material (MPa)

C = Geometry correction factor

As the stress in the alumina approaches its failure stress, even very small cracks could initiate failure. Equation 5-4 demonstrates this by showing that at a failure load of 22kN the critical crack length is only 0.0297mm.

The failure of two of the alumina cups during mechanical testing at abnormally low loads (5.95kN mean load) were calculated to be experiencing stress levels of approximately 100MPa at failure. Further calculations revealed that a critical crack length of 0.42mm would be required for failure at this load. A crack of this length would be quite considerable compared to the alumina cup and would require the crack to be modelled in the FEA as its actual geometry would act as stress raiser. The expected effect of the inclusion of the crack in the FEA would be much greater local stresses than the 100MPa predicted, therefore rendering the 0.42mm critical crack length invalid. Importantly though, the damage to the ceramic that can be seen in Fig. 73 is of large enough magnitude to cause these premature failures and that even very small cracks when approaching the alumina's stress limit could cause failure. The possibility of damage, even slight, to the alumina ceramic from the thread tapping operation is unacceptable and the design or manufacturing method must be revised to eliminate it.

5.4.4.3 Proposed Solution To Manufacturing Damage Of the Alumina

The clearance between the tapped hole and alumina cup can easily be increased to prevent damage to the alumina by a simple modification to the injection-moulding tool. The three tapered pins in the mould tool also locate the alumina cup during moulding, and therefore require modification as well as repositioning (Fig. 75 page 122).

The simple modification illustrated in Fig. 75 will increase the PCD of the drilled and tapped holes, creating greater clearance from the alumina cup. The modification of the mould tool, along with the manufacture of a simple drilling and tapping jig, will eradicate low load failures due to damage of the alumina cup.

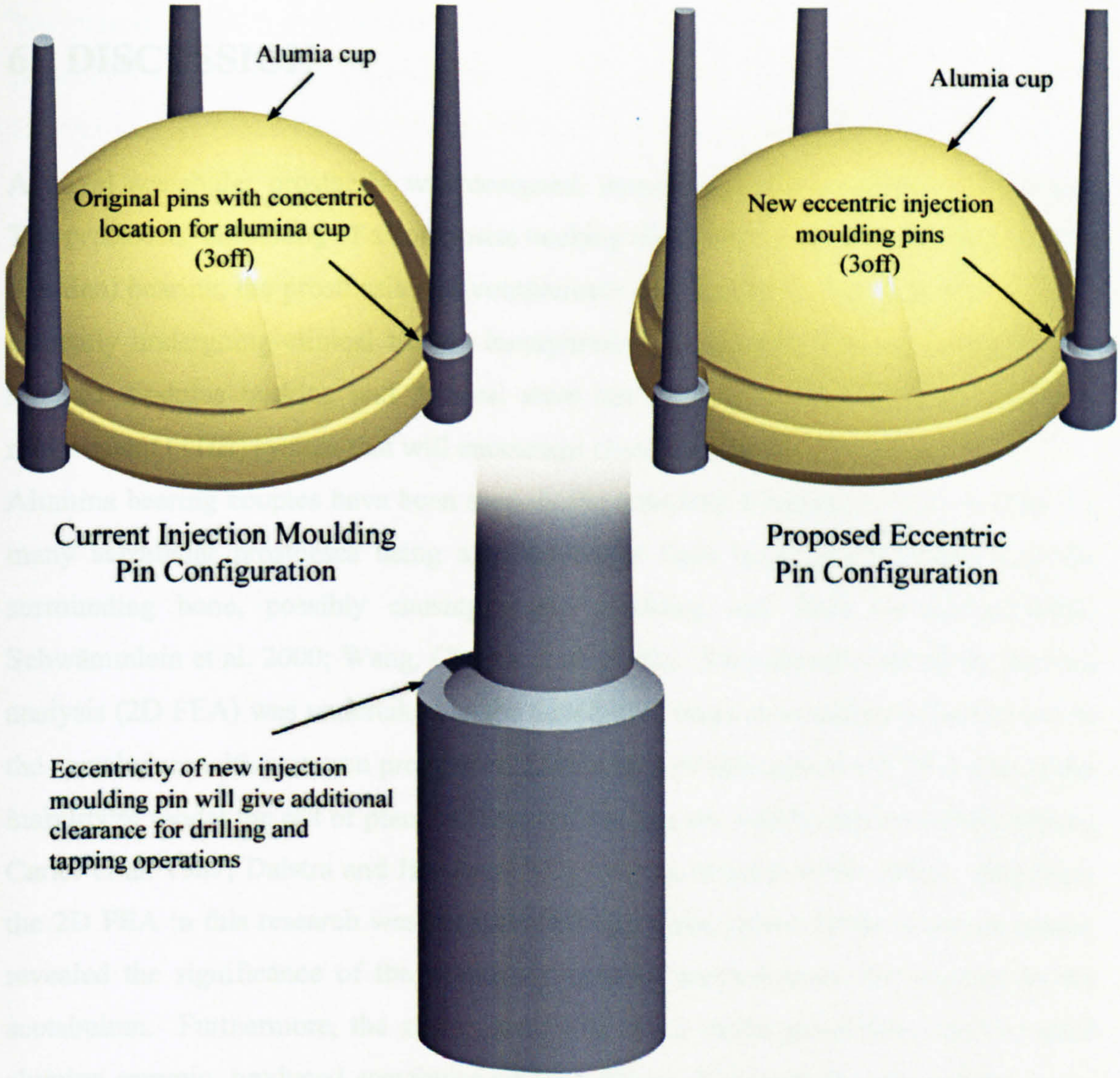

Current Injection Moulding Pin Configuration

Proposed Eccentric Pin Configuration

Detailed View Of Proposed Eccentric Pin

Fig. 75 Proposed solution to alumina cup damage during tapping

6 DISCUSSION

A novel acetabular prosthesis was designed, manufactured and mechanically tested. The prosthesis, consisting of a composite backing (Peek450CA30) and a ceramic (Vitox alumina) bearing, the prosthesis will complement the 'Bradley Composite Stem' that is currently undergoing clinical trials. Incorporating an alumina bearing couple with a reduced modulus backing and femoral stem has created a 'bone friendly' total hip replacement (THR) system that will encourage osseointegration.

Alumina bearing couples have been seen as the complete solution to wear in THR but many acetabular prostheses using alumina suffer from being much stiffer than the surrounding bone, possibly causing stress shielding and bone resorption (Pitto, Schwämmlein et al. 2000; Wang, Chopra et al. 2002). Two-dimensional finite element analysis (2D FEA) was undertaken at the conceptual stage to investigate the stresses in the acetabulum with common prostheses. Limitations of this type of 2D FEA, due to the inability to model the out of plane stiffness of the hip, are widely reported (Rapperport, Carter et al. 1987; Dalstra and Huiskes 1995; Dalstra, Huiskes et al. 1995). However, the 2D FEA in this research was incorporated into a parametric study in which results revealed the significance of the prosthesis material properties on the stresses in the acetabulum. Furthermore, the study found that much stiffer prosthesis, such as solid alumina ceramic, produced acetabular stresses orders of magnitude greater than in the natural hip. The high stresses in the solid alumina and the titanium alloy backed alumina prostheses would suggest difficulties in achieving bone ingrowth, and negative bone remodelling would be highly possible should ingrowth occur. Stress in the solid alumina was approaching the yield strength of the bone, and it is unsurprising that this type of prosthesis was widely abandoned in the 80's due to poor osseointegration. Current designs incorporate the ceramic bearing in titanium alloy backing. However, results from this study found that such designs produced stresses nearly ten times greater than that of the natural hip. Stresses of this nature could deter bone in growth and create fibrous tissue that could manifest as long or middle term failure.

The proposed PEEK 450CA30 and Vitox prosthesis displays stresses that are between those of the natural hip and the titanium alloy backed ultra high molecular weight polyethylene (UHMWPE) prosthesis. Clinically proven over many years the titanium alloy backed UHMWPE prosthesis still suffers from aseptic loosening. The cause of the aseptic loosening is still fiercely debated, but the final explanation might be sought in a combination of multiple etiologic factors including prosthesis stiffness, particulate reaction and stress shielding. The proposed prosthesis displays similar subchondral stress contour to the natural hip whilst exhibiting lower Von Mises stress to that of the titanium alloy backed UHMWPE. The high wear rates associated with UHMWPE, when compared to alumina on alumina, and the profound effects of wear debris on local tissues and fixation are well reported. The combination of PEEK 450CA30 and Vitox alumina has the advantage of lower Von Mises stresses to that of the titanium alloy backed UHMWPE, and wear rates are orders of magnitude lower than UHMWPE bearing surfaces (Zichner and Lindenfeld 1997; Willmann 2000c). Any alumina wear debris that is created is biologically inert (Christel 1992; Willmann 1998; Murray 1999; Sedel, Bizot et al. 2000), and the stresses in the subchondral bone caused by the proposed prosthesis could be further reduced by the modification of the volume fraction of the PEEK composite. With this excellent 'tune-ability' of the prosthesis, predicted Von Mises stresses can be less than that of the natural hip if required.

The prosthesis proposed by the author incorporates the alumina bearing into the reduced stiffness composite backing during the injection moulding thus avoiding problems inherent with modularity, micromotion and UHMWPE wear debris (Bobyn, Tanzer et al. 1994; Willert and Semlitsch 1996). At this time, no literature has been located describing any similar process incorporating a ceramic component into a composite injection moulding.

Mechanical testing standards worldwide (BSI, ISO, FDA) reflect the problems historically encountered with THR prostheses, but fail to address the testing of the acetabular cup prosthesis. Many mechanical testing standards are in place for femoral components, for example ISO 7206 comprises of 10 parts (BSI 1998-2002), but no specific standard exists for the mechanical testing of acetabular prostheses. The proposed anatomically orientated tests allowed fast repeatable tests to obtain ultimate compressive strength (UCS), fatigue and torque data.

The problems due to the lack of acetabular prosthesis testing standards were highlighted by the FEA work undertaken. Axial testing is the usual orientation used in testing ceramic femoral heads and commonly adopted for ceramic cups. The proposed anatomical UCS test identified stress-raising features in the alumina bearing that might not have been discovered until implantation in-vivo if axial testing had been adopted. FEA displayed a maximum principal stress increase of 23% in the alumina cup when loaded anatomically. Implications of failing to recognise the possible stress increase due to anatomical loading conditions are particularly relevant with reduced prosthesis sizes, such as those for children or the Asian market and could lead to thinner alumina bearings and therefore possible failure in-vivo.

The proposed fatigue test method allows an anatomically orientated test without the need for high cost specialist hip simulators. The proposed method can evaluate acetabular cup prosthesis fatigue life on standard servo-hydraulic test equipment at frequencies ten times faster than normally used on hip simulators. The fatigue test was developed to complement rather than replace hip simulator studies, as a fast, cheap method to assess ceramic cups fatigue resistance. The restrictive costs of the prostheses hampered the mechanical testing by limiting the number of tests that could be undertaken. Whilst the number of test undertaken was greater than the requirements to progress the project to clinical trials, further testing would give even greater confidence in the results.

The performance of this new acetabular prosthesis exceeds any relevant standard for femoral components. Fatigue tests undertaken in this study easily surpasses the required 5million cycles at over three times the load specified in the ISO standard for femoral stems, and loading of this magnitude is never experienced in-vivo (Bergmann 1993; BSI 1998-2002). The fatigue performance surpassed in-vivo loading condition so greatly that it is hard to define the cup's performance in terms of 'everyday' activities, but at the minimum load to suffer fatigue failure (7.5kN), the endurance was equivalent to over 17 years' of walking for a 36 stone (231kg) person. In regular clinical practice such a heavy patient would not undergo the procedure, and the average THR patient may well not exert loads large enough to instigate fatigue failure in this prosthesis.

THR has been a victim of its own success. Predominately THR's use was in the elderly, but now more frequently in younger, more active patients. With younger, more active patients come higher expectations that require a revised set of design goals for the

prosthesis. Sir John Charnley, who pioneered THR, predicted problems with THR in younger patients over 25 years ago (Charnley 1979). A review of the literature identified aseptic loosening as the most common type of failure of acetabular cups. High stiffness of the prosthesis is understood to be a contributing factor (Nizard and Sedel 1992; Willmann 1998; Bizot, Banallec et al. 2000; Gardelin, Seminario et al. 2000; Gualtieri, Calderoni et al. 2000; Scheller, Claus et al. 2000; Bierbaum, Barsoum et al. 2001; Park, Han et al. 2001), particularly with conventional ceramic acetabular cups (Pitto, Schwämmlein et al. 2000). The proposed acetabular prosthesis directly addresses the design goals of a prosthesis for younger more active patients. New anatomically orientated test methods proposed by the author revealed several design and manufacturing problems in the proposed THR system and test rigs. During the course of this study, all design and manufacturing problems were overcome, and it is the author's view, in light of the study's FEA and mechanical test results, that the proposed acetabular hip prosthesis be recommended for clinical trials.

7 CONCLUSIONS, LIMITATIONS AND FUTURE WORK

7.1 Conclusions

On the production of a novel acetabular cup prosthesis

A novel acetabular prosthesis was designed and manufactured with the support of Orthodynamics Ltd. The range of motion for the proposed prosthesis was analysed using Pro-Engineer three-dimensional CAD models. Results from the range of motion analysis determined that the prosthesis easily exceeds the ranges of motion required for everyday activities and no instances of impingement occurred.

Finite element analysis was undertaken to investigate the stresses in the acetabulum with acetabular prostheses and in the natural hip. The analysis results for the natural hip were in agreement with published results, validating the modelling method and giving confidence in the results incorporating prostheses. Finite element analysis incorporating current and recent materials used in acetabular prostheses identified Von Mises stresses in the acetabulum orders of magnitude higher than the natural hip, possibly leading to poor osseointegration and negative bone remodelling. Finite element analysis of the proposed composite backed ceramic prosthesis determined subchondral Von Mises stresses similar to a natural hip, and lower than those of titanium alloy backed UHMWPE prostheses. Reduction of stresses should encourage osseointegration and reduce negative bone remodelling and resorption

'Tuning' of the composite's backing volume fraction was demonstrated by finite element analysis. This displayed further reductions of subchondral Von Mises stress of up to 70% if required. The alumina bearing design was optimised using finite element analysis reducing the predicted maximum principal stress in the component by 24%.

Mechanical testing identified alumina head failures at only 8% of reported burst strength. Investigation into the failures determined that they were due to incompatible tapers. In fact, the outcome of this investigation resulted in the Medical Devices

Agency issuing a safety notice containing best practise information for ceramic femoral heads. Revised taper adaptors for use with alumina femoral heads were designed and mechanically tested. No alumina femoral head failures occurred with the revised taper adaptor design. Finite element analysis of the two new taper adaptor variants and the alumina head reported a maximum principal stress reduction of 34% and 22% respectively.

On materials and manufacture

Alumina on alumina was identified as the most suitable bearing couple for the proposed prosthesis. Advantages over traditional material, such as UHMWPE, include lower wear rates and increased biocompatibility. Wear rates orders of magnitude lower than UHMWPE have been reported for alumina on alumina bearing couples. A carbon fibre reinforced composite backing (PEEK 450CA30) was created for the alumina bearing surface by injection moulding. The reduced modulus of the composite allows the optimisation of the stress distribution in the system without compromising durability and bone ingrowth. The combination of a PEEK 450CA30 backing and an alumina bearing couple gives very low wear rates whilst avoiding the high stiffness normally inherent with a ceramic on ceramic bearing couple.

An injection moulding process that incorporates the alumina cup during manufacture was formulated. Thermally induced cracking of the alumina cup and mould filling problems were overcome in order to produce the novel acetabular prosthesis. At this time, no literature has been located describing any similar process incorporating a ceramic component into a composite injection moulding.

On the novel mechanical test methods

Investigation into THR mechanical testing standards (BSI, ISO and FDA) determined that there was no testing standards for acetabular cup prostheses. A novel UCS test method for acetabular prostheses was designed, built and tested by the author. The proposed UCS test is anatomically orientated, and therefore eliminates the possibility of not revealing stress-raising features that are not stressed when tested in the traditional

axial method. Finite element analysis of the traditional ultimate compressive strength (UCS) axial loading method and the proposed anatomically orientated UCS method was undertaken. The FEA results support the need for the proposed anatomical test method as the maximum principal stress of the alumina bearing component in an anatomically orientated acetabular prosthesis increased by 22%.

A novel anatomically orientated method for fatigue testing of acetabular prostheses was designed, built and tested by the author. Operating at 10 Hz, the novel fatigue test provides results ten times faster than a hip simulator, and has the benefit of requiring only standard material testing equipment. The production of an S/N curve for the proposed acetabular prosthesis, at times required the fatigue testing to be carried out at loads over three and half times greater than the ISO fatigue requirements for femoral stems. Fatigue testing at these loads exceeded the fatigue limit for the initially proposed fatigue test rig. A second heavy-duty fatigue rig was designed and built by the author for testing at these elevated loads. Although these elevated loads would never be experienced in-vivo, the creation of samples with fatigue failures could also allow further research into fatigue failure of alumina bearing couples in THR.

A novel test to determine adequate fixation of the ceramic bearing in the injection moulded backing during torque loading was designed, built and tested. The torque test was required as fixation of the alumina cup is created during injection moulding. The test ensured that the filling of the anti-rotation features in alumina cup during manufacture was capable of resisting torque loads under anatomical loading.

On the mechanical test results

A mean UCS of 22.02 kN was determined for the proposed prosthesis. A load of this magnitude equates to approximately 30 times body weight and would never occur in-vivo. During ultimate compressive strength testing, two samples produced unacceptably low failure loads of 6.6 kN and 5.3 kN. The cause was determined as damage to the alumina cups during the final stages of prosthesis manufacture. A simple solution to the manufacturing damage is proposed and thus further prostheses incorporating the solution will be suitable for clinical trials.

The proposed acetabular prosthesis easily achieved the minimum fatigue requirements for femoral components (5 million cycles at a sinusoidal load between 0.3 and 3.3 kN). Further testing at greater loads and longer durations produced an S/N curve for the proposed prosthesis. The loads required to produce a fatigue failure were considerably higher than those that are achieved in-vivo.

Axial torque loading of the alumina cup at anatomical loads did not cause the alumina cup to rotate in the composite backing. Undamaged bearing surfaces require just over 1Nm of torque to rotate the head in the alumina cup at a 3.3 kN axial load. 'Worst case' torque tests were undertaken incorporating damaged alumina cups and at no time did the alumina cup rotate in the composite backing.

The test results for the UCS; fatigue and torque testing provide evidence that the project is acceptable for continuation to clinical trials.

7.2 Limitations and Future Work

The limitations of using 2D FEA for the modelling of the hip are widely reported, and are discussed in Section 5.1 (page 70). A 2D model cannot account for the out-of-plane part of the acetabular wall and will therefore be too flexible. The 2D model did however lend itself ideally to the parametric study, giving results on the effect prosthesis material had on stress distributions in the acetabulum. The 2D FEA results were of fully osseointegrated prostheses and not newly press-fitted. Similar work by Taylor (1998) on a controlled stiffness femoral prosthesis proposes that, whilst a controlled stiffness femoral prosthesis is beneficial when osseointegrated, it offers no advantages over conventional stiffness femoral prosthesis when implanted as a press fit. The logical next step for future work would be to undertake further 2D FEAs on un-bonded, press-fit, prosthesis and 3D FEAs that can fully model the stiffness of the hip and acetabulum. The 3D model would also be used to investigate shear stresses and micromotion at the prosthesis to bone interface. Shear stresses and micromotion at the interface have been of concern with reduced stiffness prostheses and the 3D model

would be used to determine the effect of reducing the proposed prosthesis stiffness further on the interface.

The lower half of the proposed fatigue rig is based on the neck geometry of the femoral stem that is to be used in the proposed THR system. The stiffness of the femoral component used may affect the performance of the alumina bearing. Further work to determine the effect of stems of differing stiffness might have on the performance of the alumina bearing couple would be beneficial in the design of future THR systems.

Corrosion of the hardened insert on the fatigue rig required regular changing of the Ringer's solution. The problem was addressed with the design and manufacture of the heavy-duty rig that used a stainless steel with a higher corrosion resistance than the original 440C specification. Further tests with this rig need to be undertaken to ensure adequate corrosion resistance of the design. Further fatigue testing on the alumina cup with the heavy-duty fatigue rig would also supply additional fatigue data. The original data is limited by the prohibitive costs of the prosthesis. The prohibitive costs of the prosthesis made it impossible to undertake multiple tests at a given load, and therefore any additional testing would give further confidence in the S/N curve produced by the research.

The proposed fatigue rig can create samples suitable for the investigation into the fatigue failure mechanism of alumina ceramic. Research into fatigue failure of fine-grained alumina is lacking, with no known publications regarding the fatigue of anatomically orientated alumina acetabular prosthesis in Ringer's solution. Future research need not be limited to prosthesis design and testing. The novel manufacturing method of the proposed prosthesis could lead to other possible commercial applications for ceramic inserts in injection-moulded composites.

APPENDICIES

Appendix 1

Movements Of The Hip Joint And Typical Ranges Of Motion

A1.1 Movements of the Hip Joint

Adapted from Nordin and Frankel (2001)

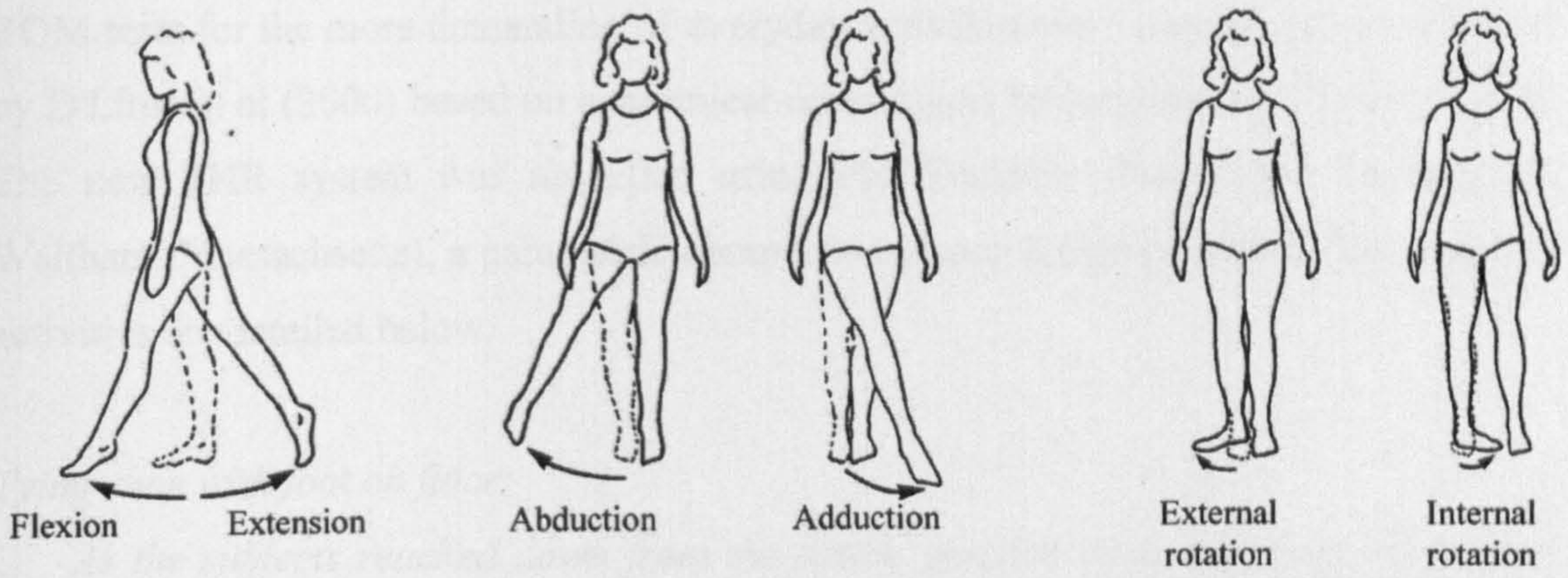

A1.2 Anatomical Planes

Adapted from BS 6324-1 (BSI 1983)

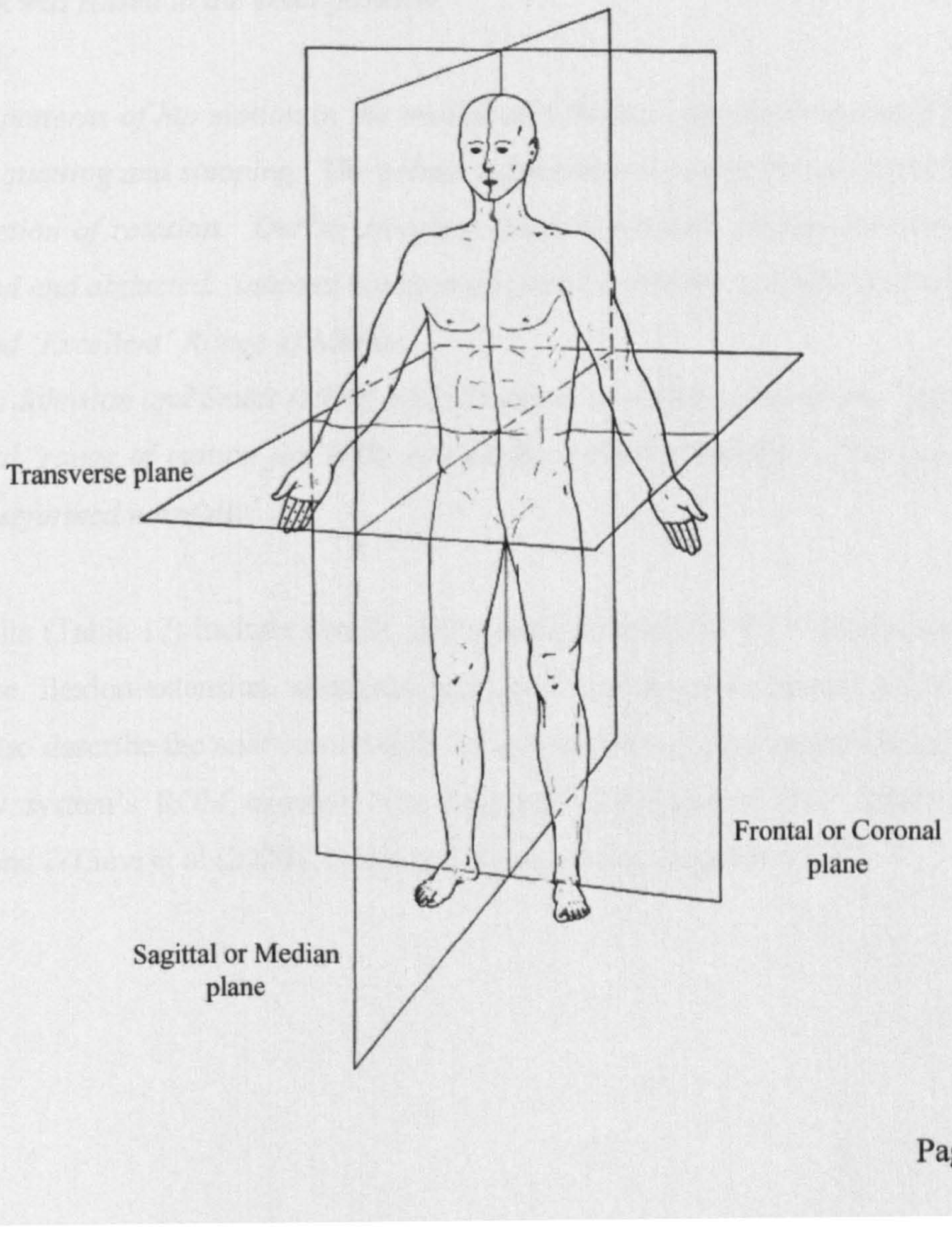

A1.3 Results For Typical Ranges of Movement During Everyday Activities

ROM tests for the more demanding of everyday activities were carried out as described by D'Lima et al (2000) based on anatomical orientations by Johnston and Smidt (1970). The new THR system was modelled using Pro Engineer (Parametric Technology, Waltham, Massachsetts), a parametric computer-assisted-design program. The common activities are detailed below:

Tying shoe with foot on floor:

As the subjects reached down from the sitting position to tie his shoe, hip motion occurred in the directions of flexion, abduction and external rotation. In the latter 2 directions the excursion was small. Extension and adduction took place as the trunk was raised to the erect position.

Stooping:

The patterns of hip motion in the medial and frontal planes are essential the same for squatting and stooping. The primary difference between the two activities is the direction of rotation. During stooping external rotation occurred as the hip was flexed and abducted. Internal rotation occurred as the hip extended and adducted.

'Ideal and 'Excellent' Range of Motion:

Both Johnston and Smidt (1970) and D'Lima et al (2000) propose an 'Excellent' or 'ideal' range of motion for THR, so that the common activities of daily living can be performed normally.

The results (Table 17) include details of the orientation of the THR system; acetabular cup angle, flexion/extension, abduction/adduction and internal/external rotation. The results also describe the additional degree of articulation to impingement in each plane. The new system's ROM exceeds both Johnston and Smidt (1970) 'ideal' range of motion and D'Lima et al (2000) 'Excellent' range of motion proposals.

Activity	Acetabular Cup Angle	Degree of Flexion (+) or Extension (-)	Additional Flexion Available Until Impingent	Degree of Abduction (+) or Adduction (-)	Additional Abduction Until Impingent	Degree of Rotation, External (+) or Internal (-)	Additional Rotation Until Impingent
Tying shoe (foot on floor)	45°	+129°	Unlimited	+18°	+26°	+13°	+54°
Stooping	45°	+125°	Unlimited	+25°	+23°	+15°	+51°
'Ideal' range of motion as proposed by Johnston and Smidt (1970)	45°	+120°	Unlimited	+20°	+17°	+20°	+43°
'Excellent' range of motion as proposed by D'Lima et al (2000)	35°	+110°	Unlimited	+45°	+1°	+45°	+2°
	35°	-30°	Unlimited	-45°	0°	+45°	Unlimited

Table 17 Range of motion results

Appendix 2

Engineering Drawings Of Novel Fatigue Testing Rig

A2.1 Fatigue Rig Assembly Drawing

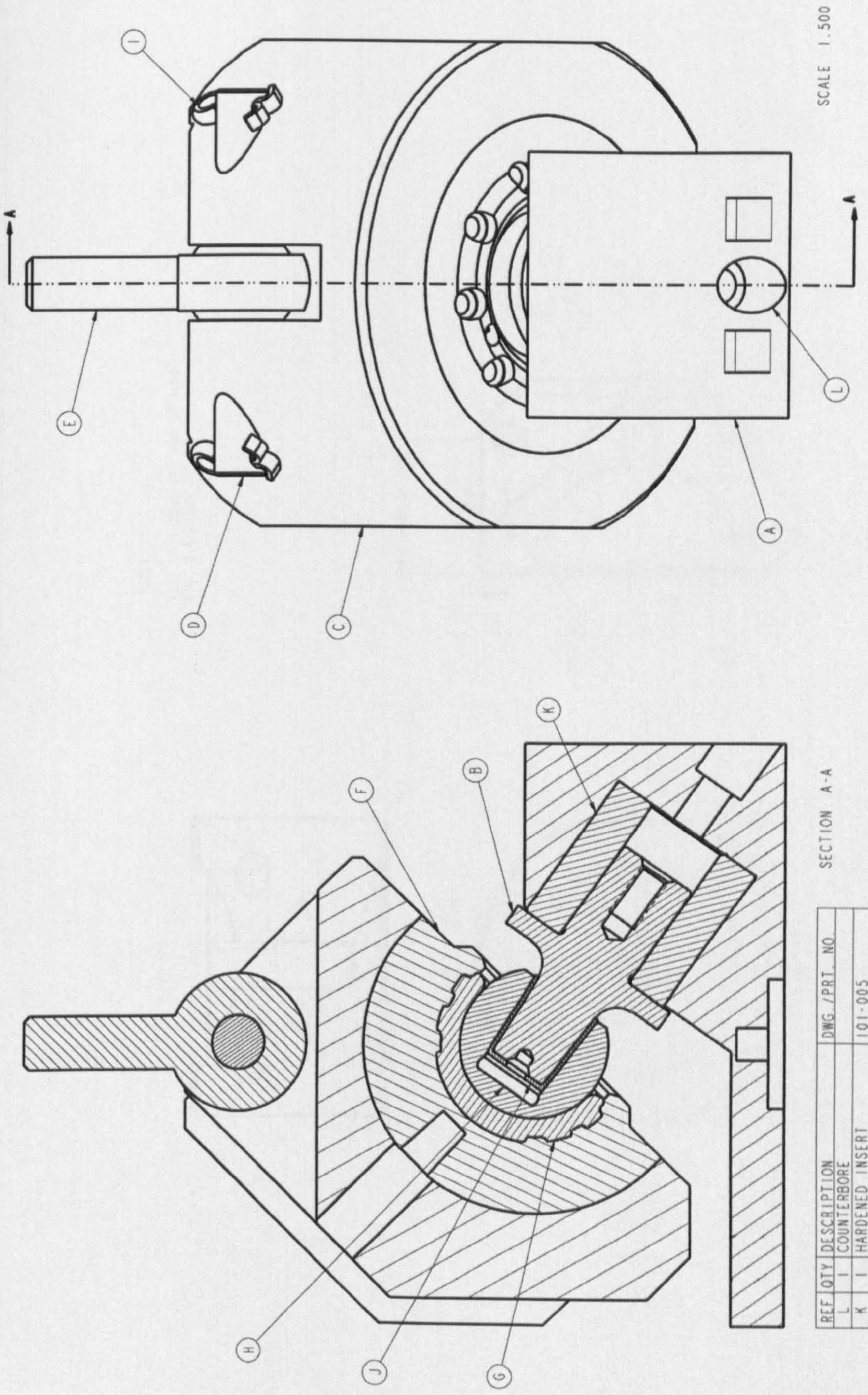

A2.2 Engineering Drawing of Fatigue Rig Top

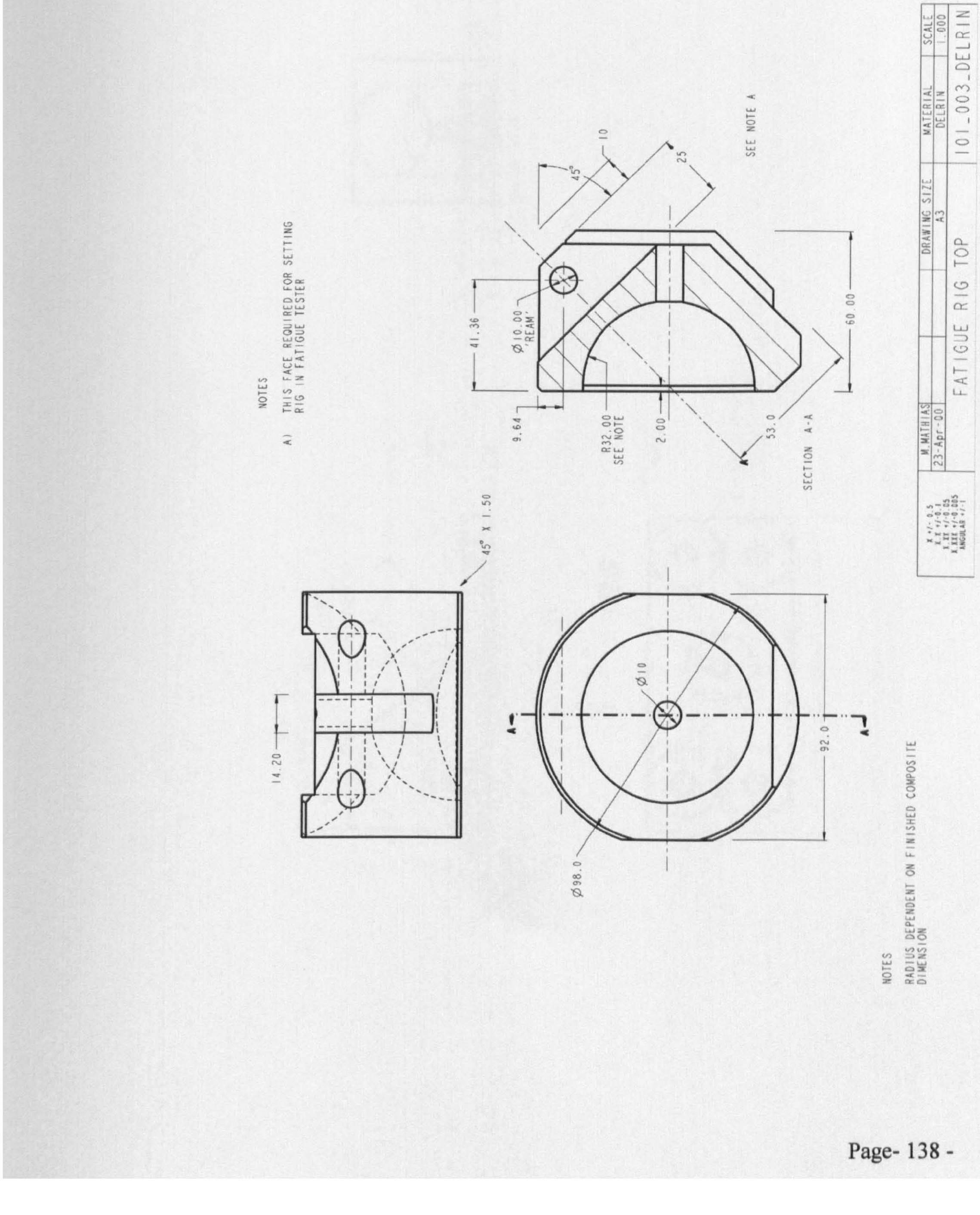

A2.3 Engineering Drawing of Fatigue Rig Base

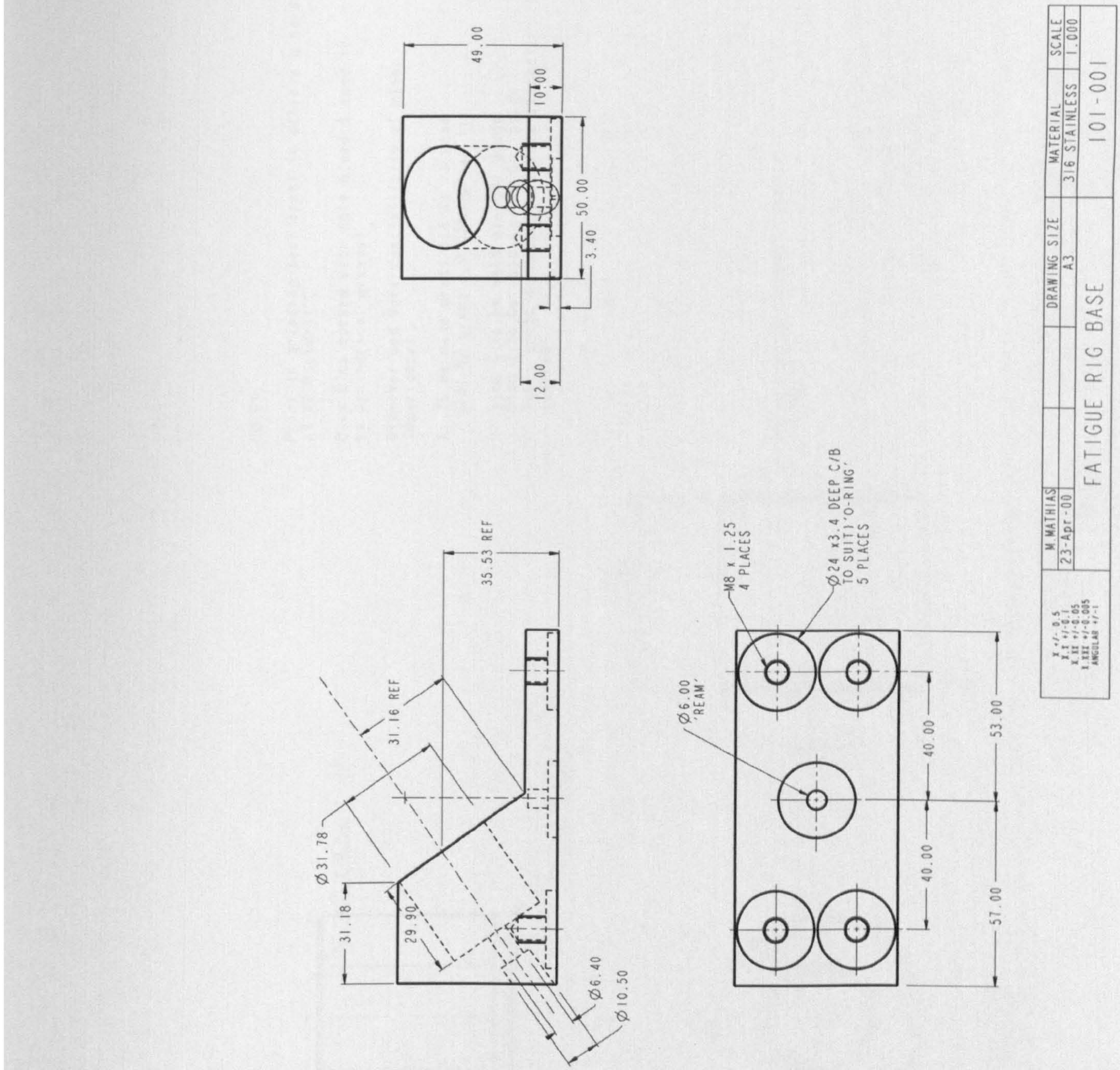

A2.4 Engineering Drawing of Fatigue Rig Hardened Insert

NOTES:

Prior to grinding heat treat to achieve a hardness of 40 Rockwell C

Only Dims marked with note A and B need to be cylindrical ground)

Diameter and bore concentricity of importance)

A: To be made press fit in to base Ø31.82 gives a 0.05mm press fit

B: Stem 6 to be used as 'GO' gauge
Stem 2 to be used as 'No Go' gauge
These gauge diameters are very slightly tapered)

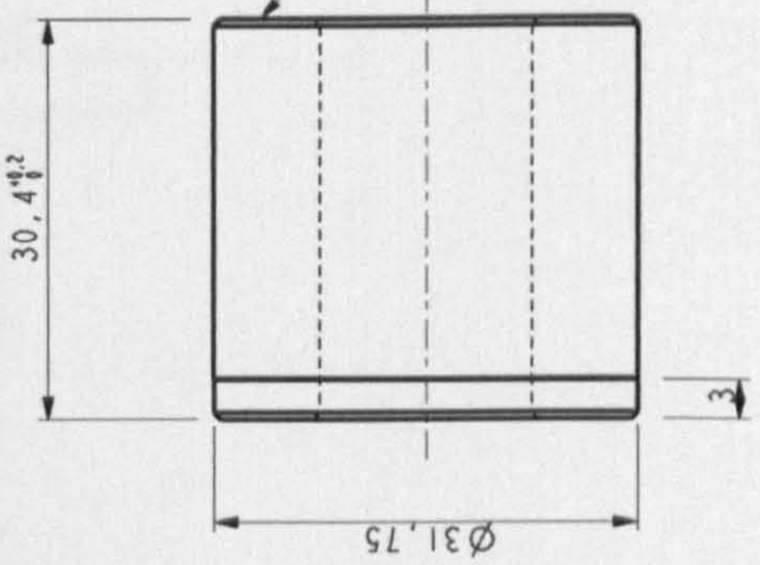

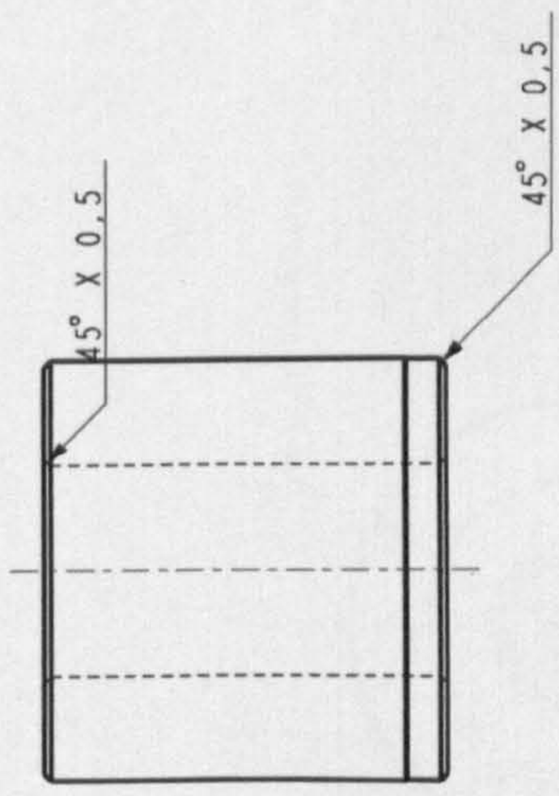

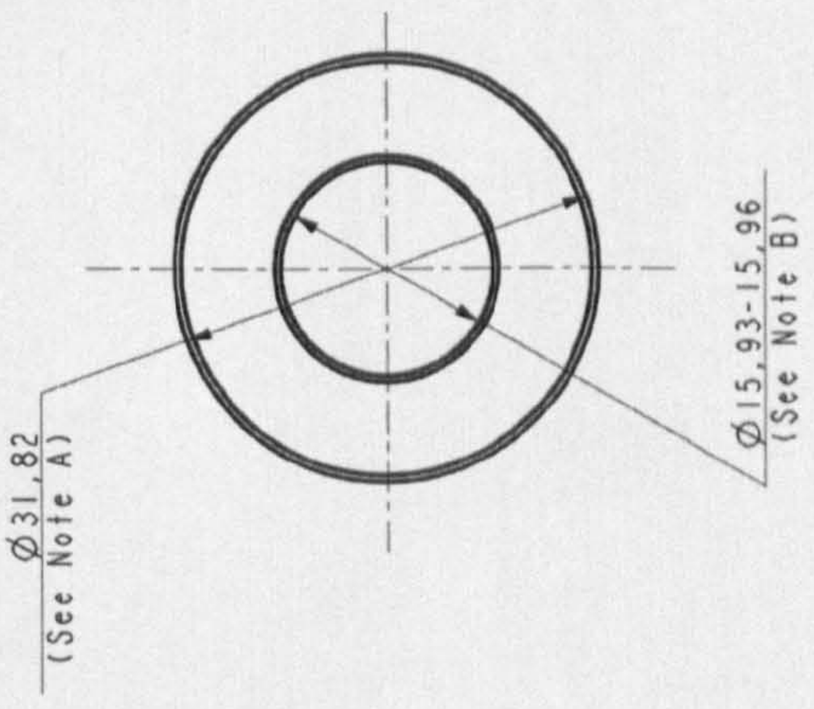

M.MATHIAS			DRAWING SIZE	MATERIAL
23-Apr-00			A3	440C STAINLESS

HARDENED INSERT

101-005

X -/- 0.5
X.X +/-0.1
X.XX +/-0.05
X.XXX +/-0.005
ANGULAR +/-1

SCALE 1.000

A2.5 Engineering Drawing of Fatigue Rig Taper

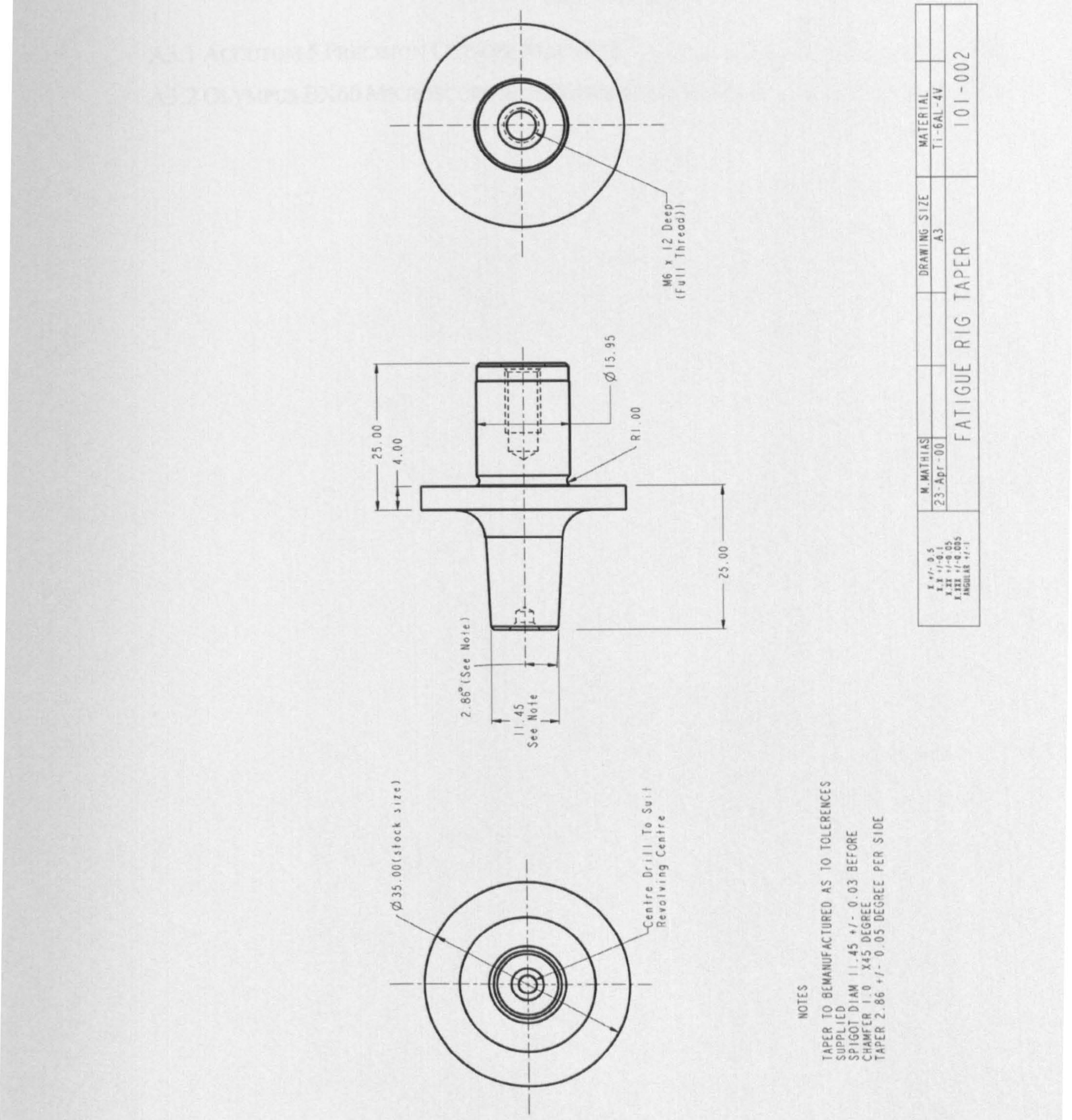

Appendix 3

Microscopy Equipment

A3.1 Accutom 5 Precision Cut-off Machine

A3.2 Olympus BX60 Microscope with Videotext Overlay

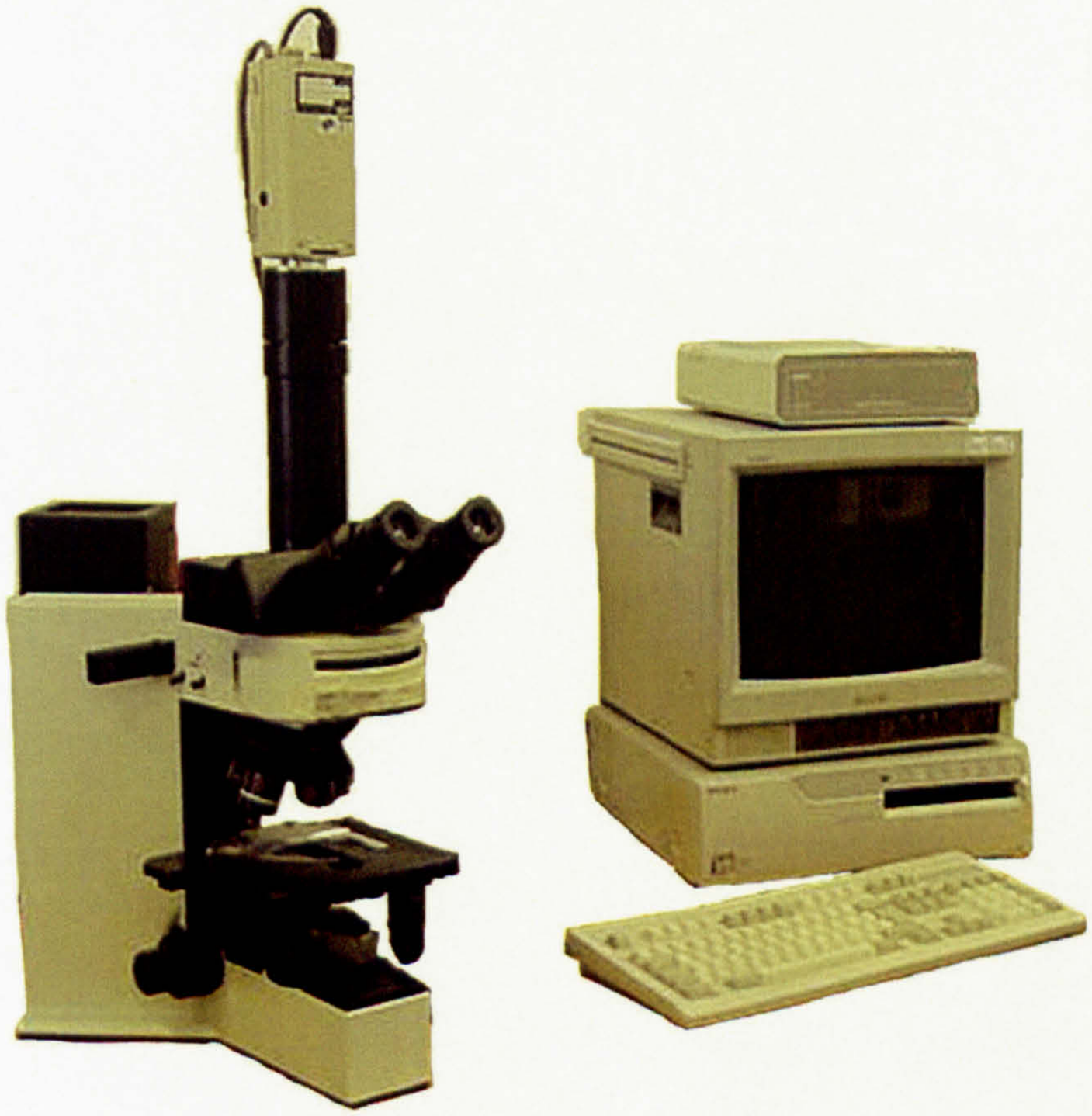

Appendix 4

Geometrical Analysis of Titanium Alloy Taper Adaptor

A4.1 Zeiss Scanware Three-Dimensional Coordinate Measuring Machine and Taylor Hobson Tally Surf.

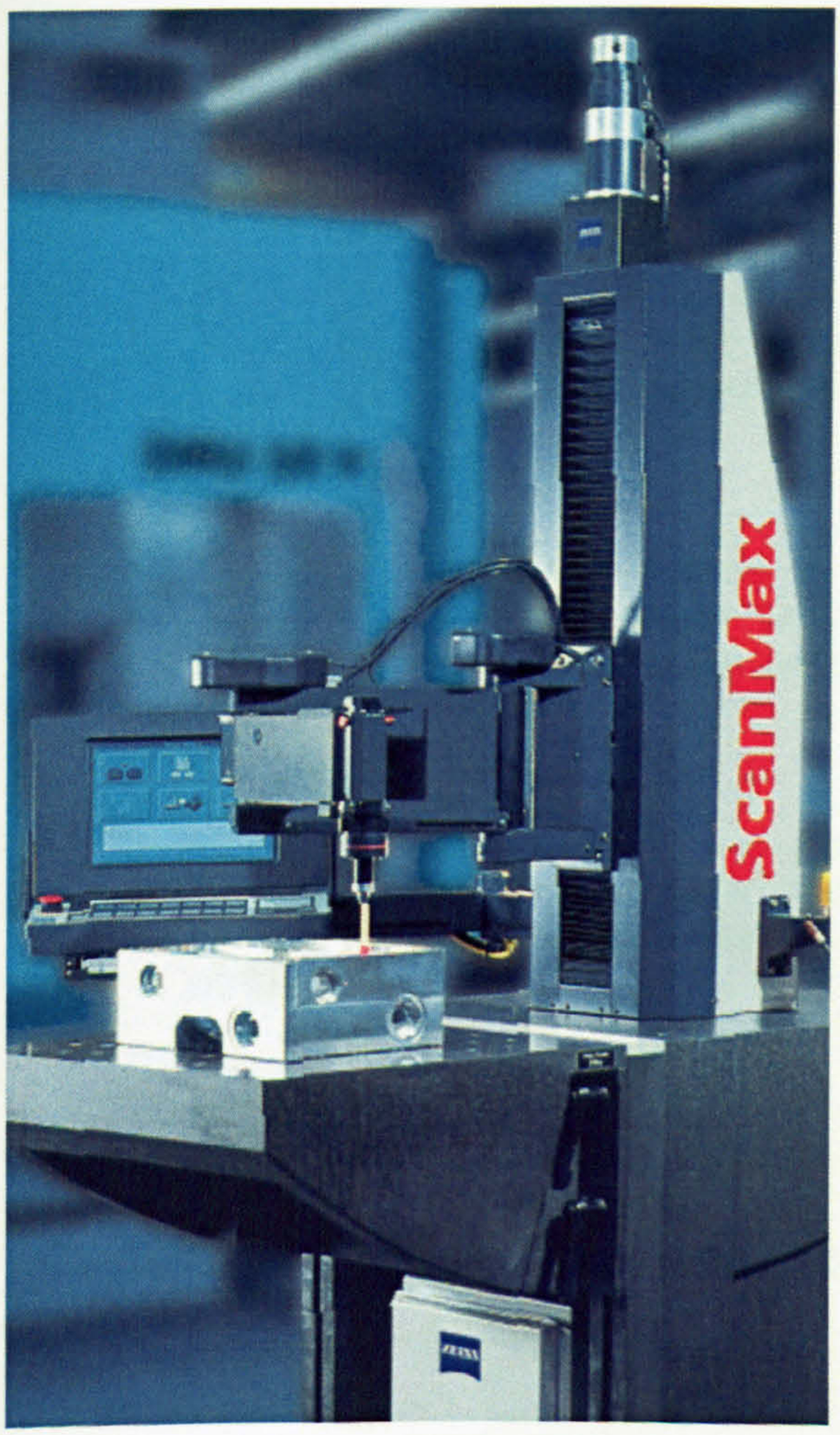

Zeiss Scanware three dimensional Coordinate Measuring Machine

Taylor Hobson Tally Surf

A4.2 Sample Output From Zeiss Scanware Three-Dimensional Coordinate Measuring Machine

ADR	TASK	ACT_MEAS
	,3 Outside Taper	
	3 Narrow cone	+0.210
		-0.182
		-6.309
		+5/39/19
		+0.001
	5 Outside Small Dia	[4,3]
	5 Cone intersection	+0.212
		-0.186
		-1.000
		+12.978
	7 Outside Large Dia	[6,3]
	7 Cone intersection	+0.207
		-0.176
		-14.500
		+14.311
	19 Inside Taper	[17,18]
	19 Narrow cone	+0.404
		-0.322
		-7.880
		+5/33/21
		+0.003
	22 Inside Large Dia	[20,19]
	22 Cone intersection	+0.406
		-0.329
		-1.001
		+12.908
	23 Inside Small Dia	[21,19]
	23 Cone intersection	+0.401
		-0.316
		-14.501
		+11.598

A4.3 Sample Output From Taylor Hobson Tally Surf

Straightness of outer surface of Adaptor A (top)

Surface finish of outer surface of Adaptor A (bottom)

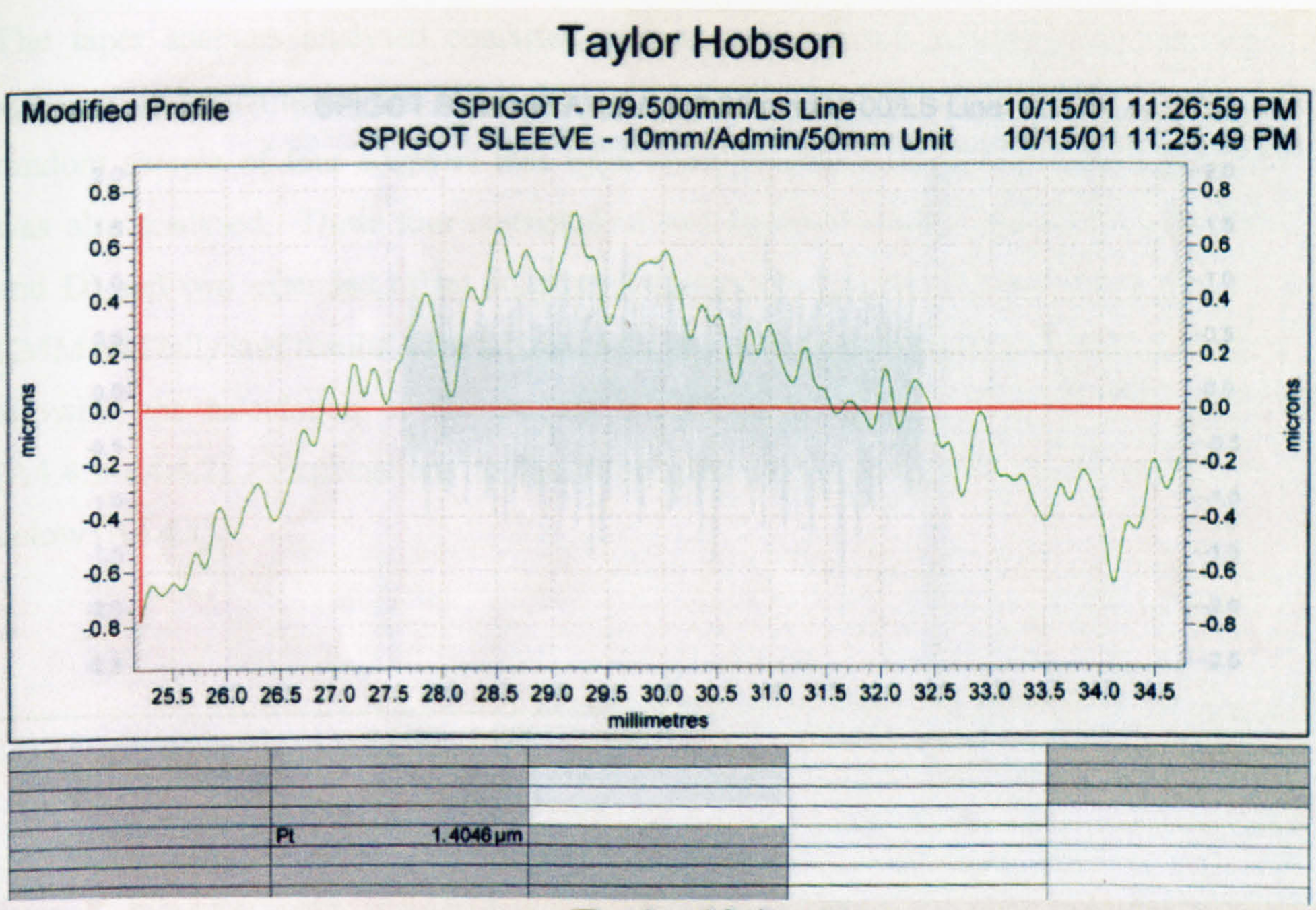

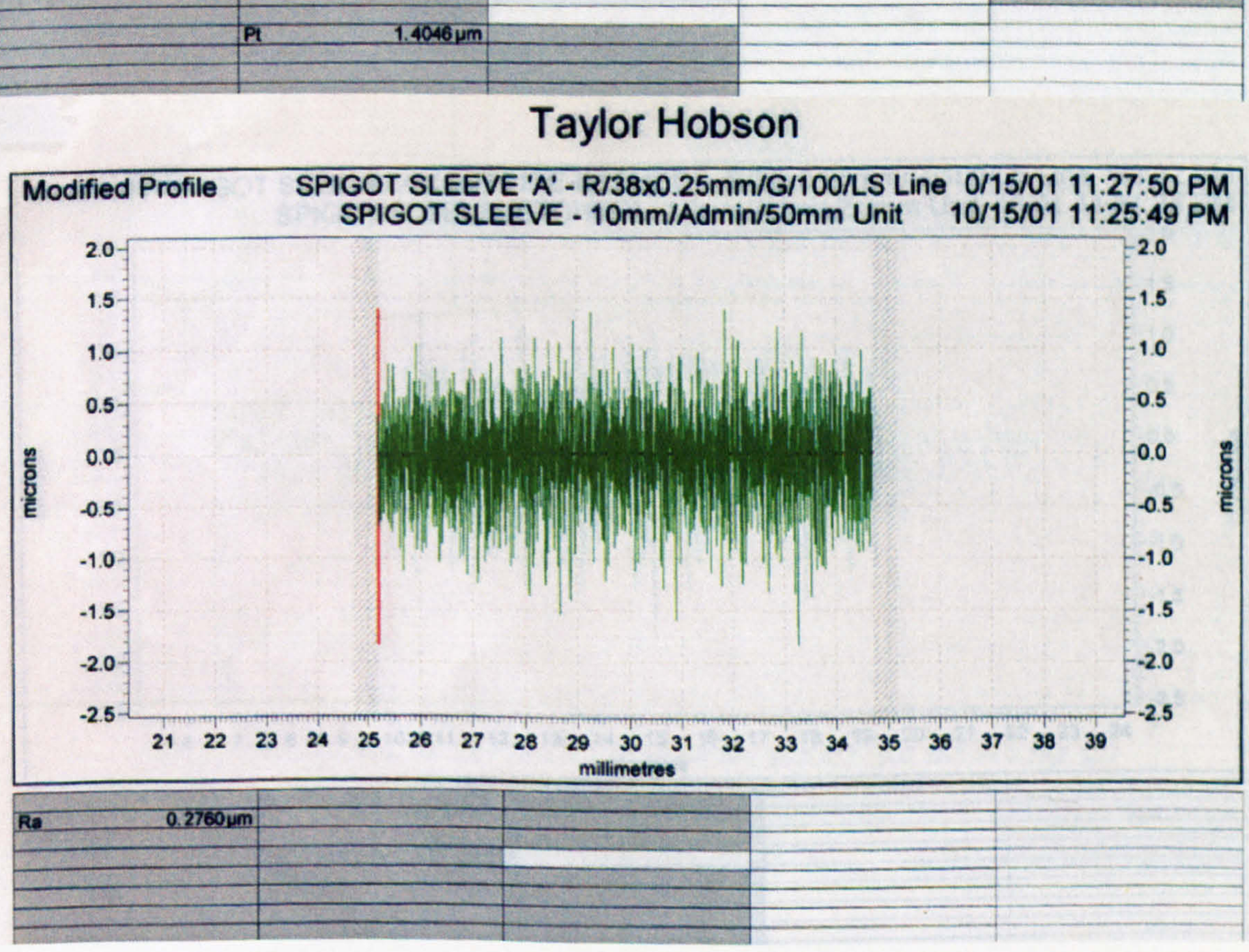

A4.4 Results of Taper Adaptor Geometric Analysis (Original Design)

The taper adaptors analysed consisted of two, sub-contract manufactured, standard adaptors on which heads had failed during mechanical testing (Adaptors A and B). A random sample of four adaptors that were manufactured in-house by Orthodynamics was also analysed. These four consisted of two standard offset adaptors (Adaptors C and D) and two extended offset adaptors (Adaptors E and F). Outputs from the 3D-CMM and tally surf results were tabulated along with original engineering drawing data allowing the calculation of the amount out of tolerance for individual dimensions (A4.4.2-A4.4.7). Explanations to the dimension measured can be found in the key below (A4.4.1).

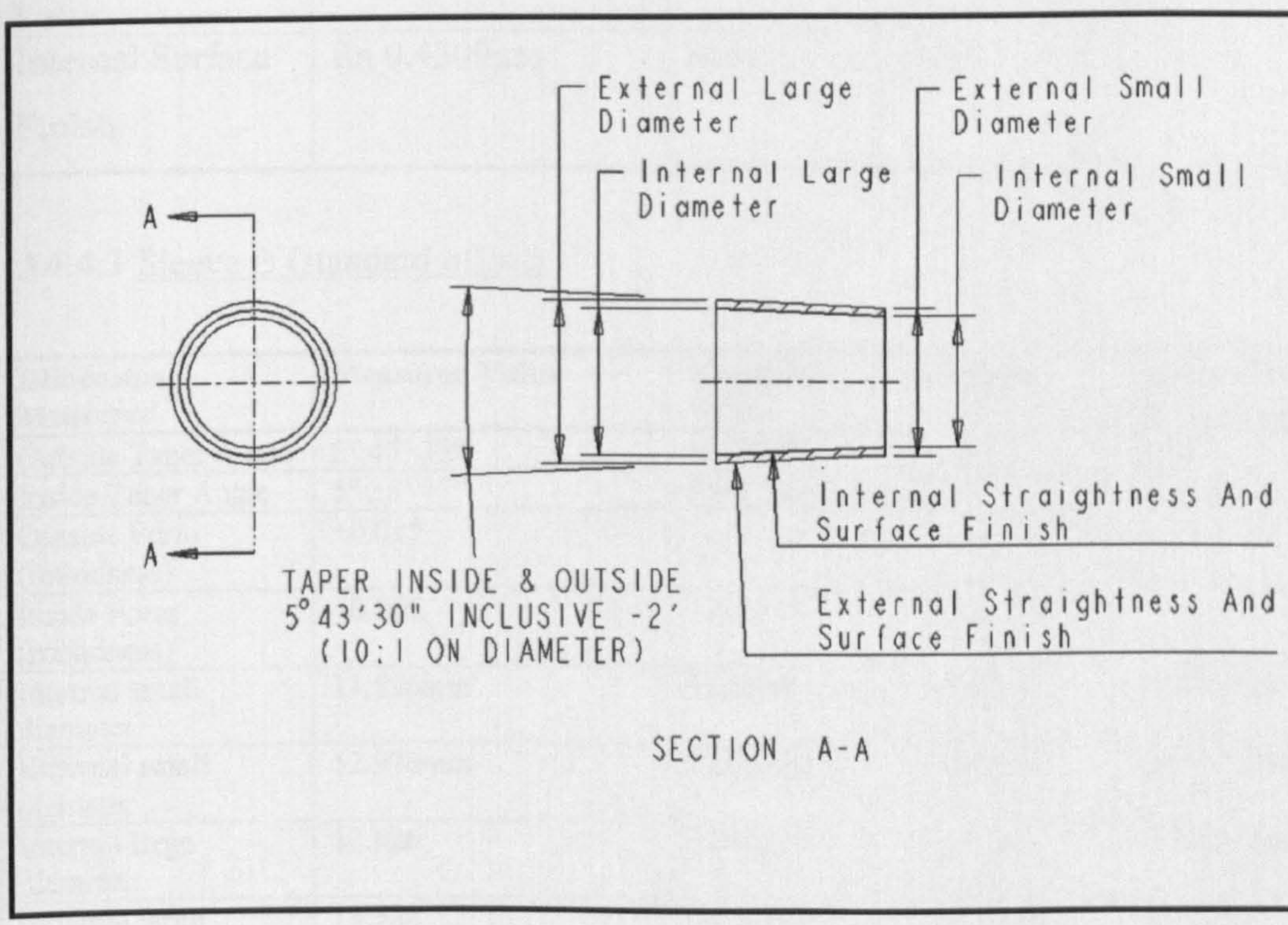

A4.4.1 Key to Original Design Dimension
(Standard Offset Shown)

A4.4.2 Sleeve A (standard offset)

Dimension Measured	Measured Value	Required Value	Tolerance	Amount Out Of Tolerance
Outside Taper Angle	5° 39' 19"	5°43'30"	-2'	Approx -2'
Inside Taper Angle	5° 33' 21"	5°43'30"	-2'	Approx -8'
Outside Form (roundness)	+0.001			
Inside Form (roundness)	+0.003			
Internal small diameter	11.598mm	11.5mm	+/- 0.03mm	+0.068mm
External small diameter	12.978mm	12.95mm	+/- 0.03mm	In Tolerance
Internal large diameter	12.908	12.95mm	+/- 0.03mm	-0.012mm
External large diameter	14.311	14.40mm	+/- 0.03mm	-0.059mm
Internal Straightness	1.8292µm	none	none	
External Straightness	1.4046 µm	none	none	
External Surface Finish	Ra 0.2760 µm	none	none	
Internal Surface Finish	Ra 0.4309µm	none	none	

A4.4.3 Sleeve B (standard offset)

Dimension Measured	Measured Value	Required Value	Tolerance	Amount Out Of Tolerance
Outside Taper Angle	5° 45' 33"	5°43'30"	-2'	Approx +2'
Inside Taper Angle	5° 38' 17"	5°43'30"	-2'	Approx -3'
Outside Form (roundness)	+0.015			
Inside Form (roundness)	+0.006			
Internal small diameter	11.596mm	11.5mm	+/- 0.03mm	+0.016mm
External small diameter	12.970mm	12.95mm	+/- 0.03mm	In Tolerance
Internal large diameter	12.926	12.95mm	+/- 0.03mm	In Tolerance
External large diameter	14.328	14.40mm	+/- 0.03mm	-0.042mm
Internal Straightness	2.1108µm	none	none	
External Straightness	0.7723 µm	none	none	
External Surface Finish	Ra 0.2829 µm	none	none	
Internal Surface Finish	Ra 0.4787µm	none	none	

A4.4.4 Sleeve C (standard offset)

Dimension Measured	Measured Value	Required Value	Tolerance	Amount Out Of Tolerance
Outside Taper Angle	5° 50' 34"	5°43'30"	-2'	0.118°
Inside Taper Angle	5° 41' 36"	5°43'30"	-2'	In Tolerance
Outside Form (roundness)	+0.005			
Inside Form (roundness)	+0.001			
Internal small diameter		11.5mm	+/- 0.03mm	
External small diameter	12.894mm	12.95mm	+/- 0.03mm	0.026mm
Internal large diameter	12.891mm	12.95mm	+/- 0.03mm	0.029mm
External large diameter		14.40mm	+/- 0.03mm	
Internal Straightness	0.6976µm	none	none	
External Straightness	3.1154µm	none	none	
External Surface Finish	Ra 0.3767µm	none	none	
Internal Surface Finish	Ra 0.3333µm	none	none	

A4.4.5 Sleeve D (standard offset)

Dimension Measured	Measured Value	Required Value	Tolerance	Amount Out Of Tolerance
Outside Taper Angle	5°49'52"	5°43'30"	-2'	0.106°
Inside Taper Angle	5°42'15"	5°43'30"	-2'	In Tolerance
Outside Form (roundness)	0.004mm			
Inside Form (roundness)	0.002mm			
Internal small diameter		11.5mm	+/- 0.03mm	
External small diameter	12.893mm	12.95mm	+/- 0.03mm	0.027mm
Internal large diameter	12.894	12.95mm	+/- 0.03mm	0.026mm
External large diameter		14.40mm	+/- 0.03mm	
Internal Straightness	2.3716µm	none	none	
External Straightness	0.6135µm	none	none	
External Surface Finish	Ra 0.3652µm	none	none	
Internal Surface Finish	Ra 0.3379µm	none	none	

A4.4.6 Sleeve E (extended offset)

Dimension Measured	Measured Value	Required Value	Tolerance	Amount Out Of Tolerance
Outside Taper Angle	5°48'9"	5°43'30"	-2'	0.078°
Inside Taper Angle	5°43'8"	5°43'30"	-2'	In Tolerance
Outside Form (roundness)	0.003mm			
Inside Form (roundness)	0.001mm			
Internal small diameter			+/- 0.03mm	
External small diameter	13.158mm	13.20mm	+/- 0.03mm	0.012mm
Internal large diameter	12.423	12.45mm	+/- 0.03mm	In Tolerance
External large diameter			+/- 0.03mm	
Internal Straightness	2.6773µm	none	none	
External Straightness	1.1085µm	none	none	
External Surface Finish	Ra 0.4583µm	none	none	
Internal Surface Finish	Ra 0.3113µm	none	none	

A4.4.7 Sleeve F (extended offset)

Dimension Measured	Measured Value	Required Value	Tolerance	Amount Out Of Tolerance
Outside Taper Angle	5°49'11"	5°43'30"	-2'	0.095°
Inside Taper Angle	5°43'46"	5°43'30"	-2'	0.044°
Outside Form (roundness)	0.002mm			
Inside Form (roundness)	0.002mm			
Internal small diameter			+/- 0.03mm	
External small diameter	13.144mm	13.20mm	+/- 0.03mm	0.026mm
Internal large diameter	12.406mm	12.45mm	+/- 0.03mm	0.014mm
External large diameter			+/- 0.03mm	
Internal Straightness	1.0925µm	none	none	
External Straightness	2.1642µm	none	none	
External Surface Finish	Ra 0.3395µm	none	none	
Internal Surface Finish	Ra 0.3239µm	none	none	

A4.5 Results of Taper Adaptor Geometric Analysis (New Design)

A random sample of four of the new design adaptors that were designed by the author and manufactured in-house by Orthodynamics was also analysed. These four consisted of two standard adaptors (Adaptors G and H) and two extended adaptors (Adaptors I and J). Outputs from the 3D-CMM and tally surf results were tabulated along with original engineering drawing data allowing the calculation of the amount out of tolerance for individual dimensions (A4.5.9-A4.5.12). Explanations to the dimension measured can be found in the key below (A4.5.8).

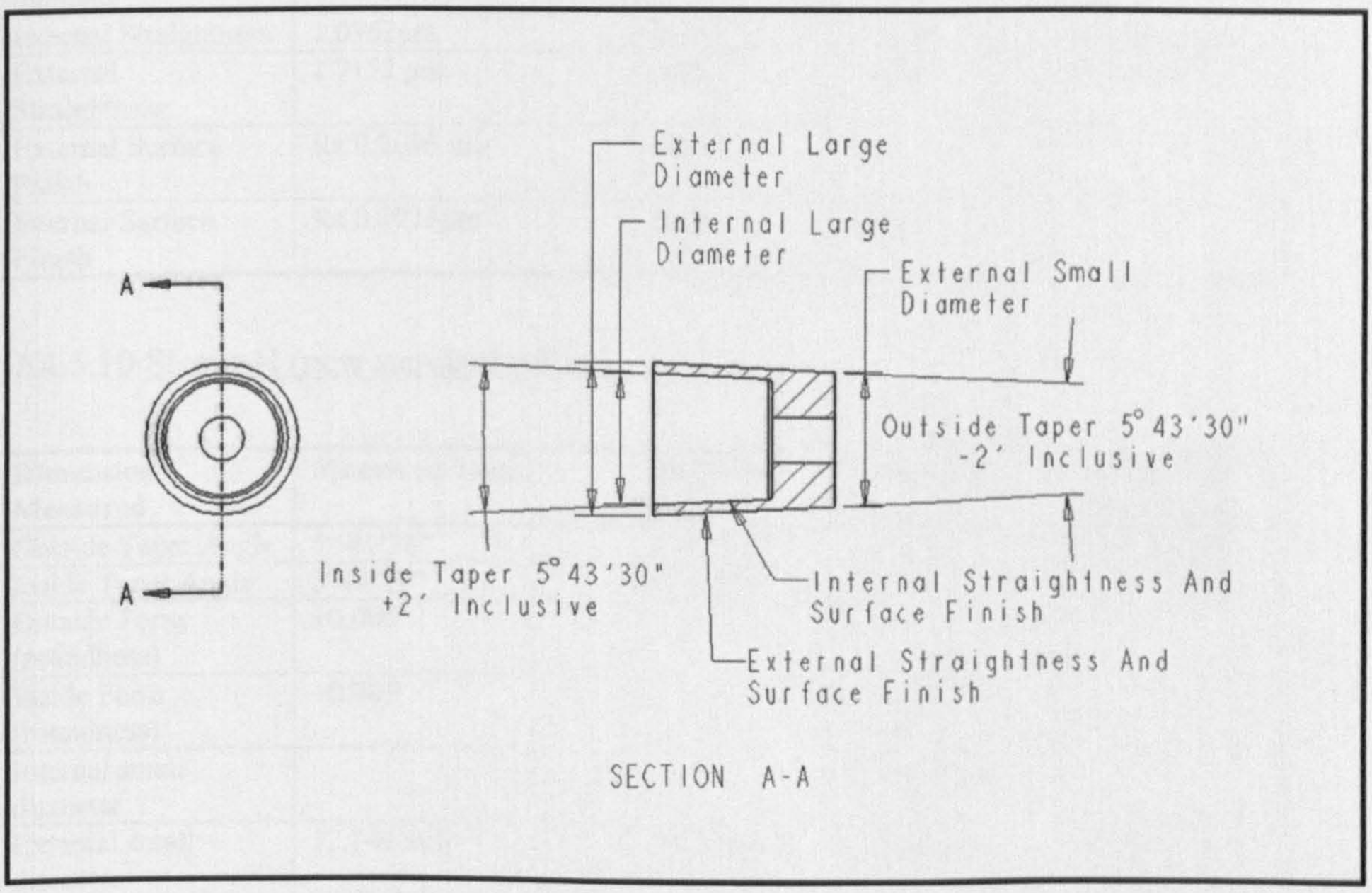

A4.5.8 Key to New Design Dimension
(Extended Offset Shown)

A4.5.9 Sleeve G (new standard offset)

Dimension Measured	Measured Value	Required Value	Tolerance	Amount Out Of Tolerance
Outside Taper Angle	5° 42'26"	5°43'30"	-2'	In Tolerance
Inside Taper Angle	5°45' 13"	5°43'30"	+2'	In Tolerance
Outside Form (roundness)	+0.004			
Inside Form (roundness)	+0.006			
Internal small diameter			+/- 0.03mm	
External small diameter	12.757 mm	12.70mm	+/- 0.03mm	+0.027
Internal large diameter	12.90 mm	12.95mm	+/- 0.03mm	-0.02
External large diameter	14.452	14.40mm	+/- 0.03mm	+0.022
Internal Straightness	1.0762µm	none	< 3µm	In Tolerance
External Straightness	1.7152 µm	none	< 3µm	In Tolerance
External Surface Finish	Ra 0.2696 µm	none	none	
Internal Surface Finish	Ra 0.2923µm	none	none	

A4.5.10 Sleeve H (new standard offset)

Dimension Measured	Measured Value	Required Value	Tolerance	Amount Out Of Tolerance
Outside Taper Angle	5° 41'36"	5°43'30"	-2'	In Tolerance
Inside Taper Angle	5°44'19"	5°43'30"	+2'	In Tolerance
Outside Form (roundness)	+0.005			
Inside Form (roundness)	+0.005			
Internal small diameter			+/- 0.03mm	
External small diameter	12.749 mm	12.70mm	+/- 0.03mm	+0.019
Internal large diameter	12.936 mm	12.95mm	+/- 0.03mm	In Tolerance
External large diameter	14.44 mm	14.40mm	+/- 0.03mm	+0.01
Internal Straightness	1.6307	none	< 3µm	In Tolerance
External Straightness	1.8625 µm	none	< 3µm	In Tolerance
External Surface Finish	Ra 0.1942 µm	none	none	
Internal Surface Finish	Ra 0.3690µm	none	none	

A4.5.11 Sleeve I (new extended offset)

Dimension Measured	Measured Value	Required Value	Tolerance	Amount Out Of Tolerance
Outside Taper Angle	5° 44'2"	5°43'30"	-2'	+0° 0'28" +0.0077°
Inside Taper Angle	5°45'5"	5°43'30"	+2'	In Tolerance
Outside Form (roundness)	+0.003			
Inside Form (roundness)	+0.004			
Internal small diameter			+/- 0.03mm	
External small diameter	12.753 mm	12.70mm	+/- 0.03mm	+0.023
Internal large diameter	12.432 mm	12.45mm	+/- 0.03mm	In Tolerance
External large diameter	14.456 mm	14.40mm	+/- 0.03mm	+0.026
Internal Straightness	2.0421 µm	none	< 3µm	In Tolerance
External Straightness	1.8228 µm	none	< 3µm	In Tolerance
External Surface Finish	Ra 0.1942 µm	none	none	
Internal Surface Finish	Ra 0.3690µm	none	none	

A4.5.12 Sleeve J (new extended offset)

Dimension Measured	Measured Value	Required Value	Tolerance	Amount Out Of Tolerance
Outside Taper Angle	5° 42'50"	5°43'30"	-2'	+0° 0'28" +0.0077°
Inside Taper Angle	5°43'57"	5°43'30"	+2'	In Tolerance
Outside Form (roundness)	+0.004			
Inside Form (roundness)	+0.004			
Internal small diameter			+/- 0.03mm	
External small diameter	12.757 mm	12.70mm	+/- 0.03mm	+0.027
Internal large diameter	12.432 mm	12.45mm	+/- 0.03mm	In Tolerance
External large diameter	14.454 mm	14.40mm	+/- 0.03mm	+0.024
Internal Straightness	2.2806 µm	none	< 3µm	In Tolerance
External Straightness	2.0414 µm	none	< 3µm	In Tolerance
External Surface Finish	Ra 0.1942 µm	none	none	
Internal Surface Finish	Ra 0.3690µm	none	none	

A4.6 Extract From MDA Safety Notice

(Medical Devices Agency 2002)

MDA SN2002(05)
February 2002

MEDICAL DEVICES AGENCY

Best practice in use of ceramic femoral heads in hip replacement implants

SAFETY NOTICE

MANUFACTURER/SUPPLIER
Various orthopaedic implant manufacturers and suppliers

PROBLEM
The orthopaedic literature describes, in general, good clinical performance of ceramic femoral heads in hip replacement implants, including reduction of wear rates. However, MDA receives periodic reports of fracture of ceramic femoral heads. Although it is often not possible to identify the reasons for the failure in individual cases, clinical practice can affect the performance of ceramic femoral heads.

For the attention of:

Health Authorities (England)	- Chief Executives
NHS Trusts (England)	- Chief Executives

ACTION

Follow manufacturers' instructions when using alumina or zirconia ceramic femoral heads in hip replacement implants. In particular:

Mix and match of design/manufacturer
1. Do not use a ceramic femoral head supplied by one manufacturer with a femoral stem supplied by another manufacturer;
2. Only use ceramic femoral heads in combination with stems or cups specifically recommended by the manufacturer;
3. Do not use femoral stem taper adaptor sleeves at the head/neck interface unless they are part of a head-sleeve-neck system provided by one manufacturer;

Surgical Technique
4. Do not use excessive force (particularly impact) during attachment of a ceramic femoral head to a stem; do not allow a metal hammer/mallet or other hard item to come into contact with the ceramic head during impaction;
5. Do not implant used, dropped or damaged ceramic femoral heads;
6. Ensure that femoral stem and ceramic femoral head tapers are clean and dry prior to implantation;

Revision
7. Do not implant a ceramic femoral head during hip replacement revision if the stem is not being revised, unless the head is specifically designed by the manufacturer for use in revision surgery;

Sterilization
8. Do not resterilize zirconia femoral heads using steam.

Appendix 5

Additional Mechanical Results Data

A5.1 Additional UCS Data

A5.1.1 Data capture depicting obvious 22 kN failure of prosthesis 01358 during UCS test

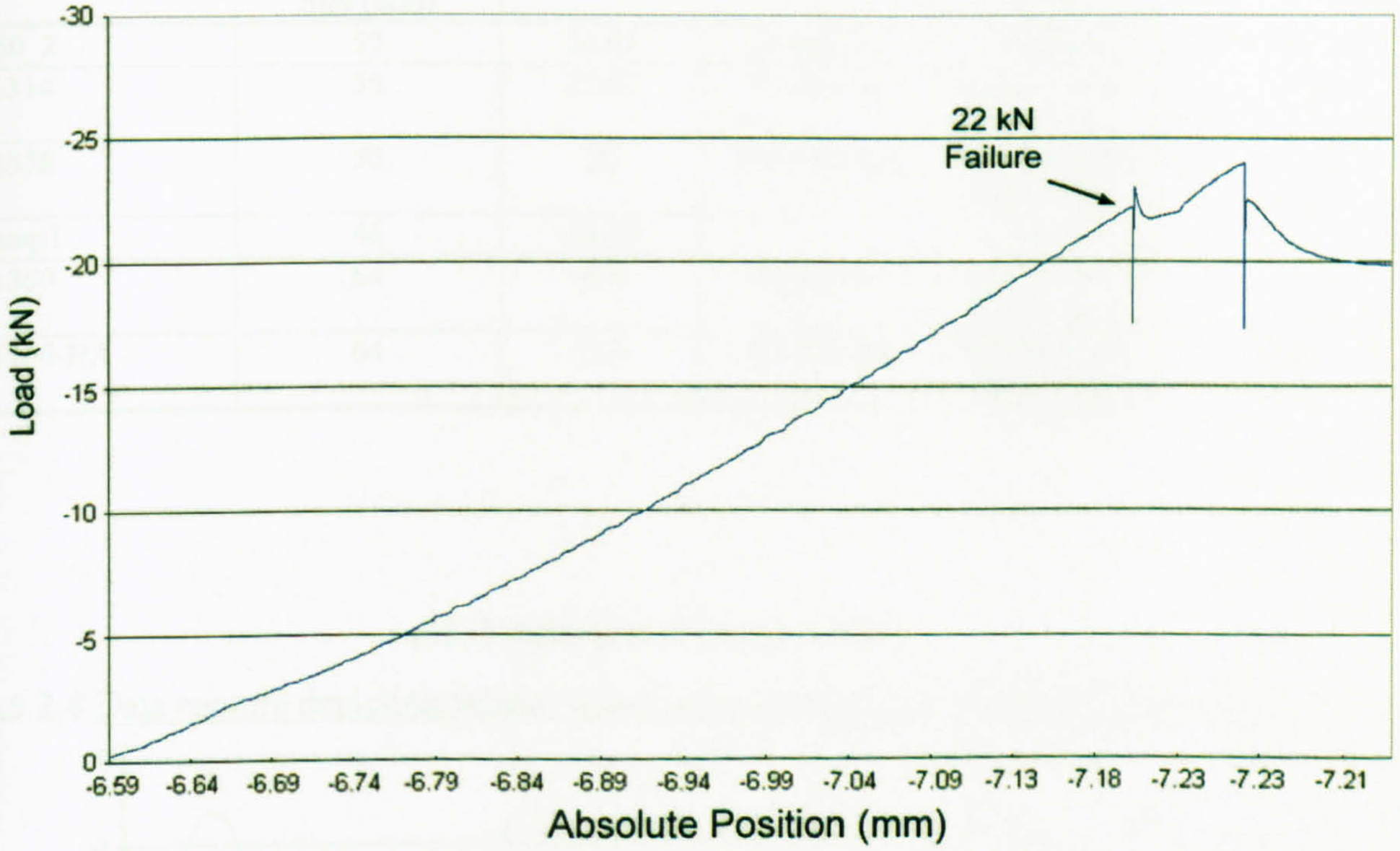

A5.1.2 Data capture depicting unobvious 22.66 kN failure of prosthesis 01314 during UCS test

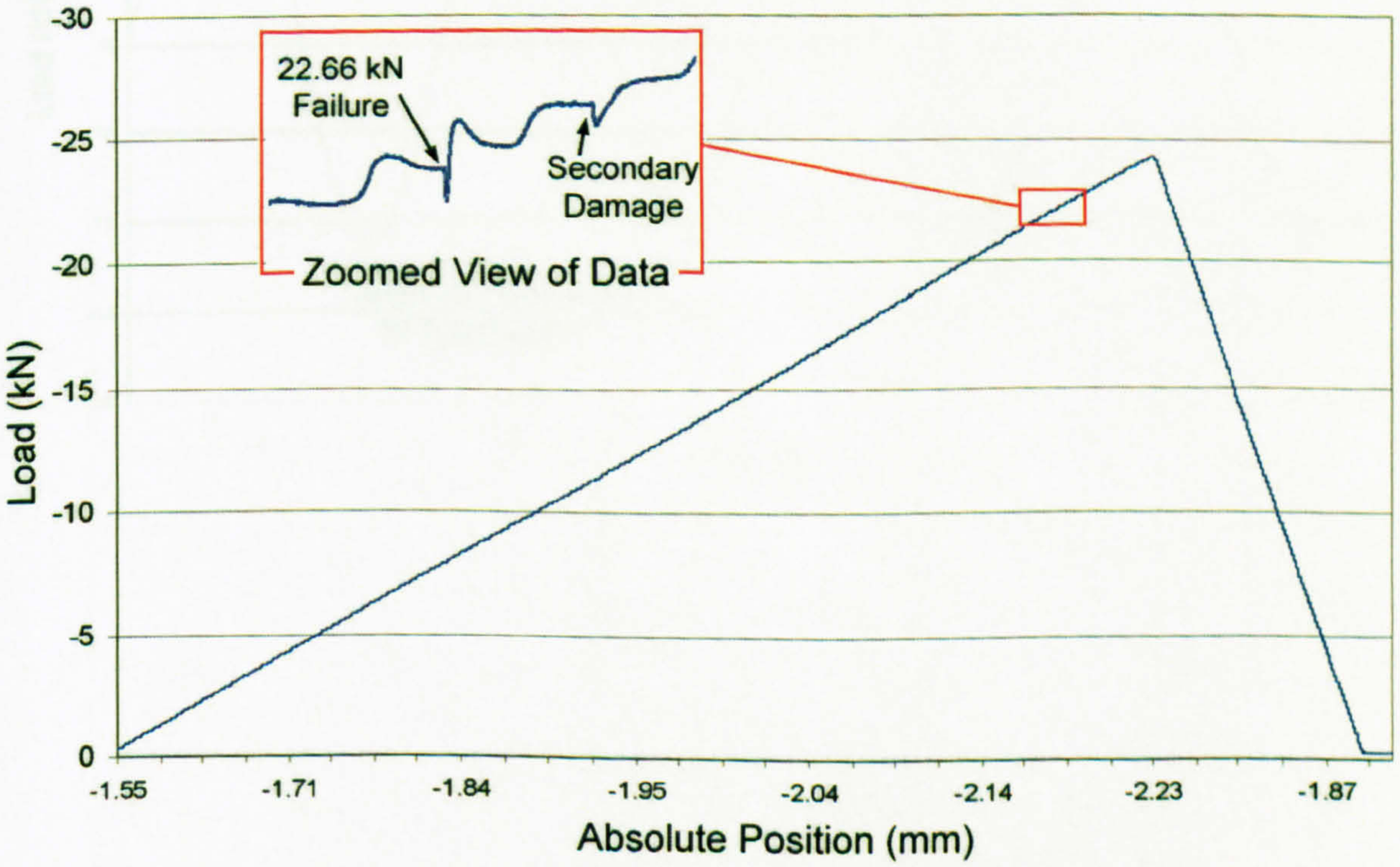

A5.1.3 Individual UCS Test Details

Specimen Number	Prosthesis Size (mm)	UCS (kN)	Load Rate	Loading Head Type
T50_2	50	24.67	2 mm/sec	Alumina
01314	50	22.67	0.1 kN/sec	Stainless Steel (REX 734)
01358	50	22	0.01 mm/sec	Stainless Steel (REX 734)
Samp1	46	18.75		Alumina
01360	64	6.6	0.1 kN/sec	Stainless Steel (REX 734)
01360-HA	64	5.3	0.1 kN/sec	Stainless Steel (REX 734)

A5.2 Additional Fatigue Data

A5.2.4 Data capture depicting fatigue failure of prosthesis 01358-3 at 577,220 cycles

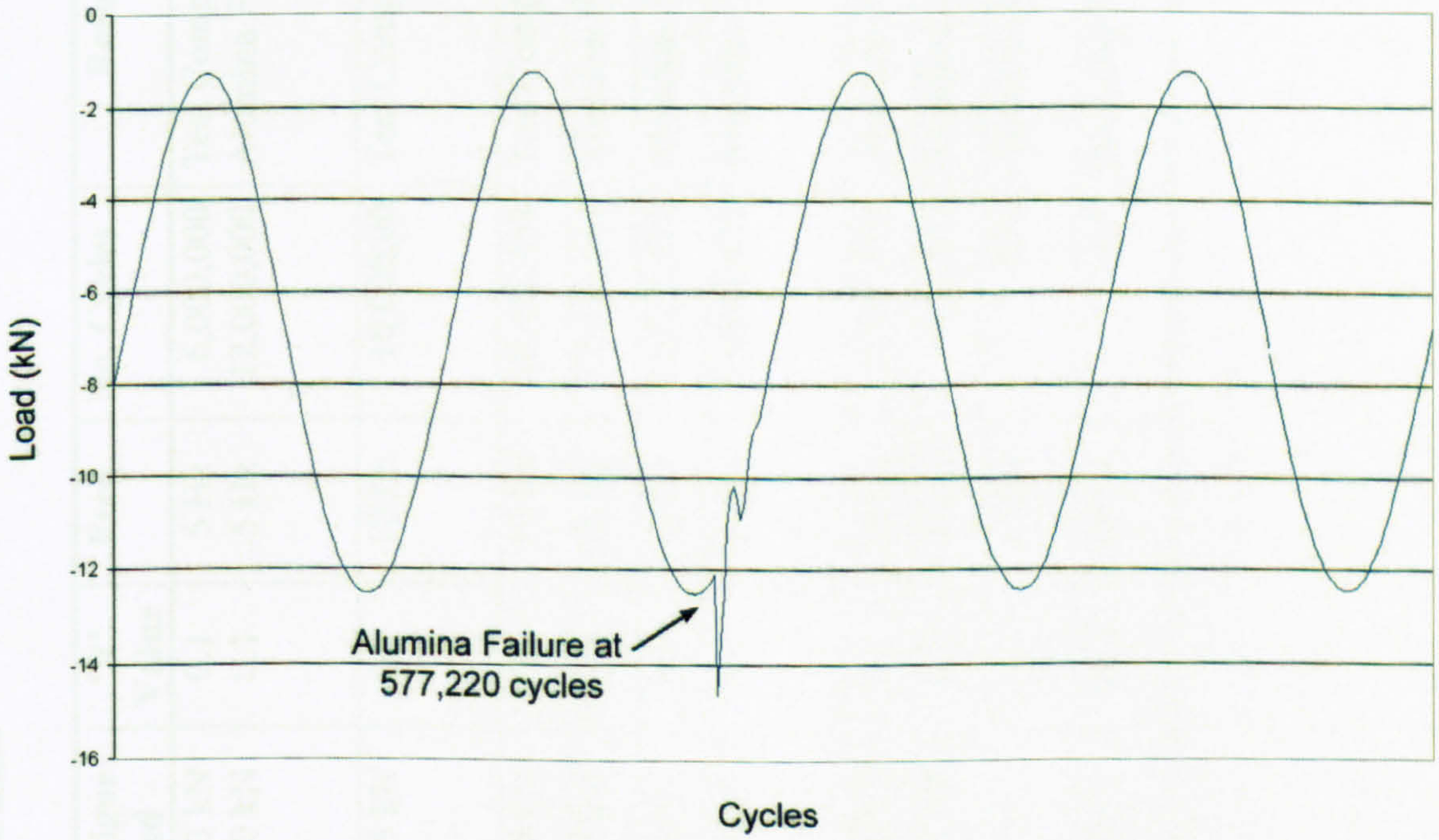

A5.2.5 Individual Fatigue Test Details

Sample Name	Sample Size	Fatigue Load	'R' Value	Freq.	No. Cycles	Result	Information
Sample 2	46mm	3.3 kN 7.0 kN	0.1 0.1	5 Hz 5 Hz	6,000,000 12,000,000	Test Completed Alumina Failure	No sign of damage to test sample on initial test, Test at higher load caused fatigue failure.
01358-1	50mm	7.5 kN	0.1	10 Hz	10,000,00	Test Completed	Acetal to WR-2 mounting epoxy interface showed signs of loosening. Create larger volume for mounting epoxy.
01314	50mm	7.5 kN	0.1	10 Hz	10,423,458	Test Completed	
01359-2	46mm	7.5 kN	0.1	10 Hz	17,054,641	Alumina Failure	
01358-2	50mm	10 kN	0.1	10 Hz	13,721,911	Alumina Failure	
01361	50mm	10 kN	0.1	10 Hz	11,648,455	Alumina Failure	Test ran to 15 million cycles but unusual displacement and inspection of data capture files pinpointed earlier failure
01358-2c	50mm	12.5 kN	0.1	10 Hz	3,015,919	Alumina Failure	
01358-3	50mm	12.5 kN	0.1	10 Hz	837,600	Alumina Failure	
01360	64mm	N/A	N/A	10 Hz	N/A	Alumina Failure	Alumina cup failure at 6.6 kN during initial ramping of load
01360-HA	64mm	N/A	N/A	10 Hz	N/A	Alumina Failure	Alumina cup failure at 5.3 kN during initial ramping of load

A5.2.6 Fatigue Failure Photograph of Standard Test Rig Caused by Creation of S/N Curve

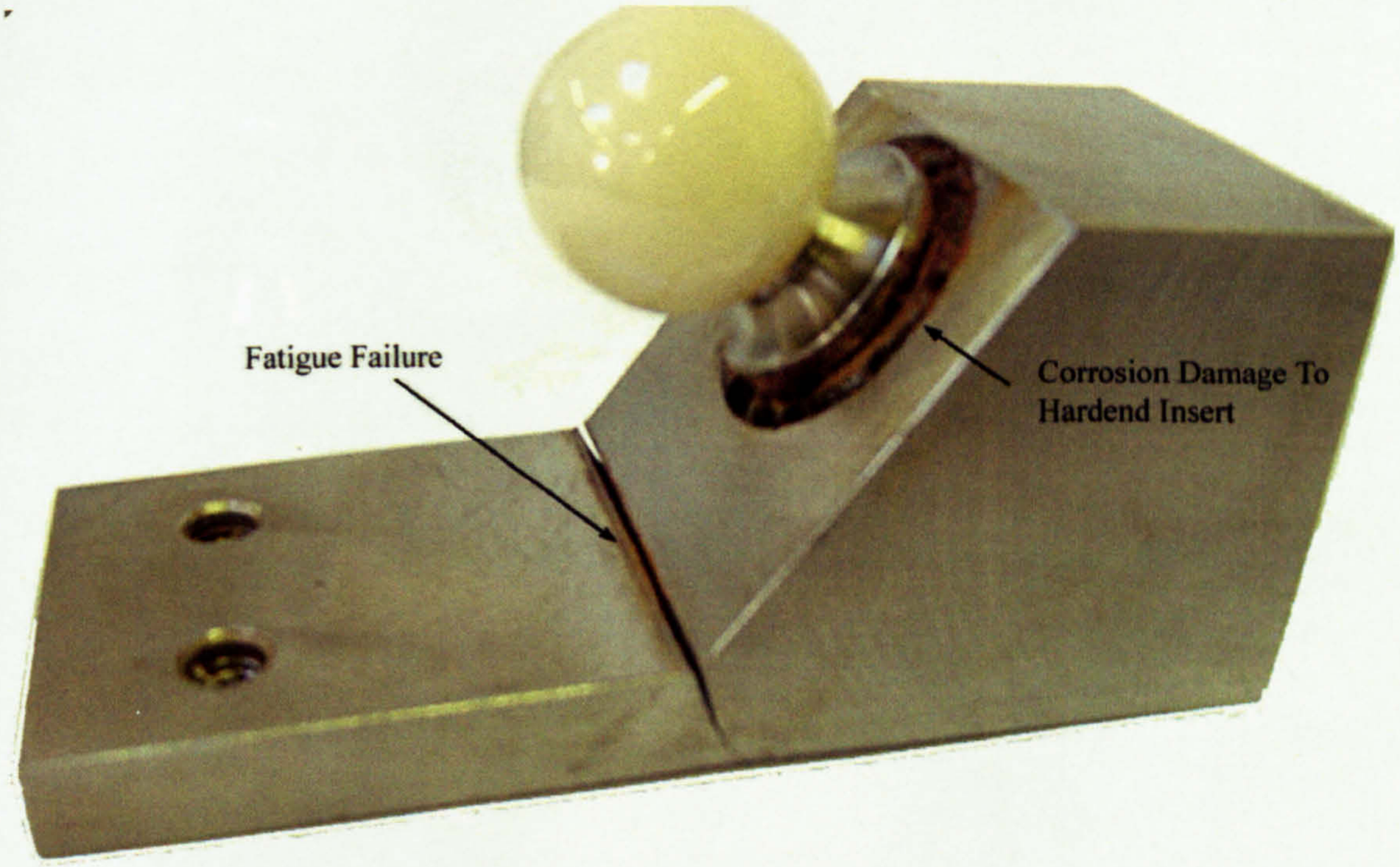

A5.2.7 Photograph of Heavy and Standard Duty Fatigue Rig Components

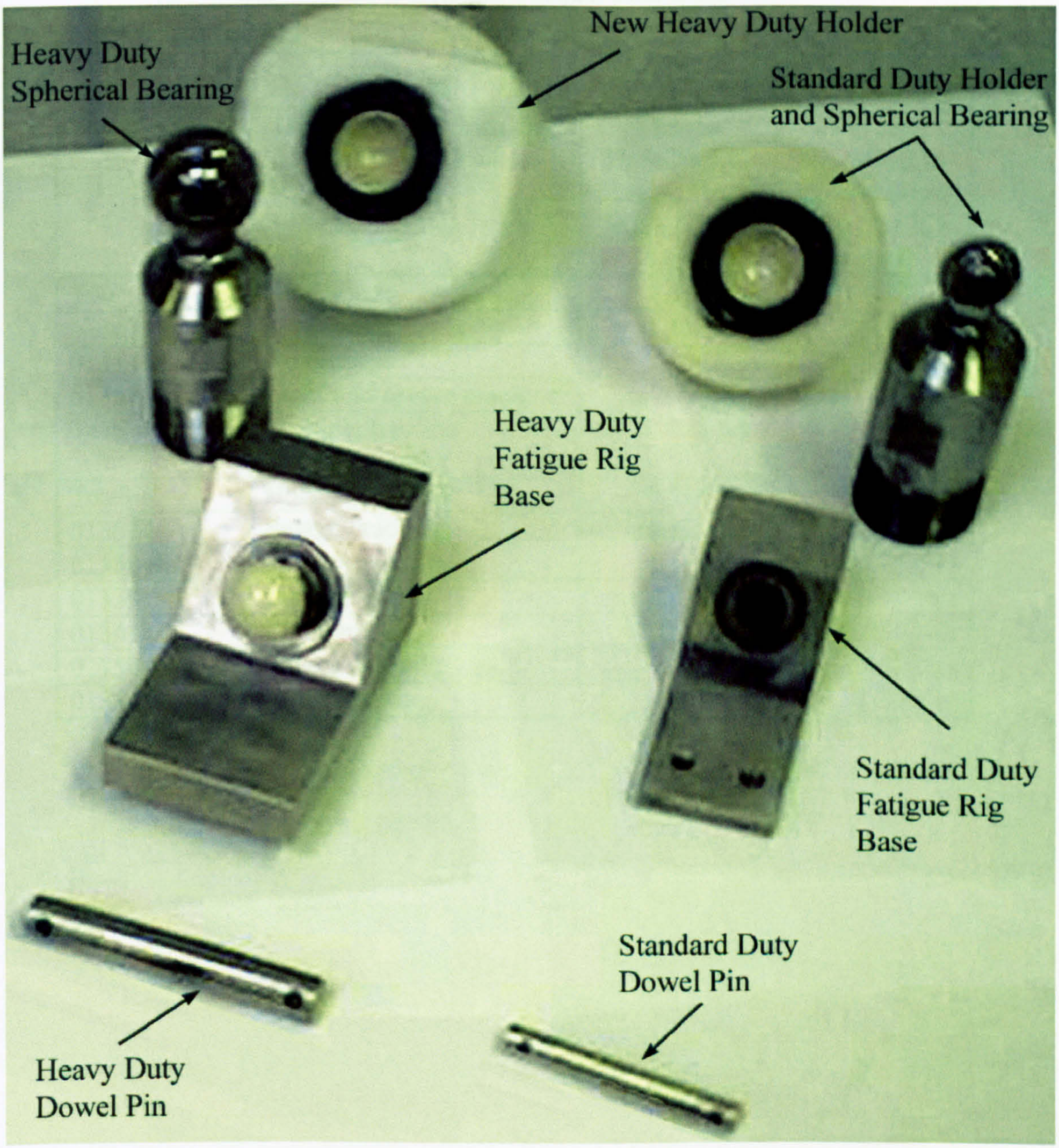

A5.3 Additional Torque Test Data

A5.3.8 Individual torque test details

Sample Name	Description of Existing Damage to Alumina Cup	Torque Required to Rotate Head With 3.3 kN Load	Torque Required to Rotate Head With 7.5 kN Load
T50	No damage	1.155 Nm	
New	No damage	1.155 Nm	2.835 Nm
01314a	No damage	1.05 Nm	3.15 Nm
01358	Light and severe cracking	1.05 Nm	4.2 Nm
Test2	Multiple hairline horseshoe craks	2.625 Nm	5.775 Nm
Test3	Horseshoe crack	0.525 Nm	1.155 Nm
01361	Severe cracking	1.575 Nm	6.3 Nm
01358-2	Severe cracking	1.575 Nm	5.775 Nm
01359	Light cracking	1.575 Nm	5.46 Nm
01364	Light cracking	0.84 Nm	2.205 Nm
01358-3	Severe cracking	1.05 Nm	2.625 Nm
01314	Light cracking	0.525 Nm	1.05 Nm

GLOSSARY

arthroplasty	The surgical repair of a joint.*
abduction	For definition when used with regard to the hip see Appendix 1part A1.1
acetabulum	The cup-shaped cavity at the base of the hipbone into which the ball-shaped head of the femur fits.**
adduction	For definition when used with regard to the hip see Appendix 1part A1.1
articular	Of or relating to joints.*
aseptic	Free from infection or septic material, sterile.*
avascular	Without blood.*
biocompatible	The property of being biologically compatible by not producing a toxic, injurious, or immunological response in living tissue.**
bioinert	Having no pharmacologic or therapeutic action.
bone mineral density	Bone mineral density is determined from a painless non-invasive test. It is the best way to determine your bone health. BMD tests can identify osteoporosis, determine risk of fractures and monitor response to an osteoporosis treatment.
cortical bone	Outer compact bone consisting of mineralised regularly ordered parallel collagen fibres.**
extension	For definition when used with regard to the hip see Appendix 1part A1.1
external rotation	For definition when used with regard to the hip see Appendix 1part A1.1
femur	Large bone in the thigh that articulates with the pelvis above and the knee below.*
flexion	For definition when used with regard to the hip see Appendix 1part A1.1
heterogeneous	Consisting of dissimilar elements or parts; not homogeneous.**
homogeneous	Uniform in structure or composition throughout.**
hyaline	Clear, transparent, granular free.*

hypertrophy	The enlargement or overgrowth of an organ or part due to an increase in size of its constituent cells.*
impingement	Impingement is defined as contact between the femoral neck and the rim of acetabular cup or insert
initial fixation	The method the prosthesis is fixed to its host bone at time of surgery
internal rotation	For definition when used with regard to the hip see Appendix 1part A1.1
isoelastic	Equal in elasticity, normally used incorrectly when describing a reduced stiffness prostheses.
medial	The side of the body or body part that is nearer to the middle or centre (median) of the body.
necrosis	The death of cells in the body.*
orthopaedic	The medical specialty concerned with the preservation, restoration, and development of form and function of the musculoskeletal system.*
osseointegration	The growth action of bone tissue, as it assimilates surgically implanted devices or prostheses to be used as either replacement parts (e.g., hip) or as anchors (e.g., dental implants).*
osteoarthritis	Non-inflammatory degenerative joint disease occurring chiefly in older persons, characterised by degeneration of the articular cartilage, hypertrophy of bone at the margins and changes in the synovial membrane. It is accompanied by pain and stiffness, particularly after prolonged activity.*
PEEK	Polyetheretherketone is the best-known example of the polyarlyletherketone group of polymers.
polymerisation	The bonding of two or more monomers to form a polymer.
primary	The first, first in order or in time of development
primary fixation	Initial method of mechanical fixation of prosthesis to bone. Giving prosthesis stability required for osseointegration.

prostheses	Artificial substitutes for body parts, and materials inserted into tissue for functional, cosmetic, or therapeutic purposes. Prostheses can be functional, as in the case of artificial arms and legs, or cosmetic, as in the case of an artificial eye. Implants, all surgically inserted or grafted into the body, tend to be used therapeutically.*
reamed	To form, shape, taper, or enlarge (a hole or bore, for example) with or as if with a reamer.
revision	The act of revising; re-examination for correction. In THR generally means the replacing of all, or part of the prosthesis.
roentgenogram	A photograph made with x-rays. Also called roentgenograph.**
subchondral	Beneath or below cartilage*
synovial fluid	A transparent, viscid, lubricating fluid*
trabecular bone	Of or pertaining to a trabecula, a transverse partition which divides or partly divides a cavity.* Normally spongeous bone within a cortical shell.

*Definitions adapted from Cancerweb (2003)

** Definitions adapted from Bartleby.com (2003)

ABBREVIATIONS

BMD	Bone mineral density
CMM	Computerised three-dimensional measuring machines
CNC	Computer numerically controlled
FEA	Finite element analysis
HA	Hydroxyapatite
HIP	Hot isostatic pressing
MDA	Medical Devices Agency
NHS	National Health Service
PCD	Pitched circle diameter
PEEK	Polyetheretherketone
PMMA	Polymethylmethacrylate
ROM	Range of motion
SCG	Slow crack growth
SEM	Scanning electron microscope
THR	Total hip replacement
UCS	Ultimate compressive strength
UHMWPE	Ultra high molecular weight polyethylene
UTS	Ultimate torque strength

REFERENCES

Abu Bakar, M. S., Cheang, P. and Khor, K. A. (2003). Mechanical properties of injection molded hydroxyapatite-polyetheretherketone biocomposites. *Composites Science and Technology,* **63**(3-4), pp421-425.

Adam, F., Hammer, D. S., Pfautsch, S. and Westermann, K. (2002). Early failure of a press-fit carbon fiber hip prosthesis with a smooth surface. *Journal of Arthroplasty,* **17**(2), pp217-223.

Adams, V. and Askenazi, A. (1999). *Building better products with Finite Element Analysis*. Santa Fe, Onword Press.

Akay, M. and Aslan, N. (1996). Numerical and experimental stress analysis of a polymeric composite hip joint prosthesis. *Journal Of Biomedical Materials Research,* **31**(2), pp167-182.

Andrew, T. A., Flanagan, J. P., Gerundini, M. and Bombelli, R. (1986). The isoelastic non-cemented total hip arthroplasty: preliminary experience with 400... *Clin. Orthop. and Related Res.,* **206**, pp127-138.

ASTM F603-00 Standard Specification for High-Purity Dense Aluminum Oxide for Surgical Implant Application. **13.01**.

Bader, R., Steinhauser, E., Willmann, G. and Gradinger, R. (2000). Limitations of artificial hip joint mobility due to wear and ceramic cup design. *Bioceramics*. Zurich-Uetikon, TRANS TECH PUBLICATIONS LTD. **192-1**, pp549-552.

Bartleby.com., The American Heritage® Dictionary of the English Language, (2000), Available: http://www.bartleby.com/61/, (Accessed: 21/4/2003)

Bauer, T. W., Stulberg, B. N., Ming, J. and Geesink, R. G. (1993). Uncemented acetabular components. Histologic analysis of retrieved hydroxyapatite-coated and porous implants. *Arthroplasty,*(Apr 8), pp167-77.

Bergmann, G. (1993). Hip joint loading during walking and running measured in two patients. *Biomech.,* **26**, pp969-990.

Bernakiewicz, M. and Viceconti, M. (1999). Parameter identification in finite element contact analysis with refrence to orthopaedic biomechanics applications.

Bierbaum, B. E., Barsoum, W. K., Puri, L., Headrick, J. and Gomes, S. (2001). Alumina-Alumina Ceramic Bearings. *6th International Biolox® Symposium 2001.*

Bizot, P., Banallec, L., Sedel, L. and Nizard, R. (2000). Alumina-on-alumina total hip prostheses in patients 40 years of age or younger. *Clinical Orthopaedics and Related Research,*(379), pp68-76.

Bobyn, J. D., Mortimer, E. S., Glassman, A. H., Engh, C. A., Miller, J. E. and Emerson Brooks, C. (1992). Producing and avoiding stress shielding: laboratory and clinical observations of noncemented total hip arthoplasty. *Clin. Orthop,* **274**, pp79-96.

Bobyn, J. D., Tanzer, M., Krygier, J., Dujovne, A. R. and Brooks (1994). Concerns with modularity in total hip arthoplasty. *Clin. Orthop.,* **298**, pp27-36.

BSI 1983. *BS 6324-1 Terms relating to surgical implants,* British Standards Institute.

BSI 1992. *ISO 7206-5 Method of determination of resistance to static load of the head and neck region of stemmed femoral components of hip joint prostheses,* British Standards Institute.

BSI 1994. *ISO 6474 Implants for surgery - Ceramic materials based on high purity alumina,* British Standards Institute.

BSI 1998-2002. *ISO 7206 (all parts),* British Standards Institute.

BSI 2002. *ISO 14242-1 Loading and displacement parameters for wear-testing machines and corresponding environmental conditions for test,* British Standards Institute.

Buckwater, J. A., Glimcher, M. J. and Cooper, R. R. (1995). Bone biology. Part 1: Strcture, blood supply, cells, matrix and mineralization. Part2: Formation form, remodelling and regulation of cell function. (Instructional Course Lecture). *Journal of Bone and Joint Surgery,* **77A**, pp1256-1289.

Burger, W. and Richter, H. G. (2000). High strength and toughness alumina matrix composites by transformation toughening and 'in situ' platelet reinforcement (ZPTA) - The new generation of bioceramics. *Bioceramics*. Zurich-Uetikon, TRANS TECH PUBLICATIONS LTD. **192-1**, pp545-548.

Cales, B. and Stefani, Y. (1998). Risks and advantages in standardization of bores and cones for heads in modular hip prostheses. *Journal of Biomedical Materials Research,* **43**(1), pp62-68.

Callaway, G., Flynn, W., Ranawat, C. and Sculco, T. (1995). Fracture of the femoral head after ceramic-on-polyethylene total hip arthroplasty. *Arthroplasty,* **10:6**(dec), pp855-9.

Cancerweb, On-Line Medical Dictionary, (2003), Available: http://cancerweb.ncl.ac.uk/omd/index.html, (Accessed: 26/3/2003)

Carter, D. R., Vasu, R. and Harris, W. H. (1982). Periacetabular stress distributions with subchondral bone retention. *Orthopaedic Scandanavica,* **54**, pp29-35.

Cartwright, K. (2003). Personal Email from Invibio.

CeramTec (2003). CereamTec Sales Literature, Biolox Forte.

Chang, F. K., Perez, J. L. and Davidson, J. A. (1990). Stiffness and strength tailoring of a hip prosthesis made of advanced composite materials. *Journal of Biomedical Materials Research,* **24**(7), pp873-899.

Charnley, J. (1979). *Low friction arthroplasty of the hip. Theory and practice.* New York, Springer-Verlag.

Chevalier, J., Olagnon, C. and Fantozzi, G. (1999). Crack propagation and fatigue in zirconia-based composites. *Composites,* **A30**, pp525-530.

Christel, P. (1992). Biocompatibility of surgical-grade dense polycrystalline alumina. *Clin. Orthop.,* **282**, pp10-18.

Christel, P., Meunier, A. and Leclercq, S. (1987). Development of a carbon-carbon hip prosthesis. *Journal of Biomed. Mater. Res. Appl. Biomater,* **21**(A2), pp191-218.

Cristofolini, L. and Viceconti, M. (1999). Towards the standardization of in vitro load transfer investigations of hip prostheses. *Journal of Strain Analysis for Engineering Design,* **34**(1), pp1-15.

Dalstra, M. and Huiskes, R. (1994). Pre-stress around the acetabulum generated by screwed cups. *Clin. Mater.,* **16**, pp145-154.

Dalstra, M. and Huiskes, R. (1995). Load transfer across the pelvic bone. *Biomech.*,(June).

Dalstra, M., Huiskes, R. and van Erning, L. (1995). Development and validation of a three-dimensional finite element model of the pelvic bone. *Biomech. Eng.*,(Aug).

D'Antonio, J. (2002). Early results for alumina-on-alumina THA look promising. *69th Annual Meeting of the American Academy Of Orthopaedic Surgeons*, Dallas.

Dauskardt, R. H. (1993a). Cyclic fatigue-crack growth in grain bridging ceramics. *Engineering Materials and Technology,* **115**, pp244.

Dauskardt, R. H. (1993b). A frictional-wear mechanism for fatigue-crack growth in grain bridging ceramics. *Acta. metall. Mater.,* **41(9)**, pp2765.

Dauskardt, R. H., James, M. R., Porter, J. R. and Ritchie, R. (1992). Cyclic fatigue-crack growth in SiC-Whisker-Reinforced Alumina ceramic composite: Long and small crack behaviour. *Am. Ceram. Soc.,* **75(4)**, pp759.

Dauskardt, R. H., Yu, W. and Ritchie, R. O. (1987). Fatigue Crack-Propagation in Transformation-Toughened Zirconia Ceramic. *Journal of the American Ceramic Society,* **70**(10), ppC248-C252.

de Oliveira Simoes, J. A. and Marques, A. T. (2001). Determination of stiffness properties of braided composites for the design of a hip prosthesis. *Composites Part A: Applied Science and Manufacturing,* **32**(5), pp655-662.

De Santis, R., Ambrosio, L. and Nicolais, L. (2000). Polymer-based composite hip prostheses. *Journal of Inorganic Biochemistry,* **79**(1-4), pp97-102.

D'Lima, D., Urquhart, A. G., Buehler, K., Walker, R. H. and Colwell, C. W. (2000). The effect of the orientation of the acetabular and femoral components on the range of motion of the hip at different head neck ratios. *Journal of Bone and Joint Surgery,* **82A**(3), pp315-321.

Dörre, E. and Dawihl, W. (1980). Ceramic Hip Endoprostheses. *Mechanical Properties of Biomaterials.* G. Hastings and D. Williams, Wiley & Sons, pp113-127.

Dunne, N. J. and Orr, J. F. (2002). Curing characteristics of acrylic bone cement. *Journal of Materials Science-Materials in Medicine,* **13**(1), pp17-22.

Engh, C. A. and Culpepper, W. J. (1997). Long-term results of use of the anatomic medullary locking prosthesis in total hip arthroplasty. *Journal of Bone and Joint Surgery-American Volume,* **79A**(2), pp177-184.

Epinette, J. (2001a). Ceramic-ceramic Bearings: Why and for Whom? *6th International Biolox® Symposium 2001.*

Epinette, J. (2001b). Hydroxyapatite-Coated Hip Implants - Current Status at 10 - 14 Years of Clinical Experience. *6th International Biolox® Symposium 2001.*

Ewalds, H. L. and Wanhill, R. J. H. (1984). *Fracture Mechanics*. Baltimore, Edward Arnold.

Eyerer, P. (1984). Biodegradation of ultra-high molecular weight polyethylene in joint endoprosthesis. *Transactions of the society of Biomaterials,* **7**, pp68.

FDA 1995a. *Guidance document for testing acetabular cup prosthesis,* U.S. Food and Drug Administration.

FDA 1995b. *Guidance document for the preparation of premarket notifications for ceramic ball hip systems,* U.S. Food and Drug Administration.

Fehring, T. K., Hurley, P. T., Braun, E. R., Mobley, C. E., Wang, P. and Griffin, W. L. (1992). Modular acetabular components: Are they really metal-backed? *Proc. AAOS 59th Annual Meting, Washington DC,*(Feb 20-25), pp82.

Finerman, G., Dorey, F., Grigoris, P. and Mc Kellop, H. (1998). *Total hip arthroplasty outcomes*. New York, Churchill Livingstone.

Gardelin, P., Seminario, J. P., Corradini, C. and Gomez, J. F. (2000). Total hip prostheses with cup and ball in ceramic and metal sockets. *Bioceramics*. Zurich-Uetikon, TRANS TECH PUBLICATIONS LTD. **192-1**, pp983-988.

Gilbert, C. J., Petrany, R. N., Ritchie, R. O., Dauskardt, R. H. and Steinbrech, R. W. (1995). Cyclic fatigue in monolithic alumina: mechanisms for crack advance promoted by frictional wear of grain bridges. *Mater. Sci.*, **30**, pp643.

Gilbert, C. J. and Ritchie, R. O. (1997). Mechanism of cyclic fatigue-crack propagation in a fine grained alumina ceramic: the role of crack closure. *Fatigue Fract. Engng Mater. Struct.*, **20(10)**, pp1453.

Glassman, A. H., Crowninshield, R. D., Schenck, R. and Herberts, P. (2001). A low stiffness composite biologically fixed prosthesis. *Clinical Orthopaedics and Related Research*,(393), pp128-136.

Gualtieri, G., Calderoni, P., Ferruzzi, A., Gnudi, S., Frontali, P., Calista, F. and Gualtieri, I. (2000). Ceramic on ceramic couplings - Twenty years' experience. *Bioceramics*. Zurich-Uetikon, TRANS TECH PUBLICATIONS LTD. **192-1**, pp989-990.

Guiu, F., Li, M. and Reece, M. (1991). Role of crack-bridging ligaments in the cyclic fatigue behavior of alumina. *Am. Ceram. Soc.*, **75(11)**, pp2976.

Havelin, L. I., Vollset, S. E. and Engesaeter, L. B. (1995). Revision for aseptic loosening of uncemented cups in 4,352 primary total hip prostheses. A report from the Norwegian Arthroplasty Register. *Acta Orthop Scand*, **66**(Dec), pp494-500.

Hernigou, P. and Le Mouel, S. (1999). Do voids in a femoral cement mantle affect the outcome? *Journal of Arthroplasty*, **14(8)**, pp1005-1010.

Hodge, W. A., Carlson, K. L., Fijan, R. S., Burgess, R. G., Riley, P. O., Harris, W. H. and Mann, R. (1989). Contact pressures from an instrumented hip endoprosthesis. *Journal of bone and joint surgery*, **71-A(9)**, pp1378-1386.

Hu, Z. and Mai, Y. (1992). Crack-Bridging Analysis for Alumina ceramics under monotonic and cyclic loading. *Am. Ceram. Soc.*, **75(4)**, pp848.

Huiskes, R. (1980). Some fundamental aspects of human joint replacement. *Acta. Orthop.Scand. Suppl.*, **185**, pp109-199.

Huiskes, R. (1987). Finite element analysis of the acetabular reconstruction. Noncemented threaded cups. *Acta. Orthop. Scand.*, **58**, pp620-625.

Huiskes, R. (1993). Failed innovation in total hip replacement. *Acta. Orthop. Scand.*, **64**, pp699-716.

Huiskes, R. and Chao, E. (1983). A survey of finite element analysis in orthopaedic biomechanics: The first decade. *Biomech.*, **16**, pp385-409.

Huiskes, R., Weinans, H. and Dalstra, M. (1989). Adaptive bone remodeling and biomechanical design considerations for noncemented total hip arthroplasty. *Orthopedics*,(Sep.), pp1255-1267.

Invibio Biomaterial Solutions (2003). PEEK Technical Literature.

Jacob, H., Huggler, A., Dietschi, C. and Schreiber, A. (1976). Mechanical function of subchondral bone as experimentally determined on the acetabulum of the human pelvis. *Biomech*, **9**, pp625-627.

Johnston, R. C. and Smidt, G. L. (1970). Hip motion measurements for selected activities of daily living. *Clinical Orthopaedics and Related Research*, **72**, pp205-215.

Juvinall, R. and Marshek, K. (2000). *Fundamentals of machine component design 3rd edition*. New York, John Wiley and Sons.

Kettunen, J., Makela, A., Miettinen, H., Nevalainen, T., Pohjonen, T., Suokas, E. and Rokkanen, P. (2001). The fixation properties of carbon fiber-reinforced liquid crystalline polymer implant in bone: an experimental study in rabbits. *Journal Of Biomedical Materials Research*, **56**(1), pp137-143.

Kishimoto, H., Ueno, A. and Okawara, S. (1994). Crack propagation behavior of polycrystalline alumina under static and cyclic load. *Am. Ceram. Soc*, **77(5)**, pp1324.

Krainess, F. E. and Knapp, W. J. (1978). Strength of a dense alumina ceramic after aging in vitro. *Journal of Biomedical Materials Research*, **12**(2), pp241-246.

Kuiper, J. H. and Huiskes, R. (1997). Mathematical optimisation of elastic properties: Application to cementless hip stem design. *Bio-mechanical Engineering*, **119**(2), pp166-175.

Kurtz, S. M., Gabriel, S. M. and Bartel, D. L. (1993). The effect of non-conformity between metal-backing and polyethylene inserts in acetabular components for total hip arthroplasty. *Trans. 39th Annual meeting ORS, San Francisco, Cal*, **15-18 feb**, pp434.

Lennon, A. B. and Prendergast, P. J. (2002). Residual stress due to curing can initiate damage in porous bone cement: experimental and theoretical evidence. *Journal of Biomechanics*, **35**(3), pp311-321.

Levenston, M. E., Beaupré, G. S., Schurman, D. J. and Carter (1993). Computer simulations of stress-related bone remodelling around non-cemented acetabular components. *Arthroplast.*, **8**, pp595-605.

Litsky, A. S. and Pophal, S. G. (1994). Initial mechanical stability of acetabular prostheses. *Orthopaedics*,(Jan 17), pp53-7.

Livermore, J., Ilstrup, D. and Morrey, B. (1990). Effect of femoral head size on wear of the polyethylene acetabular component. *Journal of Bone and Joint Surgery*, **72A**, pp518-528.

Magee, F. P., Weinstein, A. M., Longo, J. A., Koeneman, J. B. and Yapp, R. A. (1988). A canine composite femoral stem. An in vivo study. *Clinical Orthopaedics and Related Research*,(235), pp237-252.

Mann, R. W. (2002). Comment on normal hip joint contact pressure distribution in single-leg standing-effect of gender and an atomic parameters. *Journal of Biomechanics*, **35**(9), pp1291-1292.

Massin, P., Shmidt, L. and Engh, C. A. (1989). Evaluation of cementless acetabular component migration. *Arthroplasty*, **4**, pp245-251.

Matweb, Search MatWeb for Property Information, (1996-2003), Available: http://www.matweb.com/search/search.asp, (Accessed: 2/5/03)

Matweb, Vitox Properties, (1996-2003), Available: http://www.matweb.com/search/SpecificMaterial.asp?bassnum=CM0010, (Accessed: 19th June 2003)

McCormack, B. A. O. and Prendergast, P. J. (1999). Microdamage accumulation in the cement layer of hip replacements under flexural loading. *Journal of Biomechanics*, **32**(5), pp467-475.

McCormack, B. A. O., Prendergast, P. J. and O'Dwyer, B. (1999). Fatigue of cemented hip replacements under torsional loads. *Fatigue & Fracture of Engineering Materials & Structures*, **22**(1), pp33-40.

Medical Devices Agency, SN 2002(05) - Best practice in use of ceramic femoral heads in hip replacement implants, (04/03/2002), Available: http://medical-devices.gov.uk/mda/mdawebsitev2.nsf/webvwSearchResults/061A360A902310E300256B6D0050B822?OPEN, (Accessed: 31/7/03)

Medical Multimedia Group, A Patients Guide to Total Hip Replacement Surgery, (17/5/97), Available: http://www.healthpages.org/AHP/LIBRARY/HLTHTOP/THR/INDEX.HTM, (Accessed: 20/2/03)

Mendes, D. G., Said, M. and Zukermann, V. (2000). Ten Rules of Technique for Ceramic Bearing Surfaces in Total Hip Arthroplasty. *5th International CeramTec Symposium*.

Mittelmeir, H. and Heisel, J. (1992). Sixteen-years experience with ceramic hip prostheses. *Clin. Orthop.*, **282**, pp64-72.

Mjoberg, B. (1997). The theory of early loosening of hip prostheses. *Orthopedics*, **20**(12), pp1169-1175.

Morgan Matroc HIP Vitox Alumina Ceramic on Ceramic Bearings (Matroc Bioceramics Sales Literature).

Morgan Matroc Ltd. (2000). Matroc Bioceramics Sales Literature.

Morscher, E. W. (1992). Current status of acetabular fixation in primary total hip arthroplasty. *Clin. Orthop.*,(jan), pp172-93.

Murphy, B. P. and Prendergast, P. J. (2000). On the magnitude and variability of the fatigue strength of acrylic bone cement. *International Journal of Fatigue*, **22**(10), pp855-864.

Murray, M. 1999. *HIP Vitox high purity alumina for use as long term implantation devices*, Morgan Matroc Ltd,.

National Audit Office 2000. *Hip replacements: Getting it right first time*,

Nizard, R. and Sedel, L. (1992). Ten-Year survivorship of cemented ceramic-ceramic total hip prosthesis. *Clin. Orthop.*, **282**, pp53-63.

Nordin, M. and Frankel, H. (2001). *Basic Biomechanics of the Musculoskeletal System*, Lippincott Williams & Wilkins Publishers.

Norman, E., Cubitt, J., Urry, S. and Whittaker, M. (1995). *Advanced Design and Technology. Second Edition*, Longman.

Ornstein, E. (2002). Total hip replacement in general. *Acta Orthopaedica Scandinavica*, **73**, pp3-66.

Orthodynamics Ltd (1998). Internal report, Durability of material.

Orthodynamics Ltd (2003). Internal report, BMD,DEXA and composite stem.

Pandit, H. G., Hand, C. J., Ramos, J. L., Pradham, N. S. and Boyd, N. A. (1999). Middle-term results of a cementless threaded self-tapping acetabular cup. *J R Nav Med Serv*, **85**, pp174-7.

Park, Y. S., Han, K. Y., Fenollosa Gomez, J. and Benazzo, D. (2001). Clinical Results of Sandwich type Ceramic-on-ceramic Couplings in Primary Cementless Total Hip Arthroplasty. *6th International Biolox® Symposium 2001*.

Paul, J. (1999). Strength requirements for internal and external prostheses. *Journal of Biomechanics*, **32**, pp381-393.

Pedersen, D. R., Crowninshield, R. D., Brand, R. A. and Johnston, R. C. (1982). An axisymmetric model of acetabular components in total hip arthroplasty. *Biomech.*, **15**, pp305-315.

Pendegrast, P. J. (1997). Finite element modelling in tissue mechanics and orthopaedic implant design. *Clin. Biomech.*, **12**, pp343-366.

Pilliar, R. M., Lee, J. M. and Maniatopoulos, C. (1986). Observations on the Effect of Movement on Bone Ingrowth into Porous-Surfaced Implants. *Clinical Orthopaedics and Related Research,*(208), pp108-113.

Pitto, R. P., Schwämmlein, D. and Schramm, M. (2000). Modular Press-Fit Acetabular Components in Total Hip Arthroplasty. *5th International CeramTec Symposium.*

Prendergrast, P. J., Monaghan, J. and Taylor, D. (1989). Materials selection in the artificial hip joint using finite element stress analysis. *Clin. Mats.*, **4**, pp361-376.

Primal Pictures, The 3D image resource for medical education and the healthcare industry, (2003), Available: http://www.primalpictures.com/, (Accessed: 26/2/03)

Raimondi, M. and Pietrabissa, R. (1999). Modelling evaluation of the testing condition influence on the maximum stress induced in the hip prosthesis during ISO 7206 fatigue testing. *Med. Eng. Phys.*, **21**, pp353-359.

Rapperport, D. J., Carter, D. R. and Schurman, D. J. (1985). Contact finite element analysis of the hip joint. *Orthop. Res.*, **3**, pp435-446.

Rapperport, D. J., Carter, D. R. and Schurman, D. J. (1987). Contact finite element analysis of porous ingrowth acetabular cup implantation, ingrowth and loosening. *Orthop. Res.*, **5**, pp548-561.

Ray, A. K. (1998). A new technique for precracking ceramic specimens in fatigue fracture. *Journal of European Ceramic Society,* **18**, pp1655-1662.

Reinhardt, A., Advani, S. G., Santare, M. H. and Miller, F. (1999). Preliminary study on composite hip prostheses made by resin transfer molding. *Journal of Composite Materials,* **33**(9), pp852-870.

Ritchie, R., Gilbert, C. J. and McNaney, J. (2000). Mechanics and mechanisms of fatigue damage and crack growth in advanced materials. *Int. Journal of Solids and Structures,* **37**, pp311-329.

Ritchie, R. O., Dauskardt, R. H., Yu, W. K. and Brendzel, A. M. (1990). Cyclic fatigue-crack propagation, stress-corrosion, and fracture-toughness behavior in pyrolytic carbon-coated graphite for prosthetic heart valve applications. *Journal Of Biomedical Materials Research,* **24**(2), pp189-206.

Roebben, G., Steen, M., Bressers, J. and Van der Biest, O. (1996). Mechanical fatigue in monolithic non-transforming ceramics. *Progress in Material Science,* **40**, pp265-331.

Rushfeld, P., Mann, R. and W., H. (1979). The influence of cartilage geometry on the pressure distribution in the human hip. *Science,* **204**, pp413-415.

Scheller, G., Claus, A., Günther, B., Schroeder-Boersch, H. and Jani, L. (2000). MPF Modular Press Fit Cup - The Concept, Experience and First Results. *5th International CeramTec Symposium.*

Schüller, H. M., Dalstra, M., Huiskes, R. and Marti, R. K. (1993). Total hip reconstruction in acetabular dysplasia. A finite element study. *Bone and Joint Surgery,*(May).

Scotchford, C. (2001). Internal Report: Use of novel carbon fibre composite material for a section of the femoral stem component of a THR system: in vitro biological assessment. J. Bradley, Orthodesign Ltd.

Sedel, L., Bizot, P., Nizard, R., Hammadouche, M. and Hannouche, D. (2000). Long term clinical results of total joint replacement with alumina/alumina articulation. *Bioceramics*. Zurich-Uetikon, TRANS TECH PUBLICATIONS LTD. **192-1**, pp969-973.

Shaver, S., Brown, T., Hillis, S. and Callaghan, J. (1997). Digital edge-detection measurement of polyethylene wear after total hip arthoplasty. *Journal of Bone and Joint Surgery,* **79A**(5), pp693-700.

Shirandami, R. and Esat, I. I. (1990). New design of hip prosthesis using carbon fibre reinforced composite. *Journal of Biomedical Engineering,* **12**(1), pp19-22.

Simoes, J. A., Marques, A. T. and Jeronimidis, G. (2000). Design of a controlled-stiffness composite proximal femoral prosthesis. *Composites Science and Technology,* **60**(4), pp559-567.

Stoch, A., Brozek, A., Blazewicz, S., Jastrzebski, W., Stoch, J., Adamczyk, A. and Roj, I. (2003). FTIR study of electrochemically deposited hydroxyapatite coatings on carbon materials. *Journal of Molecular Structure,* **In Press, Corrected Proof.**

Sumner, D. R. and Galante, J. O. (1992). Advances in osseointegration of cementless total hip replacements. *Curr. Opinion. Orthop.*, **3**, pp427-35.

Taylor, M. (1998). Preliminary investigation of a novel controlled stiffness proximal femoral prosthesis. *Proc. Instn. Mech. Engrs.*

Taylor, M. and Tanner, K. E. (1997). Fatigue failure of cancellous bone: a possible cause of implant migration and loosening. *Journal of Bone and Joint Surgery,* **79B**, pp181-182.

Unsworth, A. and Strozzi, A. (1995). Axisymmetric finite element analysis of hip replacement with an elastomeric layer: the effects of clearance and Poisson's ratio. *Proc. Inst. Mech. Eng. (Lon),* **209H**, pp59-64.

Vasu, R., Carter, D. R. and Harris, W. H. (1982). Stress distribution in the acetabular region- before and after total joint replacement. *Biomechanics,* **15**, pp155-164.

Vekinis, G., Ashby, M. F. and Beaumont, P. W. R. (1990). R-Curve Behavior of Al_2O_3 Ceramics. *Acta Metallurgica Et Materialia,* **38**(6), pp1151-1162.

Viceconti, M., Muccini, R., Blaleani, M. and Cristofolini, L. (1999). On the numerical methods used to model contact between prostheses and host bone. *Submitted to the Journal of Biomechanics in May 1999.*

Victrex plc (2000). PEEK Properties Guide.

von Eisenhart, R., Streinlecher, M., Muller-Gerbl, M. and Eckstein, F. (1999). Quantitive determination of joint incongruity and pressure distribution during simulated gait and cartilage thickness in the human hip joint. *Orthop. Res.,* **17**, pp532-539.

Walter, A. (1992). On the material and the tribology of alumina on alumina couplings for hip joint prostheses. *Clinical Orthopedics and Related Research,* **282**, pp31-46.

Wang, A., Chopra, A. and Schmidig, G. (2002). Ceramic-On-Ceramic bearng surfaces: A complete solution to 3rd body wear problem in total hip arthroplasty. *Key Engineering Materials,* **218-220**, pp669-672.

Wilkinson, J. M., Peel, N. F., Elson, R. A., Stockley, I. and Eastell, R. (2001). Measuring bone mineral density of the pelvis and proximal femur after total hip arthroplasty. *Bone and Joint Surgery,* **83-b**(2), pp283-288.

Willert, H. G. and Semlitsch, M. (1996). Tissue reactions to plastic and metallic wear products of joint endoprostheses (Reprint). *Clinical Orthopaedics and Related Research,*(333), pp4-14.

Williams, D. (2001). New horizons for thermoplastics polymers. *Medical Device Technology*, pp8-9.

Willmann, G. (1998). Ceramics for Total Hip Replacement- What a surgeon should know. *Orthopedics,* **21**(2), pp173-177.

Willmann, G. (2000a). Ceramics for joint replacement: What are the options for this millennium. *Bioceramics*. Zurich-Uetikon, TRANS TECH PUBLICATIONS LTD. **192-1**, pp565-568.

Willmann, G. (2000b). Design of ceramic acetabular components: A retrospective. *Bioceramics*. Zurich-Uetikon, TRANS TECH PUBLICATIONS LTD. **192-1**, pp525-528.

Willmann, G. (2000c). New Generation Ceramics. *5th International CeramTec Symposium*.

Willmann, G. and Heros, R. (1998). Ceramics in total hip arthroplasty: History, Mechanical properties, Clinicla results, and current manufacturing state of the art. *Semin Arthroplasty,* **9**(2), pp114-122.

Wroblewski, B. M., Siney, P. D. and Fleming, A. (2002). Charnley low-frictional torque arthroplasty in patients under the age of 51 years - Follow-up to 33 years. *Journal of Bone and Joint Surgery-British Volume,* **84B**(4), pp540-543.

Yahiro, M. A., Gantenberg, J. B., Nelson, R., Lu, H. and Mishra, N. K. (1995). Comparison of the results of cemented, porous-ingrowth, and threaded acetabular cup fixation. A meta-analysis of the orthopaedic literature. *Arthroplasty,* **10**, pp339-50.

Yi, K. S., Cox, B. N. and Dauskardt, R. H. (1999). Fatigue crack-growth behavior of materials in viscous fluid environments. *Journal of the Mechanics and Physics of Solids,* **47**(9), pp1843-1871.

Yi, K. S., Dill, S. J. and Dauskardt, R. H. (1997). Subcritical crack growth in glasses under cyclic loads: effect of hydrodynamic pressure in aqueous environments. *Acta Materialia,* **45**(7), pp2671-2684.

Yildiz, H., Chang, F. K. and Goodman, S. (1998). Composite hip prosthesis design .2. Simulation. *Journal of Biomedical Materials Research,* **39**(1), pp102-119.

Yildiz, H., Ha, S. K. and Chang, F. K. (1998). Composite hip prosthesis design .1. Analysis. *Journal of Biomedical Materials Research,* **39**(1), pp92-101.

Zheng, X., Yan, J. and Zhao, K. (1999). Crack growth rate and cracking velocity in fatigue for a class of ceramics. *Theoretical and Applied Fracture Mechanics,* **32**, pp65-73.

Zichner, L. and Lindenfeld, T. (1997). In vivo wear of ceramics-polyethylene in comparison with metal-polyethylene. *Orthopade,* **26**(2), pp129-134.

BIBLIOGRAPHY

Adams, V.and A. Askenazi (1999). Building better products with Finite Element Analysis. Santa Fe, Onword Press.

Dowson, D. and Wright, V. (1981) Introduction to the Biomechanics of Joints and Joint Replacement. London._ Mechanical Engineering Publications

Ewalds, H. and Wanhill R. (1984). Fracture Mechanics. London, Edward Arnold Publishers

Hertzberg, R.W. (1989). Deformation and Fracture Mechanics of Engineering Materials. New York. John Wiley and Sons, Inc

Juvinall, R.C. and Marshek, K.M. (2000). Fundamentals of Machine Component Design. New York. John Wiley and Sons, Inc

Nordin, M.and Frankel, H. (2001). Basic Biomechanics of the Musculoskeletal System, Lippincott Williams & Wilkins Publishers.

Norman, E., J. Cubitt, S. Urry and M. Whittaker (1995). Advanced Design and Technology. Second Edition, Longman.

Pilkey, W.D. (1997). Peterson's Stress Concentration Factors. New York. John Wiley and Sons, Inc.

Sih, G.C. (1991). Mechanics of Fracture Initiation and Propagation. Kluwer Academic Publishers.